NORTHWESTERN UNIVERSITY

Peptide Biomimicry: Structure-Activity Relationships of Peptoid Analogues of Lung Surfactant Protein C

A DISSERTATION

SUBMITTED TO THE GRADUATE SCHOOL
IN PARTIAL FULFILLMENT OF THE REQUIREMENTS

for the degree

DOCTOR OF PHILOSOPHY

Field of Chemical Engineering

By

Nathan James Brown

EVANSTON, ILLINOIS

December 2008

© Copyright by Nathan James Brown 2008
All rights reserved

ABSTRACT

Peptide Biomimicry: Structure-Activity Relationships of Peptoid Analogues of Lung Surfactant Protein C

Nathan James Brown

The adoption of surfactant replacement therapy (SRT) for the treatment of neonatal respiratory distress syndrome (nRDS) is one of the main contributors to the dramatic decline in infant mortality rates observed in the 1980s. Despite the significant efficacy of animal-derived surfactant preparations, there are still some concerns associated with their use including: possible spread of pathogenic material, batch-to-batch variability, high cost, and limited production potential. Therefore, research has been directed at the creation of synthetic surfactant preparations. Critical to this endeavor is the development of accurate analogues of the proteins of the lung surfactant system, SP-B and SP-C. Despite SP-C's relatively short sequence length and simple secondary structure, the predominately helical protein is extremely difficult to work with due to its extreme hydrophobicity and unstable secondary structure.

One interesting approach that is particularly promising is the use of a poly-*N*-substituted glycines, or peptoids. Peptoids have close structural similarity to peptides and can be designed to form extraordinarily stable, helical structures that are resistant to protease degradation. These properties make peptoids especially promising candidates for the mimicry of peptides that rely on helical structure for their activity, such as SP-C. Here, detailed structure-activity relationships are reported for peptoid-based analogues of SP-C for use in a biomimetic SRT.

Utilizing similar design strategies as those in peptide mimics of SP-C, a range of peptoid analogues was created with specific sequence alterations to better understand the key structural

and molecular features necessary to recapitulate SP-C's unique biophysical activity. Specifically, the necessary structural requirements of the C-terminal, helical region and the unstructured, *N*-terminal region were investigated. Combining the information garnered from these studies, a peptoid-based analogue was created that mimics SP-C's extreme hydrophobicity, amphipathic patterning, and helical secondary structure, but because of its unique structure, overcomes the difficulties associated with the natural protein. When combined with a biomimetic phospholipid formulation, this analogue reproduces native SP-C's *in vitro* surface activity. With improved stability and greater production potential, peptoid SP-C mimics offer great potential not only to improve the treatment of nRDS, but also the treatment of other respiratory-related disorders.

Acknowledgements

I thank my research advisor, Dr. Annelise Barron, for her continuing assistance and support; never have I have left a research meeting feeling unenthused nor unmotivated. I also thank my committee members, Dr. Wesley Burghardt, Dr. Lyle Mockros, and Dr. David Steinhorn, who have offered support and careful critique of the research project. Partial funding for this research and financial assistance was received from the NIH Biotechnology Training Program.

I also thank past and current members of the Barron Laboratory for all your help, assistance, and comradeship. Especially to Nate Chongsiriwatana, for his continued friendship, assistance, and critical attention to detail that I will always admire. Also, thank you to Dr. Shannon Seurynck-Servoss for her assistance in introducing me to this field of research and to Michelle Dohm and Ann Czyzewski for all of your assistance and intellectual input. Also, thank you to our collaborator, Dr. Jorge Bernardino de la Serna, for hosting and providing instruction at MEMPHYS – Center for Biomembrane Physics.

I also gratefully acknowledge my mother, father, and family members for the all support, encouragement, and love that have always been in abundance.

Finally, a special thank you to Yang, who has always been there for me no matter the circumstances. I cannot imagine being here today without all of your help and support; you are a remarkable individual.

Table of Contents

ABSTRACT **3**

Acknowledgements **5**

List of Tables **12**

List of Figures **13**

Chapter 1: Biomimicry of surfactant protein C **18**

1.1 Introduction 19

1.2 Lung surfactant and respiratory distress syndrome 21

1.3 *In vitro* characterization of lung surfactant biophysical activity 23

1.3.1 Langmuir-Wilhelmy Surface Balance (LWSB) 23

1.3.2 Pulsating bubble surfactometer 27

1.4 Surfactant protein C 32

1.5 Synthetic SP-C analogues 37

1.5.1 Recombinant SP-C analogues 37

1.5.2 Synthetic SP-C peptide analogues 38

1.5.3 Peptoid analogues 40

1.6 Future implications 44

1.7 Presentation and summary of the work presented 46

Chapter 2: Lung surfactant comparators: synthesis, isolation, and characterization **48**

2.1 Introduction 49

2.2 Materials and methods 52

2.2.1 Materials 52

2.2.2 Natural surfactant isolation 53

2.2.3 Natural surfactant extraction 55

2.2.4 Peptide Synthesis 55

2.2.5 Peptide Purification 58

2.2.6 Circular dichroism 59

2.2.7 Pulsating bubble surfactometry 59

2.3 Results and discussion 61

2.3.1 Natural lung surfactant *in vitro* surface activity 61

2.3.2 SP-C peptide mimic 64

2.4 Conclusions 74

Chapter 3: Lipid composition greatly affects the *in vitro* surface activity of lung surfactant protein C mimics 76

3.1 Introduction 77

3.2 Materials and methods 81

3.2.1 Materials and reagents 81

3.2.2 Peptide and peptoid synthesis, purification, and characterization 82

3.2.3 Methods and apparatus 84

3.3 Results and discussion 87

3.3.1 Comparison of the surface-active behavior of three synthetic lipid formulations used as mimics of the non-protein portion of lung surfactant 87

3.3.2 *In vitro* surface-active behaviors of peptide and peptoid mimics in various lipid formulations 98

3.4 Conclusions 114

Chapter 4: Effects of hydrophobic helix length and side chain chemistry on biomimicry in peptoid analogues of surfactant protein C 118

4.1 Introduction 119

4.2 Materials and methods 124

4.2.1 Materials 124

4.2.2 Protein design and synthesis 124

4.2.3 Peptoid synthesis 127

4.2.4 Circular dichroism spectroscopy 128

4.2.5 Langmuir-Wilhelmy surface balance and fluorescent microscopy 128

4.2.6 Pulsating bubble surfactometer 129

4.3 Results and discussion 130

4.3.1 Peptoid design and rationale 130

4.3.2 Secondary structure 132

4.3.3 Langmuir-Wilhelmy surface balance studies 134

4.3.4 Fluorescence microscopy imaging of film morphology 138

4.3.5 Static adsorption 141

4.3.6 Dynamic cycling 143

4.4 Conclusions 148

Chapter 5: *N*-terminal alkylation of a peptoid analogue of surfactant protein C 152

5.1 Introduction 153

5.2 Materials and methods 159

5.2.1 Materials 159

5.2.2 Peptoid synthesis 160

5.2.3 Circular dichroism spectroscopy 162

5.2.4 Pulsating bubble surfactometer 162

5.2.5 Langmuir-Wilhelmy surface balance and fluorescent microscopy 163

5.3 Results and discussion 164

5.3.1 Peptoid design and rationale 164

5.3.2 Secondary structure 166

5.3.3 Langmuir-Wilhelmy surface balance studies 168

5.3.4 Fluorescence microscopy imaging of film morphology 171

5.3.5 Static-bubble pulsating bubble surfactometry 175

5.3.6 Dynamic pulsating bubble surfactometry 178

5.4 Conclusions 181

Chapter 6: Side chain chemistry of the C-terminal helix of a peptoid analogue of SP-C: balancing structural rigidity and biomimicry 186

6.1 Introduction 187

6.2 Materials and methods 192

6.2.1 Materials 192

6.2.2 Peptoid synthesis 193

6.2.3 Circular dichroism spectroscopy 195

6.2.4 Langmuir-Wilhelmy surface balance and fluorescent microscopy 196

6.2.5 Pulsating bubble surfactometer 197

6.3 Results and discussion 198

6.3.1 Peptoid design and rationale 198

6.3.2 Circular dichroism 199

6.3.3 Langmuir-Wilhelmy surface balance 201

6.3.4 Fluorescent microscopy 205

6.3.5 Static adsorption 207

6.3.6 Dynamic cycling 209

6.4 Conclusions 213

Chapter 7: SP-C peptoid biomimicry: combining structural rigidity and side chain biomimicry in one peptoid residue 216

7.1 Introduction 217

7.2 Materials and methods 220

7.2.1 Materials 220

7.2.2 Peptoid synthesis 221

7.2.3 Natural lung surfactant isolation and extraction 223

7.2.4 Peptide synthesis 224

7.2.5 Peptide and peptoid fluorescent labeling 225

7.2.6 Circular dichroism spectroscopy 226

7.2.7 Pulsating bubble surfactometer 226

7.2.8 Giant unilamellar vesicles 227

7.3 Results and discussion 228

7.3.1 Peptoid design and rationale 228

7.3.2 Circular dichroism 230

7.3.3 Static bubble adsorption 232

7.3.4 Dynamic compression-expansion cycling 235

7.3.5 Fluorescently labeled SP-C mimics in lipid bilayers 238

7.4 Conclusions 241

Chapter 8: Summary and future directions 244

8.1 Impact of the work presented 244

8.2 Future directions 245

8.2.1 Biomimetic SP-C structures 245

8.2.2 Biophysical characterization 246

8.2.3 Formulation of a peptoid-based surfactant replacement therapy 249

8.2.4 Peptoid biocompatibility 250

8.3 Conclusion 251

References 253

Appendices 273

Appendix A: SP-C Peptoid *N*- and C-terminal sequence biomimicry 273

List of Tables

Table 1.1: Structure of native SP-C and SP-C analogues.. 33

Table 2.1: Structures of native SP-C and SP-C peptide analogues..... 57

Table 3.1: Peptide and peptoid sequences and molecular weights. 83

Table 3.2: Molar percentages of added peptide or peptoid in each lipid formulation. 84

Table 4.1: Peptide and peptoid sequences. 126

Table 5.1: Structure of porcine SP-C and peptoid-based SP-C analogues. 161

Table 6.1: Structures of peptoid-based SP-C analogues. 194

Table 7.1: Structures of peptoid-based SP-C analogues. 222

List of Figures

Figure 1.1: Schematic of a Langmuir-Wilhelmy surface balance (LWSB) consisting of a Teflon trough, two Teflon barriers to control film area, and a Wilhelmy plate to monitor surface pressure. 24

Figure 1.2: A model Langmuir-Wilhelmy surface balance (LWSB) isotherm showing the various lipid phases and phase transitions present in pulmonary surfactant as the surface area is reduced. Adapted from [21]..... 26

Figure 1.3: Schematic diagram of the pulsating bubble surfactometer (PBS) used to monitor interfacial surface tension during both static adsorption and dynamic cycling at quasi-physiological conditions. Adapted from [25]. 28

Figure 1.4: Static bubble (A) and dynamic bubble (B) adsorption results from the pulsating bubble surfactometer (PBS) Infasurf. Dynamic data were collected at 20 cycles/min and loop direction is clockwise. Measurements were taken at a bulk surfactant concentration of 1 mg/mL lipids and at 37°C. Data are reproduced from Seurynck et al [27]. 31

Figure 1.5: Hypothesized SP-C disposition in a LS film at the alveolar air-liquid interface. In a monolayer film, the SP-C helix is oriented nearly parallel to the air-liquid interface, while in a phospholipid bilayer, the SP-C helix aligns nearly parallel with the lipid acyl chains and perpendicular to the interface. The figure also shows how the palmitoyl chains of SP-C may act to anchor either the flexible *N*-terminal region in the same phospholipid film or to an adjacent layer, forming a surface-associated surfactant reservoir..... 35

Figure 1.6: (A) Peptide and peptoid structures and (B) submonomer synthesis scheme for peptoid oligomers..... 42

Figure 2.1: Isolation and extraction procedure for the hydrophobic constituents of natural lung surfactant. Procedure adapted from [80-83]. 54

Figure 2.2: Static bubble (A) and dynamic bubble (B) adsorption results from the pulsating bubble surfactometer in buffer at 37°C for SLSE. Dynamic data were collected at 20 cycles/min and loop directions are clockwise. 62

Figure 2.3: HPLC elution profile of SP-$C_{F,F}$ synthesized using standard Fmoc chemistry with NMP as the coupling solvent and 20% piperidine in NMP for Fmoc deprotection (black line) and using Fmoc chemistry with DMSO as the coupling solvent and 4% DBU:piperidine (1:1) in DMF for Fmoc deprotection (red line). Desired compounds are indicated by *. 0-100% solvent B in solvent A over 90 minutes on a C4 RP-HPLC column where solvent A = 0.1% TFA in water and solvent B = 0.1% TFA in isopropanol. The largest peak in each elution profile was normalized to 1. 68

Figure 2.4: (A) CD spectra of SP-$C_{F,F}$ and di-pSP-$C_{F,F}$ in methanol showing characteristic features of a peptide α-helix; (B) CD spectra of SP-$C_{F,F}$ and di-pSP-$C_{F,F}$ in 5 mM liposomes in 10 mM Tris·HCl, pH = 6.90. Spectra were acquired at a peptide concentration of ~ 60 μM at room temperature. 70

Figure 2.5: Static bubble (A) and dynamic bubble (B) adsorption results from the pulsating bubble surfactometer in buffer at 37°C for Tanaka lipids, Tanaka lipids + 1.6 mol% SP-$C_{F,F}$, and Tanaka lipids + 1.6 mol% di-pSP-$C_{F,F}$. Dynamic data were collected at 20 cycles/min and loop directions are clockwise. 72

Figure 3.1: Surface pressure-surface area isotherms obtained using the Langmuir-Wilhelmy surface balance at 25 °C (A) and 37°C (B) for PCPG lipids, Tanaka lipids, and synthetic Infasurf lipids. 91

Figure 3.2: Fluorescent microscopic images of PCPG lipids (A, B), Tanaka lipids (C, D), and synthetic Infasurf lipids (E, F) at ~ 35 mN/m (A, C, E) and ~ 50 mN/m (B, D, F) on buffer at 37°C, collected with a barrier speed of 5 mm/min. 94

Figure 3.3: Static bubble (A) and dynamic bubble (B) adsorption results from the pulsating bubble surfactometer in buffer at 37°C for PCPG lipids, Tanaka lipids, and synthetic Infasurf lipids. Dynamic data were collected at 20 cycles/min and loop directions are clockwise. 96

Figure 3.4: Surface pressure-surface area isotherms obtained using the Langmuir-Wilhelmy surface balance at 37°C for PCPG lipids (A), Tanaka lipids (B), and synthetic Infasurf lipids (C) along with added SP-C mimics. Molecular areas include both lipids and mimics. 100

Figure 3.5: Fluorescent microscopic images for PCPG lipids (A and B), PCPG lipids with added SP-$C_{F,F}$ (C and D) and Peptoid C (E and F) on buffer at 37ºC, collected with a barrier speed of 5 mm/min. Images shown for Π ~ 35 mN/m (A, C, and E) and Π ~ 50 mN/m (B, D, and F). 103

Figure 3.6: Fluorescent microscopic images for Tanaka lipids (A and B), Tanaka lipids with added SP-$C_{F,F}$ (C and D) and Peptoid C (E and F) on buffer at 37ºC, collected with a barrier speed of 5 mm/min. Images shown for Π ~ 35 mN/m (A, C, and E) and Π ~ 50 mN/m (B, D, and F). 104

Figure 3.7: Fluorescent microscopic images for synthetic Infasurf lipids (A and B), synthetic Infasurf lipids with added SP-$C_{F,F}$ (C and D) and Peptoid C (E and F) on buffer at 37ºC, collected with a barrier speed of 5 mm/min. Images shown for Π ~ 35 mN/m (A, C, and E) and Π ~ 50 mN/m (B, D, and F). 106

Figure 3.8: Static bubble adsorption results from the pulsating bubble surfactometer in buffer at 37°C for PCPG lipids (A), Tanaka lipids (B), and synthetic Infasurf lipids (C) along with added SP-C mimics. 108

Figure 3.9: Dynamic bubble adsorption results from the pulsating bubble surfactometer in buffer at 37°C for PCPG lipids (A), Tanaka lipids (B), and synthetic Infasurf lipids (C) along with added SP-C mimics. Data were collected at 20 cycles/min and loop directions are clockwise..... 110

Figure 4.1: (A) Circular dichroism (CD) spectra of the SP-C_{Lff} peptide as well as of the varied-length *N*spe-based peptoid SP-C mimics (Mimics 1-8, 1-11, and 1-14), showing qualitatively similar features characteristic of peptide and peptoid helices, respectively; and (B) CD spectra of the varied-length *N*ssb-based peptoid SP-C mimics (Mimics 2-8, 2-11, and 2-14) displaying the characteristic features of polyproline type I peptide helices. Spectra were acquired in methanol at a concentration of 60 μM, at room temperature. 133

Figure 4.2: LWSB studies at 25°C (A) Π-A isotherms obtained for DPPC:POPG:PA (68:22:9, by weight) alone, and with 1.6 mol% SP-C_{Lff} peptide; (B) 1.6 mol% *N*spe-based peptoids (Mimics 1-8, 1-11, and 1-14) ; (C) 1.6 mol% *N*ssb-based peptoids (Mimics 2-8, 2-11, and 2-14). Isotherms were collected on a buffered subphase (150 mM NaCl, 10 mM HEPES, 5 mM $CaCl_2$, pH=6.90). 136

Figure 4.3: FM micrographs at 37°C corresponding to Π of ~ 35 mN/m and ~ 50 mN/m for DPPC:POPG:PA (68:22:9, by weight) alone (panels A and E), with 1.6 mol% SP-C_{Lff} peptide (panels B and F), with 1.6 mol% Mimic 1-14 (panels C and G), and with 1.6 mol% Mimic 2-14 (panels D and H). Average size of the dark LC domains for each film is indicated in the lower left of each panel. 139

Figure 4.4: Static PBS results displaying surface tension as a function of time. Measurements were taken at a bulk surfactant concentration of 1 mg/mL lipids and at 37°C. (A) Lipid mixture alone and with 1.6 mol% SP-C_{Lff} and *N*spe-based peptoids (Mimics 1-8, 1-11, and 1-14); (B) Lipid mixture alone and with 1.6 mol% *N*ssb-based peptoids (Mimics 2-8, 2-11, and 2-14)... 142

Figure 4.5: Dynamic PBS results displaying surface tension as a function of surface area at an oscillation frequency of 20 cycles/min, after 10 minutes of initial cycling. Measurements were taken at a bulk surfactant concentration of 1 mg/mL lipids and at 37°C. (A) Lipid mixture alone and with 1.6 mol% SP-C_{Lff}; (B) Lipid mixtures with 1.6 mol% *N*spe-based peptoids (Mimics 1-8, 1-11, and 1-14); (C) Lipid mixtures with 1.6 mol% *N*ssb-based peptoids (Mimics 2-8, 2-11, and 2-14). 145

Figure 5.1: Circular dichroism (CD) spectra of peptoid-based SP-C mimics (Mimics C, pC, and di-pC), showing qualitatively similar characteristics of peptoid helices. Spectra were acquired in methanol at a concentration of ~ 60 μM at room temperature. 167

Figure 5.2: Langmuir-Wilhelmy surface balance (LWSB) studies at 37°C. (A) Surface pressure-area isotherms obtained for DPPC:POPG:PA (68:22:9, by weight) alone, and with 1.6 mol% SP-C; (B) Lipids with 1.6 mol% peptoid-based SP-C mimics (Mimics C, pC, and di-pC). Isotherms were collected on a buffered subphase (150 mM NaCl, 10 mM HEPES, 5 mM $CaCl_2$, pH=6.90) at 37°C. 169

Figure 5.3: Fluorescence microscopy (FM) micrographs at 37°C corresponding to a surface pressure of ~ 35 mN/m and ~ 50 mN/m for DPPC:POPG:PA (68:22:9, by weight) alone (panels A and F), with 1.6 mol% SP-C (panels B and G), Mimic C (panels C and H), Mimic pC (panels D and I), and Mimic di-pC (panels E and J). Average size of the dark LC domains for each film is indicated in the lower left of each panel. 173

Figure 5.4: (A) Static pulsating bubble surfactometry (PBS) results displaying surface tension as a function of time and (B) dynamic PBS results displaying surface tension as a function of surface area at an oscillation frequency of 20 cycles/min after 5 minutes of cycling. Measurements were taken at a bulk surfactant concentration of 1 mg/mL lipids at 37°C. 176

Figure 6.1: Circular dichroism (CD) spectra of the peptoid-based SP-C mimics (Mimics C, CIle1, CIle2, and di-pCIle2) showing qualitatively similar characteristics of peptoid helices. As the aliphatic content is increased, the CD spectra display features that are progressively similar to a polyproline type I peptide helix. Spectra were acquired in methanol at a concentration of ~ 60 μM at room temperature. 201

Figure 6.2: Langmuir-Wilhelmy surface balance (LWSB) studies at 37°C. (A) Surface pressure-area isotherms obtained for DPPC:POPG:PA (68:22:9, by weight) alone, with 1.6 mol% SP-C, and with 1.6 mol% Mimic C; (B) Lipids with 1.6 mol% Mimic CIle1, Mimic CIle2, and Mimic di-pCIle2. Isotherms were collected on a buffered subphase (150 mM NaCl, 10 mM HEPES, 5 mM $CaCl_2$, pH=6.90). 202

Figure 6.3: Fluorescence microscopy (FM) micrographs at 37°C corresponding to a surface pressure of ~ 35 mN/m and ~ 50 mN/m for DPPC:POPG:PA (68:22:9, by weight) alone (panels A and G), with 1.6 mol% SP-C (panels B and H), Mimic C (panels C and I), Mimic CIle (panels D and J), Mimic CIle2 (panels E and K), and Mimic di-pCIle2 (panels F and L). Average size of the dark LC domains for each film is indicated in the lower left of each panel. 206

Figure 6.4: Static pulsating bubble surfactometry (PBS) results displaying surface tension as a function of time. (A) Lipid mixture alone and with 1.6 mol% SP-C and Mimic C; (B) Lipid mixture with 1.6 mol% Mimics CIle1, CIle2, and di-pCIle2. 208

Figure 6.5: Dynamic pulsating bubble surfactometry (PBS) results displaying surface tension as a function of surface area at an oscillation frequency of 20 cycles/min, after 5 minutes of initial cycling. (A) Lipid mixture alone and with 1.6 mol% SP-C and Mimic C. (B) Lipid mixtures with 1.6 mol% Mimics CIle1, CIle2, and di-pCIle2. Measurements were taken at a bulk surfactant concentration of 1 mg/mL lipids and at 37°C. 211

Figure 7.1: Circular dichroism (CD) spectra of the peptoid-based SP-C mimics showing qualitatively similar characteristics of peptoid helices. As the aliphatic content is increased, the CD spectra display features that are progressively similar to a polyproline type I peptide helix. Spectra were acquired in methanol at a concentration of ~ 60 µM at room temperature. 231

Figure 7.2: Static pulsating bubble surfactometry (PBS) results displaying surface tension as a function of time. (A) Natural lung surfactant and lipid mixture alone and with 1.6 mol% SP-C; (B) Lipid mixture with 1.6 mol% Mimics C, CLeu2, CLeu3, and di-pCLeu3. Measurements were taken at a bulk surfactant concentration of 1 mg/mL lipids and at 37°C. 233

Figure 7.3: Dynamic pulsating bubble surfactometry (PBS) results displaying surface tension as a function of surface area at an oscillation frequency of 20 cycles/min. (A) Natural lung surfactant and lipid mixture alone and with 1.6 mol% SP-C. (B) Lipid mixtures with 1.6 mol% Mimics C, CLeu2, CLeu3, and di-pCLeu3. Measurements were taken at a bulk surfactant concentration of 1 mg/mL lipids and at 37°C. 236

Figure 7.4: Confocal fluorescence microscopy imaging of giant unilamellar vesicles (GUVs) of lipids alone (A and E), lipids with 10 wt% di-pSP-C (B and F), lipids with 10 wt% Mimic CLeu3 (C and G), and lipids with 10 wt% Mimic di-pCLeu3. Scale bars correspond to 5 µm. Fluorescence images were taken at 21°C and are representative of the population observed. Red corresponds to the fluorescently labeled lipid species and yellow to the labeled peptide and peptoids. 239

Chapter 1: Biomimicry of surfactant protein C

Reproduced with the permission of Accounts of Chemical Research, **2008**, 41, 1409-1417.
Copyright 2008, American Chemical Society.

Since the widespread use of exogenous lung surfactant to treat neonatal respiratory distress syndrome, premature infant survival and respiratory morbidity have dramatically improved. Despite the effectiveness of the animal-derived surfactant preparations, there still remain some concerns and difficulties associated with their use. This has prompted investigation into the creation of synthetic surfactant preparations. However, to date, no clinically used synthetic formulation is as effective as the natural material. This is largely because the previous synthetic formulations lacked analogues of the hydrophobic proteins of the lung surfactant system, SP-B and SP-C, which are critical functional constituents. As a result, recent investigation has turned towards the development of a new generation of synthetic, biomimetic surfactants that contain synthetic phospholipids along with a mimic of the hydrophobic protein portion of lung surfactant.

In this Chapter, efforts towards creating accurate mimics of SP-C for use in a synthetic surfactant replacement therapy are detailed. Despite SP-C's seemingly simple structure, the predominantly helical protein is extraordinarily challenging to work with given its extreme hydrophobicity and structural instability, which greatly complicates the creation of an effective SP-C analogue.

Drawing inspiration from Nature, two promising biomimetic approaches have led to the creation of rationally designed biopolymers that recapitulate many of SP-C's molecular features. The first approach utilizes detailed SP-C structure-activity relationships and amino acid folding propensities to create a peptide-based analogue, SP-C33. In SP-C33, the problematic and

metastable poly-valine helix is replaced with a structurally stable, poly-leucine helix and includes a well placed positive charge to prevent aggregation. SP-C33 is both structurally stable and eliminates the association propensity of the native protein. The second approach follows the same design considerations, but makes use of a non-natural, poly-*N*-substituted glycine or "peptoid" scaffold to circumvent the difficulties associated with SP-C. By incorporating unique, biomimetic side chains in a non-natural backbone, the peptoid mimic captures both SP-C's hydrophobic patterning and helical secondary structure.

Despite the differences in structure, both SP-C33 and the SP-C peptoid mimic capture many requisite features of SP-C. In a surfactant environment, these analogues also replicate many of the key surface activities necessary for a functional biomimetic surfactant therapy while overcoming the difficulties associated with the natural protein. With improved stability, greater production potential, and elimination of possible pathogenic contamination, these biomimetic surfactant formulations offer the potential not only to improve the treatment of respiratory distress syndrome, but also the opportunity to treat other respiratory-related disorders.

1.1 Introduction

In spite of the seemingly simple building blocks from which they are constructed, proteins constitute enormously complex and powerful molecular tools. Utilizing a bottom-up design approach, Nature has engineered proteins to perform a wide range of life-essential tasks that participate in almost every biological process. Proteins are able to carry out such diverse functions because they adopt specific, compact conformations with high precision and fidelity, allowing exact, three-dimensional positioning of the functional groups and facilitating the necessary interactions of the active site.

The diverse and precise bioactivities of proteins have made them coveted therapeutic agentsand are currently being used to in a variety of applications including in the treatment of diabetes, cancer, and to combat infection. Because of their size, peptides have several advantages over small molecules and antibodies for therapeutic applications. Therapeutic peptides are large enough (10-50 AA) that their interaction with desired targets are more specific with lower toxicity profiles than other small molecules. Likewise, peptides are small enough to have improved storage/stability, tissue penetration, and immunogenicity over antibody-based therapeutics. Despite this, peptide-based therapeutics are only recently seeing wider spread use, largely, because peptides are generally more difficult than small molecules to produce on a large scale, are rapidly cleared *in vivo*, and lack *in vivo* stability due to protease degradation [1].

To date, the vast majority of engineered synthetic and recombinant peptide therapeutics are based upon sequences originating from natural sources, as these peptides have undergone natural selection for both efficacy and stability [1]. Recent advances in genomics and structural proteomics have led to a deeper understanding of how a protein's amino acid sequence lends itself to the formation of stable, secondary structural elements such as α-helices, β-sheets, and turns; and how these structural elements give rise to tertiary and quaternary structures of folded, biologically active proteins. This improvement in translating amino acid sequences into protein structures and related functions, while not complete and still developing, has led to the ability to prepare some peptide sequences *de novo* with predictable structures [2]. In addition, researchers are also expanding Nature's code with the inclusion of non-natural amino acids and, in some cases, using totally synthetic polymeric scaffolds, or "foldamers" [3]. These novel structures are beginning to become increasingly efficacious and have the possibility to possess improved properties over native peptides, increasing the tools available to the protein scientist.

Researchers have developed novel sequences of amino acids, non-natural polymers, and hybrids of the two that can be efficiently produced with improved stability, bioavailability, and, in some instances, improved functionality in comparison to the mimicked peptide. One interesting application with clinical relevance concerns the mimicry of the predominantly helical, hydrophobic protein of the lung surfactant (LS) system, surfactant protein C (SP-C). SP-C, in addition to SP-B, is an important constituent of exogenous LS material for the treatment of respiratory distress syndrome (RDS). However, working with the natural protein and sequence-identical analogues is extremely challenging due SP-C's extreme hydrophobicity and metastable secondary structure [4]. These attributes make the isolation and storage of SP-C very difficult and may also contribute to the limited shelf-life of therapeutic preparations containing the protein [5]. The utilization of recombinant and synthetic peptides as well as non-natural, peptidomimetic approaches offer promise for overcoming these difficulties. Below, the requisite surface activities of a functional LS formulation and the key SP-C structural and molecular features are detailed followed by the ongoing approaches to mimic this difficult protein.

1.2 Lung surfactant and respiratory distress syndrome

LS is a complex mixture of over 50 lipid species and four surfactant proteins, which lines the alveolar air-liquid interface and is required for proper respiration, as its absence or dysfunction leads to severe respiratory disease [6, 7]. No single component is solely responsible for LS's unique biophysical activity [7, 8]. Phospholipids are the main constituent of LS, representing > 80% of its mass, while neutral lipids and surfactant proteins each constitute approximately 10% [8, 9]. In the airways, the lipid-protein mixture has three main properties that are essential for respiration: 1) rapid adsorption to the air-liquid interface of the alveoli, 2)

dramatic reduction of the alveolar surface tension to near-zero values upon compression or exhalation, preventing collapse of the alveoli due to contractile forces of the alveolar liquid lining, and 3) rapidly respread to the air-liquid interface upon expansion or inhalation, reducing maximum surface tension and diminishing the work of breathing [10].

An absence of functional LS in premature infants leads to the occurrence of neonatal RDS (nRDS). Without properly functioning LS, lung compliance is reduced and respiration is greatly impaired, ultimately resulting in alveolar collapse and suffocation without treatment. While nRDS was once a leading cause of infant mortality, it is now routinely treated by administration of animal-derived exogenous surfactant preparations into the lungs of afflicted individuals [7]. These surfactant replacement therapies (SRTs) consist of modified mammalian surfactant either extracted directly from animal lungs by lavage or isolated from homogenized lung tissue. Despite the efficacy of natural SRTs, there are some drawbacks associated with their use [11]. Natural preparations present a possibility of cross-species transfer of infectious agents as well as high production costs and batch-to-batch variability. In addition, SRTs may also be beneficial in the treatment of other respiratory-related disorders such as acute RDS; however, this requires significantly more material than current isolation techniques can supply [12]. To address these concerns, synthetic surfactants composed of synthetic phospholipids and surface-active chemical additives were developed. However, these synthetic preparations had reduced efficacies compared to natural surfactants and are no longer used, likely, a result of the absence of the hydrophobic LS proteins, SP-B and SP-C, which are both critical constituents of functional LS [13, 14]. Therefore, there has been increasing interest in the development of a third category of SRTs: biomimetic SRTs that utilize an entirely synthetic surfactant containing a mimic of the hydrophobic protein portion of LS, which functions as well as the natural material

and eliminates the concerns associated with animal-derived surfactants [12, 15]. This endeavor requires a detailed understanding of the molecular interactions between the hydrophobic surfactant proteins and the LS phospholipids and how these interactions relate to surface activity [16].

1.3 *In vitro* characterization of lung surfactant biophysical activity

Over the past 50 years, a variety of techniques have been utilized to characterize the surface-active properties of lung surfactant as well as the specific behaviors of the individual surfactant components. These techniques have largely evolved from methods originally developed for interfacial phenomena research with specific modifications to better suit the unique requirements of lung surfactant research. Many of the specialized techniques attempt to mimic conditions occurring in the alveoli to investigate the underlying mechanisms governing lung surfactant's unique biophysical activity, which include: interfacial adsorption, surface tension reduction, and film respreading [16]. Four experimental methods that comprise the bulk of surfactant instrumentation are the Langmuir-Wilhelmy surface balance (LWSB), an adsorption surface balance with minimized diffusion, the pulsating bubble surfactometer (PBS), and the captive bubble surfactometer (CBS). The major features of the complementary LWSB and PBS instruments are described below.

1.3.1 Langmuir-Wilhelmy Surface Balance (LWSB)

Instruments that measure the surface pressure (Π)-area (A) characteristics of a spread surface film are termed surface balances. The LWSB is the most common surface balance used for the characterization of the surface-active behaviors of lung surfactant and was first used for lung surfactant research by Clements in 1957 [17]. Since then, the LWSB has proven to be a

valuable instrument to assess surface film structure and surface activity. A schematic of a typical LWSB used for pulmonary research is depicted in Figure 1.1.

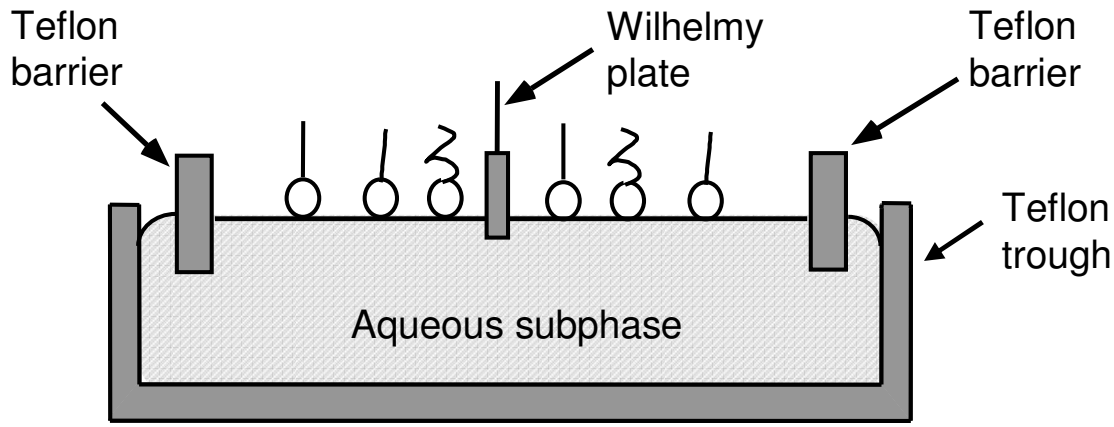

Figure 1.1: Schematic of a Langmuir-Wilhelmy surface balance (LWSB) consisting of a Teflon trough, two Teflon barriers to control film area, and a Wilhelmy plate to monitor surface pressure.

A typical LWSB consists of a Teflon trough that holds a liquid subphase, one or two Teflon barriers that compress and expand the surface film, and a Wilhelmy plate to monitor surface pressure. The surfactant film is typically formed at the air-liquid interface of the trough by spreading from an immiscible organic solvent (chloroform or hexane) or by adsorption from the aqueous subphase. The film is then compressed and expanded by movement of the trough barriers. The surface pressure of the interface is then determined with a force transducer connected to a Wilhelmy slide situated just below the surface of the liquid. Surface pressure (Π) is defined as the difference in surface tension in the presence of a monolayer (γ) relative to that of a clean interface (γ^o) as shown in Eq. 1.1.

$$\Pi = \gamma^o - \gamma \qquad \text{Eq. 1.1}$$

By monitoring the surface pressure of the liquid subphase and surfactant film, the amount by which the surface tension is reduced due to the presence of the surface-active film as a function of surface area can be determined. The LWSB also allows measurement of the respreading behavior and hysteresis properties of surfactant films as surface area is altered, separate from the influence of adsorption [7]. A typical plot of surface pressure vs. molecular area (LWSB isotherm) is shown in Figure 1.2. The important features of a LWSB isotherm of lung surfactant are an early lift-off, a biomimetic plateau region between 40 and 50 mN/m, and a high collapse pressure, ~ 70 mN/m, corresponding to very low surface tension. Upon subsequent cycles of compression-expansion, the film should also have little offset in area, which is indicative of minimal loss of surfactant material to the subphase or favorable respreading characteristics.

A major utility of the LWSB is that it can be combined with other instrumentation techniques such as fluorescence microscopic (FM) imaging, Brewster angle microscopic (BAM) imaging, and atomic force microscopy (AFM) to reveal detailed information on the surfactant film morphology [18-20]. Of these techniques, FM is most commonly used as it offers the ability to easily monitor the phase morphology as a function of surface pressure and the distribution of the membrane associated proteins at the air-liquid interface. In this technique, a small amount of a fluorescently labeled lipid molecules and/or proteins are added to the

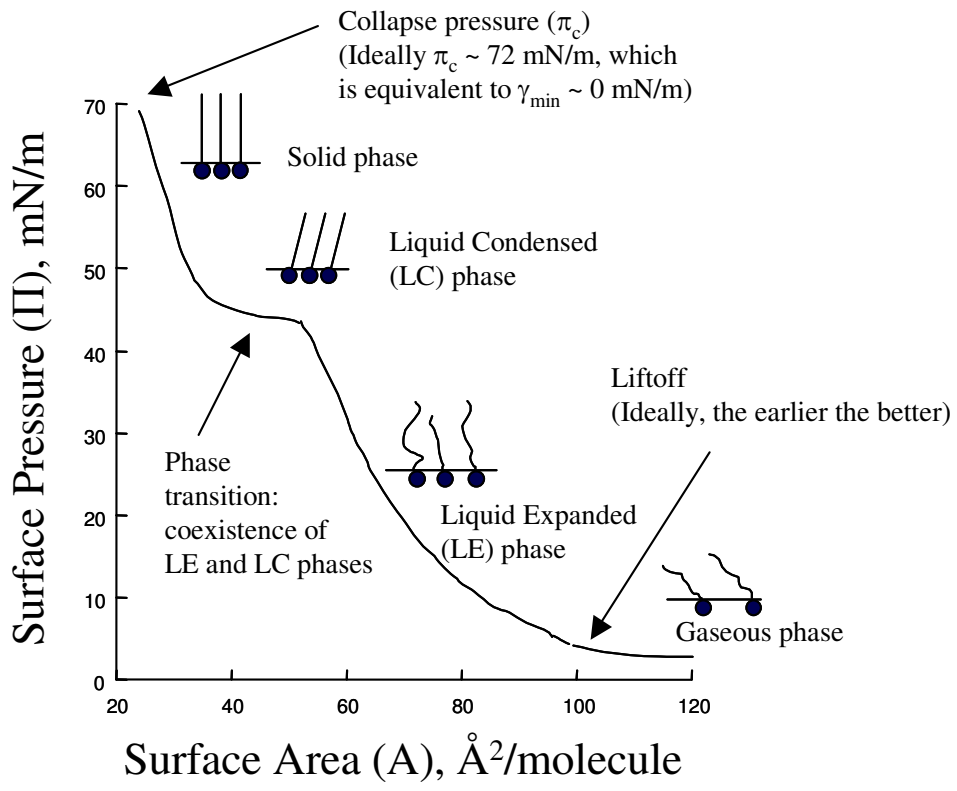

Figure 1.2: A model Langmuir-Wilhelmy surface balance (LWSB) isotherm showing the various lipid phases and phase transitions present in pulmonary surfactant as the surface area is reduced. Adapted from [21].

formulation and imaged with a fluorescence microscope. Typically, the bulky fluorescently labeled lipid species preferentially partition into the less ordered phase of the monolayer, allowing differentiation between the liquid expanded (LE) and the liquid condensed (LC) phases of the surfactant film [22].

One of the drawbacks of the LWSB is that it is a quasi-static method for surface tension measurements; interfacial films are compressed and expanded at a rate much slower than physiological rates and do not fully reflect a dynamic process like breathing. To address this, LWSB studies of lung surfactant are typically combined with *in vitro* studies performed at physiological cycling rates such as in the PBS and/or CBS instruments.

1.3.2 Pulsating bubble surfactometer

To complement the quasi-static characterization technique of the LWSB, more physiologically relevant instruments have been developed that better reflect a dynamic process like breathing [23, 24]. One instrument of particular utility is the PBS originally developed by Enhorning in 1977 [23]. The PBS has been used extensively in lung surfactant research to determine the dynamic surface tension lowering ability of surfactants dispersed in aqueous solutions. The PBS closely approximates many of the parameters in the alveoli with physiologically relevant cycling rates, compression ratio, temperature, and humidity. Surface tension measurement in the PBS also reflects a sum of contributions from adsorption and dynamic film behavior, which is analogous to the conditions in the airways.

The PBS instrument consists of three main components: a sample chamber, a volume-displacement piston, and a pressure transducer (Figure 1.3). The surfactant material dispersed in an aqueous suspension is first loaded into the PBS sample chamber and then placed onto the

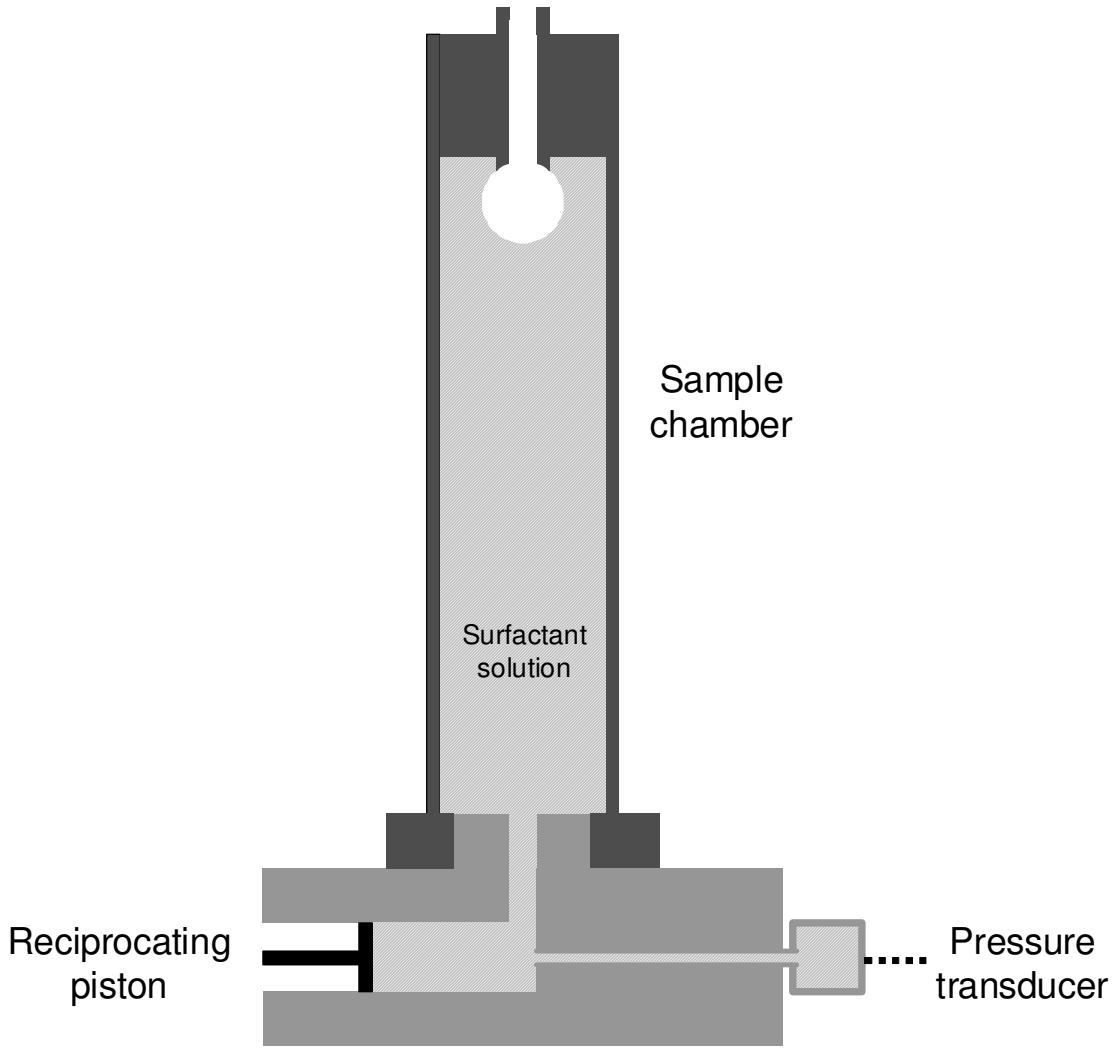

Figure 1.3: Schematic diagram of the pulsating bubble surfactometer (PBS) used to monitor interfacial surface tension during both static adsorption and dynamic cycling at quasi-physiological conditions. Adapted from [25].

PBS instrument. Next, a volume displacement piston is then used to pull air through the small capillary at the top of the sample chamber, forming a bubble of a known volume in the aqueous surfactant suspension. The pressure transducer is then used to continuously monitor the pressure differential across the bubble. By knowing the pressure drop (ΔP) and bubble radius (r), the surface tension (γ) of the bubble during static adsorption or dynamic cycling can then be determined using the Laplace equation for a sphere shown in Equation 1.2.

$$\Delta P = \frac{2r}{\gamma} \qquad \text{Eq. 1.2}$$

One of the drawbacks of the commercial PBS instrument is that the PBS does not dynamically determine the bubble size and shape during experimentation. This leads to inaccuracies in the calculated surface tension due to bubble growth or elliptical bubble shape that frequently occur during experimentation [26]. Also, the oscillatory volume changes of the pulsating bubble are slightly different than those assumed by the software of the commercial unit [27]. This leads to errors in both surface area and surface tension measurements. To address this, an image-acquisition system has been combined with the PBS to accurately determine the bubble size and shape, which results in the accurate determination of surface area and surface tension of the bubble [27]. The image-acquisition system is able to dynamically fit an ellipse to the bubble, determining the bubble's shape, size, and surface tension utilizing Equation 1.3:

$$\gamma = \frac{\Delta P}{\frac{1}{R_1} + \frac{1}{R_2}} \qquad \text{Eq. 1.3}$$

where, assuming an ellipsoid, at the side of the bubble the two radii of curvature, R_1 and R_2, are $R_1 = b^2/a$ and $R_2 = a$ and at the apex, $R_1 = R_2 = a^2/b$ (where a is the major radius and b is the minor radius of the bubble.

The PBS instrument can be operated in one of two modes to collect either static or dynamic adsorption data. In the static mode, the bubble is first formed in the surfactant suspension and the surface area is held constant. The surface tension of the static bubble is then monitored over time, allowing for the rate determination of surfactant adsorption to the air-liquid interface. Figure 1.4A shows a typical PBS plot for the adsorption of a commercial surfactant preparation, Infasurf, to the air-liquid interface of a bubble [27]. An essential characteristic of lung surfactant is that it rapidly adsorbs to the air-liquid interface, almost immediately reaching and equilibrium surface tension of approximately 25 mN/m [10].

The second operational mode of the PBS is the dynamic monitoring of surface tension as the bubble area is cycled. This allows for the determination of how surface tension varies with surface area. A typical PBS loop of surface tension vs. bubble area for Infasurf is shown in Figure 1.4B. The important characteristics of natural lung surfactant are that upon compression of the bubble area, the surface tension rapidly drops to near-zero values, preventing the collapse of the alveoli due to the contractile forces of
the alveolar liquid lining and that upon expansion of the bubble area, the surface tension rises to only ~ 35 mN/m [10].

Using a combination of the techniques mentioned here as well as other biophysical technologies a wealth of information has been revealed about the surface-active

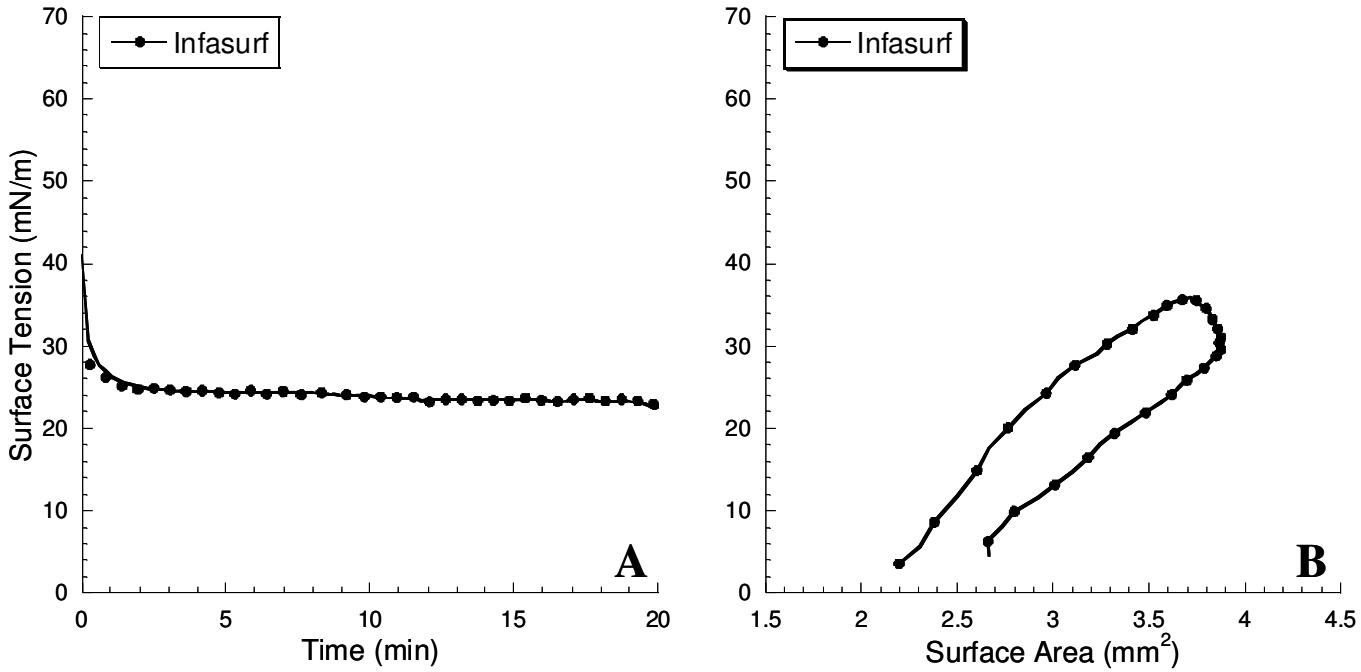

Figure 1.4: Static bubble (A) and dynamic bubble (B) adsorption results from the pulsating bubble surfactometer (PBS) Infasurf. Dynamic data were collected at 20 cycles/min and loop direction is clockwise. Measurements were taken at a bulk surfactant concentration of 1 mg/mL lipids and at 37°C. Data are reproduced from Seurynck et al [27].

properties of lung surfactant. This has also lead to a better understanding of the functional importance of the individual components of lung surfactant including the phospholipids and the surfactant-associated proteins, SP-B and SP-C.

1.4 Surfactant protein C

Both SP-B and SP-C are key functional constituents of LS and are included in exogenous SRTs for the treatment of nRDS [13, 16]. SP-B catalyzes the transport of surfactant to the air-liquid interface and assists in the folding and respreading of surfactant material during the respiration cycle. While many of SP-C's biophysical properties overlap with those of SP-B, SP-C is ubiquitously expressed in all mammals and other non-mammalian species that breathe air via alveolar-like lung structures and lacks sequence homology to any other known protein [16]. These observations suggest that SP-C's role in LS is both unique and necessary in addition to SP-B.

SP-C is synthesized in the distal airspace by the alveolar type II cells and is secreted as a final 35 amino acid surface-active lipopeptide. The mature protein contains a high number of valine, leucine, and isoleucine residues as well as a dipalmitoylation modification near the *N*-terminus (Table 1.1). The abundant hydrophobic residues, along with the palmitoyl motif, make SP-C one of the most hydrophobic proteins known to exist in any biological system [7]. SP-C's unique sequence is highly conserved amongst all species expressing the protein [28].

The three-dimensional structure of SP-C in an apolar solvent has been determined by 2D-NMR and was found to lack any tertiary structure while its secondary structure is dominated by a large α-helical region encompassing residues 9 to 34 [29]. The length of this helical region, 37 Å, matches that of a fluid DPPC bilayer and within this region resides a 23 Å-long, valyl-rich

Table 1.1: Structure of native SP-C and SP-C analogues. The table shows how two classes of SP-C analogues utilize different techniques to mimic the various conserved regions. Colored residues signify the different conserved regions of SP-C: residues in the flexible *N*-terminal region of SP-C are blue, the basic residues are red, and the hydrophobic, helical region is in green.

Compound	Structure
Human SP-C	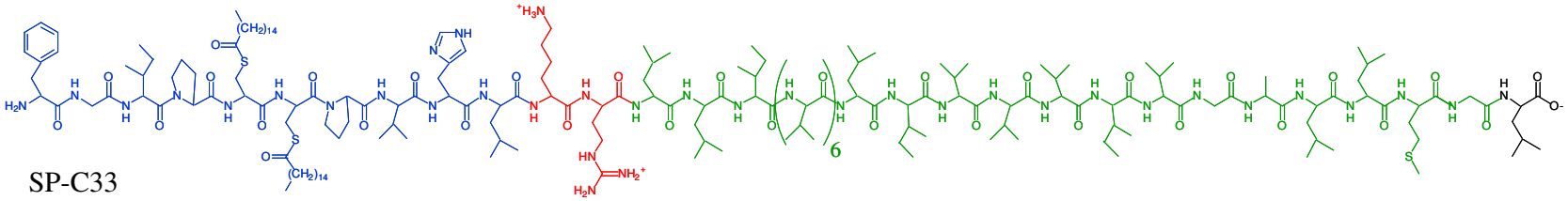
SP-C33	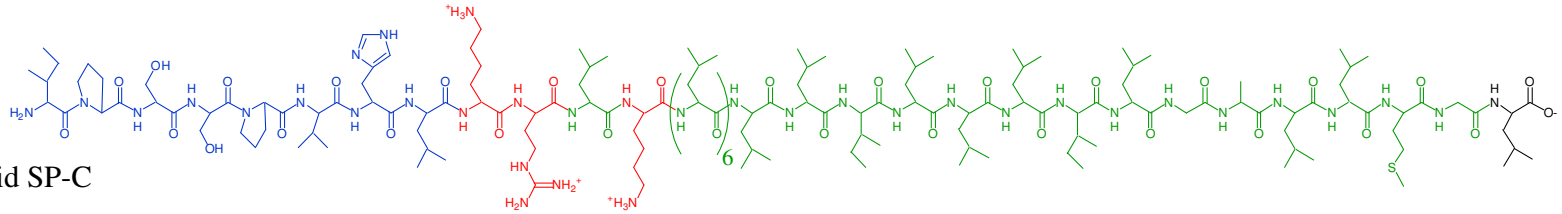
Peptoid SP-C	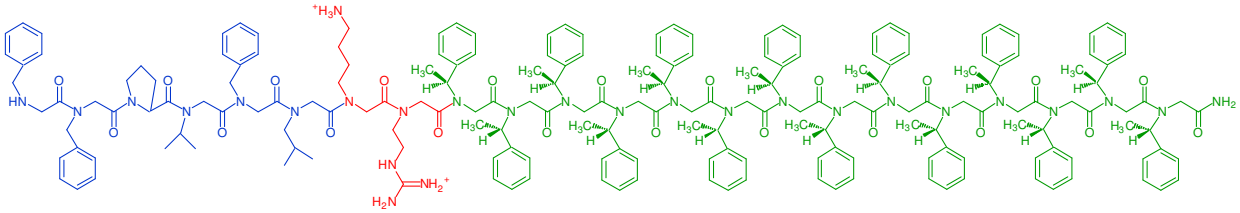

stretch of hydrophobic amino acids that also closely matches the alkyl chain length of a DPPC bilayer. The unstructured *N*-terminal region of the mature peptide was found to assume a flexible disordered orientation in solution, but more recent studies have suggested that this segment adopts an amphipathic conformation in the presence of phospholipid monolayers and membranes [30, 31].

SP-C's unique molecular characteristics make it ideally suited for interacting with LS phospholipids [7]. Strong hydrophobic forces and the lack of charged or bulky side-chains cause SP-C's helical region to associate and interact with the interior of phospholipid acyl chains. In a DPPC monolayer, SP-C orientates at a 70° tilt relative to the interfacial plane and orients nearly parallel with the lipid acyl chains within a bilayer, maximizing interactions between the poly-valyl helix and the acyl chains [32, 33]. The two positively charged residues, lysine and arginine, also promote binding to a phospholipid monolayer or bilayer through ionic interactions between the basic residues and the head groups of the anionic phospholipids [34]. The exact function of the palmitoylated cysteines is not completely known, but they appear also to contribute to SP-C's association with phospholipids, as well as in the possible maintenance of its helical structure [33, 35-37]. A depiction of SP-C's believed disposition in a surfactant film is shown in Figure 1.5.

While only a minor component of LS, ~ 1% (w/w), SP-C has a substantial effect on the surface activity of the LS phospholipids. The addition of SP-C to surfactant phospholipids dispersed in an aqueous subphase accelerates the adsorption and transfer of surfactant phospholipids from the subphase, rapidly forming a surfactant layer at the interface [38]. SP-C

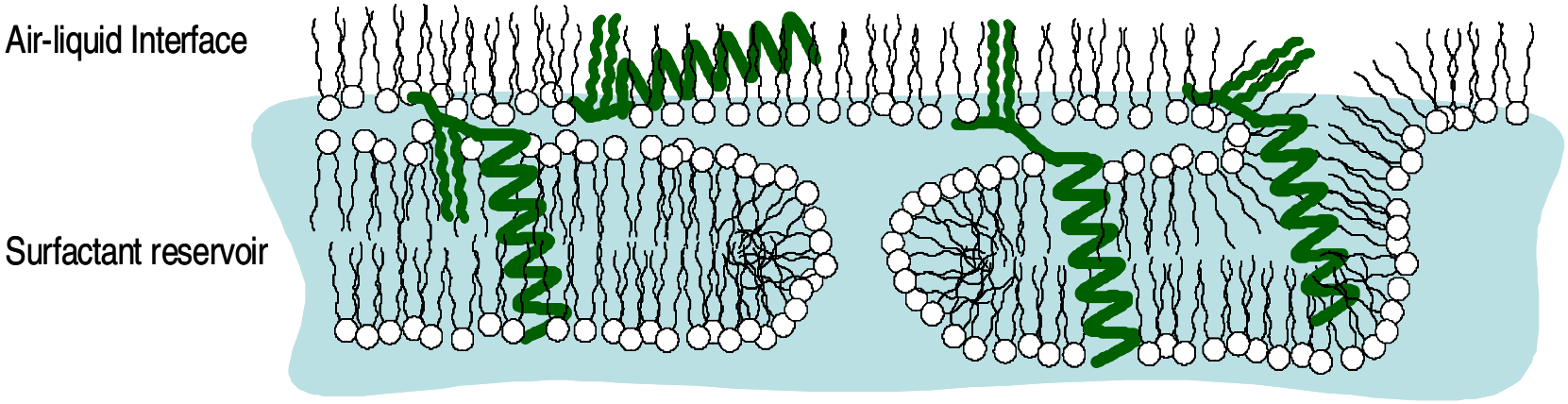

Figure 1.5: Hypothesized SP-C disposition in a LS film at the alveolar air-liquid interface. In a monolayer film, the SP-C helix is oriented nearly parallel to the air-liquid interface, while in a phospholipid bilayer, the SP-C helix aligns nearly parallel with the lipid acyl chains and perpendicular to the interface. The figure also shows how the palmitoyl chains of SP-C may act to anchor either the flexible *N*-terminal region in the same phospholipid film or to an adjacent layer, forming a surface-associated surfactant reservoir.

also promotes further binding of dispersed lipid vesicles to the newly formed surfactant layer, creating a surface-associated surfactant reservoir [37].

Once at the air-liquid interface, SP-C acts as a molecular lever and hydrophobic lipid anchor during respiration [32]. Upon exhalation, the LS film is compressed causing a reduction of surface tension. This compression leads to the exclusion of some material from the interface, resulting in the formation of bilayer and multilayered structures of surfactant that remain associated with the interface [20]. This multilayer formation is significantly enhanced by the presence of the hydrophobic SP-C protein [20]. Figure 1 depicts how SP-C may facilitate the formation of three dimensional surfactant structures. As the film is compressed, SP-C's helical region reorients, aligning its helix with the lipid acyl chains [39]. At the same time, a number of lipid molecules are also drawn out of the monolayer surface and inverted to form a retained local bilayer structure [40]. SP-C's helix as well as the palmitoylated cysteines are thought to assist in surfactant retainment, whereby the palmitoyl groups remain associated with the compressed surface film while the helix is anchored with the excluded phospholipids [40, 41]. This surfactant reservoir could then readily be inserted upon expansion or inhalation. The SP-C-specific catalyzed multilayered structures are also believed to be responsible for SP-C's regulation of surfactant viscosity, which prevents surfactant outflow from the alveoli to the upper airways at very low surface tensions [42].

Despite SP-C's many important biophysical properties, working with and studying the native protein is quite difficult as SP-C's poly-valyl helix is discordant, i.e. it is composed of amino acids with a high propensity to form β-strands [4]. The SP-C helix is consequently metastable in solution and can spontaneously convert into β-sheet aggregates and amyloid fibrils

that have inferior surface activity compared to the correctly folded, helical protein [43-45]. The instabilities of SP-C pose serious challenges either in isolating the native protein or the creation of synthetic analogues that retain the SP-C's requisite α-helical structure and corresponding surface activity. As a result, researchers have employed a variety of unique strategies to overcome these problems by producing and mimicking SP-C in heterologous systems, synthetic peptide synthesis, and non-natural peptidomimetic materials.

1.5 Synthetic SP-C analogues

The high degree of SP-C sequence conservation and uniqueness suggests the main molecular and structural features of SP-C must be preserved to retain the full repertoire of SP-C-related functionality [28]. These features include SP-C's extreme hydrophobicity, its helical secondary structure, the flexible *N*-terminal region, and the two basic, charged residues. The palmitoylation motif has also been shown to have significant *in vitro* functionality; however, the *in vivo* importance of this motif has yet to be definitively proven [30, 31, 41]. In addition, the resulting analogues must resist misfolding and degradation over time and be amenable to efficient, larger-scale production.

1.5.1 Recombinant SP-C analogues

The expression of SP-C in heterologous systems allows for more efficient, large-scale production of the troublesome protein than isolation of the native protein with the ability to introduce designed sequence variations, improving handling and efficacy [46-48]. A form of recombinant SP-C (rSP-C) is currently used in Venticute [49]. This rSP-C analogue from Nycomed shares a nearly identical sequence with human SP-C except that the palmitoylated cysteines are absent and have been replaced with phenylalanines to eliminate protein

oligomerization [48]. The phenylalanine substitution makes this protein analogue similar to canine SP-C, which contains one phenylalanine at position 6 and preserves, to some extent, the hydrophobicity of the palmitoyl groups. The addition of palmitoyl chains in a similar analogue did not enhance *in vivo* efficacy of the rSP-C-based formulation [46].

rSP-C has shown good efficacy, improving lung function in premature animal models of RDS [48]. In clinical trials for the treatment of ARDS resulting from both indirect and direct lung injury, Venticute has shown a positive effect on gas exchange, but, ultimately, did not have a beneficial effect on long-term survival [49]. However, a post-hoc analysis suggested that Venticute may have survival benefits in patients with direct lung injury. As a result, Venticute is currently being used in a Phase III clinical trial for the reduction of mortality in adult patients with RDS resulting only from severe acute pneumonia or aspiration of gastric contents (NCT00074906). The forthcoming results of this study are highly anticipated by clinicians and researchers of the LS community.

1.5.2 Synthetic SP-C peptide analogues

SP-C's lack of a tertiary structure and relatively simple secondary structure make it feasible to mimic the native protein by synthetic peptides. This is especially enticing given the difficulties associated with isolation, purification, and storage of the native protein from natural or recombinant sources. Utilizing structural and biophysical information gained from the native protein, synthetic SP-C analogues have been created to mimic the key lipid-interaction domains [5, 10, 50, 51]. These synthetically engineered peptides not only address some of the inherent difficulties associated with SP-C, but also facilitate the production of sufficient quantities for use in a synthetic SRT. In fact, many of these polypeptide biomimetics have been found to have comparable *in vitro* activity as the native protein as well as favorable *in vivo* performance in

animal models. However, the metastability of the helical region still remains a challenging problem in sequences that retain the poly-valyl helix.

To address the metastability of the poly-valyl helix, a novel series of valine-to-leucine substituted SP-C analogues have been created [50, 52, 53]. One of the first was SP-C(Leu), which is a non-acylated SP-C variant based upon the sequence of human SP-C, but replaces the valine residues in the α-helical region with leucine residues and the palmitoylated cysteines with serines [50]. The substitution of the β-sheet-promoting valine residues with the α-helix promoting leucines of SP-C(Leu) results in an analogue that spontaneously forms an α-helical structure in solution, even after acid treatment, which can be produced efficiently on a large scale. When combined with a phospholipid formulation, SP-C(Leu) adopted a transbilayer orientation and showed favorable *in vitro* surfactant spreading properties, similar to the native protein, reducing both minimum and maximum surface tensions during dynamic cycling. However, in an animal model of nRDS, the biomimetic formulation offered only a modest improvement in lung function [50]. This was due to unwanted oligomerization of the poly-leucine helix at high concentrations, caused by leucine zipper-like association.

To circumvent this problem, SP-C(LKS) was created in which three evenly spaced leucine residues in the helical region were replaced with lysine residues [53]. The location of the positive charges around the helical circumference prevented self-association and when combined with phospholipids, exhibited rapid adsorption and favorable modulation of surface tension during dynamic cycling [53]. However, SP-C(LKS) was unable to produce sufficient improvement of lung function *in vivo*. The reason for the poor *in vivo* performance is not well understood, but the introduction of the positively charged lysine residues in the nonpolar, helix

may either disrupt the region's hydrophobic interaction with the lipids or the SP-C dipole moment [52].

The latest generation of the leucine-based synthetic peptide analogues, SP-C33, utilizes specific design features from both SP-C(Leu) and SP-C(LKS) to overcome the solubility and aggregation problems of SP-C(Leu) with improved *in vivo* performance relative to SP-C(LKS) [52]. SP-C33 is similar to the other valine to leucine-substituted analogues, but contains an *N*-terminal region that is truncated by two residues to increase synthesis efficancy and, most notably, replaces Leu 14 with lysine to prevent peptide oligomerization while not disrupting the hydrophobicity of the aliphatic helix. This analogue was found to prevent oligomerization and improve the dynamic surface activity of a lipid formulation [52]. When used to treat premature newborn animals, a SP-C33 containing formulation was as effective in increasing inspiration volumes as a modified natural surfactant preparation that contained both SP-B and SP-C [54]. Surprisingly, despite the demonstrated *in vitro* importance of the SP-C palmitoyl groups, an acylated SP-C33 analogue did not enhance the *in vivo* performance [52]. Airway openness at end expiration was lower in animals treated with SP-C33 than those treated with a natural SRT, suggesting that other components, such as SP-B, are necessary to maintain alveolar stability [13]. Despite this difference, the synthetic peptide is as effective as native SP-C in improving surface properties of lipids *in vitro* and *in vivo* and represents a successful engineering approach to overcome the numerous difficulties associated with the native protein.

1.5.3 Peptoid analogues

In an alternative approach to creating recombinant or synthetic peptide analogues, recent work has been aimed at the development of a new category of synthetic surfactant protein mimics utilizing poly-*N*-substituted glycines or "peptoids" [3]. Peptoids have close structural

similarity to peptides, but have their side chains appended to the amide nitrogens rather than to the α-carbons. This feature renders peptoids essentially invulnerable to protease degradation, making them more biostable than peptides and reducing specific recognition by the immune system [55]. So far, studies have shown peptoids to induce only very low-level antibody response and, certain sequences, have been found to be bioactive, nontoxic, and nonimmunogenic [56, 57]. Despite the achirality of the *N*-substituted glycine backbone and its lack of hydrogen bond donors, peptoids are able to adopt extraordinarily stable, chiral helices. When substituted with α-chiral, sterically bulky side chains, steric and, in some instances, electronic repulsion between adjacent residues cause peptoids to adopt a secondary structure similar to a polyproline type I helix with ~ 3 residues per turn and a pitch of ~ 6 Å [58, 59]. These helical structures are extremely stable and do not appreciably denature over time as their formation does not depend on hydrogen bonding along the backbone [60]. Peptoids also have the added advantage of being relatively easy and cost-effective to synthesize compared to peptides [3]. Utilizing a solid-phase, submonomer synthesis approach (Figure 1.6), peptoids up to 50 residues in length can be synthesized in high yield, with coupling efficiencies comparable to those of Fmoc peptide synthesis (> 98.5%). Efficient synthesis and the ability to form stable, helical structures make peptoids an excellent platform for mimicry of bioactive molecules that rely on helical structure for proper function, such as the hydrophobic protein, SP-C.

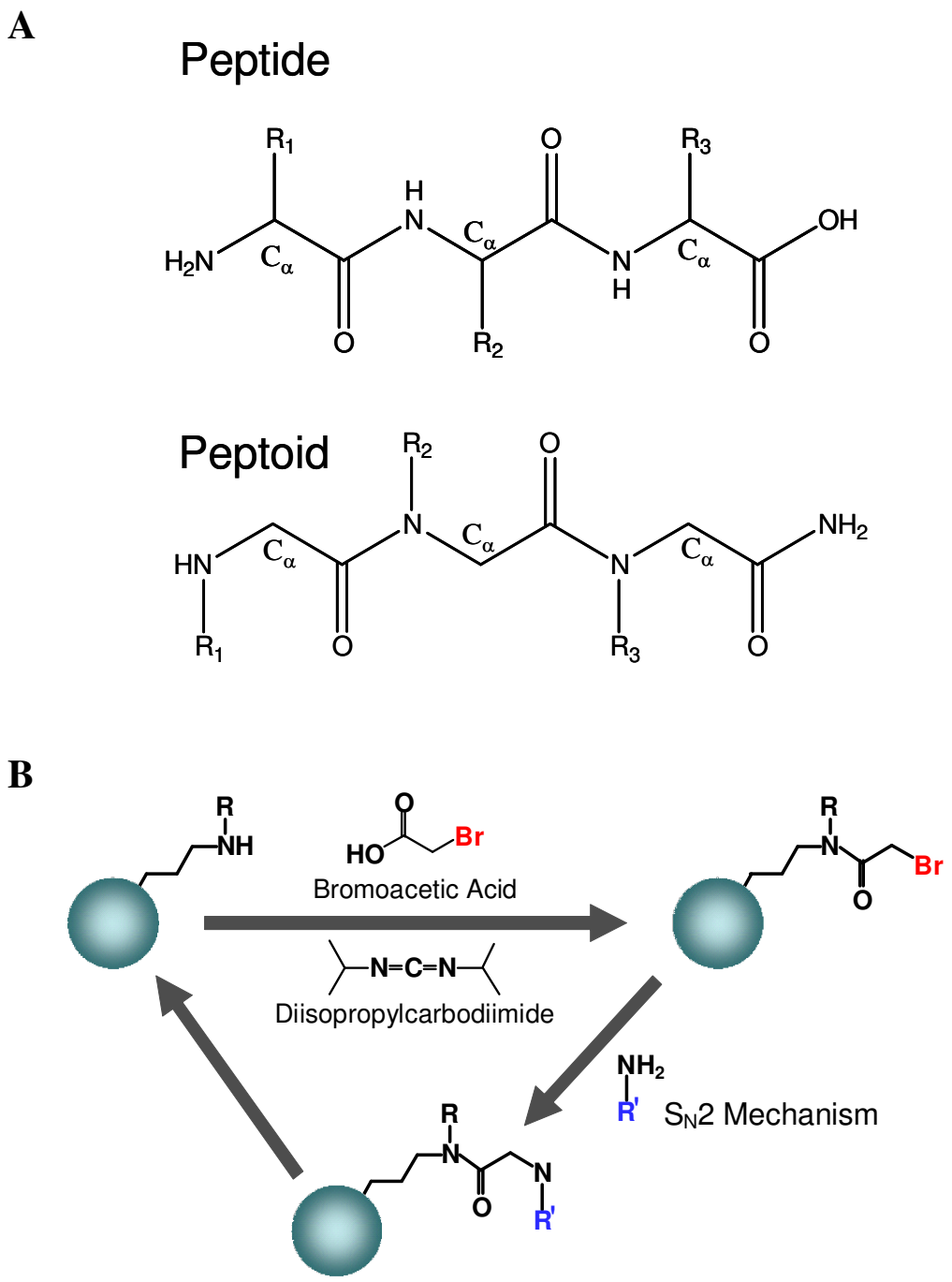

Figure 1.6: (A) Peptide and peptoid structures and (B) submonomer synthesis scheme for peptoid oligomers.

Utilizing design strategies similar to those that were used in the design of recombinant and synthetic peptide analogues of SP-C, a variety of non-acylated, sequence-specific peptoid analogues of SP-C(5-32) have been developed [61, 62]. The sequences of the biomimetic analogues were designed to emulate the key structural features of the native protein, with a hydrophobic, α-chiral, helical region, mimicking SP-C's helix, and an *N*-terminal amphipathic, achiral region containing side chains that are largely analogous to those present in human SP-C. To gain a greater understanding of the structural requirements in peptoid-based analogues of SP-C, systematic alterations were introduced in the sequences [61]. Two main classes of mimics were created, containing either α-chiral, aromatic- or α-chiral, aliphatic-based helices, which contained 8, 11, and 14 residues to determine both the side chain preference and the optimal helix length for a peptoid-based mimic of SP-C. Circular dichroism spectroscopy showed that the analogues were predominantly helical in solution with the longer mimics having the highest helical propensity. In addition to being highly helical, the analogues were stable and not prone to misfolding in solution over time.

When combined with a synthetic phospholipid formulation, the peptoid-based SP-C mimics all showed improved *in vitro* surface activity over the lipid system alone; however, the mimics containing the more rigid, aromatic helix yielded superior surface activity in comparison to the more biomimetic, aliphatic-based mimics. The optimal surface activity of the SP-C mimics was also dependent on the presence of a helical region of 14 peptoid monomers in length (~ 28 Å), which is similar in length to the poly-valyl region of native SP-C (26 Å). In a lipid film, the aromatic-based mimic altered the surface pressure-area isotherms (obtained on a Langmuir-Wilhelmy surface balance) in a manner similar to a synthetic SP-C peptide. Film

morphology studies revealed that the presence of the aromatic-based mimic, but not the aliphatic-based mimic, resulted in the nucleation of bright vesicle domains, likely three-dimensional structural changes in the film, at higher surface pressures, similar to SP-C. In a pulsating bubble surfactometer, the aromatic-based mimic also accelerated surfactant adsorption to the air-liquid interface as well as greatly reduced the minimum and maximum surface tensions, all of which properties were similar to the SP-C peptide.

These results were somewhat surprising, as the native protein contains only aliphatic side chains in the helical region; however, it is believed that the aromatic monomers more effectively constrain the peptoid backbone into the polyproline type I-like helical conformation because it exhibits both steric repulsions between bulky side chains and electronic repulsions between aromatic π and carbonyl lone-pair electrons [58]. This indicates that it is more important to capture the extreme hydrophobicity and highly helical structure of SP-C rather than its exact side chain chemistry, which is consistent with previous studies of peptide analogues [63].

Taken together, peptoid-based mimics of SP-C seem very promising, since they exhibit *in vitro* biophysical activities highly similar to that of the SP-C peptide. It was also found that the same design considerations occurring in SP-C peptide variants are applicable in the development of peptoid-based mimics of SP-C. Therefore, the results observed seem to provide a basis for the development of a peptoid-based biomimetic, SRT for the treatment of RDS or other medical applications, and this work is ongoing.

1.6 Future implications

While current SRT formulations are highly efficacious in the treatment of nRDS, there are still drawbacks associated with their use, which has prompted researchers to devise synthetic

sources of the surface-active material, specifically creating mimics of the hydrophobic surfactant proteins, SP-B and SP-C. The importance of SP-C as a functional constituent of a biomimetic SRT is evidenced not only by its inclusion in natural exogenous surfactant formulations, but also by its ubiquitous expression in mammalian airwaysand its uniqueness, lacking any known sequence homologues. However, isolation and storage of either the native SP-C protein or sequence-identical analogues is extraordinarily difficult due to its extreme hydrophobicity and metastable secondary structure. As a result, researchers have drawn inspiration from Nature in redesigning the naturally selected protein to overcome these difficulties. Utilizing detailed structural information and biophysical insight about native SP-C, coupled with protein folding preferences, investigators have created a number of novel peptide and peptoid-based analogues that mimic SP-C's key molecular and structural motifs, but because of their side chain chemistry and/or their unique backbone structure, reduce or eliminate many of the difficulties associated with the native protein and sequence identical analogues. Utilizing synthetic approaches, it is also conceivable that future SP-C analogues may contain other non-natural, sequence modifications that further improve stability and activity in comparison to the native and recombinant species. Further improvements in biomimetic SRT efficacy will also likely involve the inclusion of a SP-B mimetic as both constituents play a critical role in surfactant homeostasis. With improved stability, greater production potential, and elimination of possible pathogenic contamination, not only do biomimetic SRTs offer the potential to improve the treatment of nRDS, but they may also see wider application in the treatment of other, more prevalent, respiratory-related disorders where greater quantities of the surface-active material are required, such as in the treatment of acute RDS.

1.7 Presentation and summary of the work presented

The aim of the presented work focuses on the development of a peptoid-based analogue of SP-C to address the clinical need for a biomimetic SRT that's as efficacious as the animal-derived material for the treatment of neonatal RDS and, possibly, acute RDS. The work detailed in Chapters 4, 5, 6, and 7 focuses on detailed structure-function studies, in which specific modifications have been engineered into a peptoid scaffold to determine molecular and structural requirements for the biomimicry of SP-C. These studies reveal key features that are required for the retainment of SP-C's biophysical activity in a phospholipid environment. These findings are not only applicable to the development of a non-natural analogue of SP-C, but are also applicable to other platforms mimicking SP-C, such as synthetic peptides or recombinant proteins.

The information detailed in Chapter 2 details the process of obtaining either natural or synthetic lung surfactant components that are used as comparators for these studies. Specifically, the isolation and purification of animal-derived lung surfactant material is detailed along with a successful strategy for the synthesis of a non-acylated and a uniquely acylated SP-C peptide mimic. The surface activities of the natural and synthetic materials are also characterized and are useful comparators in the development of a fully functional, synthetic SRT.

The composition of natural surfactant is quite complex and varies greatly not only from species-to-species, but also amongst individuals of the same species [8]. Due to the complexity and compositional variance, it is difficult to determine which components are necessary to fully capture lung surfactant's dynamic biophysical activity. To address this, Chapter 3 focuses on the effect of synthetic lipid composition on a peptoid and peptide analogue of SP-C. Here, it is found that a relatively simple lipid formulation, DPPC:POPG:PA (68:22:9) or Tanaka lipids,

captures many of natural lung surfactant's surface activity with combined with the synthetic analogues.

Finally, Chapter 8 presents the major conclusions of this research and its relevance to lung surfactant and peptidomimetic research. Also presented are future recommendations for this project.

Chapter 2: Lung surfactant comparators: synthesis, isolation, and characterization

Animal-derived, exogenous surfactant preparations are routinely used to treat respiratory distress syndrome (RDS) in premature infants and have significantly reduced the morbidity and mortality associated with lung immaturity. Despite the clinical effectiveness of the animal-derived material, there still exist some concerns associated with the use of the exogenous material including cost, availability, and possible safety concerns. Because of this, research has focused on the development of a synthetic lung surfactant formulation that eliminates these concerns while retaining the functionality of the natural material. This endeavor requires a detailed understanding of the biophysical activities of the natural material as well as that of the individual molecular components, including the hydrophobic surfactant proteins, SP-B and SP-C, which are critical constituents of lung surfactant. This chapter details the isolation and characterization of native lung surfactant from excised lungs as well as the successful synthesis and characterization of an acylated and non-acylated peptide mimic of SP-C. The synthesis of the peptide mimics is notable, in that, specific alterations in the coupling and deprotection protocols were made to prevent on-resin aggregation and to improve the Fmoc deprotection efficacy. These modifications lead to an improvement in yield of this extraordinarily "difficult sequence." The acylated SP-C peptide also utilizes a unique method for the on-resin alkylation of the peptide that is both selective and stable, being efficiently incorporated during solid phase synthesis. The acquisition and *in vitro* characterization of native lung surfactant material as well as a peptide analogue of SP-C is needed in the development and assessment of biomimetic

surfactant replacement therapies (SRTs), ensuring that the biomimetic SRTs fully capture the critical biophysical activities of lung surfactant and associated species.

2.1 Introduction

Lung surfactant is a complex mixture of lipids and proteins found at the air-liquid interface within the lungs and is required for proper respiration. This highly specialized biomaterial functions to reduce and regulate surface tension within the alveoli during respiration, greatly diminishing the work of breathing and preventing alveolar collapse. Lung surfactant is composed of approximately 90% lipids and 10% proteins [9, 64]. No single constituent of lung surfactant is solely responsible for its unique dynamic surface behavior. Phospholipids comprise the bulk, ~ 80%, of lung surfactant's mass and are the chief surface-active component. Dipalmitoyl phosphatidylcholine (DPPC), the main lipid component of lung surfactant, along with other saturated phospholipids enable lung surfactant to reach very low minimum surface tensions upon dynamic compression. However, the molecular characteristics that allow DPPC and other saturated lipids to reach very low surface tensions, prevent them from rapidly readsorbing and respreading upon expansion [9]. The inclusion of fluid, unsaturated phospholipids provides better respreadability and slightly improved surfactant adsorption to the air-liquid interface, but results in an increase in minimum surface tension [9]. While the hydrophobic proteins of lung surfactant, SP-B and SP-C, represent only a small portion of lung surfactant, they are an essential component and are necessary for the proper biophysical function of lung surfactant. SP-B and SP-C greatly enhance surfactant adsorption, stability, and recycling of phospholipid films [65-67]. In fact, the presence of these surfactant-specific proteins is

required for proper respiration as their absence in either genetically manipulated animal models or in individuals with inherited genetic deficiencies leads to lethal respiratory failure [68-71].

A clinically relevant condition that arises from a developmentally regulated deficiency of functional lung surfactant in the immature airways of premature infants is neonatal RDS (nRDS). The deficiency of functional lung surfactant in premature infants is due to a lack of mature alveolar type II cells in the epithelial lining of the lungs and is a leading cause of infant mortality [7]. Without sufficient surface-active material in the airways, lung compliance is reduced and respiration is greatly impaired, ultimately resulting in alveolar collapse and suffocation without treatment. Today, infants at risk for nRDS are routinely treated with exogenous surfactant material that functions in place of the native material until the afflicted individual is able to produce functional surfactant [72]. The adoption of SRT to treat nRDS was a significant factor in the dramatic decline in infant mortality rates observed during the 1980s [72]. Current SRT formulations are animal-derived surfactants, consisting of the entire hydrophobic portion of lung surfactant including most of the phospholipid species as well as the hydrophobic proteins, SP-B and SP-C [8].

Despite the efficacy of animal-derived SRTs, there are some drawbacks associated with their use [11]. Because the natural surfactants are extracted from animal lungs, there is a possibility of cross-species transfer of antigenic or infectious agents as well as high costs, limited production potential, and batch-to-batch variability [8, 73-76]. Therefore, there has been increasing interest in the development of a new category of SRTs: biomimetic SRTs that utilize an entirely synthetic surfactant containing an accurate mimic of the hydrophobic protein portion

of lung surfactant that functions as well as the natural material while eliminating the concerns associated with animal-derived surfactants [11, 15]. The developments of lucinactant (Surfaxin), Venticute, and SP-C33 have shown promise as efficacious biomimetic SRTs; however, these novel surfactants are not yet clinically available [48, 52, 77]. Therefore, there still remains a tremendous opportunity for innovation in the development of lung surfactant replacements that are increasingly efficacious, cost-effective, and provide a long therapeutic window for the treatment of lung disorders. Also, with an increased production potential, biomimetic SRTs have the potential for use in the treatment of other respiratory-related disorders in adults where significantly more material would be required [49, 78, 79].

In order to develop a biomimetic SRT for the treatment of respiratory-related disorders, a detailed understanding of the biophysical properties of natural lung surfactant and the surfactant-specific molecular components is necessary. It is well known that lung surfactant fulfills three main activities in the airways: 1) rapid adsorption to the alveolar air-liquid interface, forming an interfacial surfactant layer; 2) regulating surface tension as a function of surface area to stabilize the alveoli and respiratory bronchioles against collapse and reducing surface tension to very low values upon compression during expiration, maintaining alveolar patency; and 3) efficiently respreading upon expansion during inhalation, re-establishing the surfactant film for the next respiration cycle; however, it is necessary to quantify the extent of these activities *in vitro* to efficiently evaluate and optimize the surface-active properties of a synthetic surfactant formulation in relation to the native materials [10].

Here, the isolation and extraction of native lung surfactant from excised lungs is detailed as well as a modified method for the synthetic synthesis of the hydrophobic surfactant protein,

SP-C. First, natural lung surfactant was isolated from whole, excised lungs and processed to obtain the functional hydrophobic surfactant portion by organic extraction. The *in vitro* surface activity of the sheep lung surfactant extract (SLSE) was then characterized using a modified pulsating bubble surfactometer (PBS) to assess the material's unique surface-active properties. To assess the surface-active properties of a SP-C peptide, a modified methodology is reported for the solid phase synthesis of a non-acylated SP-C peptide analogue. The synthesis modifications overcome some of the difficulties associated with the synthesis of this "difficult" protein. An acylated version was also synthesized that utilizes a peptoid submonomer protocol to incorporate two alkyl chain motifs in the *N*-terminal region, mimicking the native SP-C palmitoyl chains. These amide-link modifications have several advantages over the other techniques used to incorporate thioester-linked palmitoyl chains in proteins including: on-resin incorporation, selectivity, and stability. The secondary structure and *in vitro* surface activity of these peptide mimics were also characterized by circular dichroism (CD) spectroscopy and PBS, respectively.

2.2 Materials and methods

2.2.1 Materials

Peptide synthesis reagents were purchased from Applied Biosystems (Foster City, CA) and Sigma-Aldrich (Milwaukee, WI). Fmoc-protected amino acids, resins, and di-tert-butyl dicarbonate were purchased from NovaBiochem (San Diego, CA). All organic solvents used for sample synthesis, purification, and preparation were HPLC-grade or better. The organic solvents and reagents for the phospholipid assay were purchased from Fisher Scientific (Pittsburgh, PA). The synthetic phospholipids DPPC and palmitoyloleoyl phosphatidylglycerol (POPG) were

purchased from Avanti Polar Lipids (Alabaster, AL) and were used as received. Palmitic acid (PA) was purchased from Sigma-Aldrich in the highest purity available.

2.2.2 Natural surfactant isolation

Native lung surfactant (SLSE) was obtained from freshly slaughtered ovine lungs (Chiappetti Lamb and Veal, Chicago, IL) following procedures previously reported and depicted in Figure 2.1 [80-82]. Briefly, excised lungs with trachea and bronchi intact were lavaged with ~ 2 liters of cold (4°C) 0.15 M NaCl under 25 cm H_2O of pressure within 1 hour of tissue procurement. After instillation of the saline solution, the filled lungs were elevated and the return collected by passive drainage. Collected lavage material showing any signs of contamination with blood was discarded. Blood-free lavage fluid was then pooled and centrifuged at 150 x g at 4°C for 10 minutes to remove any cellular debris. The supernatant containing the surfactant material was retained and pooled again. The crude surfactant was then harvested by medium-speed centrifugation at 20,000 x g at 4°C for 45 minutes. The pelleted surfactant was resuspended in 0.15 M NaCl and dispersed by injection through a syringe fitted with a 22-gauge needle. The resuspended material was then layered over 0.8 M sucrose in 0.15 M NaCl and centrifuged at 30,000 x g at 4°C for 45 minutes using a swinging bucket rotor. Pellicles at the interface were aspirated, pooled, and resuspended in 0.15 M NaCl as before. The collected material was then ultracentrifuged at 60,000 x g at 4°C for 30 minutes to wash and concentrate the whole surfactant. The supernatant from this step was discarded and the pelleted material was resuspended in a small amount of 0.15 M NaCl.

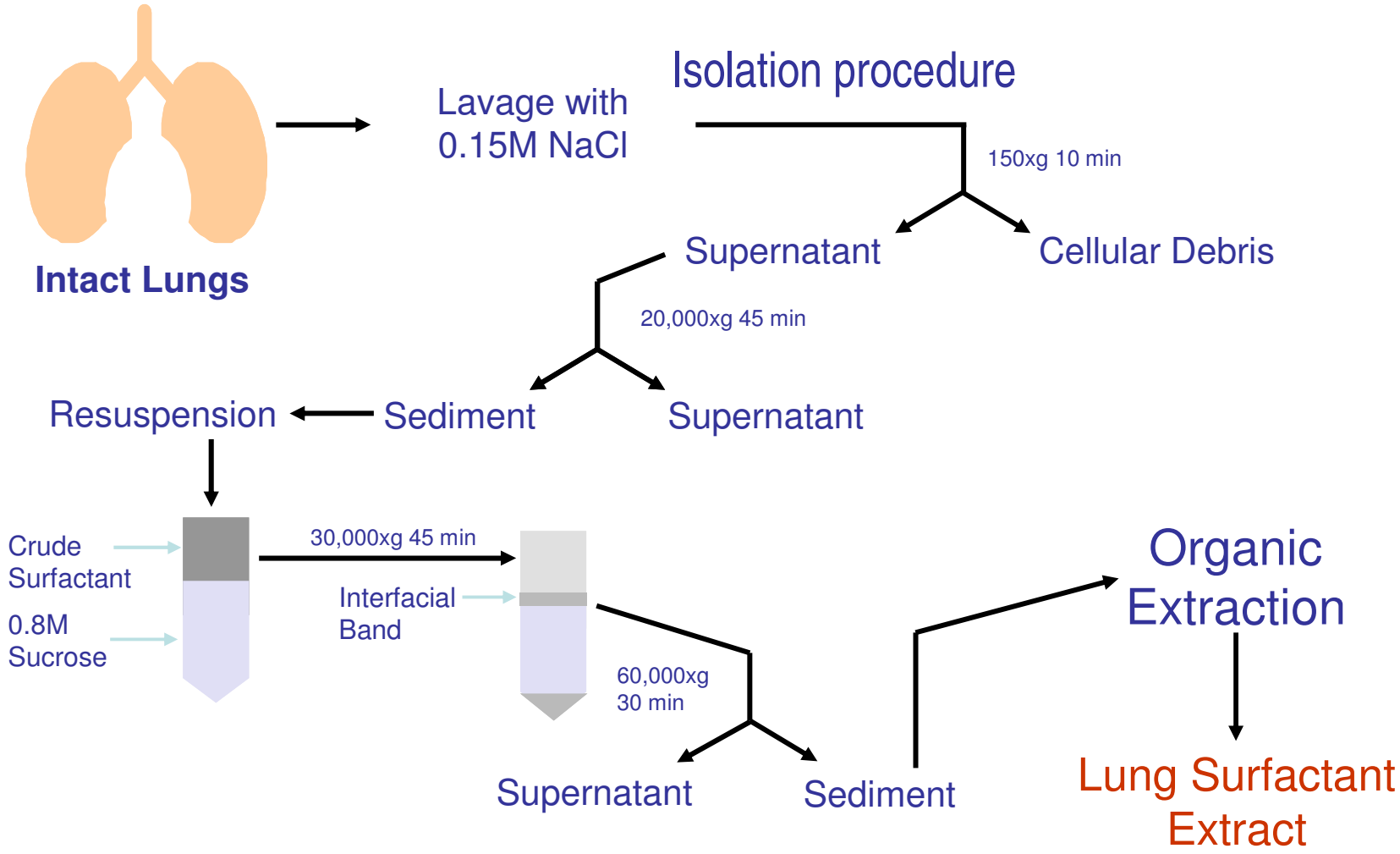

Figure 2.1: Isolation and extraction procedure for the hydrophobic constituents of natural lung surfactant. Procedure adapted from [80-83].

2.2.3 Natural surfactant extraction

The surfactant lipids and the hydrophobic proteins were extracted from the isolated whole surfactant by the method of Bligh and Dyer [83]. Briefly, for each 1 mL of suspended surfactant, 3.75 mL of 1:2 (v/v) chloroform:methanol was slowly added under constant agitation. This slurry was then vortexed for 1 minute. 1.25 mL chloroform was then added and the solution vortexed for 30 seconds. Finally, 1.25 mL water was added and the slurry vortexed for an additional 30 seconds. The mixture was then left undisturbed for ~ 1 minute, allowing the organic and aqueous phases to separate. Approximately 90% of the bottom organic phase containing the phospholipids and hydrophobic proteins was then recovered with a Pasteur pipette. The recovered organic material was then filtered through a Whattman No. 2 filter to remove any undissolved material. The filtrate solvent was then removed by drying with a stream of nitrogen. The dried surfactant material was then placed under high vacuum for at least 1 hour to remove any remaining solvent.

The fully dried material was then reconstituted by adding a small amount of aqueous buffer (0.15 M NaCl, 5 mM $CaCl_2$, and 10 mM HEPES at pH 6.90) and aspirated through a 22-gauge needle. The lipid concentration of the purified SLSE material was then quantified using the method of Stewart while the protein content was determined using a BCA protein assay kit (Thermo Fisher Scientific, Rockford, IL) [84].

2.2.4 Peptide Synthesis

A non-palmitoylated SP-C peptide mimic was designed with a sequence modified to prevent aggregation and preserve the hydrophobicity of the *N*-terminal region. This peptide mimic, SP-$C_{F,F}$, includes valine-to-leucine, cysteine-to-phenylalanine, and methonine-to-isoleucine

substitutions to prevent misfolding, oligomerization, and partial oxidation, respectively (sequence shown in Table 2.1) [48, 50]. Two methods were utilized for the synthesis of the non-palmitoylated SP-C peptide. The first synthesis method utilized standard Fmoc chemistry on a solid support while the second method used a modified methodology designed to better address the difficulties associated with this "difficult" protein. An acylated SP-C peptide analogue was also created using the modified synthetic strategy.

2.2.4.1 Standard Fmoc solid phase peptide synthesis

Solid phase synthesis of the SP-$C_{F,F}$ peptide was carried out on a 0.25 mmol scale on an Applied Biosystems 433A automated peptide synthesizer, using standard Fmoc chemistry, and a prederivatized Wang-Leu resin (0.64 mmol/g substitution). Briefly, the presubstituted solid phase resin was swollen by washing with dichloromethane (DCM) and *N*-methylpyrrolidine (NMP). After the initial resin swelling step, the amine-protecting Fmoc group was removed with the addition of 20% piperidine in NMP for 12 minutes with periodic vortexing. The deprotection step was repeated a minimum of three times until conductivity peak heights did not change, indicating no additional Fmoc-piperidine adduct was being produced. Next, 4 molar equivalents of the amino acid residue was then activated by adding an equivalent amount of 2-(1H-benzotriazol-1-yl)-1,1,3,3-tetramethyluronium hexafluorophosphate (HBTU), *N*-hydroxybenzotriazole (HOBt), and diisopropylethylamine (DIEA) dissolved in NMP. The OBt ester-activated residue was then immediately added to the solid phase resin for coupling to the growing peptide chain. The coupling step was carried out for approximately 1.5 hours with periodic vortexing. The amino acid coupling step was repeated twice for each residue to increase coupling efficiency. After coupling, the resin was washed repeatedly with NMP and any

Table 2.1: Structures of native SP-C and SP-C peptide analogues.

Compound	Structure
Human SP-C	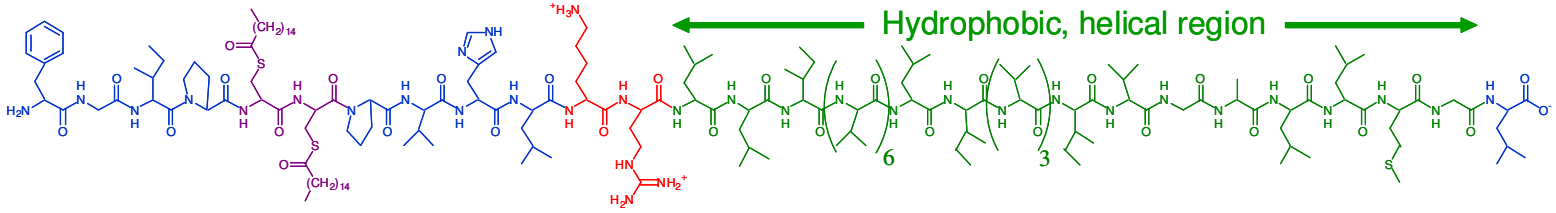
SP-$C_{F,F}$	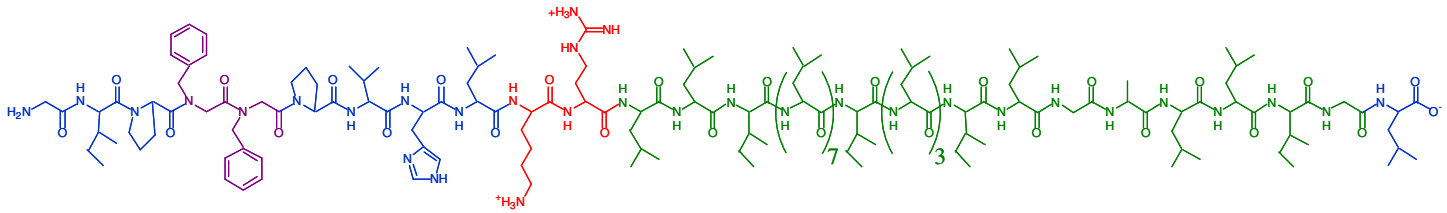
di-pSP-$C_{F,F}$	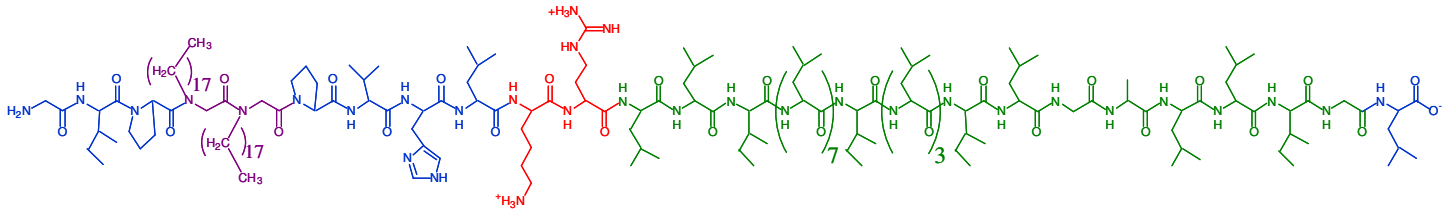

unreacted polypeptide chains were capped with an acetic anhydride solution. The deprotection and coupling steps were repeated until the desired polypeptide was created.

2.2.4.2 Modified Fmoc solid phase synthesis

To increase the efficiency of the SP-$C_{F,F}$ peptide synthesis, several modifications to the standard Fmoc synthesis procedure were made. The standard presubstituted Wang-Leu resin was replaced with a lower loading Wang-Leu resin (0.24 mmol/g substitution). The NMP solvent typically used during the coupling step was replaced with dimethyl sulfoxide (DMSO). For the Fmoc removal step, a solution of 2% 1,8-diazabicyclo-[5.4.0]undec-7-ene (DBU) and 2% piperidine dissolved in *N,N*-dimethylformamide (DMF) was used as an alternative to the 20% piperidine in NMP [85].

An acylated peptide mimic of SP-C was also synthesized using this peptide synthesis strategy. Two peptoid residues were introduced at positions 4 and 5 following the submonomer protocol developed by Zuckermann et al [86]. For this, the deprotected amine of the peptide chain was first acylated with bromoacetic acid. The side chain, *N*-octadecylamine (*N*ocd), was then introduced as a primary amine, which undergoes incorporates via nucleophilic displacement of the bound halogen. The procedure was repeated for the second *N*ocd residue and then the peptide synthesis protocol was resumed for the remaining three residues. The mass of the synthesized peptides was confirmed to be correct by electrospray ionization.

2.2.5 Peptide Purification

After completion of the peptide syntheses, the resin-bound oligomers were simultaneously cleaved from the resin and deprotected with 90% trifluoroacetic acid (TFA) along with necessary scavengers for 2 hours. The cleaved material was then immediately diluted

with isopropanol and water, frozen, and lyophilized to yield the crude peptide. The crude products were then purified by reverse-phase HPLC on a Waters system with either a C4 or C18 column utilizing a linear gradient of 60-100% B in solvent A (solvent A = 0.1% TFA in water and solvent B = 0.1% TFA in isopropanol).

2.2.6 Circular dichroism

CD measurements were performed on a Jasco model 715 spectropolarimeter (Easton, MD). Stock solutions for dilution to appropriate concentrations for CD were made immediately before analysis in tared vials by precise weighing of added solvent and at least 2 mg of lyophilized peptoid powder, to produce a sample of accurately known concentration. The peptide samples were prepared in methanol or, when liposomes were used, lipids (5 mM) and buffer (10 mM Tris·HCl, pH = 6.90), to a final peptide concentration of ~ 60 μM. CD spectra were acquired in a quartz cylindrical cell (Hellma model 121-QS, Forest Hills, NY) with a path length of 0.02 cm, employing a scan rate of 100 nm/min between 185-280 nm with 0.2 nm data pitch, 1 nm bandwidth, 2 second response, 100 mdeg sensitivity, and 40 successive spectral accumulations. Data are expressed in terms of per-residue molar ellipticity (deg cm^2/dmol), as calculated per mole of oligomer residues and normalized by the molar concentration of peptide.

2.2.7 Pulsating bubble surfactometry

Static and dynamic characterization of surfactant film properties were performed on a modified PBS (General Transco, Seminole, FL) as described by Seurynck et al., in which an imaging system is employed to accurately track bubble size and shape throughout the experiment [27]. This methodology results in more accurate determination of bubble surface tension based on bubble size [27]. The major differences observed with the image analysis system, in

comparison to the commercial system, are higher maximum surface tensions, reduced hysteresis in the data loop, and a reduced slope upon expansion of the bubble. These differences reflect a more accurate measurement and representation of the surface-active behaviors of lung surfactant formulations [27].

For PBS sample preparation, SLSE dispersed in aqueous buffer was diluted with the same buffer to a phospholipid concentration of 1.0 mg/mL and a final volume of 80 μL. Samples were then mixed 40 times with a pipette to form a uniform suspension. The samples were then loaded into a plastic PBS sample chamber (General Transco) using a modified leak-free methodology [26]. The sample preparation for the synthetic surfactant formulations differed from the natural material preparation, in that, the lipid mixture (DPPC:POPG:PA, 68:22:9 (by weight)) was initially dissolved in chloroform:methanol (3:1) with or without 1.6 mol% SP-C mimic. Just prior to experimentation, the samples were added to Eppendorf tubes, dried under vacuum, and resuspended at room temperature in an aqueous buffer solution (0.15 M NaCl, 5 mM $CaCl_2$, and 10 mM HEPES at pH 6.90) to a phospholipid concentration of 1.0 mg/mL, with a final volume of 70-80 μL. Samples were then mixed with a pipette 20 times, twice sonicated with a probe sonicator for 15 seconds, and then mixed again 20 times with a pipette to form a uniform suspension. The samples were then loaded into the plastic PBS sample chamber as before.

After preparation and loading of the sample chamber, a bubble with a radius of 0.4 mm was then formed and an imaging acquisition system was used to determine the bubble size. Trans-film bubble pressure was recorded as a function of time while holding bubble radius static for 20 minutes during static adsorption experiments. Following static adsorption, dynamic

measurements of surface tension as a function of bubble surface area were collected by cycling the bubble radius between approximately 0.4 mm and 0.55 mm at an oscillation frequency of 20 cycles/min for 10 minutes. The trends reported for both static and dynamic adsorption experiments were consistent with all repeated experiments for each surfactant formulation.

2.3 Results and discussion

2.3.1 Natural lung surfactant *in vitro* surface activity

As previously mentioned, lung surfactant has many unique properties that are necessary for proper respiration. To assess its *in vitro* surface activity of the SLSE material as well as to determine if the SLSE was free from contamination, the extracted material was characterized on a modified PBS instrument. Static-bubble PBS experiments were first performed to characterize the adsorption kinetics of the SLSE to the air-liquid interface of a bubble (Figure 2.2A). Natural lung surfactant is expected to cause a rapid decline in surface tension almost immediately upon bubble formation, reaching a static surface tension of ~ 25 mN/m within one minute [27, 87]. As shown in Figure 2.2A, the SLSE material, as expected, adsorbs very rapidly to the interface of the bubble, reducing the surface tension to < 25 mN/m in less than one minute.

The dynamic surface activity of the SLSE material was then characterized by collecting surface tension vs. surface area data loops on the PBS instrument with a cycling rate of 20 cycles/min, which is comparable to the rate of respiration in an adult. A typical plot of the compression-expansion loop for SLSE is shown in Figure 2.2B. The maximum surface tension during dynamic cycling for the natural material is ~ 33 mN/m and the minimum surface tension reached is less than 1 mN/m. These values are consistent with other studies of natural lung

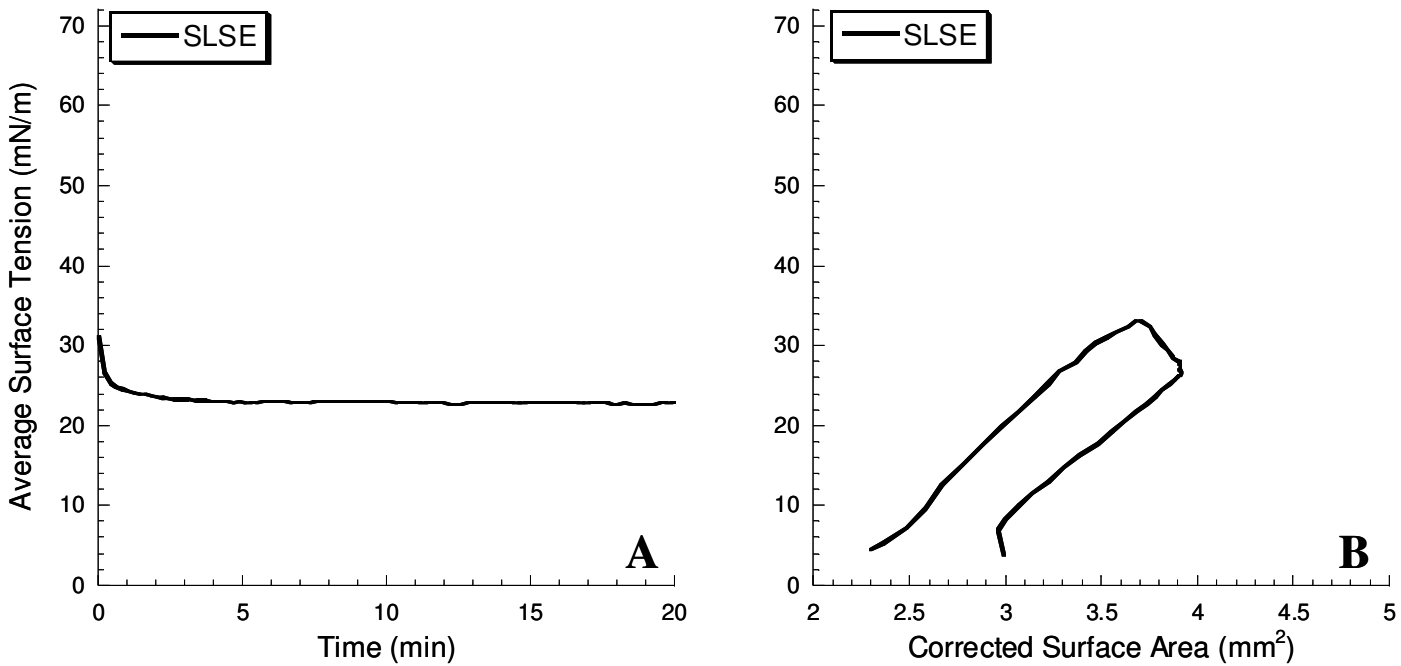

Figure 2.2: Static bubble (A) and dynamic bubble (B) adsorption results from the pulsating bubble surfactometer in buffer at 37°C for SLSE. Dynamic data were collected at 20 cycles/min and loop directions are clockwise.

surfactant material [27, 82]. It is noted that at very low surface tensions that there is a "break" in the PBS cycling loop. This is due to an inability of the image-analysis system to accurately determine the size of the bubble at very low surface tensions because it varies significantly from that of an ellipse; however, given the very low pressure drop across the bubble and the amount of bubble deformation observed, it is clear that the surface tension is near zero for this "missing" portion of the data loop [27]. An unusual phenomenon near maximum bubble area is also observed in the compression-expansion PBS loop in Figure 2.2B. As the bubble is expanded near the maximum surface area, there is a slight decrease in surface tension during the expansion. This counterintuitive characteristic is due to a change in the rate of surface area expansion. While the change in bubble volume is constant during cycling, the rate of surface area expansion and compression is not. At this point, surface adsorption overcomes the rate of surface area expansion and the surfactant adsorption to the interface outpaces the change in surface area, which causes a decrease in surface tension. This feature is only seen in rapidly adsorbing surfactant materials.

The results from the static PBS adsorption and dynamic cycling experiments for SLSE demonstrate that the functional constituents of the natural material are retained during the isolation and extraction procedures. The SLSE material rapidly adsorbs to the air-liquid interface and dramatically alters the surface tension vs. surface area characteristics, displaying very low maximum and minimum surface tensions. These results also indicate that the SLSE material is essentially free of surface-active contaminants, such as albumin and other blood plasma species. The characterization of SLSE surface behavior is necessary for the development and study of synthetic lung surfactants as these surface-active features serve as *in vitro*

benchmarks for a biomimetic SRT formulation to treat RDS. In addition to the surface-active properties of the entire hydrophobic content of lung surfactant, it is also necessary to characterize the *in vitro* activities of the hydrophobic proteins of lung surfactant.

2.3.2 SP-C peptide mimic

2.3.2.1 SP-C peptide synthesis

SP-C is the smaller of the two hydrophobic lung surfactant proteins, at just 35 monomers in length (Table 2.1). SP-C's sequence is highly conserved and unique, containing a high amount of hydrophobic, β-branched amino acids, mainly valine, leucine, and isoleucine [88]. The properly folded protein SP-C does not possess any tertiary structure; however, the secondary structure is dominated by a poly-valyl α-helix comprising residues 9-34 [29]. In lung surfactant films, SP-C promotes phospholipid insertion into the air-liquid interface, and thereby enhances the rate of lipid adsorption as well as the respreading of the alveolar film upon inhalation [37, 38, 89, 90]. The presence of SP-C has also been shown to lower, to some extent, the minimum surface tension of various lipids, stabilize the surfactant film upon compression, and greatly increase the surface viscosity at lower surface tensions [42, 89].

Given SP-C's lack of a tertiary structure and relatively modest size, it is feasible to chemically synthesize full-length analogues of SP-C; however, this is not a trivial task. Due to its large number of nonpolar residues (> 70%) and the two palmitoyl chains, SP-C is the most hydrophobic naturally occurring mammalian protein known [7]. In addition to SP-C's extreme hydrophobicity, the poly-valyl helix is also discordant, i.e. it is composed of amino acids with a high propensity to form β-strands [4]. The SP-C helix is consequently metastable in solution and can spontaneously convert into β-sheet aggregates and amyloid fibrils [43, 44]. These misfolded

and aggregated structures have inferior surface activity compared to the correctly folded, helical protein [45]. SP-C's hydrophobicity and metastable secondary structure make working with the natural protein extraordinarily difficult [43, 44, 91]. This difficulty has led to the development of synthetic and recombinant analogues of SP-C in order to reproduce the biophysical behavior of the natural protein while minimizing the tendency for aggregation or misfolding [50, 51, 92]. These analogues have offered many insights concerning the structure-activity relationships of SP-C, and researchers have identified several biomimetic polypeptide candidates for use with phospholipids in order to treat RDS [10, 51, 93, 94]. One interesting approach replaces the valine residues in the helical region with leucine residues that more readily form α-helical structures [50]. This analogue is more structurally stable than either the natural protein or sequence identical analogues; however, the sequence is still resistant to efficient assembly in appreciable yield by standard Fmoc solid phase synthesis procedures as it is prone to aggregation during synthesis (unpublished observations). The challenge facing the synthesis of sequences with strong aggregation propensities is commonly referred to as the "difficult sequence" phenomena [95].

While the successful synthesis of a human identical SP-C peptide has been reported by routine Fmoc solid phase synthesis, many researchers have pursued other avenues of production including tert-butyloxycarbonyl chemistry and recombinant protein expression to combat on-resin sequence aggregation [47, 48, 50, 96]. In a modified approach, the standard Fmoc peptide synthesis protocol was modified to overcome the inherent difficulties associated with the synthesis of SP-C. Using this protocol a non-acylated peptide mimic, SP-$C_{F,F}$, and an acylated mimic, di-pSP-$C_{F,F}$, were synthesized (Table 2.1). The SP-$C_{F,F}$ analogue is based upon the work

of Nilsson and coworkers and includes a valine-to-leucine, cysteine-to-phenylalanine, and methonine-to-isoleucine substitutions to prevent misfolding, oligomerization, and partial oxidation, respectively (sequence shown in Table 2.1) [48, 50].

Some of the main factors that contribute to a "difficult peptide" synthesis are resin substitution level, Fmoc deprotection efficiency, and extent of peptide-resin solvation [97]. To address these issues, a lower substitution resin was used (0.24 mmol/g vs. 0.64 mmol/g) to separate adjacent peptide chains, decreasing the effective concentration and aggregation propensity. Fmoc deprotection was also carried out utilizing 2% of the non-nucleophilic base, 1,8-diazabicyclo-[5.4.0]undec-7-ene (DBU), and 2% piperidine dissolved in DMF as an alternative to the 20% piperidine in NMP solution that is typically used for this step [85]. DBU is a stronger base than piperidine and more readily displaces the Fmoc protecting group. This is especially beneficial with a peptide that is prone to on-resin aggregation as the encountered steric hindrance can cause the Fmoc-protected end of the peptide to become much less accessible to reagents, dramatically decreasing the deprotection efficiency even with extension and repetition of the deprotection step. This decreased deprotection efficiency is a major cause of either reduced yield or failed syntheses in aggregation prone sequences (Peter White, personal communication). A small amount of piperidine is still needed in the deprotection step to scavenge the dibenzofulvene formed upon Fmoc removal.

On-resin sequence aggregation also hinders the acylation step of peptide synthesis, drastically reducing amino acid coupling efficiencies. Both DMF and NMP are routinely used as solvents during this step as both are compatible with the acylating reagents and effectively solvate non-aggregating peptide chains; however, for sequences termed "difficult sequences,"

DMF and NMP do not effectively solvate the growing peptide chain. To address this, DMSO was used as the solvent during the acylation step with no further modification of the acylation step procedure. DMSO has been demonstrated to inhibit peptide aggregation and to improve acylation efficiency relative to DMF and NMP [97, 98].

Figure 2.3 shows the analytical HPLC elution profile for the non-acylated SP-$C_{F,F}$ peptide synthesized using the standard Fmoc solid phase synthesis procedure as well as for the same non-alkylated peptide synthesized with the modified synthesis protocol. The desired product in each elution profile is indicated and a slight shift in retention time is observed due to a difference in column manufacturer; however, the separation efficiency of these columns is comparable. By utilizing DMSO as the solvent during the acylation step as well as the mixture of 2% DBU and 2% piperidine in DMF for Fmoc deprotection during synthesis, the crude peptide yield was improved, resulting in fewer truncated sequences as observed by the reduction in number and peak areas of the contaminant species. The improvement in synthesis efficiency not only improves the crude purity, but also improves the subsequent HPLC purification of the peptide. These synthetic strategies enable the successful obtainment of a synthetic peptide analogue of human SP-C in high purity and sufficient yield.

The alkylated peptide, di-pSP-$C_{F,F}$, was also synthesized using the modified Fmoc solid phase synthesis protocol. The structure of the alkylated mimic is shown in Table 2.1. This sequence is unique, in that, instead of the native thioester-linked palmitoyl chains, two peptoid residues that incorporate the *N*ocd submonomer were used. *N*ocd mimics the length and hydrophobicity of the native palmitoyl groups; however, because of the amide linkage, the alkyl chains are stable against hydrolysis in an alkaline environment and, as a result, are readily

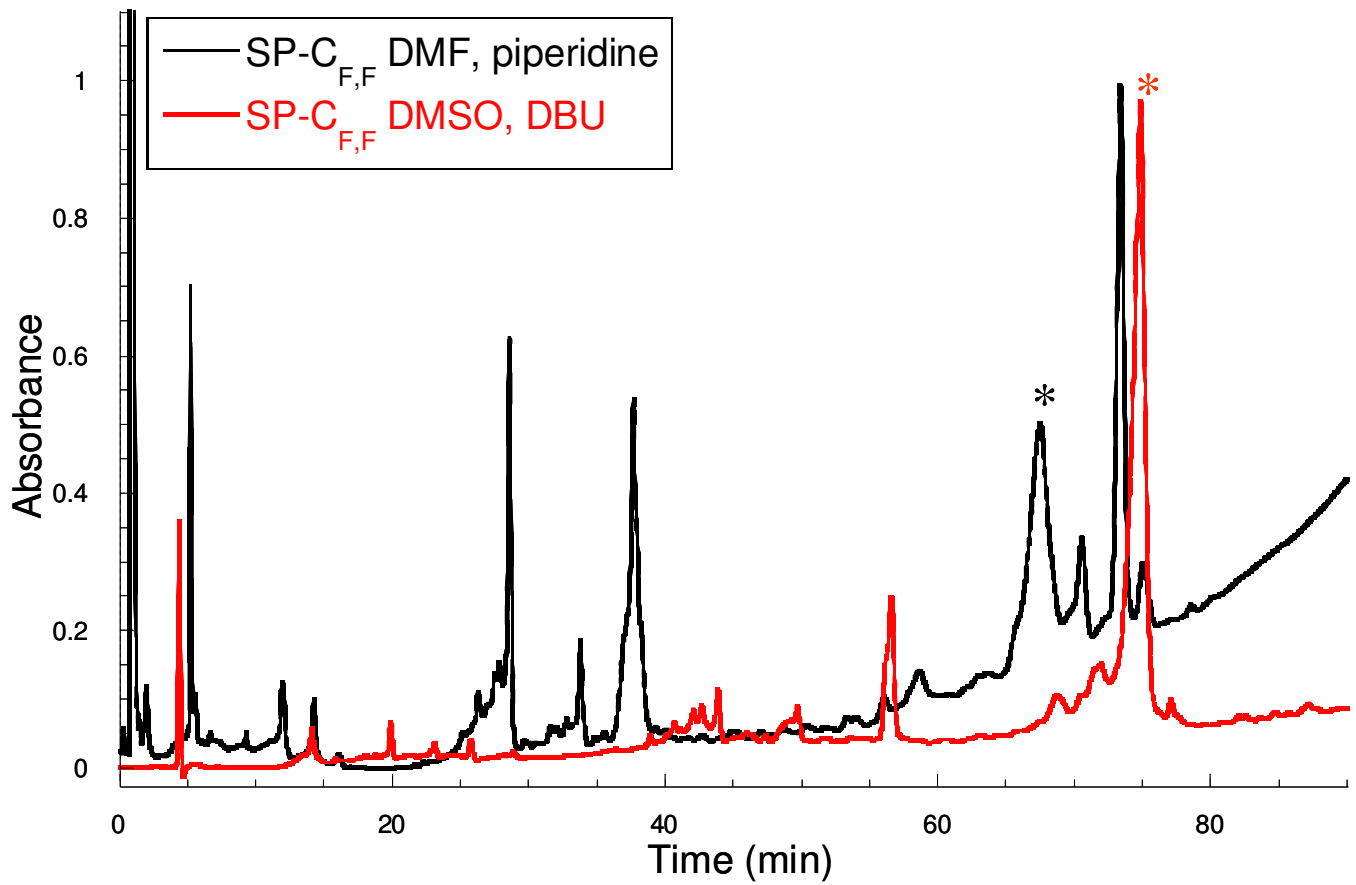

Figure 2.3: HPLC elution profile of SP-$C_{F,F}$ synthesized using standard Fmoc chemistry with NMP as the coupling solvent and 20% piperidine in NMP for Fmoc deprotection (black line) and using Fmoc chemistry with DMSO as the coupling solvent and 4% DBU:piperidine (1:1) in DMF for Fmoc deprotection (red line). Desired compounds are indicated by *. 0-100% solvent B in solvent A over 90 minutes on a C4 RP-HPLC column where solvent A = 0.1% TFA in water and solvent B = 0.1% TFA in isopropanol. The largest peak in each elution profile was normalized to 1.

incorporated into the growing peptide chain at selective sites during peptide synthesis. These features are advantageous in comparison to other methods that have been used to palmitoylated SP-C, which are unstable to alkaline environments and must be performed post-synthesis, requiring additional purification steps [99].

2.3.2.2 SP-C secondary structure characterization

SP-C's secondary structure is dominated by a long α-helical region that is essential to its biophysical activity in lung surfactant [50, 63, 96, 99, 100]. CD was used to characterize and compare the secondary structures of the non-acylated and acylated SP-C peptides, ensuring proper folding. CD spectra of the modified SP-C peptides in methanol are displayed in Figure 2.4A. SP-$C_{F,F}$ displays CD spectral features that are characteristic of an α-helix with a double minima at λ ~ 208 nm and ~ 220 nm and an intense maximum at λ ~ 192. This is consistent with previously published results for SP-C [96]. The addition of the alkyl chains to the *N*-terminal region of the peptide does not significantly alter the CD spectrum; however, a slight decrease in spectral intensity is observed, indicating a slight reduction in helicity. This is somewhat surprising as several studies have show that the palmitoyl groups increase the helical propensity of SP-C [33, 43, 89]; however, other studies have shown that the palmitoyl groups either decreases or has no influence on the helical content of the peptide [101-103]. Despite this, both peptides are properly folded and highly helical in solution.

In order to characterize the conformation of the peptide mimics in an environment more similar to that of lung surfactant, CD spectrometry was performed in an aqueous solution of lung surfactant-mimetic liposomes, with an overall lipid concentration of 5 mM (Figure 2.4B). The lipid formulation used, DPPC:POPG:PA 68:22:9 by weight (Tanaka lipids), has been shown to

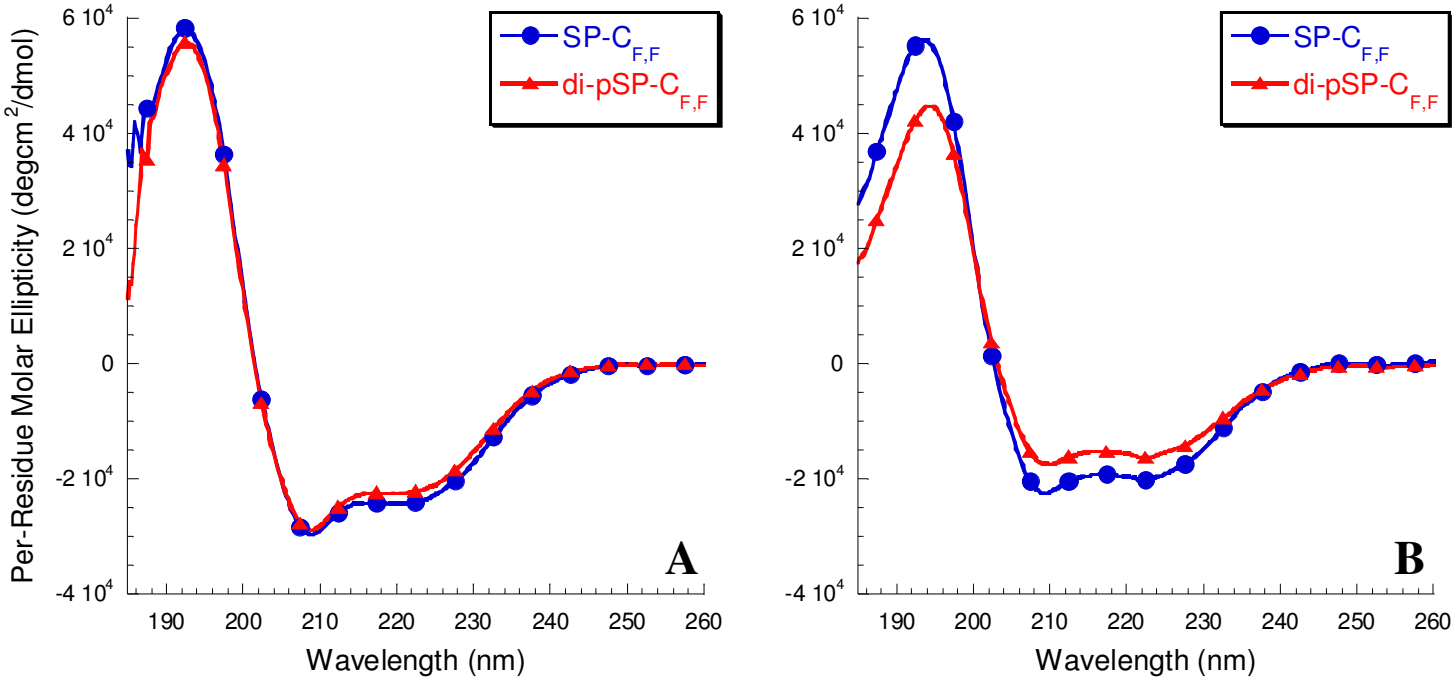

Figure 2.4: (A) CD spectra of SP-$C_{F,F}$ and di-pSP-$C_{F,F}$ in methanol showing characteristic features of a peptide α-helix; (B) CD spectra of SP-$C_{F,F}$ and di-pSP-$C_{F,F}$ in 5 mM liposomes in 10 mM Tris·HCl, pH = 6.90. Spectra were acquired at a peptide concentration of ~ 60 μM at room temperature.

be a good mimic of the lipid fraction of lung surfactant [104]. In the Tanaka liposomes both of the SP-C peptides retain their helical secondary structure; however, the intensities of the spectra are reduced slightly from that in methanol, indicating a slight decrease in helicity for both peptides in the liposomes. This is not unexpected as the secondary structure of SP-C is already fully developed outside the lipid environment and this finding is consistent with other studies of SP-C in lipid micelles [45, 105].

2.3.2.3 SP-C *in vitro* surface activity

In vivo, lung surfactant rapidly adsorbs to the alveolar air-liquid interface and immediately forms a surface-active layer [7, 10]. The hydrophobic proteins of lung surfactant, SP-B and SP-C, are crucial for this surface-active property as their addition greatly accelerates the surfactant adsorption kinetics [106-108]. The *in vitro* adsorption kinetics of the Tanaka lipid formulation alone and with the addition of the synthetic peptides, SP-$C_{F,F}$ and di-pSP-$C_{F,F}$, was characterized with a modified PBS run in static mode with a bubble radius of approximately 0.40 mm at 37°C. Figure 2.5A displays the adsorption surface tension as a function of time for the synthetic surfactant formulations. In the absence of the SP-C peptides, the lipid mixture displays very slow adsorption kinetics and fails to reach an equilibrium surface tension lower than 52 mN/m even after 20 minutes of static adsorption. The addition of SP-$C_{F,F}$ to the lipid formulation significantly accelerates the kinetics of lipid adsorption to the interface, allowing the film to reach a surface tension of ~ 30 mN/m in less than 1 minute and reaching ~ 24 mN/m after 4 minutes. The addition of the alkylated peptide, di-pSP-$C_{F,F}$, also accelerates the surfactant adsorption kinetics, reaching a surface tension below 30 mN/m almost instantaneously and dropping to ~ 20 mN/m after 4 minutes. Both of the mimics catalyze the adsorption of surfactant

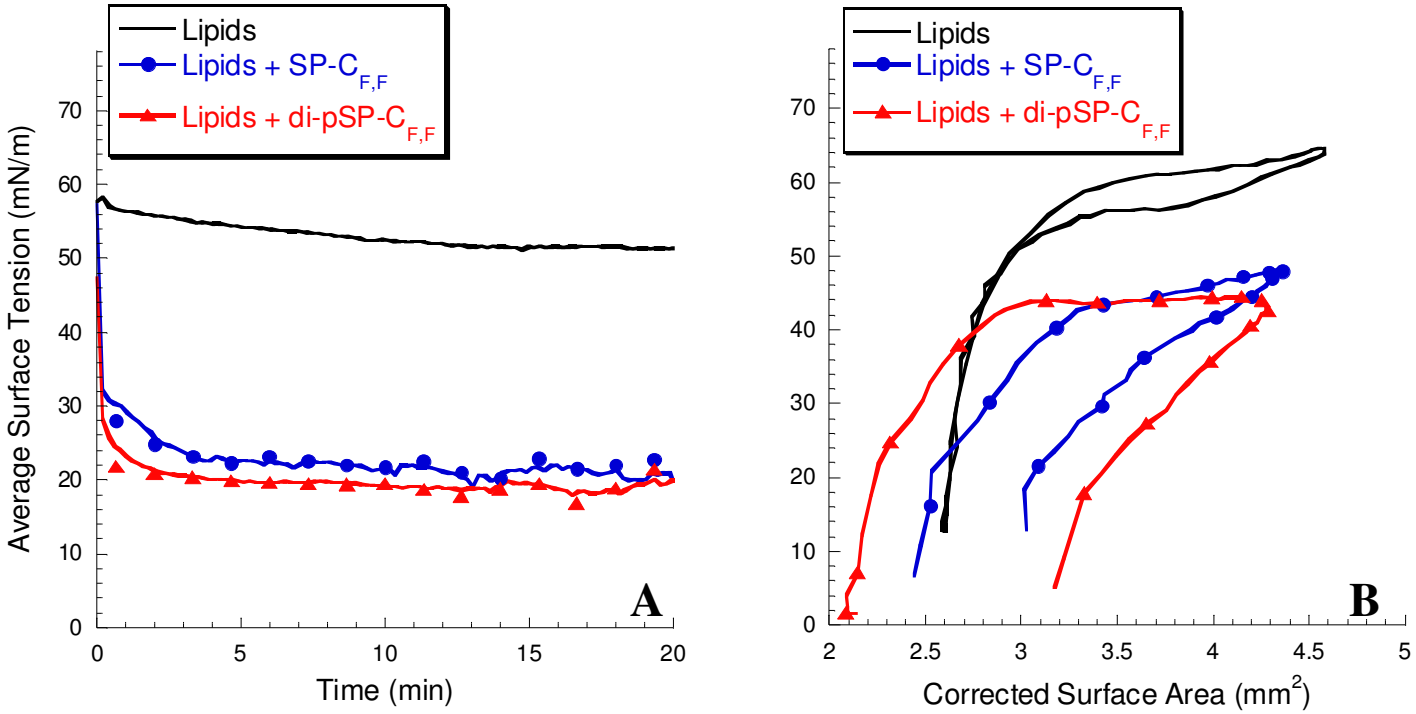

Figure 2.5: Static bubble (A) and dynamic bubble (B) adsorption results from the pulsating bubble surfactometer in buffer at 37°C for Tanaka lipids, Tanaka lipids + 1.6 mol% SP-$C_{F,F}$, and Tanaka lipids + 1.6 mol% di-pSP-$C_{F,F}$. Dynamic data were collected at 20 cycles/min and loop directions are clockwise.

material to the air-liquid interface; however, the presence of the alkyl chains in di-pSP-$C_{F,F}$ results in slightly faster adsorption kinetics, which may be a result of either the increased hydrophobicity or an increased ability to perturb the lipid packing, facilitating the inter-membrane phospholipid transfer.

The presence of SP-B and SP-C also significantly alter the dynamic cycling properties of the phospholipids of the lung surfactant system, reducing both the maximum and minimum surface tensions during expansion and compression of the film [16]. Figure 2.5B shows the surface tension as a function of bubble surface area for lipid mixture with and without the SP-C peptides. The lipid mixture, when used alone, exhibits high minimum surface tension and maximum surface tensions of ~ 12 mN/m and ~ 65 mN/m, respectively. With these properties, this material would be inadequate as a lung surfactant. The addition of SP-$C_{F,F}$ to the lipid mixture dramatically improves the surface activity of the film relative to that of the lipids alone, as indicated by the significantly lower minimum surface tension of < 1 mN/m and lower maximum surface tension of ~ 48 mN/m (Figure 2.5B). The addition of SP-$C_{F,F}$ to the lipid formulation also significantly decreases the compressibility of the surfactant, requiring much less compression to reach a minimum surface tension. Adding di-pSP-$C_{F,F}$ to the lipid formulation similarly improves the surface-active properties of the surfactant. Both the minimum and maximum surface tensions are reduced to < 1 mN/m and ~ 45 mN/m, respectively. It is interesting to note, that the presence of the alkyl chains in di-pSP-$C_{F,F}$ causes a slight decrease in the maximum surface tension as well as a PBS loop with much more hysteresis indicating that the surfactant film is less compressible.

2.4 Conclusions

Here a method is detailed for the successful isolation and extraction of native lung surfactant from excised animal lungs as well as a modified synthetic procedure for the synthesis of a non-alkylated and an alkylated SP-C peptide mimic, SP-$C_{F,F}$ and di-pSP-$C_{F,F}$, respectively. The synthesis of the peptide mimics is notable, in that, specific alterations in the coupling and deprotection protocols were made to prevent on-resin aggregation and to improve the Fmoc deprotection efficacy. These modifications lead to an improvement in yield of this extraordinarily "difficult sequence." The acylated SP-C peptide also utilizes a unique method for the on-resin alkylation of the peptide that is both selective and stable, being efficiently incorporated during solid phase synthesis. The applicability of this alkylation method has merit not only in the study of SP-C functionality, but also in the investigation of other lipoprotein species.

The *in vitro* surface activities of the lung surfactant material and SP-C peptides were also characterized with a PBS instrument. The extracted lung surfactant material and the SP-C peptides, when combined with a synthetic phospholipid formulation, both display remarkable surface activity. These materials rapidly adsorb to the air-liquid interface, reaching an equilibrium surface tension below 30 mN/m in less than one minute. During dynamic cycling, the native lung surfactant displays low maximum and minimum surface tensions of ~ 33 mN/m and < 1 mN/m, respectively. Both the SP-C peptides cause a dramatic reduction in minimum surface tension to below 1 mN/m; however, neither peptide is able to reproduce the low maximum surface tension observed with the natural lung surfactant material. The SP-$C_{F,F}$- and di-pSP-$C_{F,F}$-containing formulations exhibit maximum surface tensions of ~ 48 mN/m and ~ 45

mN/m, respectively. The *in vitro* characterization of these materials is beneficial in the development and assessment of a biomimetic SRT, ensuring that the dominant surface-active features are accurately captured by the synthetic SRT formulation.

Chapter 3: Lipid composition greatly affects the *in vitro* surface activity of lung surfactant protein C mimics

Reproduced with the permission of *Colloids and Surfaces B: Biointerfaces*, **2007**, 57, 37-55. Copyright 2007, Elsevier Inc.

A crucial aspect of developing a functional, biomimetic lung surfactant replacement is the selection of the synthetic lipid mixture and surfactant proteins (SPs) or suitable mimics thereof. Studies elucidating the roles of different lipids and surfactant proteins in natural lung surfactant have provided critical information necessary for the development of synthetic lung surfactant replacements that offer performance comparable to the natural material. In this study, the *in vitro* surface-active behaviors of peptide- and peptoid-based mimics of the lung surfactant protein C (SP-C) were investigated using three different lipid formulations. The lipid mixtures were chosen from among those commonly used for the testing and characterization of SP mimics: (1) dipalmitoyl phosphatidylcholine : palmitoyloleoyl phosphatidylglycerol 7:3 [w/w] (PCPG), (2) dipalmitoyl phosphatidylcholine : palmitoyloleoyl phosphatidylglycerol : palmitic acid 68:22:9 [w/w] (TL), and (3) dipalmitoyl phosphatidylcholine : palmitoyloleoyl phosphatidylcholine : palmitoyloleoyl phosphatidylglycerol : palmitoyloleoyl phosphatidylethanolamine : palmitoyloleoyl phosphatidylserine : cholesterol, 16:10:3:1:3:2 [w/w] (IL). The lipid mixtures and lipid/peptide or lipid/peptoid formulations were characterized *in vitro* using a Langmuir-Wilhelmy surface balance, fluorescent microscopic imaging of surface film morphology, and a pulsating bubble surfactometer. Results show that the three lipid formulations exhibit significantly different surface-active behaviors, both in the presence and absence of SP mimics, with desirable *in vitro* biomimetic behaviors being greatest for the TL

formulation. Specifically, the TL formulation is able to reach low surface tensions at physiological temperature as determined by dynamic PBS and LWSB studies, and dynamic PBS studies show this to occur with a minimal amount of compression, similar to natural lung surfactant.

3.1 Introduction

Lung surfactant, a complex biomaterial that coats internal pulmonary surfaces, is essential for normal breathing [109]. This surface-active material functions to reduce and regulate surface tension within the alveoli during respiration [109]. The most important attributes of lung surfactant are its ability to (i) adsorb rapidly to the air-water interface, (ii) reach near-zero surface tension upon film compression, preventing alveolar collapse, and (iii) respread at the air-water interface through multiple expansions and contractions of film surface area. The congenital absence or dysfunction of lung surfactant results in neonatal respiratory distress syndrome (nRDS), a leading cause of infant mortality in the United States [7]. Currently, premature infants suffering from nRDS are treated by intratracheal instillation of an exogenous lung surfactant replacement, typically animal-derived, into the lungs [7]. However, there are significant concerns associated with the use of animal-derived lung surfactant replacements, including high production and purification costs, batch-to-batch variability, and the potential for pathogen transmission [7]. Less expensive, synthetic lung surfactant replacements have been developed, but are not commonly used due to their generally inferior efficacy in the treatment of nRDS [7]. This poor performance is attributed to the lack of the hydrophobic surfactant proteins (SPs) present in animal-derived surfactant that are necessary for the proper biophysical functioning of lung surfactant [7]. Hence, there is a need for a safe, cost-effective, entirely

synthetic lung surfactant replacement that contains good functional mimics of both the hydrophobic SPs and the lipid portion of lung surfactant.

In order to create a useful synthetic lung surfactant replacement, the role of each lung surfactant component must be considered carefully. Lipids comprise approximately 90% of lung surfactant by weight, and SPs approximately 10% [109]. The hydrophobic SPs, SP-B and SP-C, are thought to be critical for facilitating the proper interfacial lipid dynamics and maintaining respreadability of the lipid film [7]. The addition of SP-B and/or SP-C to natural or synthetic lipid mixtures results in a faster rate of adsorption, lower minimum surface tensions, and better respreadability of the film compared to the film without added SP [7].

The major lipid class in lung surfactant is phosphatidylcholine (PC), which comprises approximately 65 – 75% of lung surfactant lipids; dipalmitoyl phosphatidylcholine (DPPC) is the most prevalent single component of lung surfactant, comprising 40 – 60% of the PC species. Monolayers of DPPC are able to maintain near-zero surface tensions upon compression due to the tight packing ability of saturated phospholipids [7]. However, this stiff and rigid monolayer adsorbs slowly to the air-aqueous interface and respreads poorly upon successive compressions and expansions of film area [7]. The addition of unsaturated phospholipids such as palmitoyloleoyl phosphatidylcholine (POPC) and palmitoyloleoyl phosphatidylglycerol (POPG) or other lipids and hydrophobic molecules such as palmitic acid (PA) and cholesterol has been shown to enhance the adsorption rate of the lipid film as well as improve its respreadability; however, the minimum surface tension upon compression is thus increased relative to DPPC films [9].

There is general agreement that a functional replacement for natural lung surfactant must either contain SP-B and/or SP-C or comprise good functional mimics of these small, amphipathic proteins. Both have unique structural attributes that are not trivial to mimic with synthetic peptides or peptidomimetics. SP-C is an exceedingly hydrophobic, amphipathic, helical protein, comprised of 35 amino acids [7]. SP-C contains two cationic residues at positions 11 and 12 that interact with anionic phospholipid head groups of a lipid film [34] and post-translationally palmitoylated cysteines at positions 5 and 6 that are believed to be important for proper function; however, their exact role and the extent of their importance are a matter of debate [35, 37, 40, 89, 103]. SP-C's structure is dominated by an α-helix that is approximately 37 Å long, and within this helical region is a 23 Å-long, valyl-rich stretch of hydrophobic amino acids. The lengths of the helix and valyl-rich region closely match the thickness of a DPPC bilayer and its acyl-chain portion, respectively, suggesting that SP-C can traverse a phospholipid bilayer [29], or form a transbilayer orientation, interacting with the hydrophobic lipid acyl chains [32]. Due to extreme hydrophobicity and a strong tendency to aggregate and misfold in the absence of lipids, several simplified peptide mimics of SP-C have been created and studied [45, 51, 94, 110, 111]. Takei *et al.* synthesized various non-palmitoylated, full-length and truncated forms of SP-C, and found that a core sequence (residues 5-31 or 6-32) is required for biophysical activity comparable to the full-length protein [51]. Nilsson *et al.* created an SP-C analog by replacing valines with leucines and cysteines with serines, which showed surface activity comparable to native SP-C, but with a much-reduced tendency for hydrophobic aggregation and misfolding [50, 52].

In previous studies, the surface-active behaviors of peptoid-based mimics of both SP-B and SP-C in lipid films were investigated, and compared the activity of the peptoids to the respective peptide mimics [62, 112]. Peptoids represent an alternate derivative of a polypeptide backbone, with the side chains attached to the amide nitrogens rather than to the α-carbons [86, 113]. The *N*-substituted backbone of this class of molecules resists proteolysis, resulting in enhanced bioavailability and the potential for reduced specific recognition by the immune system [55, 114]. Such properties are of course extremely sequence- and size-dependent, and the biocompatibility of longer peptoid oligomers has not yet been assessed. Although peptoids are not able to form backbone-backbone hydrogen bonds like peptides to stabilize secondary structure [115], structural studies have shown that peptoid sequences with homochiral side chains form stable helical structures with a chiral sense, similar to polyproline helices in peptides [116]. Peptoid helices have a helical pitch of approximately 6 Å and a periodicity of 3 residues per turn, and are stabilized primarily by steric and electronic repulsions [115].

The peptoid-based SP-C mimics previously reported were designed to capture the essential structural features of the cognate peptide: The peptoid mimics were helical and longitudinally amphipathic [62]. The surface-active behaviors of the peptoid mimics as well as of comparator peptides were characterized in biomimetic lipid films using a Langmuir-Wilhelmy surface balance (LWSB) and a pulsating bubble surfactometer, while film phase morphologies were observed using fluorescence microscopy in conjunction with an LWSB. The peptoid mimics were found to exhibit surface-active behaviors and film phase morphologies that were in many ways similar to, though not identical to the model peptide mimics [62].

It has been shown that lipid composition can play an important role in the surface activity and structure of SP mimics in a lipid film [117]. In this study, the *in vitro* function of a peptide- and a peptoid-based SP-C mimics in three different lipid formulations were studied to further investigate SP-C mimic/lipid interactions. The lipid mixtures were chosen from among those commonly used for the testing and characterization of SP-C mimics: (1) dipalmitoyl phosphatidylcholine : palmitoyloleoyl phosphatidylglycerol 7:3 [w/w] (PCPG), (2) dipalmitoyl phosphatidylcholine : palmitoyloleoyl phosphatidylglycerol : palmitic acid 68:22:9 [w/w] (TL), and (3) dipalmitoyl phosphatidylcholine : palmitoyloleoyl phosphatidylcholine : palmitoyloleoyl phosphatidylglycerol : palmitoyloleoyl phosphatidylethanolamine : palmitoyloleoyl phosphatidylserine : cholesterol, 16:10:3:1:3:2 [w/w] (IL). The results show that these three lipid formulations exhibit significantly different surface-active behaviors as determined by LWSB, FM, and PBS studies, both in the presence and absence of the SP-C mimics. Additionally, the lipid composition has a dramatic effect on the surface-active behaviors of both peptoid- and peptide-based mimics, which has important implications for their use in biomimetic lung surfactant replacement formulations.

3.2 Materials and methods

3.2.1 Materials and reagents

Peptide and peptoid synthesis reagents were purchased from Applied Biosystems (Foster City, CA) and Aldrich (Milwaukee, WI). Resins and Fmoc-protected amino acids were purchased from NovaBiochem (San Diego, CA), while 2,2,5,7,8-pentamethylchroman-6-sulfonyl chloride (PMC) was purchased from Omega Chemical (Quebec, CA), and primary amines and di-*tert*-butyl dicarbonate (Boc) were purchased from Aldrich. Acetonitrile, isopropanol, and

trifluoroacetic acid (TFA) were purchased from Fisher Scientific (Pittsburgh, PA). DPPC, POPG, POPC, POPE, POPS, and cholesterol were purchased from Avanti Polar Lipids (Alabaster, AL), PA was purchased from Aldrich, and Texas Red® 1,2-dihexadecanoyl-*sn*-glycero-3-phosphoethanolamine, triethylammonium salt (TR-DHPE) was purchased from Molecular Probes (Eugene, OR). All chemicals were purchased in high purity form and were used without further purification.

3.2.2 Peptide and peptoid synthesis, purification, and characterization

A non-palmitoylated SP-C-mimetic peptide was synthesized with a sequence modified to prevent aggregation and preserve the hydrophobicity of the *N*-terminal region, SP-$C_{F,F}$, which included valine-to-leucine and cysteine-to-phenylalanine substitutions (sequence shown in Table 3.1) [48, 50]. The SP-C peptide was synthesized by standard Fmoc chemistry on solid support (pre-loaded Wang resin) using an ABI 433A automated peptide synthesizer (Applied Biosystems).

A peptoid mimic of SP-C, Peptoid C, mimics residues 5-32 from human SP-C, with close sequence mimicry at the *N*-terminus and maintenance of the *C*-terminal hydrophobic helix (structure shown in Table 3.1) [62]. The SP-C peptoid was synthesized using an ABI 433A on Rink amide resin by the sub-monomer protocol as previously described [86]. All molecules were cleaved from the resin with TFA, along with the appropriate scavenging reagents, for 10 minutes for the peptoid mimic or 1 hour for SP-$C_{F,F}$ (the longer time is necessary to remove the PMC protecting group from guanidine side chains in the acid-stabile SP-$C_{F,F}$ peptide). SP-C mimics were purified by RP-HPLC using a linear gradient of 30%-80% solvent B in solvent A over 50 minutes (solvent A is 0.1% TFA in water [v/v] and solvent B is 0.1% TFA in

Table 3.1: Peptide and peptoid sequences and molecular weights.

Molecule	**Sequence/Structure**	**Molecular Weight (Da)**
SP-$C_{F,F}$	FGIPFFPVHLKRLLILLLLLLLLILLLILGALLMGL	3924
Peptoid C	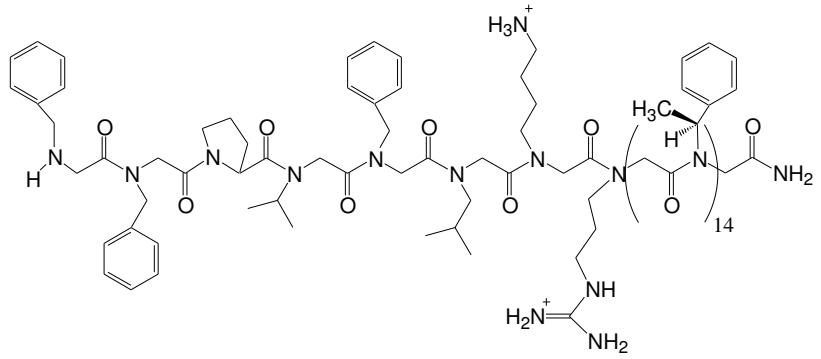	3309

acetonitrile-isopropanol 1:1 [v/v] for Peptoid C and 0.1% TFA in isopropanol [v/v] for SP-$C_{F,F}$). The final purities of the molecules were confirmed to be > 97% by analytical RP-HPLC, and molecular weights were confirmed by electrospray ionization mass spectrometry (Table 3.1). The extent of helicity of the peptides and peptoids was confirmed by circular dichroism spectroscopy [62, 112].

3.2.3 Methods and apparatus

3.2.3.1 Sample preparation

Each lipid was individually dissolved in chloroform/methanol (3/1 [v/v]) to a precisely known concentration (~ 4 mg/mL). The lipids were then combined to make three different formulations, which is termed: "PCPG lipids" (DPPC:POPG, PCPG, 7:3 [w/w]), "Tanaka lipids" (TL, DPPC:POPG:PA, 68:22:9 [w/w]), and "synthetic Infasurf lipids" (IL, DPPC : POPC : POPG : POPE : POPS : cholesterol, 16:10:3:1:3:2 [w/w]) with total lipid concentrations of ~ 2 mg/mL.

Peptide and peptoid mimics were dissolved in methanol to a known concentration (~ 2 mg/mL). The modified SP-$C_{F,F}$ peptide was added to the lipid mixtures at 10 weight percent, which is similar to the total protein content in lung surfactant. The SP-C peptoid mimic was added to each of the lipid formulations at an equivalent mole percentage (see Table 3.2) comparable to those used in other studies [118].

Table 3.2: Molar percentages of added peptide or peptoid in each lipid formulation.

	PCPG (mole%)	**TL (mole%)**	**IL (mole%)**
SP-$C_{F,F}$/Peptoid C	1.9	1.6	1.8

3.2.3.2 Langmuir-Wilhelmy surface balance studies

Surface pressure-molecular area isotherms were obtained using a home-built Langmuir-Wilhelmy surface balance, as previously described [112]. The trough was filled with 300 mL of aqueous buffer (150 mM NaCl, 5 mM $CaCl_2$, 10 mM HEPES, pH 6.9) and heated to either 25 or 37˚C. The surfactant formulation was spread at the air-water interface from a chloroform/methanol solution using a glass syringe and allowed to equilibrate for 10 minutes. The barriers were then compressed and expanded at a rate of 30 mm/min. Surface pressure was measured using a Wilhelmy plate (Riegler and Kirsten GMBH, Berlin). The average surface area per molecule was calculated including both the lipids and the protein mimics. Experiments were repeated a total of six times per temperature for each surfactant formulation and gave reproducible results. Error bars fall within the thickness of the lines.

3.2.3.3 Fluorescence microscopic imaging

In order to obtain fluorescence microscopic images of the lipid films on the Langmuir trough, a Nikon MM40 compact microscope stand with a 100W mercury lamp (Tokyo, Japan) was used in conjunction with an LWSB. Fluorescence was detected by a Dage-MTI three-chip color camera (Dage-MTI, Michigan City, IN) in conjunction with a generation II intensifier (Fryer, Huntley, IL). Samples were spiked with 0.5 mol% of a fluorescently labeled lipid, TR-DHPE, for detection. Previous studies have shown that inclusion of the labeled lipid at this concentration does not alter surfactant film morphology [119]. Experiments were performed on an aqueous buffered subphase at 25 and 37ºC with a barrier speed of 5 mm/min, and were repeated a total of three times per temperature for each surfactant formulation; results were reproducible.

3.2.3.4 Pulsating bubble surfactometry

A modified pulsating bubble surfactometer (General Transco, Largo, FL), which has been previously described, was used to obtain both static-bubble and dynamic-bubble adsorption data [27]. An image acquisition system has been added to a commercial PBS in order to track bubble shape and size in real time. Images and pressure data from the instrument are sent to a LabVIEW program that is used to fit the bubble to an ellipse and calculate both the surface tension and the surface area of the bubble, resulting in more accurate determination of bubble surface tension based on bubble size [27]. Some of the major differences observed with the image analysis system, relative to the simpler commercial system, are higher maximum surface tensions, reduced hysteresis in the data loop, and a reduced slope upon expansion of the bubble. These differences have been shown to reflect a more accurate measurement and representation of the surface-active behaviors of biomimetic lung surfactant formulations [27]. In addition, it is possible to visually detect any movement (leakage) of surfactant up the capillary or formation of particulates in the sample. Runs that showed either of these phenomena were removed from further analysis.

Surfactant formulations were dried from the chloroform/methanol solution using a DNA 120 Speedvac (Thermo Electron, Holbrook, NY), forming a pellet. The pellet was suspended in an aqueous buffer (150 mM NaCl, 5 mM $CaCl_2$, 10 mM HEPES, pH 6.9) to 1.0 mg lipid/mL, with a final volume of 70-80 μL. The surfactant formulations were mixed with a micropipette, sonicated briefly with a Fisher Model 60 probe sonicator, and then mixed with a micropipette again to form a uniform suspension. Samples were loaded into a plastic PBS sample chamber

(General Transco) with putty placed on the capillary end of the sample chamber to prevent sample leakage; the putty was removed before experiments were performed [26].

All experiments were performed at physiological temperature, 37ºC. Static adsorption surface tension data were collected for 20 minutes, starting with a bubble radius of 0.4 mm and allowing the bubble size to drift (grow) throughout the adsorption period. Following static adsorption, dynamic adsorption data were obtained at a frequency of 20 cycles/min for at least 10 minutes or until the shape of the hysteresis loop remained unchanged for at least 2 minutes, again starting with a minimum bubble radius of 0.4 mm and allowing the bubble size to drift (grow) throughout the experiment. PBS experiments were repeated a total of six times for each surfactant formulation, and gave reproducible results. The trends reported for both static and dynamic adsorption experiments were consistent with all repeated experiments for each surfactant formulation.

3.3 Results and discussion

3.3.1 Comparison of the surface-active behavior of three synthetic lipid formulations used as mimics of the non-protein portion of lung surfactant

3.3.1.1 Composition and efficacy of each lipid formulation

The surface-active behavior of SP mimics can vary greatly with lipid composition, and therefore SP mimics have been characterized in a multitude of different lipid formulations, including pure monolayers of DPPC [35, 120], dipalmitoyl phosphatidylglycerol (DPPG) [35, 121], and PA [22]. Since SP-C is cationic and is thought to interact with anionic PG head groups [38, 122, 123] and since DPPC is necessary for reaching low surface tensions, formulations

composed of both DPPC and POPG have also often been used for the surfactometry characterization of SPs and their mimics in lipid films [38, 124-128].

Tanaka *et al.* investigated 25 different surfactant formulations containing varying combinations of phospholipids (DPPC, PG, phosphatidylserine (PS), phosphatidylinositol (PI), phosphatidylethanolamine (PE), and sphingomyelin), fatty acids (PA, palmitoleic acid, stearic acid, or oleic acid), acylglycerols, and a lipid-bound protein isolated from lung surfactant [104]. Of these 25 formulations, they found three surfactant mixtures with good, apparently biomimetic, *in vitro* surface activities, all containing 68.6% DPPC, 22.2% PG or PS, 9.1% fatty acid (palmitic acid or stearic acid), and 0.9% protein [w/w]. Based on these results, a similar lipid formulation containing DPPC, POPG, and PA (68:22:9 [w/w], the so-called "Tanaka lipids" (TL)) has since been used widely to investigate the surface activity of SP mimics both *in vitro* and in animal models of RDS [53, 62, 112, 119, 129-134].

While the Tanaka lipids have been shown to facilitate the biomimetic functioning of surfactant protein replacements both *in vivo* and *in vitro*, this simple formulation has a composition that differs greatly from that of natural lung surfactant lipids. Most notably, the DPPC content of the Tanaka lipids (69%) is significantly higher than that of natural lung surfactant and also of successful, commercially available lung surfactant replacements such as Infasurf™ (55%) [117]. In addition, the inclusion of PA in Tanaka lipids is highly debated; while PA does not comprise a significant portion of natural lung surfactant lipids and increases the viscosity of the lipid film, it has been successfully included in effective clinical preparations and widely used for both *in vitro* and *in vivo* testing. Natural lung surfactant also contains other anionic phospholipids that are likely to interact with the cationic amino acid side chains of SP-B

and SP-C, such as PI, PE, and PS, as well as cholesterol, which is believed to contribute to fluidization of the lipid film [135-142]. Walther *et al.* recently investigated the surface activity of three lipid formulations, including (1) lipids isolated from lung lavage, (2) a more complex formulation designed to be the synthetic equivalent of the natural lung surfactant lipids, and (3) the Tanaka lipids, in combination with dimeric SP-B_{1-25} peptide both *in vitro* (captive bubble surfactometer) and *in vivo* (a rat washout model of RDS) [143]. Studies performed on the captive bubble surfactometer indicate that formulation (2), the synthetic lung lavage lipid formulation that more closely mimics the composition of natural lung lavage lipids, containing DPPC, DOPC, POPG, POPE, POPS, and cholesterol (16:10:3:1:3:2 [w/w]), reached a minimum surface tension similar to that of both natural lipids and the Tanaka lipids. In addition, studies in a rat model of RDS revealed higher oxygenation levels with the natural lipids or the synthetic lung lavage lipids than with the Tanaka lipids. Therefore, this synthetic lipid formulation that more closely mimics the composition of natural lung surfactant seems to show greater promise for *in vivo* use as part of a biomimetic lung surfactant replacement.

Here the surface activities of two SP-C mimics, peptide- and peptoid-based, were investigated in three different lipid formulations: "PCPG", composed of DPPC and POPG (7:3 [w/w]); "Tanaka lipids (TL)", composed of DPPC, POPG, and PA (68:22:9 [w/w]); and "synthetic Infasurf lipids (IL)", based on the composition of the lipid portion of natural lung surfactant [143] and composed of DPPC, POPC, POPG, POPE, POPS, and cholesterol (16:10:3:1:3:2 [w/w]). The *in vitro* surface activities of the three lipid formulations, with and without added SP-C mimics, were investigated using a Langmuir-Wilhelmy surface balance (LWSB), fluorescence microscopic (FM) imaging, and a pulsating bubble surfactometer (PBS).

3.3.1.2 Langmuir-Wilhelmy surface balance results

An LWSB is typically used to record surface pressure (Π) - molecular area (A) isotherms. Lipids are spread at the air-aqueous interface in the 2D gas-liquid coexistence region, at a high enough molecular area so that the lipid tails do not interact with one another and the surface pressure is essentially independent of molecular area. As the barriers are compressed, lipid tails begin to interact, entering the liquid expanded (LE) phase, and an increase in surface pressure is observed (referred to as lift-off). For natural lung surfactant, lift-off is expected to occur at a high molecular surface area (> 100 $Å^2$/molecule) [144]. As the barriers are further compressed, a coexistence of LE and liquid condensed (LC) phases is observed. A biomimetic plateau in the isotherm between 40 and 50 mN/m, which is thought to correspond to a 2D phase transition and/or the structured removal of material from the monolayer [144], is typically observed for effective lung surfactant formulations. Finally, at high surface pressures the solid phase is observed, and for biomimetic lung surfactant formulations, a collapse pressure near 70 mN/m is expected, which corresponds to a surface tension near 0 mN/m [144].

Π-A isotherms taken at 25 °C for the three lipid formulations with no SP mimic added (Figure 3.1A) reveal that TL exhibit a much later lift-off (~ 95 $Å^2$/molecule) than either PCPG or IL (~ 110 $Å^2$/molecule). This trend is also observed, though much less dramatically, at 37°C (Figure 3.1B), with a lift-off area of ~ 100 $Å^2$/molecule for TL, ~ 110 $Å^2$/molecule for PCPG, and ~ 120 for IL. All Π-A isotherms exhibit at least a small kink at ~ 55 mN/m at 25 °C, with more pronounced plateaus for TL and IL; at 37°C, all lipid formulations exhibit plateaus at ~ 50 mN/m. Finally, with the exception of IL at 37°C, collapse pressures are near 70 mN/m. Interestingly, at 37°C, the IL film exhibits a low collapse pressure, of approximately 55 mN/m.

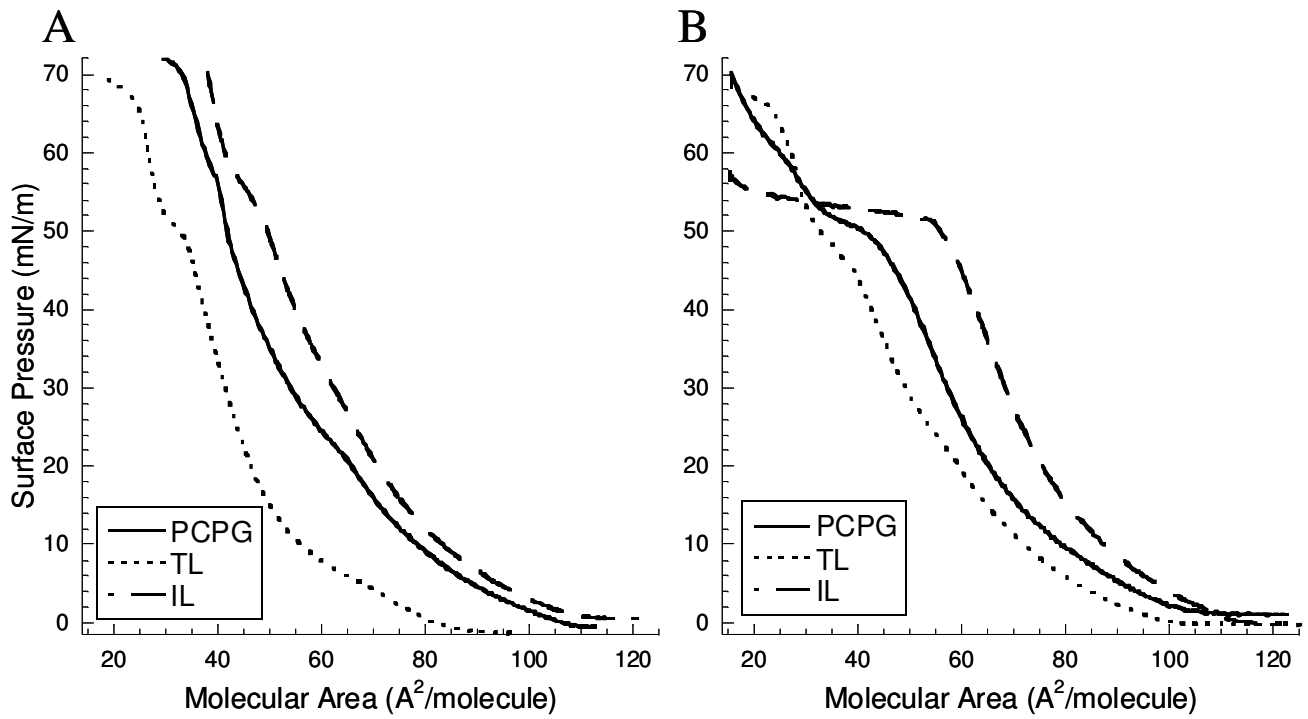

Figure 3.1: Surface pressure-surface area isotherms obtained using the Langmuir-Wilhelmy surface balance at 25 °C (A) and 37°C (B) for PCPG lipids, Tanaka lipids, and synthetic Infasurf lipids.

To our knowledge, this phenomenon has not previously been reported. While IL films have been previously studied, LWSB results were not reported by Walther *et al.* [143].
The later lift-off area observed with the TL film in comparison to those of PCPG and IL is likely due to the inclusion of PA in only the TL formulation. Because PA is a single-chain lipid with a small head group relative to DPPC or unsaturated phospholipids, it occupies less space in the monolayer and therefore it takes a greater degree of film compression for the lipid tails in the IL formulation to begin interacting with one another. Furthermore, IL contains more unsaturated lipids, which have kinked tails and take up more space in the monolayer, than either PCPG or TL (~ 49% for IL versus ~ 30% for PCPG and ~ 22% for TL), leading to lift-off at a higher molecular area for IL films. The inclusion of cholesterol in the IL formulation is known to fluidize lipid monolayers above the transition temperature (T_c), especially at higher surface pressures and temperatures [7]. This provides an explanation for why the IL lipid film is not able to reach high surface pressures, or to make the transition from the LE/LC phase to a solid phase without film collapse, once the temperature is elevated to 37°C.

3.3.1.3 Fluorescence microscopic imaging

The surface phase morphologies of the lipid films were observed using FM imaging in conjunction with the LWSB. FM images were obtained by spiking the samples prepared for LWSB studies with 0.5 mol% TR-DHPE. The bulky fluorescent tag is attached to the DHPE lipid head group, and resides predominantly in the LE phase, which appears as the bright regions in the images, while the probe excluded LC phase appears relatively dark. In all of the presented FM figures, the panels on the left (at lower surface pressure) depict films in that are either entirely (PCPG and IL) or predominantly (TL) in the LE phase, and which therefore are quite

bright in intensity. As surface pressure increases, the intensity of the fluorescent lipid in the LE phase typically decreases, and in the case of LC phases, the fluorescently labeled lipid is completely excluded from certain regions. As a result, the FM images on the right (at higher surface pressure) appear significantly darker overall, and when bright spots (termed 'vesicles' here) are present, the surrounding phases appear almost completely dark. In Figure 3.2, FM images are shown for PCPG (A-B), TL (C-D), and IL (E-F) films at 37°C, from a point on the isotherm just before the plateau, ~ 35 mN/m (left panels: A, C, E), and within the plateau, ~ 50 mN/m (right panels: B, D, F). At ~ 35 mN/m, no distinct LC domains are observed for either PCPG or IL, indicating that a fluid disordered LE phase is present, while dark LC domains are seen in the TL film. These domains in the TL film are consistent with the known DPPC:PA close packing that occurs in DPPC:PA and DPPC:POPG:PA films [119, 145]. The lipid-fatty acid interactions promote mixed crystalline condensed solid phases that form in the noncondensable fluid phase, which contains POPG. Thus, LC domains are observed in TL, but not PCPG, films [119, 145]. The IL film displays what appears to be a homogeneous fluid phase, though cholesterol is known to induce lipid-cholesterol short-range order almost independent of surface pressure over only a few molecules at a time [146]. At ~ 50 mN/m, some vesicle formation is observed for all of the lipid formulations (as evidenced by the appearance of small bright domains), and in the TL film, bright vesicle formations coexist with the dark LC domains. Interestingly, the fundamental phase morphologies at ~ 50 mN/m are very different for the three formulations. In the cases of both the PCPG and IL films, the vesicles are large and are likely forming below the monolayer [147], confirming that material is removed from the monolayer in the plateau region [148-150]. The TL film exhibits LC domains of about the same

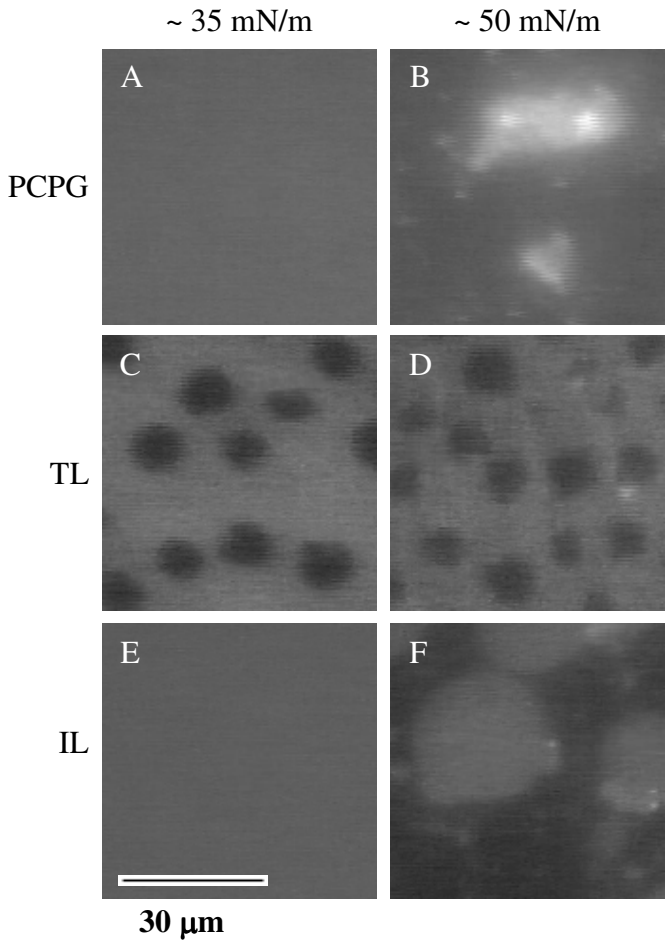

Figure 3.2: Fluorescent microscopic images of PCPG lipids (A, B), Tanaka lipids (C, D), and synthetic Infasurf lipids (E, F) at ~ 35 mN/m (A, C, E) and ~ 50 mN/m (B, D, F) on buffer at 37°C, collected with a barrier speed of 5 mm/min.

size as those observed at ~ 35 mN/m, but with several small vesicles (bright spots) interspersed throughout. The diverse but distinct phase morphologies and variations in bright vesicle size and shape observed in all three lipid formulations at high surface pressure (low surface tension) indicate that the mechanism through which material is removed from the interfacial lipid layer upon compression is probably different in each case.

3.3.1.4 Static bubble pulsating bubble surfactometry results

Static-bubble PBS experiments were performed to observe the kinetics of adsorption of the three surfactant formulations to the air-liquid interface of a bubble. Natural lung surfactant is expected to show a rapid decrease in surface tension on the PBS, reaching 25 mN/m within less than one minute of initial adsorption [27, 87]. The hydrophobic surfactant proteins are thought to play a significant role in enabling this fast adsorption. Not unexpectedly, the lipid formulations with no added SP mimics do not absorb rapidly to the interface, nor do they reach low equilibrium surface tensions (Figure 3.3A). After 20 minutes of adsorption, PCPG reaches an equilibrium surface tension of ~ 55 mN/m, TL ~ 46 mN/m, and IL ~ 55 mN/m. The lower equilibrium surface tension reached by the TL film versus the PCPG film is likely due to a higher fluidity of the TL film caused by the presence of PA, which occupies a smaller molecular area in the monolayer than DPPC or POPG. The higher surface tension obtained with the IL film may be attributed, in part, to the highly ordered phases that cholesterol induces at low surface pressures, which can preclude lipid adsorption to the interface in certain regions. Although the role of cholesterol in the surface-active behavior of lipid films is not well understood, it is known to be partially immiscible with phospholipids, depending on the T_c and the phase of the lipids,

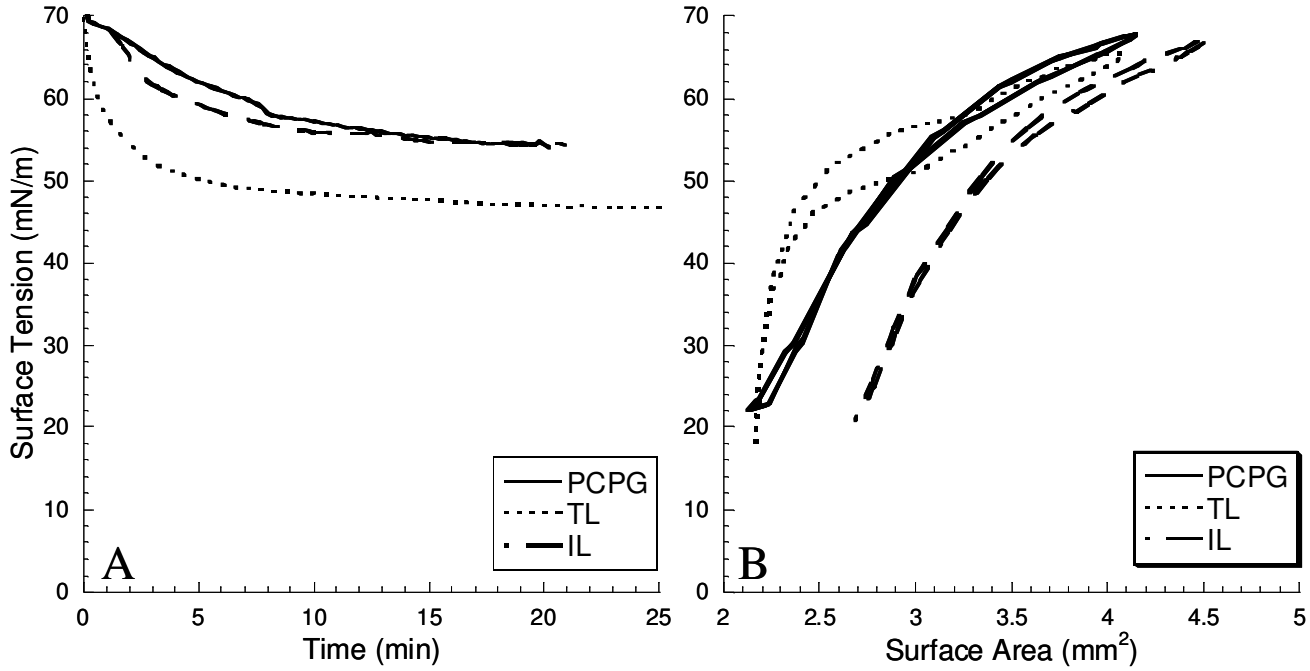

Figure 3.3: Static bubble (A) and dynamic bubble (B) adsorption results from the pulsating bubble surfactometer in buffer at 37°C for PCPG lipids, Tanaka lipids, and synthetic Infasurf lipids. Dynamic data were collected at 20 cycles/min and loop directions are clockwise.

and may either fluidize or rigidify the monolayer as a result [7, 146]. The overall effect on biophysical activity is still under investigation.

3.3.1.5 Dynamic bubble pulsating bubble surfactometry results

Surface tension (γ) vs. surface area (A) data loops may be collected by running the PBS in the dynamic-bubble mode, with a cycling rate similar to that for adult respiration (20 cycles/min). The γ-A loop for natural lung surfactant containing SPs is expected to exhibit a maximum surface tension (γ_{max}) of about 35 mN/m and a minimum surface tension (γ_{min}) near zero, with near-zero surface tension reached after a small amount of compression [27, 87]. The γ-A loops obtained using the modified PBS for PCPG, TL, and IL are shown in Figure 3.3B. As expected, both γ_{max} and γ_{min} for all formulations are significantly higher than what is typically observed for natural lung surfactant (with γ_{max} ~ 65 mN/m and γ_{min} ~ 20 mN/m for all three lipid formulations), and do not differ greatly from one another. In addition, no appreciable hysteresis in any of the data loops was observed. Interestingly, although the composition of the PCPG and IL films is drastically different, these loops are nearly identical. Furthermore, the addition of one component (PA) to a PCPG film (*i.e.* the TL film) does result in a slightly lower γ_{max} and γ_{min}, and a significantly different loop shape. The slope upon expansion of the TL film is quite steep, indicating that the elasticity of the film is increased with the presence of PA. This is not the case for either the PCPG or IL films, which have substantially lower apparent film elasticities [82].

Though definitive correlations between LWSB and PBS data have not yet been established, it seems that the *in vitro* quasi-equilibrium (LWSB), as well as the adsorptive and dynamic (PBS) surface-active behaviors of all three lipid formulations are similar, with TL film showing the most unique surface-active behavior. The most apparent differences of TL from IL

or PCPG in the current *in vitro* testing are in the lipid phase formation and general elasticity and respreadability of the lipid film. However, no specific data would predict poor *in vivo* efficacy in the lung for TL *vs.* IL or PCPG. To further investigate the overall adsorption, respreading, and phase formation of the different lipid mixtures in an *in vitro* setting, their surface-active behaviors were characterized in the presence of SP-B and SP-C peptide and peptoid mimics using the same *in vitro* techniques.

3.3.2 *In vitro* surface-active behaviors of peptide and peptoid mimics in various lipid formulations

3.3.2.1 Description of peptoid addition to lipid formulations

To investigate different lipid-lipid and lipid-peptide/peptoid interactions, experiments were performed with SP-$C_{F,F}$, or Peptoid C (Table 3.1) added to each of the three lipid formulations. SP-$C_{F,F}$ was added to each lipid formulation at 10 weight percent, similar to the total protein concentration in lung surfactant, while Peptoid C was added to the lipid formulations at the mole percentage equivalent to 10 weight percent of the SP-$C_{F,F}$ peptide (Table 3.2). The effect of varying the weight percentage of peptoid-based mimics (5%, 10%, and 20%) on the surface activity in a lipid film was also investigated [11]. It was found that at low weight percentages ($\leq$ 5%) the surface activity was inferior relative to 10%, while at high weight percent (20%) there was little change in activity over 10%. Surface activities were investigated using the LWSB, FM imaging, and the PBS. Although many separate features of LWSB and PBS data correlate to the unique behavior and physiological functions of natural lung surfactant, it is not yet conclusively known which of these properties are most important for biomedical efficacy. However, it is assumed that a formulation that closely emulates the *in vitro*

surface-active behaviors of natural lung surfactant is most likely to provide *in vivo* activity that is similar to that of natural lung surfactant.

3.3.2.2 Langmuir-Wilhelmy surface balance results

3.3.2.2.1 Effect of peptide or peptoid addition to PCPG films

Π-A isotherms obtained at 37°C reveal that when any of the mimics is added to any one of the lipid formulations, the lift-off area is increased and the resulting plateau (when applicable) is more pronounced (Figure 3.4). Similar results are observed at 25 °C (data not shown). An increase in lift-off area is expected for lipid formulations containing additional peptide or peptoid, as additives alter the available area per molecule, and presumably, the presence of surface-active SP mimics facilitates lipid-lipid and lipid-peptide/peptoid interactions, causing increased film organization and a subsequent surface pressure increase at a larger molecular area relative to the lipid mixture without added spreading agents. Since a plateau in the isotherm is thought to correspond to structural reorganization and material removal from the interface, a more pronounced plateau is considered desirable, as it mimics that of the natural lung surfactant film.

For the PCPG film at 37°C (lift-off area ~ 107 Å^2/molecule), the addition of either SP-$C_{F,F}$ or Peptoid C increases the lift-off area to ~ 120 Å^2/molecule (Figure 3.4A). Up to a surface pressure of ~ 45 mN/m, both the peptide and peptoid containing formulations are very similar to the lipid formulation, just shifted to a higher molecular area. At ~ 45 mN/m, the addition of the SP-$C_{F,F}$ peptide to PCPG results in a low film collapse pressure of ~ 50 mN/m, indicating that the film is not able to a stable solid phase. With Peptoid C added to the PCPG film, the biomimetic plateau region is more pronounced, which indicates a greater amount of structural

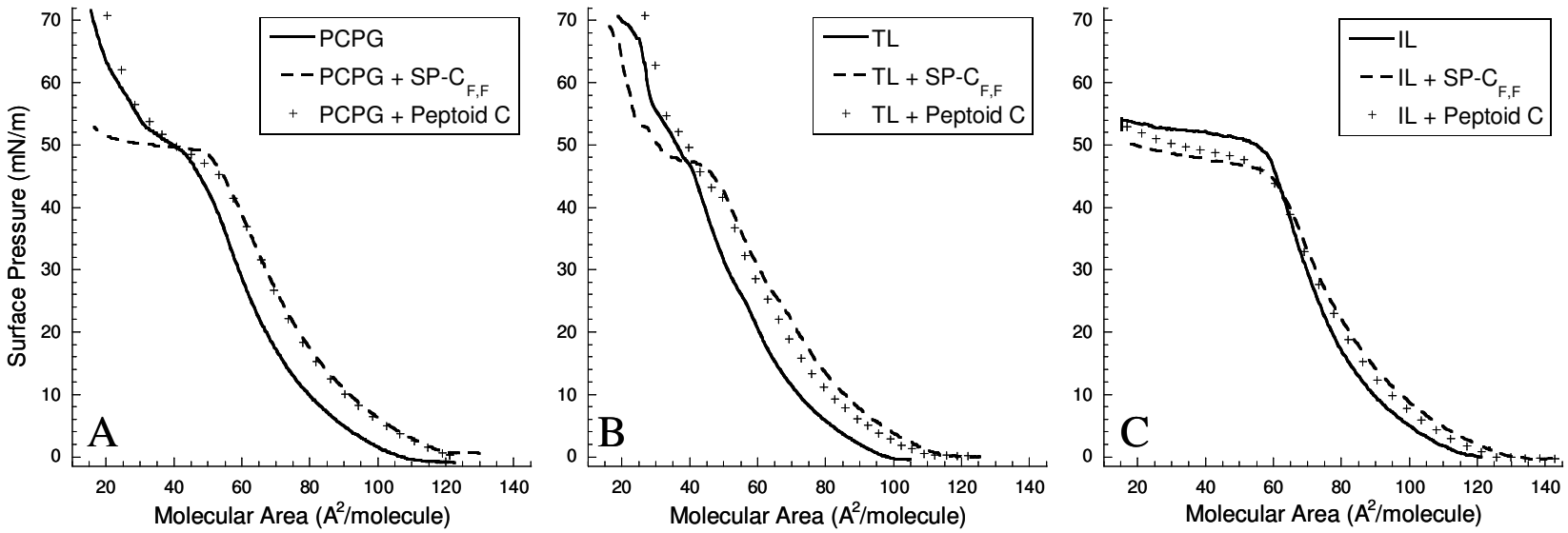

Figure 3.4: Surface pressure-surface area isotherms obtained using the Langmuir-Wilhelmy surface balance at 37°C for PCPG lipids (A), Tanaka lipids (B), and synthetic Infasurf lipids (C) along with added SP-C mimics. Molecular areas include both lipids and mimics.

rearrangement at this surface pressure. Past the plateau region, the PCPG film with and without Peptoid C is very similar, collapsing at a surface pressure ~ 70 mN/m.

3.3.2.2.2 Effect of peptide or peptoid addition to TL films

In the TL film, SP-$C_{F,F}$ exhibits a lift-off area of ~ 120 $Å^2$/molecule, and Peptoid C exhibits a lift-off area of ~ 115 $Å^2$/molecule, versus ~ 100 $Å^2$/molecule for the TL film without any additives (Figure 3.4B). The significant changes in lift-off area for peptides and peptoids in TL relative to the PCPG lipid mixture indicate that the area occupied by the added surface-active SP-C mimics at the interface is not the sole determinant for the increased lift-off area values. In all instances, the collapse pressure for the TL formulations is high (~ 70 mN/m) and a kink or plateau is observed between 45 and 50 mN/m, with more pronounced plateaus for the films with added SP-$C_{F,F}$. SP-$C_{F,F}$ in the TL film is also able to reach collapse at a high surface pressure, though there is only one lipid component difference between the TL and PCPG films (PA). Specific, electrostatic interactions between anionic PA and the cationic residues at positions 11 and 12 in SP-C_{FF} may play a role in stabilizing the film at higher surface pressures. In reaching a higher collapse pressure, an extended plateau region is observed, which is significantly different from all other plateau regions presented here. Amongst the TL films, the SP-$C_{F,F}$-containing film exhibits a slightly earlier lift-off area and a more pronounced plateau than the film containing the peptoid-based mimic, indicating overall better surface activity for the peptide, although the differences overall are relatively small.

3.3.2.2.3 Effect of peptide or peptoid addition to IL films

The lift-off area for the IL film is increased with the addition of the SP-C mimics (to ~ 135 $Å^2$/molecule for SP-$C_{F,F}$ and ~ 130 $Å^2$/molecule for Peptoid C (Figure 3.4C)). These lift-off

areas are significantly higher than those observed for either the PCPG or TL films, probably due to the higher concentrations of unsaturated lipids with bulky tails. It is again observed here, as in the PCPG and TL films, that the addition of the peptide SP-C mimic results in a slightly higher lift-off area than the presence of the peptoid SP-C mimic. However, as with the IL-only films, the IL films in the presence of SP mimics are still unable to reach high surface pressures, with a collapse pressure that is significantly lower (~ 50 mN/m), indicating that these films do not form stable LC phases. As previously mentioned, this early collapse is likely due to the tendency of cholesterol to create disordered, fluid phases at higher surface pressures [7]. As a result, all of the formulations exhibit extended plateau regions until the point of film collapse, at ~ 50 mN/m.

3.3.2.3 FM imaging results

To gain further insight into lipid phase transitions and general phase morphology, FM images were captured for these lipid-peptide/peptoid films. In Figure 3.5, FM images are shown for PCPG alone (A and B) and with added SP-$C_{F,F}$ (C and D), or Peptoid C (E and F) at 37°C from before the plateau, ~ 35 mN/m (A, C, E), and during the plateau, ~ 50 mN/m (B, D, F). FM images for TL and IL films without and with added mimics are similarly shown in Figures 3.6 and 3.7 respectively (panels labeled as described above). At ~ 35 mN/m, no LC domain formation is observed for any of the PCPG or IL formulations with the added SP mimics, while dark LC domains are observed for all of the TL formulations, as was observed for the lipid-only films (Figure 3.2). For PCPG and IL films, the addition of peptide or peptoid does not induce observable phase separation at this lower surface pressure. For TL films, both the size and

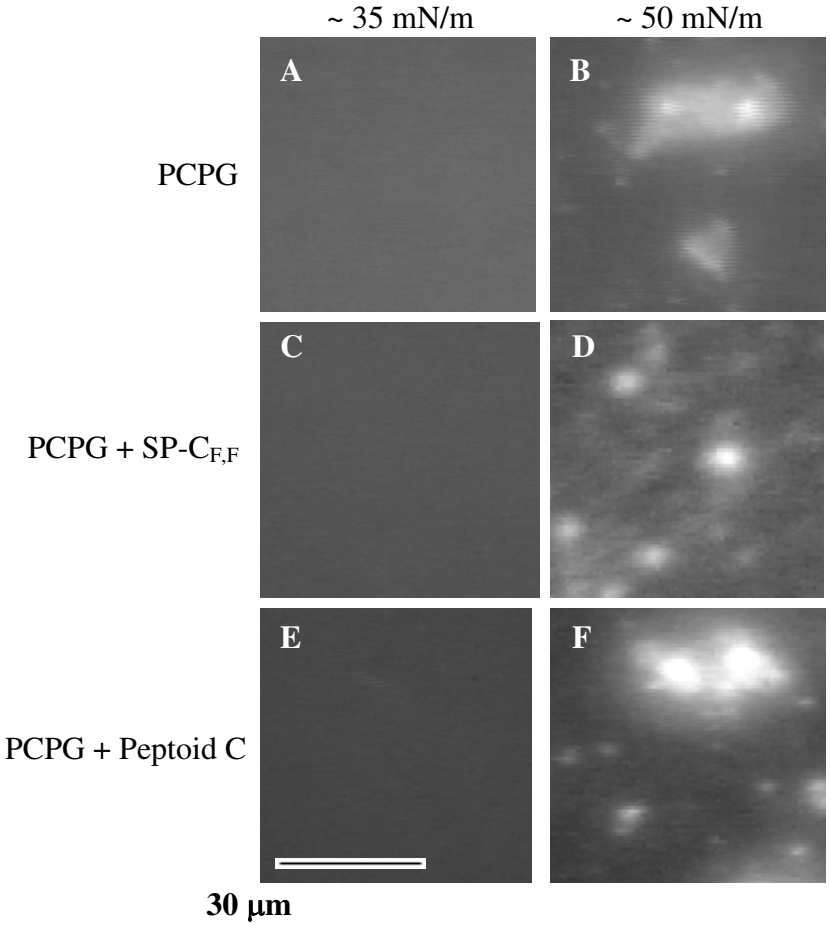

Figure 3.5: Fluorescent microscopic images for PCPG lipids (A and B), PCPG lipids with added SP-$C_{F,F}$ (C and D) and Peptoid C (E and F) on buffer at 37ºC, collected with a barrier speed of 5 mm/min. Images shown for Π ~ 35 mN/m (A, C, and E) and Π ~ 50 mN/m (B, D, and F).

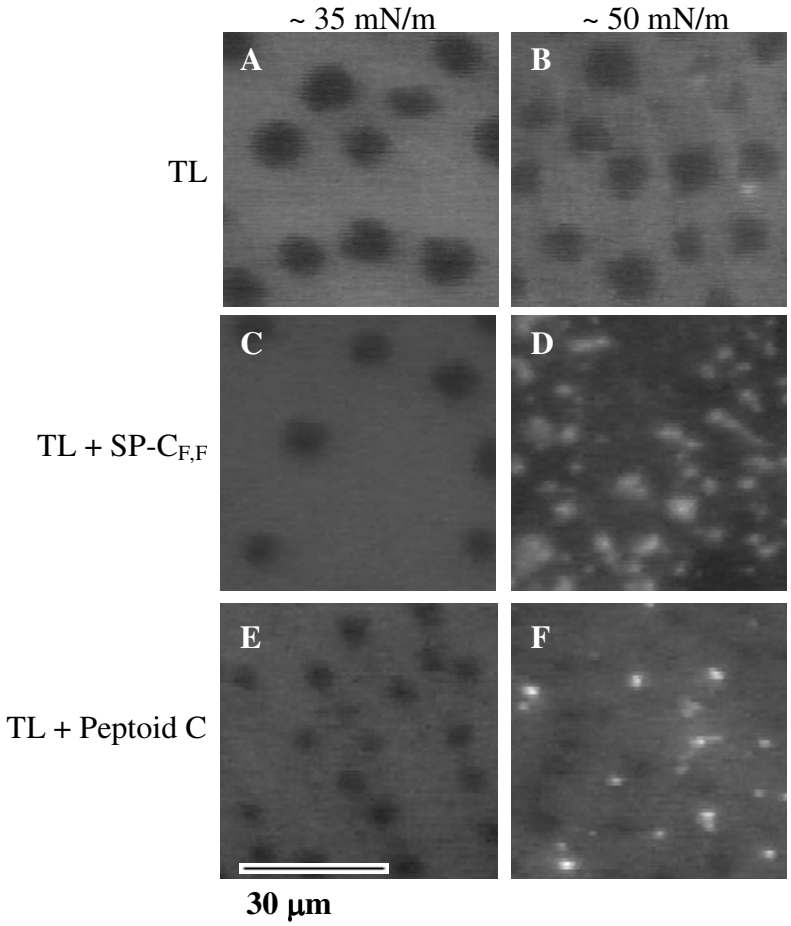

Figure 3.6: Fluorescent microscopic images for Tanaka lipids (A and B), Tanaka lipids with added SP-$C_{F,F}$ (C and D) and Peptoid C (E and F) on buffer at 37ºC, collected with a barrier speed of 5 mm/min. Images shown for Π ~ 35 mN/m (A, C, and E) and Π ~ 50 mN/m (B, D, and F).

spacing of the domains are similar for the films except that containing Peptoid C, which shows significantly smaller LC domains and a slightly tighter packing density. Thus, Peptoid C is able to affect lipid domain packing and density at lower surface pressures when compared to the other mimics, which is an indication of increased surface activity.

At ~ 50 mN/m, domain formation is observed for all of the films. Bright domains, indicative of vesicle formation, are observed for all of the PCPG films (Figure 3.5). The addition of SP-$C_{F,F}$ or Peptoid C results in the formation of bright vesicles. These types of domains are indicative of vesicle formation below the monolayer, which may point to a specific mechanism of material removal from the monolayer and submonolayer organization for each of these SP mimics [147]. Note that although the PCPG film with Peptoid C was able to reach collapse at a high surface pressure, the type of vesicle formation observed here is very similar to that of PCPG + SP-$C_{F,F}$ (Figures 3.5D and 3.5F). At ~ 50 mN/m dark LC domains are still observed for the TL films, although they may not be discernable in the presented FM images (Figure 3.6). However, for those films containing SP-C mimics, scattered small, bright vesicles are also observed. The Peptoid C containing film exhibits a significant amount of bright vesicles while the SP-$C_{F,F}$ film shows an even larger number, making it difficult to observe the dark LC domains. Note that the formation of very large vesicle domains is not observed in any TL films. The IL films possess phase morphology very similar to that of PCPG, where bright vesicle domains are observed at ~ 50 mN/m (Figure 3.7). The IL films containing the SP-C mimics also show large numbers of small bright vesicles.

Overall, the presence of SP-$C_{F\text{-}F}$ or Peptoid C in these films tends to result in numerous, smaller, bright vesicular domains. As SP-C has often been pointed to as the protein that anchors

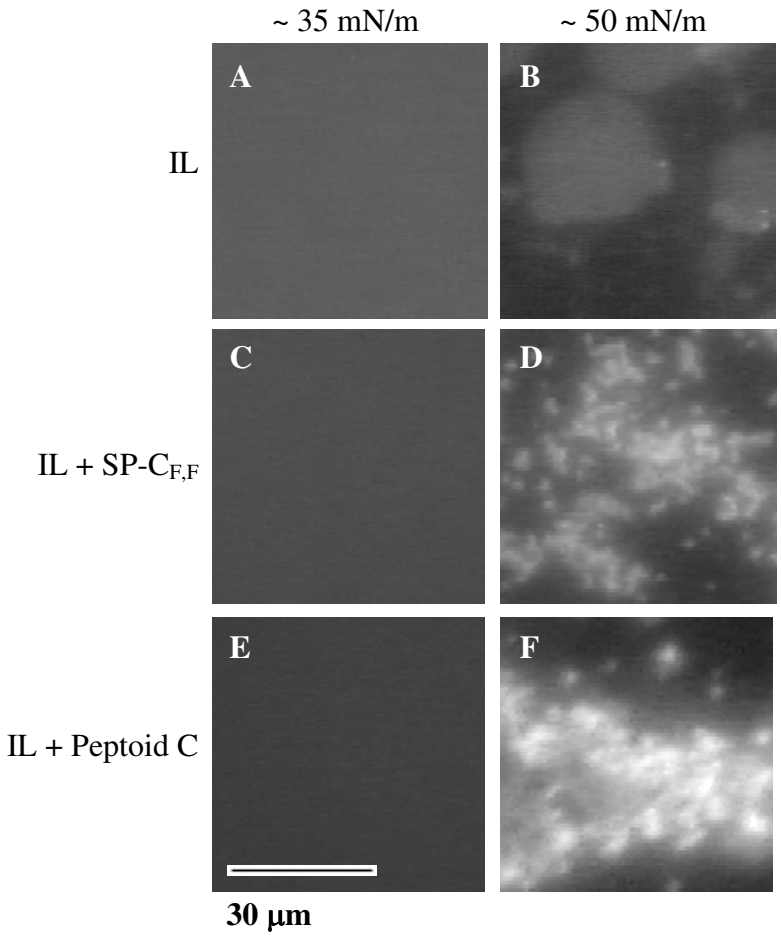

Figure 3.7: Fluorescent microscopic images for synthetic Infasurf lipids (A and B), synthetic Infasurf lipids with added SP-$C_{F,F}$ (C and D) and Peptoid C (E and F) on buffer at 37ºC, collected with a barrier speed of 5 mm/min. Images shown for Π ~ 35 mN/m (A, C, and E) and Π ~ 50 mN/m (B, D, and F).

lipids to the interface for easy incorporation upon film area expansion, it would be logical to hypothesize that it facilitates the formation of smaller vesicle domains for this reason. In general, the significance of the size, shape, and degree of vesicles formed during compression has not been extensively investigated, although their presence is the obvious result of lipid-lipid and lipid-peptide/peptoid interactions and overall structural reorganization at the interface as surface pressure increases and available film area becomes smaller [144].

Also notable is that, of the three lipid formulations, TL in the presence of any of the SP-C mimics consistently produces smaller bright domains when compared to the PCPG or IL mixtures. If vesicle domain size correlates inversely with enhanced elasticity or respreadability, it is expected that TL (the most elastic of the films) would produce smaller domains independent of the presence of SP-C mimics, which is what is observed. This phenomenon could explain why TL has up to this point been considered a very good *in vitro* mimic of the non-protein portion of lung surfactant, despite its reportedly poorer *in vivo* efficacy.

3.3.2.4 Static-bubble pulsating bubble surfactometry results

Static-bubble adsorption data collected using the PBS reveal a substantial increase in the surfactant adsorption rate and an enormous decrease in equilibrium surface tension values reached with the addition of the SP-C mimics to any of the lipid formulations (Figure 3.8). In a PCPG film (panel A), SP-$C_{F,F}$ inclusion leads to much more rapid adsorption to the interface with an equilibrium surface tension of ~ 25 mN/m reached in less than one minute. Peptoid C films also reach an equilibrium surface tension of ~ 25 mN/m, but requires nearly 10 minutes for complete adsorption. The greater number of hydrophobic amino acids in the peptide-based SP-C

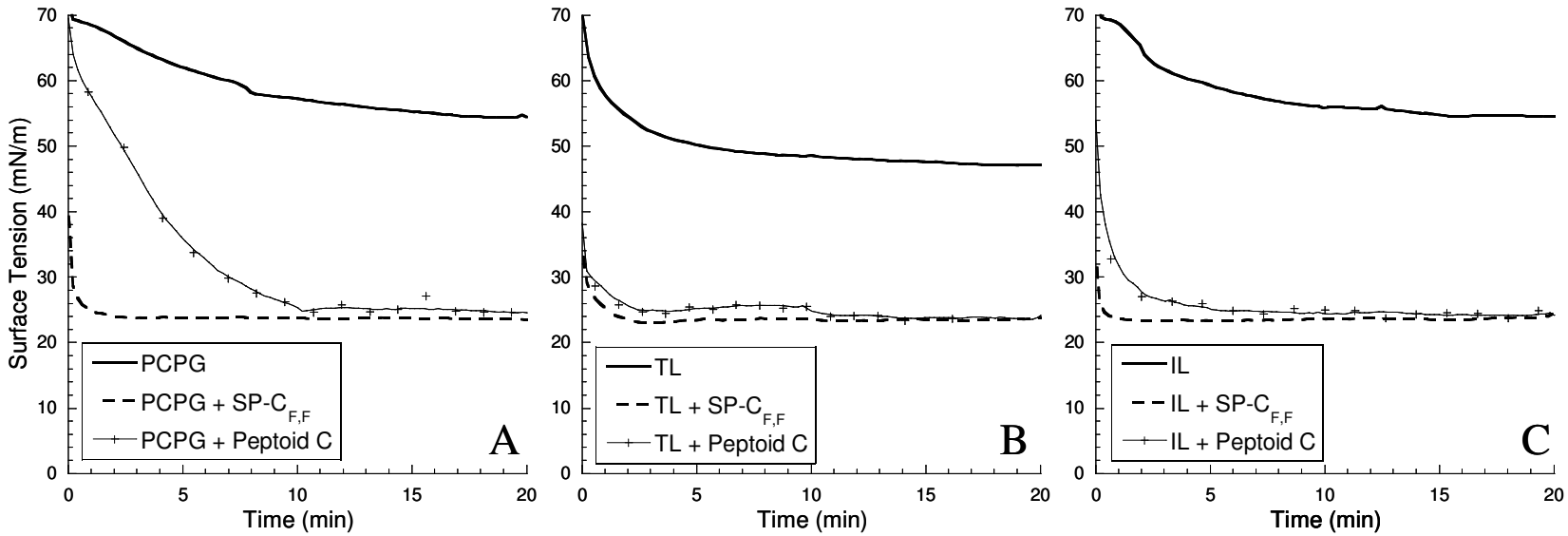

Figure 3.8: Static bubble adsorption results from the pulsating bubble surfactometer in buffer at 37°C for PCPG lipids (A), Tanaka lipids (B), and synthetic Infasurf lipids (C) along with added SP-C mimics.

mimic (relative to the shorter peptoid) may contribute to the faster adsorption kinetics observed with the peptide-containing film relative to those of the peptoid-containing film.

In TL (panel B), films containing either SP-$C_{F,F}$ or Peptoid C reach the low equilibrium surface tension of ~ 25 mN/m seen in PCPG films very rapidly, after only about 2 minutes. In IL (panels E and F), films containing SP-$C_{F,F}$ and Peptoid C again reached the desirably low equilibrium surface tension of ~ 25 mN/m, with an adsorption time of less than a minute for SP-$C_{F,F}$ and about 2 minutes for Peptoid C. Therefore, the presence of the SP-C mimics in all lipid films greatly reduces the equilibrium surface tensions reached during adsorption, to nearly that of natural lung surfactant (~ 25 mN/m). The values reached are consistent for both the peptide- and peptoid-based SP-C mimics. It is intriguing that though the respective equilibrium surface tensions reached for the different lipid films in the presence of each SP-C mimic are nearly the same, the relative rates of adsorption are different. These results point to the importance of carefully selecting both a good synthetic lipid mixture and good SP mimics (appropriately paired) for *in vivo* and *in vitro* testing. Overall, the *in vitro* performance of the TL formulation is best for the SP-C mimics studied based on these static-bubble adsorption data.

3.3.2.5 Dynamic-bubble results

Dynamic-bubble PBS experiments also reveal a substantial increase in biomimetic surfactant activity with the added SP-C mimics as expected, but the differences between the formulations are quite significant once again (Figure 3.9). For all SP-C mimic-containing films, a decrease in the maximum surface tension (γ_{max}) and an increase in data loop hysteresis are observed. However, the γ_{max} reached by films containing the peptide-based mimic are significantly lower than for films containing the peptoid-based mimic. In PCPG films (Figure

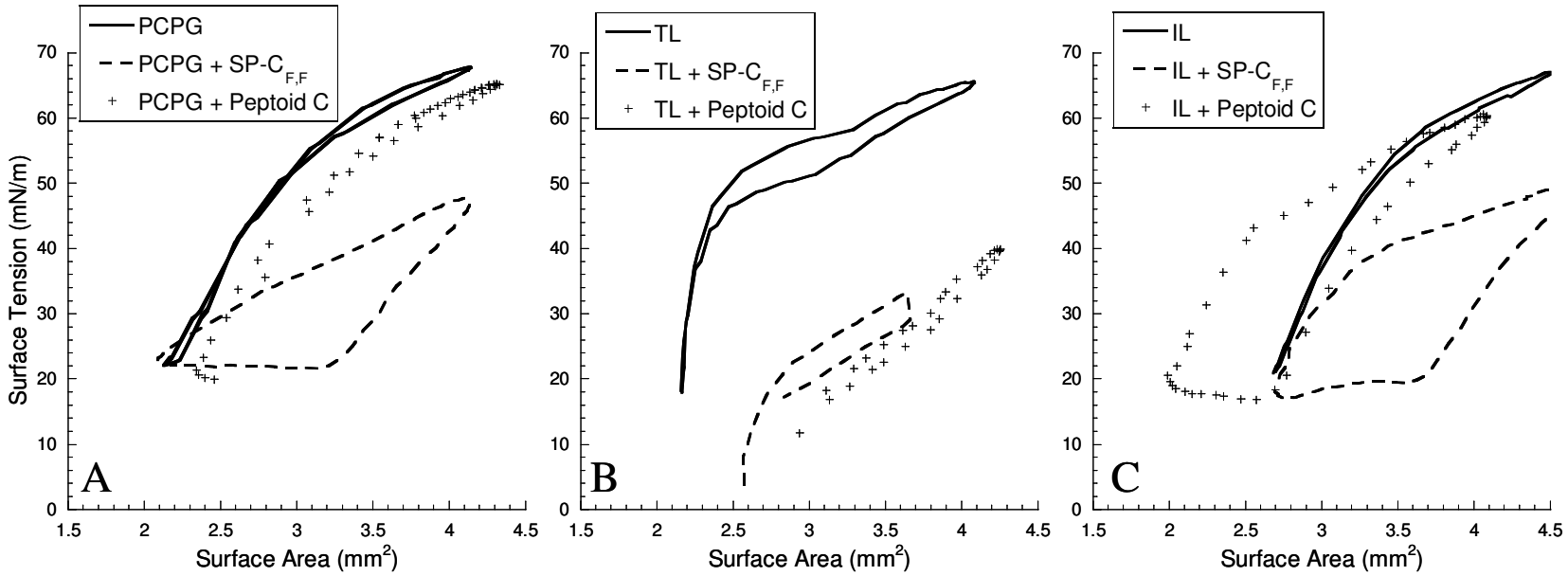

Figure 3.9: Dynamic bubble adsorption results from the pulsating bubble surfactometer in buffer at 37°C for PCPG lipids (A), Tanaka lipids (B), and synthetic Infasurf lipids (C) along with added SP-C mimics. Data were collected at 20 cycles/min and loop directions are clockwise.

3.9A) an increase in hysteresis at low surface areas is observed for films containing SP-$C_{F,F}$. High hysteresis at low surface tension corresponds to an ability to reach low surface tension with only a small amount of film area compression, similar to lung surfactant. Interestingly, Peptoid C-containing PCPG films show only a slight decrease in γ_{max} and very little increase in hysteresis at low surface tensions, and otherwise the shape of the data loop is very similar to the PCPG film containing no additives. This indicates that Peptoid C is not significantly enhancing the dynamic surface activity of this lipid film, which is surprising considering the experimental findings obtained with the LWSB and FM, as well as the static PBS results. Here, the overall dynamic *in vitro* performance of all the PCPG films is poor; films do not reach near-zero surface tensions upon compression with the added peptoid or the added peptide that is known to mimic the native protein fairly well.

The shape of the bubble loop significantly changes for both mimics in TL films as compared to PCPG films. In TL films (Figure 3.9B), γ_{max} is reduced to ~ 32 mN/m with added SP-$C_{F,F}$ and γ_{max} ~ 40 mN/m with added Peptoid C, as compared to ~ 65 mN/m for the pure lipid film. Peptoid C, which in PCPG films failed to enhance surface activity when compared to pure PCPG, shows a dramatic increase in surface activity in TL films, with γ_{max} values significantly lower than for all mimics but SP-$C_{F,F}$. Again, the PA component appears to have the pronounced effect of improving the surface activity of TL in the presence of SP-C mimics, relative to the surface activity of the mimics in PCPG films without PA. Additionally, the γ_{min} is decreased to nearly zero (as is desirable) for all SP-C mimic-containing TL films. Note that since for these formulations bubble shape greatly deforms from that of an ellipse at near-zero surface tensions, the image analysis system is not able to track a symmetrical bubble shape and calculate the

surface area nor surface tension of the bubble. However, it is clear that near-zero surface tensions are obtained in these instances because the pressure drop is very low and the bubble shapes are highly deformed. Note however that these low-surface tension data points are not shown on the plots; these low-γ data were omitted from the dynamic PBS plots for the TL/SP-$C_{F,F}$ and TL/Peptoid C films (Figure 3.9B). A general increase in data loop hysteresis is observed for films containing both SP-$C_{F,F}$, and Peptoid C, which is generally thought to be a good biomimetic feature.

In IL formulations (Figure 3.9C), γ_{max} is decreased and hysteresis is increased with added SP-C mimics, while γ_{min} remains approximately the same as the lipid-only film at ~ 20 mN/m. Similar to the PCPG and TL films, γ_{max} is decreased to a greater extent with SP-$C_{F,F}$ (~ 45 mN/m) than Peptoid C (~ 60 mN/m). Films containing SP-$C_{F,F}$ or Peptoid C show increased hysteresis at both high and low surface areas. However, like PCPG films, all the IL films fail to reach the near-zero surface tensions considered critical for efficacy of an lung surfactant formulation.

Based on the dynamic-bubble PBS results, it appears that only TL formulations with added SP-C mimics are able to reach near-zero minimum surface tensions upon film compression. However, IL formulations with added SP-C mimics tend to have a greater amount of hysteresis than the TL formulations, which is considered desirable in an lung surfactant formulation. The main difference between these lipid formulations is that TL contains PA and IL contains cholesterol. To greater elucidate the role and importance of these two different surfactant components, five additional lipid formulations were designed, in which cholesterol was either excluded from, or PA added to, the IL formulation. No significant differences in the

minimum surface tensions nor the extent of hysteresis in the PBS data loops were observed for these variant IL lipid formulations in combination with the peptoid analogue (data not shown). Hence, these compositional differences do not appear to be exclusively responsible for the unusual behavior of IL-based films. It could also be reasoned that the difference in unsaturated phospholipid content among the formulations influenced the amount of compression required to reach minimum surface tensions in the presence of the SP-C mimics. IL has significantly higher unsaturated phospholipid content than either PCPG or TL, and the increased extent of lipid acyl chain interactions with the SP-C mimics may promote more rapid changes in surface tension with small amounts of compression.

3.3.2.6 Notes on the surface-active behavior of DPPC-containing films at low surface tensions

Recent work by Gopal and Lee [151] has lent valuable insight into the collapse and low-surface-tension behaviors of DPPC-containing mixed lipid monolayers, which may be applied to the current investigation. Through the study of Langmuir isotherms and 2D bulk moduli of DPPC:PA and DPPC:DMPA mixtures with increasing mole fractions of DPPC (χ_{DPPC}) at 30 °C, it was determined that a sudden transition in collapse pressure (from 50-65 mN/m to 70+ mN/m) occurs in the range of 0.6 to 0.8 χ_{DPPC}, before which, the collapse pressures were < 60 mN/m. These data were further compared to that of DPPC:POPG:PA (TL) and DPPC: cholesterol mixtures, and very similar trends were observed [119, 151, 152]. A simple rigidity percolation treatment argument was applied to explain this phenomenon, and a quantitative explanation for the 'coincidental' widespread empirical use of 70% DPPC in lung surfactant replacement formulations for *in vitro* use was provided. Based on the χ_{DPPC} of the three lipid mixtures

studied here (0.71 χ_{DPPC} for PCPG, 0.60 χ_{DPPC} for TL, and 0.46 χ_{DPPC} for IL), the differences in collapse pressures on the LWSB may now be clearly explained. The χ_{DPPC} in IL (which also contains cholesterol) is lower than the 'key' range of 0.6-0.8 χ_{DPPC}, and therefore, a low collapse pressures (~ 55 mN/m) was observed in all IL-containing LWSB isotherms at higher temperature. As both PCPG and TL films are above the 0.6 χ_{DPPC} threshold for DPPC-containing lipid mixtures, collapse pressures > 70 mN/m (~ 2 mN/m surface tension) are reached. These results clearly support the work of Gopal and Lee. However, all three lipid formulations exhibit significantly elevated minimum surface tensions on the dynamic-bubble PBS (~ 20 mN/m), where a monolayer-only system no longer exists. Surprisingly, only the TL formulation reaches near-zero surface tensions in the presence of the SP-C mimics on the PBS. As the low surface tension/high surface pressure regime is believed to be of critical importance in designing and testing lung surfactant replacements containing SPs or their mimics, these differences in the interfacial behaviors of mono- vs. multilayer DPPC-containing lipid films will continue to be explored.

3.4 Conclusions

Previous work has shown that the addition of Peptoid C to TL improves the surface-active behavior of the lung surfactant replacement relative to what is observed for the lipids alone, and that both peptoid-based SP-C mimics show surface activities in TL that are similar to or in some ways better than that of their respective peptide analogues [61, 62]. Although peptoid-containing surfactant film properties compared well with those exhibited by the TL/peptide formulations, they are so far unable to achieve the exact performance exhibited by natural lung surfactant [27, 87]. In particular, dynamic-bubble PBS experiments revealed that

the TL/Peptoid B formulation was able to reach near-zero γ_{min}, but that γ_{max} was significantly higher than the 35 mN/m expected for natural lung surfactant [112]. In order to create a fully functional, synthetic lung surfactant replacement, the optimal lipid formulation must be further investigated; and most likely, better SP mimics will also need to be created.

In this paper, the *in vitro* surface behavior of peptide- and peptoid-based SP-C mimics were investigated in combination with three commonly used lung surfactant-mimetic lipid formulations: PCPG, TL, and IL. These lipid formulations are composed of different types of lipids, allowing the investigation of lipid-lipid and SP-C mimic/lipid interactions. Among the three lipid formulations, significantly different surface activities were observed. Although the lipid mixtures themselves do not exhibit drastic differences on the PBS, there are significant differences in the LWSB isotherms and FM images at higher surface pressures. The inability of the IL film to sustain high surface pressure/low surface tension at higher temperature would clearly inhibit us from obtaining information about added SP-C mimics in this region, which is non-ideal given that surface-active behavior in the low surface tension regime is considered critical for assessing *in vitro* efficacy. Additionally, although the film phase formation observed in this study *via* FM is not conclusively understood, the presence of dark LC domains in the TL film clearly sets its phase behavior apart from the other lipid mixtures. Previous work in our group has demonstrated that the average domain sizes change depending on the peptoid or peptide added, which may give indications regarding increased surface activity. The effect of this phase morphology on *in vivo* studies has not been definitively assessed, although TL has been reported to have overall poorer *in vivo* efficacy relative to the IL mixture [143].

Additionally, these studies have shown that lipid composition markedly affects the *in vitro* surface activities of the SP-C mimics added to the formulations. Specifically, combination of SP-C mimics with all lipid films results in a significantly higher lift-off. However, the PCPG and IL films are not always able to reach the desired high collapse pressures. While TL films form LC domains at both ~ 35 mN/m and ~ 50 mN/m, FM imaging of PCPG or IL films reveals no domain formation at ~ 35 mN/m and only vesicle formation at ~ 50 mN/m. Static-bubble PBS results indicate that though equilibrium surface tensions are similar for all lipid films with added mimics, the rate of adsorption can vary tremendously depending on lipid composition. Finally, dynamic bubble PBS results show that SP-C mimics in PCPG or IL films are not able to reach near-zero minimum surface tensions, while SP-C mimics in TL films are. However, IL films in particular are able to reach a minimum surface tension after a small amount of compression. Further investigation of lipid formulations containing varying amounts of cholesterol or PA in the IL film revealed little effect on the amount of hysteresis and the minimum surface tension.

None of these SP-C mimic/lipid formulations are able to precisely emulate the surface-active behavior of natural lung surfactant, however the TL formulation appears to be most promising for continued *in vitro* study and this is particularly the case for the peptoid-based SP mimics under development in our lab. While a more complex lipid formulation based on the lipid composition of Infasurf™ also showed some promising aspects, even with added SP-C mimics the collapse surface pressure as observed by LWSB is quite low (~ 50 mN/m) and the minimum surface tension as observed by dynamic-bubble PBS experiments is quite high (~ 20 mN/m). In terms of biomimetic characteristics, which must be seen with *in vitro* testing in order

to assess the functioning of added SP-C mimics, the TL lipid mixture is the only one to satisfy the requirement of reaching low dynamic surface tensions on both the LWSB and the PBS. Further experiments will be performed using *in vivo* animal models of RDS to study the efficacy of these formulations, and to shed further light on the relationship between these types of *in vitro* observations of surfactant behavior and the physiological functioning of surfactant replacements for the treatment of respiratory distress syndrome.

Chapter 4: Effects of hydrophobic helix length and side chain chemistry on biomimicry in peptoid analogues of surfactant protein C

Reproduced with the permission of Biochemistry, **2008**, 47, 1808-1818.
Copyright 2008, American Chemical Society.

The hydrophobic proteins of lung surfactant, SP-B and SP-C, are critical constituents of an effective surfactant replacement therapy for the treatment of respiratory distress syndrome. Due to concerns and difficulties associated with animal-derived surfactants, recent investigation has focused on the creation of synthetic analogues of the lung surfactant proteins. However, creating an accurate mimic of SP-C that retains its biophysical surface activity is extraordinarily challenging given the lipopeptide's extreme hydrophobicity and propensity to misfold and aggregate. One successful approach that overcomes these difficulties is the use of poly-*N*-substituted glycines, or "peptoids," to mimic SP-C. In order to develop a non-natural, bioactive mimic of SP-C and to investigate the effects of side chain chemistry and length of the helical, hydrophobic region, two classe of peptoid SP-C mimics were synthesized, purified, and characterized: those having a rigid, α-chiral, aromatic helix and those having a biomimetic, α-chiral, aliphatic helix. The length of the two classes of mimics was also systematically altered. Circular dichroism spectroscopy gives evidence that all of the peptoid-based mimics studied here emulate SP-C's secondary structure, forming stable, helical structures in solution. Langmuir-Wilhelmy surface balance, fluorescence microscopy, and pulsating bubble surfactometry experiments provide evidence that the aromatic-based SP-C peptoid mimics, in conjunction with a synthetic lipid mixture, have superior surface activity and biomimetic film morphology in

comparison to the aliphatic-based mimics, and that there is an increase in surface activity corresponding with increasing helical length.

4.1 Introduction

Lung surfactant is a complex mixture of lipids and proteins found at the air-water interface within the lungs that is required for proper respiration. This unique biomaterial functions to reduce and regulate surface tension within the alveoli during respiration, greatly diminishing the work of breathing and preventing alveolar collapse. No single constituent of lung surfactant is solely responsible for its unique dynamic surface behavior. Lung surfactant is composed of approximately 85-90% saturated and unsaturated phospholipids, 6-8% proteins, and 4-7% neutral lipids [7]. Saturated phospholipids such as dipalmitoyl phosphatidylcholine (DPPC), the main lipid component of lung surfactant, enable lung surfactant to reach very low minimum surface tensions upon dynamic compression. However, the molecular characteristics that allow DPPC and other saturated lipids to reach very low surface tensions, prevent them from rapidly readsorbing and respreading upon expansion. The inclusion of fluid, unsaturated phospholipids in lung surfactant provides better respreadability and slightly improved surfactant adsorption to the air-water interface, but results in an increase in minimum surface tension [9]. While the hydrophobic proteins of lung surfactant, SP-B and SP-C, represent only a small portion of lung surfactant, they are an essential component of lung surfactant and are necessary for the proper biophysical function of lung surfactant. The inclusion of SP-B and SP-C along with the phospholipid components greatly enhances surfactant adsorption, stability, and recycling of the lipid film, enabling proper respiration [65, 66].

An absence or a disruption of functional lung surfactant leads to the occurrence of two clinically relevant respiratory diseases: neonatal respiratory distress syndrome (nRDS) and acute respiratory distress syndrome (ARDS). nRDS arises from a deficiency of functional lung surfactant in premature infants due to a lack of mature alveolar type II cells in the epithelial lining of the lungs and is a leading cause of infant mortality [7]. ARDS, on the other hand, is a more complex disorder than nRDS, resulting from multiple pulmonary and nonpulmonary causes and occurs in both children and adults. While ARDS patients initially exhibit symptoms associated with the underlying disorder, they eventually display symptoms associated with respiratory failure due to inactivation or alterations of the native lung surfactant pool. Without properly functioning lung surfactant in either nRDS or ARDS, lung compliance is reduced and respiration is greatly impaired, ultimately resulting in alveolar collapse and suffocation without treatment.

Currently there is no efficacious treatment for ARDS; however, nRDS is routinely treated by the administration of exogenous surfactant preparations into the lungs of premature infants. There are two main categories of exogenous surfactant replacement therapies (SRTs) currently used in the treatment of nRDS: synthetic formulations and natural, animal-derived formulations. Synthetic surfactants are protein-free formulations comprised of synthetic phospholipids and surface-active additives while natural surfactants consist of surfactant extracted from animal lungs by lavage or isolated from homogenized lung tissue. Natural surfactants show significantly improved efficacy over synthetic surfactants, likely due to the presence of the hydrophobic proteins, SP-B and SP-C [14]. Despite the good efficacy of natural surfactants, there are some drawbacks associated with their use [11]. Because natural surfactants are

extracted from animal lungs, there is a possibility of cross-species transfer of antigenic or infectious agents as well as high costs and batch-to-batch variability [73-76]. Additionally, the large amounts of surfactant material required for the treatment of ARDS are beyond current production potential. Therefore, there has been increasing interest in the development of a third category of SRT: biomimetic SRTs that utilize an entirely synthetic surfactant containing an accurate mimic of the hydrophobic protein portion of lung surfactant, which functions as well as the natural material while eliminating the concerns associated with animal-derived surfactants. The developments of lucinactant (Surfaxin), Venticute, and SP-C33 have shown promise as efficacious biomimetic SRTs; however, these novel surfactants are not yet clinically available; therefore, there still remains a tremendous opportunity for innovation in the development of lung surfactant replacements that are increasingly efficacious, cost-effective, and provide a long therapeutic window for the treatment of lung disorders [48, 52, 77].

SP-C is the smaller of the two hydrophobic lung surfactant proteins, at just 35 monomers in length, and is the only surfactant protein that is exclusively expressed in the lungs, lacking any known homologous proteins [153, 154]. The three-dimensional structure of human SP-C has been determined by 2D-NMR in an apolar solvent. SP-C is predominantly helical with an α-helix ~ 37 Å long, comprising residues 9-34 [29]. Within this region, residues 13-28 comprise a 23 Å-long, valyl-rich stretch of hydrophobic amino acids that closely matches the alkyl chain length of a DPPC bilayer. Polarized FT-IR spectroscopic studies have shown that the SP-C α-helix orients in a transbilayer orientation in a lipid bilayer, where the helical region interacts with lipid acyl chains [33]. Two adjacent, positively charged residues, lysine and arginine, at positions 11 and 12 interact with the anionic phospholipid head groups and promote surfactant

protein binding to the monolayer or bilayer by ionic interactions [34]. In human SP-C, cysteine residues at positions 5 and 6 are post-translationally modified with palmitoyl groups and are thought to be important; however, the extent of importance is debated in the literature [35, 37, 40, 89, 103]. In lung surfactant films, SP-C promotes phospholipid insertion into the air-liquid interface, and thereby enhances the rate of lipid adsorption as well as the respreading of the alveolar film upon inhalation [37, 38, 89, 90]. The presence of SP-C has also been shown to lower, to some extent, the minimum surface tension of various lipids, stabilize the surfactant film upon compression, and greatly increase the surface viscosity at low surface tensions [42, 89].

Due to its large number of nonpolar residues (> 70%) and the two palmitoyl chains, SP-C is the most hydrophobic naturally occurring mammalian protein known [7]. SP-C's extreme hydrophobicity coupled with its unstable secondary structure makes working with the natural protein extraordinarily difficult [43, 44, 91]. This difficulty has led to the development of synthetic and recombinant analogues of SP-C in order to reproduce the biophysical behavior of the natural protein while minimizing the tendency for aggregation or misfolding [50, 51, 92]. These analogues have offered many insights concerning the structure-activity relationships of SP-C, and researchers have identified several biomimetic polypeptide candidates for use with phospholipids in order to treat RDS [10]. Despite the advantages of these synthetic and recombinant SP-C peptide mimics over the native protein, these mimics still have inherent difficulties associated with them such as being difficult to synthesize in appreciable yield, arduous purification, and marginal stability.

Recent work in our laboratory has been aimed at the development of a new category of synthetic surfactant protein mimics utilizing poly-*N*-substituted glycines or "peptoids" [62, 112].

Peptoids have close structural similarity to peptides, but have their side chains appended to the amide nitrogens rather than to the α-carbons. This feature renders peptoids essentially invulnerable to protease degradation, making them more biostable than peptides [55]. Despite the achirality of the *N*-substituted glycine backbone and its lack of hydrogen bond donors, peptoids are able to adopt extraordinarily stable, chiral helices when substituted with α-chiral, sterically bulky side chains [59, 60, 116]. This ability to form stable helices makes peptoids an excellent candidate for mimicry of bioactive molecules that rely on helical structure for proper function, such as the hydrophobic proteins of lung surfactant.

A peptoid-based mimic of SP-C with a biomimetic sequence of side chains and a longitudinally amphipathic, helical secondary structure was shown to mimic many of the essential biophysical properties of SP-C when combined with a synthetic phospholipid formulation [62]. The peptoid-based surfactant formulation was able to reach a low equilibrium surface tension and to reduce and control surface tension as a function of surface area as observed by pulsating bubble surfactometry. The biomimetic formulation also exhibited film phase behavior and film morphology similar to that of a formulation containing a modified SP-C peptide analogue. Here the previous work is expanded by investigating the biophysical behavior of several peptoid-based mimics of SP-C by systematically varying the length and chemistry of the helical, hydrophobic region, which is critical to the function of the natural protein [63]. Two classes of mimics were created containing either α-chiral, aromatic- or α-chiral, aliphatic-based helices of either 8, 11, or 14 residues in length, in order to determine the side chain preference and the optimal helical length of a peptoid-based mimic of SP-C. The findings show that the incorporation of a rigid, aromatic helix in a peptoid mimic of SP-C provides surface activity

superior to a more biomimetic, aliphatic helix, indicating that it is more important to capture the extreme hydrophobicity and highly helical structure of SP-C rather than its exact side chain chemistry. An improvement in surface activity is observed that corresponds with longer helical length, suggesting that the optimal surface activity of these SP-C mimics is dependent on the presence of a helical, hydrophobic C-terminus that is 14 *N*spe monomers in length (~ 28 Å).

4.2 Materials and methods

4.2.1 Materials

Peptide and peptoid synthesis reagents were purchased from Applied Biosystems (Foster City, CA) and Sigma-Aldrich (Milwaukee, WI). Fmoc-protected amino acids, resins, and di-tert-butyl dicarbonate were purchased from NovaBiochem (San Diego, CA). The 2,2,5,7,8-pentamethylchroman-6-sulfonyl chloride (PMC) protecting group was purchased from Omega Chemical (Quebec, Canada). The primary amines and PA were purchased from Sigma-Aldrich in the highest purity available. All organic solvents used for sample synthesis, purification, and preparation were HPLC-grade or better and were purchased from Fisher Scientific (Pittsburgh, PA). The synthetic phospholipids DPPC and POPG were purchased from Avanti Polar Lipids (Alabaster, AL) and were used as received. Texas-Red® 1,2-dihexadecanoyl-*sn*-glycero-3-phosphoethanolamine, triethylammonium salt (TR-DHPE) was purchased from Molecular Probes (Eugene, OR).

4.2.2 Protein design and synthesis

Due to SP-C's extreme hydrophobicity and strong tendency to misfold and aggregate in the absence of phospholipids, a peptide analogue, SP-C_{Lff}, was synthesized in which all valine residues in positions 13-28 were replaced with leucines, and the palmitoylcysteines at positions 5

and 6 were replaced by phenylalanine residues (Table 4.1) [44, 50, 91, 155]. This peptide analogue is based upon the SP-C analogues developed by Nilsson et al. in which leucine residues replace the transmembrane valine residues for improved solubility and stability of the α-helical secondary structure and the recombinant mimic developed by Ikegami and Jobe where the palmitoylcysteines were replaced by phenylalanines [50, 92]. Both peptide mimics were shown to have favorable surface activity when combined with a biomimetic phospholipid formulation.

SP-C_{Lff} was synthesized on a 0.25 mmol scale on an Applied Biosystems 433A automated peptide synthesizer, using standard Fmoc chemistry, and a prederivatized Wang-Leu resin. Cleavage and deprotection of the peptide-resin was carried out by mixing with aqueous 90% TFA and necessary scavengers for 2 hours. The reaction mixture was then immediately filtered, diluted with isopropanol and water, frozen, and lyophilized to yield the crude peptide. The crude material was then redissolved in isopropanol.

The crude SP-C peptide was purified on a Waters reversed-phase HPLC system (Waters Corp., Milford, MA) with a Vydac C4 column (Vydac, Hesperia, CA,) with a linear gradient of 25-100% solvent B in solvent A over 50 min (solvent A = 0.1% TFA in water and solvent B = 0.1% TFA in isopropanol). The resulting fractions were lyophilized to remove excess solvent and trace amounts of TFA. The dried fractions were then reconstituted in TFA-free isopropanol and analyzed by analytical HPLC. Fractions, which were determined to be pure, were then combined and lyophilized at least twice more. The final purity of the peptide was determined by reversed-phase HPLC to be > 97%. Electrospray mass spectrometry confirmed the molar mass of the purified peptide to match that of the desired compound (3924 Da).

Table 4.1: Peptide and peptoid sequences.

Molecule	Sequence/Structure
SP-C_{Lff}	FGIPFFPVHLKRLLILLLLLLLLILLLILGALLMGL
Mimic 1-n n = 8, 11, 14	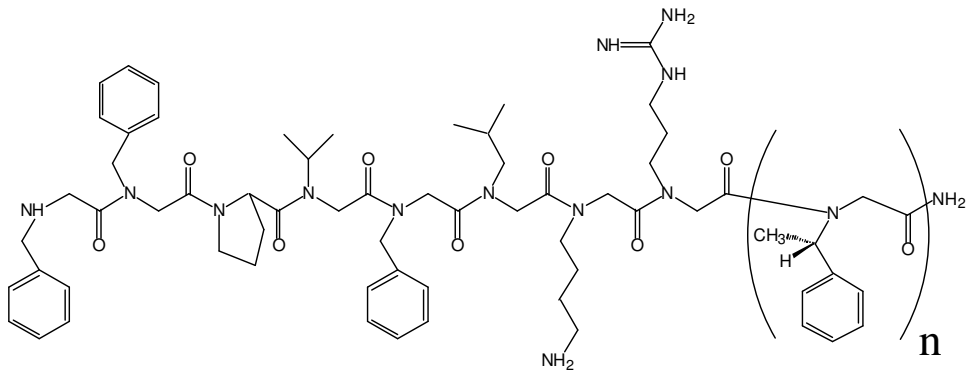
Mimic 2-n n = 8, 11, 14	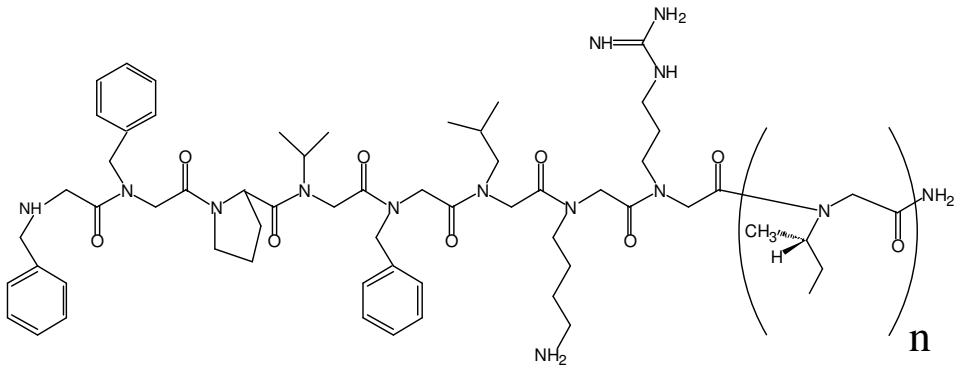

4.2.3 Peptoid synthesis

The peptoid-based SP-C mimics shown in Table 4.1 were synthesized on an automated 433A ABI Peptide Synthesizer (Foster City, CA) on solid support (Rink amide resin), following a two-step submonomer method as described by Zuckermann et al. [86]. Briefly, synthesis was carried out on 0.25 mmol Rink amide resin (NovaBiochem, San Diego, CA). After the removal of the first Fmoc protecting group from the resin with 20% piperidine in *N,N*-dimethylformamide (DMF) and rinsing of the resin with DMF, the monomer addition cycle was performed by first acetylating the resin with the addition of 1.2 M bromoacetic acid in DMF, followed by *N,N*-diisopropyl carbodiimide (DIC) in DMF. The acetylation step was carried out for 45 minutes and then the resin was washed with DMF. The resin-bound halogen was then displaced by 1.0 M primary amine submonomer in *N*-methylpyrrolidinone (NMP), which was added to the resin and allowed to react for 90 minutes. The two-step cycle was repeated until the desired length and sequence of the peptoid was obtained, except for the addition of the *N*lys, *N*arg, and proline residues. The displacement step for the PMC-protected *N*arg and Boc-protected *N*lys residues was extended to 120 minutes while for the addition of the proline residue, a PyBrop activating system was employed. After the proline addition, the Fmoc group was removed with piperidine as before and the peptoid cycle was continued.

Peptoid oligomers were cleaved from the resin and deprotected with 90% TFA along with necessary scavengers for either 15 minutes for Mimics 1-n or 40 minutes for Mimics 2-n (Table 4.1). The crude products were then purified by preparative HPLC on a Waters system with a Vydac C4 column and a linear gradient of 30-80% solvent C in solvent A over 70 minutes (solvent C = 0.1% TFA in isopropanol:acetonitrile, 1:1). The final purity of the peptoids was

confirmed by reversed-phase HPLC to be > 97%. Electrospray mass spectrometry was used to confirm correct molar masses.

4.2.4 Circular dichroism spectroscopy

CD measurements were performed on a Jasco model 715 spectropolarimeter (Easton, MD). Stock solutions for dilution to appropriate concentrations for CD were made immediately before analysis in tared 4.0-mL vials by precise weighing of added solvent and at least 2 mg of lyophilized peptoid powder, to produce a sample of accurately known concentration. The stock solutions were then diluted to CD sample concentration (~ 60 μM). CD spectra were acquired in a quartz cylindrical cell (Hellma model 121-QS, Forest Hills, NY) with a path length of 0.02 cm, employing a scan rate of 100 nm/min. CD spectra reported here represent the average of 40 successive spectral accumulations. Data are expressed in terms of per-residue molar ellipticity (deg cm^2/dmol), as calculated per mole of amide groups present and normalized by the molar concentration of peptoid. The α-helical content of the SP-C peptide, SP-C_{Lff}, was estimated using the graphical interface DICHROWEB employing the SELCON3 analysis program [156-158]. Repeat measurements were conducted approximately two months later and no significant changes in CD spectra were observed.

4.2.5 Langmuir-Wilhelmy surface balance and fluorescent microscopy

Surface pressure (Π)-area (*A*) isotherms were obtained using a home-built Langmuir-Wilhelmy surface balance as previously described [112]. For each experiment, the subphase was filled with a buffered suphase (0.15 M NaCl, 5 mM $CaCl_2$, and 10 mM HEPES at pH 6.90) and heated to either 25°C or 37°C. A Wilhelmy surface balance (Reigler & Kirstein, Berlin, Germany) was then calibrated and used to monitor the surface pressure as the area of the trough

was either expanded or compressed. The surfactant material in an organic solution was spread at the air-water interface using a syringe and allowed to equilibrate for 10 minutes. The barriers were then compressed at a rate of 30 mm/min. Determination of the surfactant respreadability was also performed for each formulation [7, 159].

In order to obtain fluorescence microscopic images, a Nikon MM40 compact microscope stand with a 100W mercury lamp (Tokyo, Japan) was used in conjunction with the Langmuir trough. Fluorescence was detected by a Dage-MTI three-chip color camera (Dage-MTI, Michigan City, IN) in conjunction with a generation II intensifier (Fryer, Huntley, IL). Samples were spiked with 0.5 mol% of a fluorescently labeled lipid, TR-DHPE, for detection. Previous studies have shown that inclusion of the labeled lipid at this concentration does not alter surfactant film morphology [119]. Experiments were performed on an aqueous buffered subphase at 37ºC with a barrier speed of 5 mm/min. The images were resized and enhanced in contrast and brightness within reasonable limits to make the features discernible for the purpose of display when warranted [147].

4.2.6 Pulsating bubble surfactometer

Static and dynamic characterization of surfactant film properties were performed on a modified PBS (General Transco, Largo, FL) as described by Seurynck et al. in which an imaging system is employed to accurately track bubble size and shape throughout the experiment [27]. Briefly, the lipid mixture (DPPC:POPG:PA, 68:22:9 (by weight)) was dissolved in chloroform:methanol (3:1) and spiked with 1.6 mol% SP-C mimic, analogous to 10 wt% SP-C peptide [104]. The samples were prepared in Eppendorf tubes, dried under vacuum, and resuspended at room temperature in an aqueous buffer solution (0.15 M NaCl, 5 mM $CaCl_2$, and

10 mM HEPES at pH 6.90) to a phospholipid concentration of 1.0 mg/mL. Samples were then mixed with a pipette 20 times, sonicated with a probe sonicator for 15 seconds twice, and then mixed again 20 times with a pipette. Samples were then loaded into the sample chamber using a modified leak-free methodology [26]. The sample chamber was placed in the PBS at a temperature of 37°C. A bubble with a radius of 0.4 mm was then formed and an imaging acquisition system was used to determine the bubble size. Trans-film bubble pressure was recorded as a function of time while holding bubble radius static for 20 minutes during static adsorption experiments. Dynamic measurements of surface tension as a function of bubble surface area were subsequently collected by cycling the bubble radius between approximately 0.4 mm and 0.55 mm at an oscillation frequency of 20 cycles/min for 10 minutes.

4.3 Results and discussion

4.3.1 Peptoid design and rationale

Our previous work with a peptoid-based mimic of SP-C utilized similar design strategies to those that have been employed in the design of peptide-based SP-C analogues. Specifically, the peptoid mimic was designed to emulate essential features of SP-C, including extreme hydrophobicity, patterning of hydrophobic and polar residues, and highly helical structure. The peptoid-based mimic of SP-C used in those studies contained a helical, hydrophobic stretch composed of 14 α-chiral, aromatic (*N*spe) monomers and an achiral, amino-terminal stretch composed of 8 peptoid monomers with side chains analogous to those present in positions 5-12 of human SP-C. This mimic was shown to yield a helical secondary structure similar to that of an SP-C peptide as well as its surface activity when combined with a biomimetic phospholipid formulation despite the presence of a hydrophobic, aromatic helix[62]. This suggested that the

critical features of SP-C are its longitudinally amphipathicity and highly helical structure rather than the exact side chain chemistry. However, it was not known if the incorporation of a more biomimetic helical region utilizing aliphatic side chains, which are more similar to valine side chains of that predominate mammalian SP-C, in a peptoid mimic would have a beneficial impact on surface activity.

In this study, the effects of varying both the side chain chemistry and the length of the hydrophobic, helical region of a SP-C peptoid mimic were investigated. Two main categories of SP-C mimics were studied: those utilizing α-chiral, aromatic side chains (*N*spe) in the helical region (Mimics 1-n) and those utilizing α-chiral, aliphatic side chains (*N*ssb) in the helical region (Mimics 2-n). The length of the helical region of the mimics was also systematically varied in order to determine the effect of helix length on surface activity. The side chains and the sequences of the various peptoid mimics studied are shown in Table 4.1.

Sequences composed of *N*spe residues form extremely stable helices, an important feature in mimicking SP-C; however, the aromatic side chains have a very different structure than that present in the helix of mammalian SP-C, which is entirely aliphatic, consisting of valine, leucine, and isoleucine residues. Therefore, peptoid mimics incorporating more biomimetic side chains (*N*ssb) were investigated that also form stable right-handed helices of the same class [58]. While both classes of mimics form stable right-handed helices with three residues per turn, the α-chiral, aromatic side chains of *N*spe are able to adopt a tighter, more rigid secondary structure with a helical pitch of ~ 6.0 Å as opposed to ~ 6.7 Å per turn for aliphatic-based peptoid helices. Both classes of mimics were studied in order to gain greater insight into whether the helical stability or side chain biomimicry has a greater impact on its

surface activity in a lipid environment. In addition to side chain chemistry, the specific length of the hydrophobic, helical region was also investigated by varying the number of α-chiral, helix-forming peptoid residues in this region in order to determine the minimal helical length of a SP-C peptoid mimic. Both classes of mimics were varied approximately one turn of the helix by incorporating 8, 11, and 14 helix inducing residues. A distinct advantage of both classes of peptoid mimics over the natural SP-C protein or peptide SP-C analogues is the absence of any observable aggregation over time in the absence of phospholipids.

4.3.2 Secondary structure

Circular dichroism (CD) was used to characterize and compare the secondary structure of the SP-C peptide and the various peptoid-based SP-C mimics. It has been previously shown that both a non-palmitoylated human-identical SP-C peptide and a dipalmitolyated peptide mimic of SP-C form predominantly α-helical structures as observed by CD [50, 96, 99, 100]. The highly helical nature of SP-C has been shown to be essential for its surfactant activity [63]. CD spectra of the modified SP-C peptide, as well as that of the peptoid-based SP-C mimics, are displayed in Figure 4.1. SP-C_{Lff} displays CD spectral features that are characteristic of an α-helix, consistent with previously published results, having an estimated α-helical content of 74% [96]. The peptoid-based SP-C mimics containing α-chiral, aromatic residues (*N*spe) exhibit CD features that are similar to the SP-C peptide, with each showing an intense maximum at λ ~ 192 nm and double minima at λ ~ 205 nm and ~ 220 nm (Figure 4.1A). These spectral features are characteristic signatures of a helical peptoid structure in oligomers of this class, with highly ordered backbone amide bonds [59]. The intensities of the helical spectrum for the aromatic-based mimics are very similar, with Mimic 1-14 (22mer) displaying the strongest intensity and

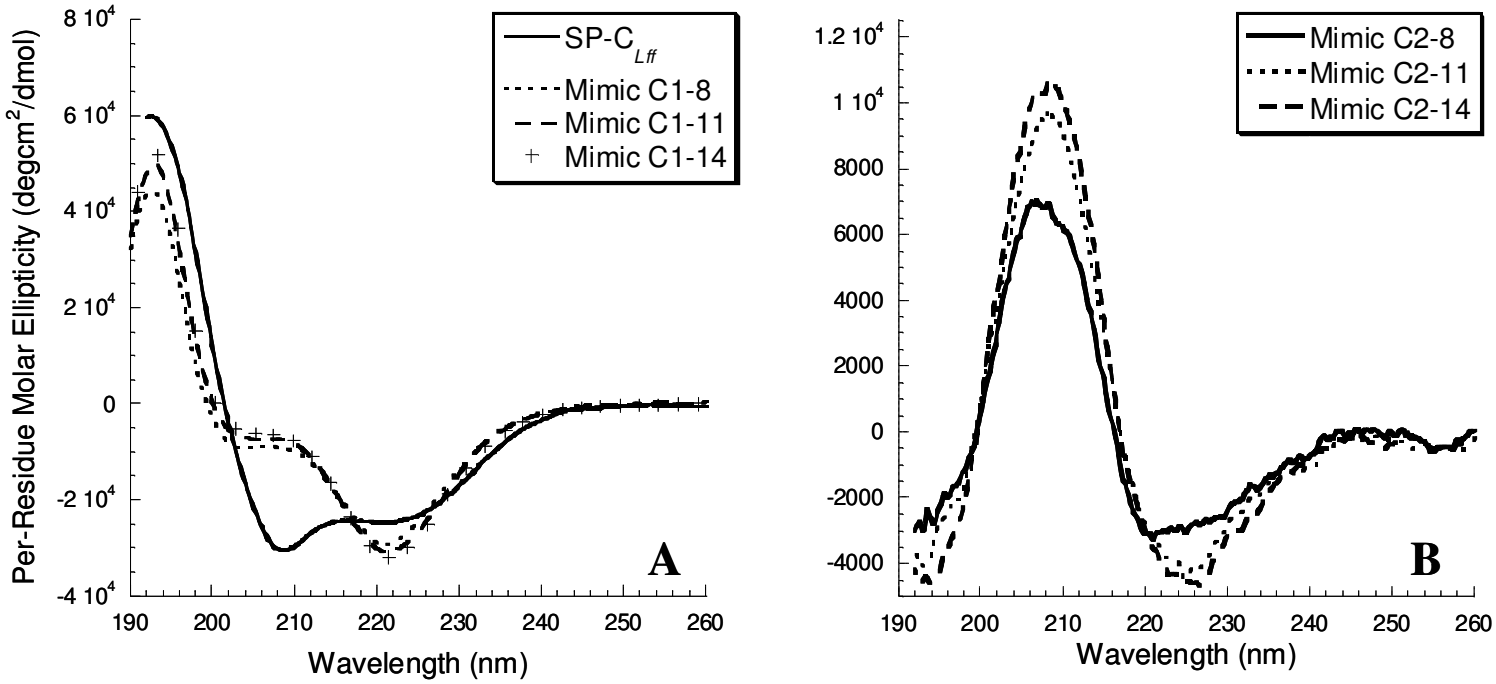

Figure 4.1: (A) Circular dichroism (CD) spectra of the SP-C_{Lff} peptide as well as of the varied-length *N*spe-based peptoid SP-C mimics (Mimics 1-8, 1-11, and 1-14), showing qualitatively similar features characteristic of peptide and peptoid helices, respectively; and (B) CD spectra of the varied-length *N*ssb-based peptoid SP-C mimics (Mimics 2-8, 2-11, and 2-14) displaying the characteristic features of polyproline type I peptide helices. Spectra were acquired in methanol at a conc entration of 60 μM, at room temperature.

that of Mimics 1-11 (19mer) and 1-8 (16mer) being only slightly weaker. The decrease in intensity of the helical signal coincides with a reduction in the length of the helical, hydrophobic stretch of the mimics, similar to what has been observed with other peptoid oligomers [160].

A different type of CD spectrum is observed for the peptoid SP-C mimics with α-chiral, aliphatic residues (*N*ssb) in the helical region (Figure 4.1B). These peptoid mimics exhibit CD spectral features that are similar to those characteristic of a polyproline type I peptide helix, but blue-shifted, which is characteristic of peptoids of this class [58, 161] Mimic 2-14 (22mer) displays the strongest CD intensity while Mimics 2-11 (19mer) and 2-8 (16mer) display progressively weaker CD signal intensities, similar to the aromatic-based mimics. Despite differences in the type of CD spectra observed for the various compounds, all of the SP-C mimics are shown to be helical and structured, satisfying one of the structural criteria, helicity, believed to be of importance for the surface activity of SP-C [63].

4.3.3 Langmuir-Wilhelmy surface balance studies

In order to determine the effect of the *N*spe- and *N*ssb-based SP-C peptoid mimics on the monolayer phase behavior of the lipid formulation, the mimics were combined at 1.6 mol% with an optimized lipid formulation comprised of DPPC:POPG:PA (68:22:9, by weight). This formulation has been shown to closely mimic the behaviors of the lipid portion of lung surfactant [104, 162]. While PA does not constitute a significant portion of natural lung surfactant, it has been successfully included in effective clinical preparations and is widely used for both *in vitro* and *in vivo* testing. The resulting formulations were studied on the LWSB as previously described. The Π-A isotherms for the lipid formulation alone and with SP-C_{Lff} at 25°C are

shown in Figure 4.2A and the *N*spe- and *N*ssb-based peptoid formulations are shown in Figures 4.2B and 4.2C, respectively.

The Π-A isotherm observed for lipids alone has a liftoff point (defined as the A where Π first increases) of ~ 90 $Å^2$/molecule. The slope of the Π−A isotherm is relatively small up to a Π of ~10 mN/m, indicating high compressibility typical of the LE phase. As the surface layer is further compressed from 10 mN/m to ~ 44 mN/m, the slope of the isotherm increases indicating a less compressible film and consistent with the formation of condensed domains of DPPC that are co-crystallizing with PA and co-existing with the LE phase [145, 163]. Further compression of the lipid film leads to a slight kink in the Π−A isotherm at ~ 44 mN/m and eventually a collapse pressure of ~ 70 mN/m. The addition of SP-C_{Lff} to the lipid mixture shifts the liftoff point to a greater molecular area (~ 108 $Å^2$/molecule vs. ~ 90 $Å^2$/molecule) indicating increased surface activity and an earlier transition to a LE state due to the presence of the SP-C peptide at the air-liquid interface. At low surface pressure, the Π−A isotherm is similar to lipids alone, only shifted towards higher molecular area. However, further compression results in the occurrence of a dramatic plateau region beginning at Π ~ 48 mN/m. The isotherm plateau is also observed for natural lung surfactant and is theorized to indicate a phase transition in the lipid film or the reversible removal of lipids and proteins from the monolayer, forming a surface-associated reservoir near the interface [149].

The presence of such a surfactant reservoir offers an explanation for how the SP-C protein is able to interact with lipids to provide low surface tension upon compression, and also to respread rapidly on expansion [149, 164]. A dramatic increase in surface viscosity is also observed for SP-C containing films at or above the plateau and is thought to help minimize the

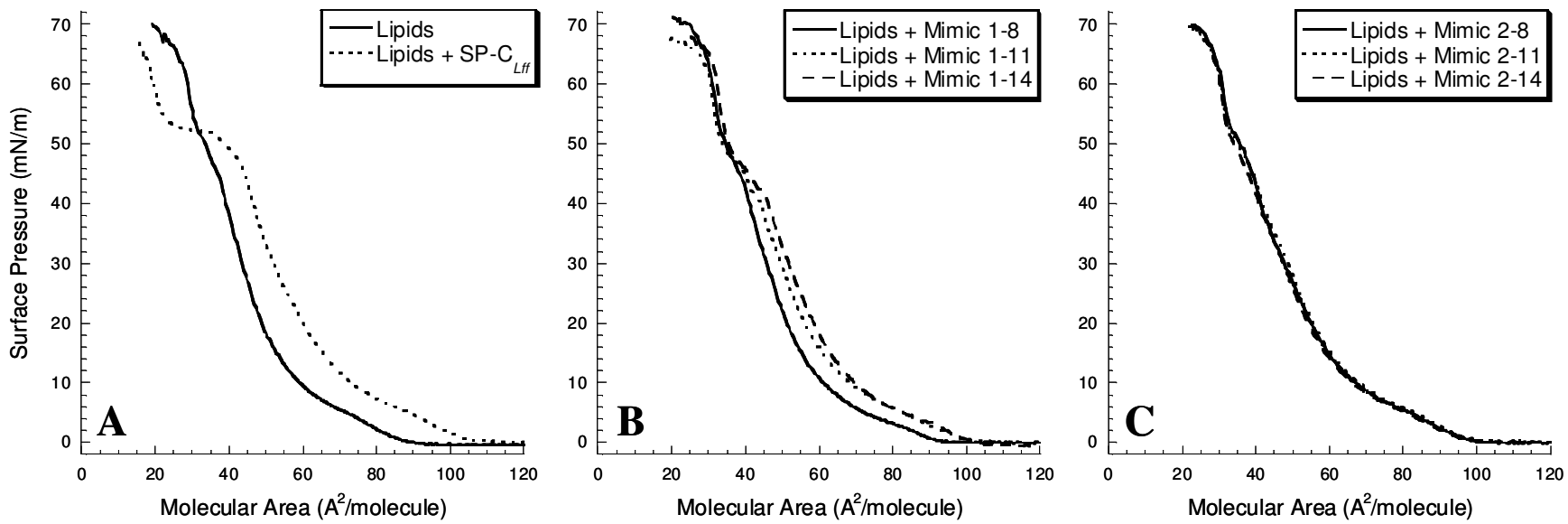

Figure 4.2: LWSB studies at 25°C (A) Π-A isotherms obtained for DPPC:POPG:PA (68:22:9, by weight) alone, and with 1.6 mol% SP-C_{Lff} peptide; (B) 1.6 mol% *N*spe-based peptoids (Mimics 1-8, 1-11, and 1-14) ; (C) 1.6 mol% *N*ssb-based peptoids (Mimics 2-8, 2-11, and 2-14). Isotherms were collected on a buffered subphase (150 mM NaCl, 10 mM HEPES, 5 mM $CaCl_2$, pH =6.90).

loss of surfactant material from the alveoli at low surface tensions, and is also partially responsible for the high collapse pressure associated with lung surfactant [42]. Further compression of the SP-C containing formulation leads to a high collapse pressure of ~ 70 mN/m.

The addition of Mimic 1-8 to the lipid formulation results in a Π-A profile very similar to that of the lipid mixture alone, with a very slight increase in lift-off to A ~ 95 $Å^2$/molecule compared to ~ 90 $Å^2$/molecule for the lipid system and a similar kink in the isotherm at Π ~ 44 mN/m (Figure 4.2B). Increasing the helical length from 8 to 11 *N*spe residues results in an additional increase in molecular area lift-off of ~ 105 $Å^2$/molecule and a slightly more pronounced kink/plateau in the isotherm beginning at Π ~ 42 mN/m. Further increase of the helical length to 14 residues, Mimic 1-14, results in a similar lift-off as the formulation containing Mimic 1-11 and with a Π–A isotherm that overlays Mimic 1-11 up to a Π of ~ 10 mN/m. Further compression of the Mimic 1-14 system past Π ~ 10 mN/m results in a surface layer that is slightly less compressible than the Mimic 1-11 system. At Π ~ 42 mN/m a biomimetic plateau is present in the Mimic 1-14 system, which occurs at the same Π as the Mimic 1-11 system, but is slightly more pronounced (although not as prominent as in the SP-C peptide system). These Π-A features make the formulation containing Mimic 1-14 the closest in monolayer phase behavior to the SP-C peptide system. Given SP-C's helical length, orientation in a lipid environment, and ability to catalyze the formation of lipid bilayers, it is reasonable that Mimic 1-14, which most closely approximates the helical length of SP-C, should have the most similar monolayer phase behavior as the SP-C peptide[41, 118].The addition of Mimic 2-8 to the lipid formulation results in an increase in the lift-off to ~ 100 $Å^2$/molecule with a very slight kink

in the isotherm that is similar to the lipid system (Figure 4.2C). Unlike the *N*spe-based mimics, further lengthening of the hydrophobic region does not improve the surface activity of the surfactant for the *N*ssb-based mimics. The addition of either Mimic 2-11 or Mimic 2-14 to the lipid system results in a similar lift-off of A ~ 100 $Å^2$/molecule and just a slight kink in the isotherm at Π ~ 48 mN/m. The isotherms for all of the *N*ssb-based mimics essentially overlay one another, suggesting a relative insensitivity to helical length in relation to surface activity and only a minor alteration of surface activity and lipid organization due to the presence of this class of mimics. It is possible that the less rigid *N*ssb-based helices are less efficient in forming the requisite three dimensional structures that normally coincide with an extended plateau region in the Π−A isotherm of lung surfactant.

In order to determine the respreadability of the surfactant films, the surface layers were compressed as before except that compression was continued approximately 10 Å/molecule past collapse. The surface films were then expanded and compressed to the same point. By comparing the ratio of the two collapse plateau regions of the Π-A isotherms, the relative respreadability was determined for each preparation [7, 159]. All surfactants with added peptoid-based SP-C analogues had similar respreadabilities, ~ 82%, which were superior to the lipids alone, ~73% (data not shown).

4.3.4 Fluorescence microscopy imaging of film morphology

To gain more detailed information about the interactions of the lipids and the SP-C mimics, the surface phase morphology of the surfactant films with and without SP-C_{Lff} and the longer length peptoid mimics, Mimics 1-14 and 2-14, were investigated. Figure 4.3 displays the FM images of the surfactant films at Π ~ 35 mN/m (panels A-D) and at Π ~ 50 mN/m (panels E-

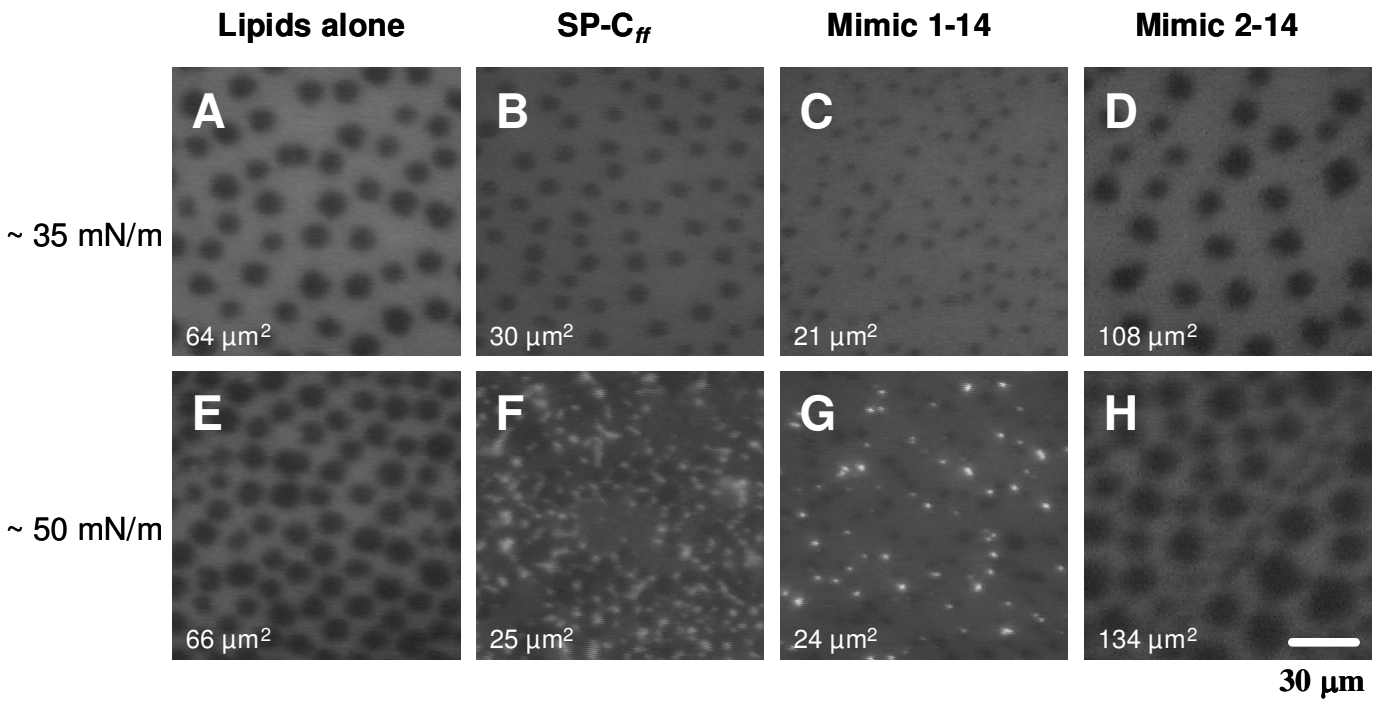

Figure 4.3: FM micrographs at 37°C corresponding to Π of ~ 35 mN/m and ~ 50 mN/m for DPPC:POPG:PA (68:22:9, by weight) alone (panels A and E), with 1.6 mol% SP-C_{Lff} peptide (panels B and F), with 1.6 mol% Mimic 1-14 (panels C and G), and with 1.6 mol% Mimic 2-14 (panels D and H). Average size of the dark LC domains for each film is indicated in the lower left of each panel.

H). The pure lipid system displays nucleation of the dark liquid condensed (LC) domains beginning at Π ~ 20 mN/m, and a continuous growth of larger, circular-shaped LC domains with increased compression (Figure 4.3, panel A and E). The coexistence of both LE and LC domains is a common feature of most lung surfactant formulations. This phase coexistence is important in controlling surface viscosity and film mechanical properties, promoting high collapse pressure. At a Π of ~ 35 mN/m, the lipid film exhibits circular LC domains of ~ 64 μm^2 that occupy ~ 23% of the total film area. This is similar to the morphology observed at Π ~ 50 mN/m, but with the appearance of a few small vesicles (bright spots) scattered throughout the film at the increased Π (Figure 4.3, panel E).

At ~ 35 mN/m, the film containing the SP-C peptide has a morphology similar to the lipids alone with the appearance of circular LC domains; however, the LC domains are significantly smaller, ~ 30 μm^2, and occupy approximately 15% of the film area. The LC domains for Mimic 1-14 are also smaller in size than the lipids alone, ~ 21 μm^2, and occupy only 10% of the film area (Figure 4.3, panels B, C, D). Adding Mimic 2-14 to the lipid film surprisingly results in larger LC domains, ~ 108 μm^2, that occupy roughly 23% of the film area. Increasing the surface pressure to ~ 50 mN/m, results in varied film morphology for the different surfactant formulations. The addition of SP-C_{Lff} to the lipid film results in nucleation of numerous bright vesicle domains or likely three dimensional protrusions throughout the film (Figure 4.3, panel F). The domains for the SP-C_{Lff} containing film remain approximately the same size and area as at the lower pressure. The lipid film containing Mimic 1-14 shows a similar film morphology and LC domain size to that of the SP-C_{Lff} film, although with less vesicle formation (Figure 4.3, panel G). Interestingly, the addition of Mimic 2-14 to the lipid

film results in a film morphology that is very similar to the "lipids–alone" film with minimal vesicle formation (Figure 4.3, panel H). The greater extent of biomimicry of the *N*spe-based formulation versus the *N*ssb-based formulation is consistent with the results of the LWSB experiments.

4.3.5 Static adsorption

One of the biophysical characteristics that is important to mimic with a lung surfactant replacement is the ability of natural lung surfactant to adsorb rapidly to an air-water interface, forming a surface-active layer [7, 10]. The adsorption kinetics of the lipid mixture alone, and with the addition of 1.6 mol% SP-C mimics, were characterized with a modified PBS run in static mode with a bubble radius of approximately 0.40 mm at 37°C. Figure 4.4 displays the adsorption surface tension (γ_{ads}) as a function of time for the various lipid formulations. In the absence of SP-C mimics, the lipid mixture displays very slow surface adsorption and fails to reach a γ_{ads} lower than 57 mN/m even after 20 minutes of static adsorption (natural, animal-derived lung surfactant reaches γ_{ads} ~ 20-25 mN/m within a few seconds) [165]. The addition of SP-C_{Lff} to the lipid formulation significantly accelerates the kinetics of lipid adsorption to the interface, allowing the film to reach a γ_{ads} of approximately 30 mN/m in just over one minute, with γ_{ads} dropping below 25 mN/m after 5 minutes. The addition of the shorter-length *N*spe-based mimic, Mimic 1-8, to the lipid formulation similarly results in accelerated adsorption kinetics over lipids alone, but the rate is slower and this formulation is only able to reach a γ_{ads} of ~ 37 mN/m after 20 minutes. The addition of Mimics 1-11 and 1-14 also improve the adsorption kinetics of the lipid film. An increase in adsorption kinetics is observed with increasing peptoid helix length. The formulation containing Mimic 1-14 is able to reach a γ_{ads} of ~ 30 mN/m after

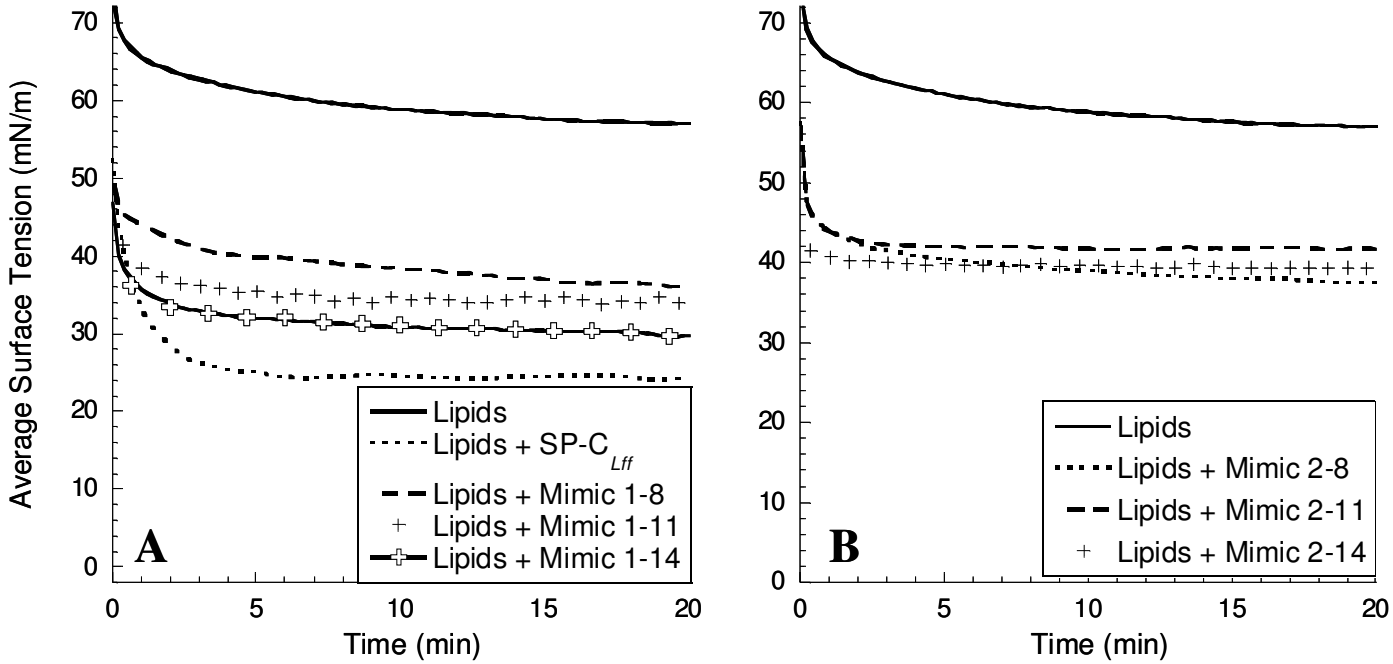

Figure 4.4: Static PBS results displaying surface tension as a function of time. Measurements were taken at a bulk surfactant concentration of 1 mg/mL lipids and at 37°C. (A) Lipid mixture alone and with 1.6 mol% SP-C_{Lff} and *N*spe-based peptoids (Mimics 1-8, 1-11, and 1-14); (B) Lipid mixture alone and with 1.6 mol% *N*ssb-based peptoids (Mimics 2-8, 2-11, and 2-14).

20 minutes and is most similar to the formulation containing the SP-C peptide, but still does not perform as well. The inclusion of Mimics 2-n in the lipid formulation also improves the adsorption to the interface over lipids alone; however, to a much lesser extent than the *N*spe-based mimics and, unlike Mimics 1-n, no improvement in adsorption is observed with increasing helical length. The *N*ssb-based mimic formulations only reach a γ_{ads} of ~ 40 mN/m after 20 minutes.

Based upon these results, the kinetic adsorption behavior of the surfactant is found to be enhanced with the addition of either class of peptoid mimics to the lipid formulation. However, the aromatic-based mimics are able to adsorb to lower surface tensions than the aliphatic-based mimics, suggesting that the greater hydrophobicity and structural rigidity of the aromatic helix is better able facilitate surfactant adsorption to the air-water interface. An improvement in adsorption corresponding to greater helical length is also observed with the aromatic-based mimics, suggesting that a minimum helical length of 14 *N*spe residues is required to mimic the adsorption behavior of SP-C_{Lff}.

4.3.6 Dynamic cycling

To investigate the effectiveness of the peptoid-based SP-C mimic formulations to reduce and control surface tension as a function of surface area, PBS experiments were performed in a dynamic mode at an oscillation frequency of 20 cycles/min and ~ 50% reduction in surface area. Features that are important in the compression-expansion loop for biomimetic surfactant film behavior include: (1) the ability to reach a very low surface tension with a small percentage of compression; (2) an ability to respread rapidly, and (3) an ability to control surface tension as a function of bubble surface area with the lowest minimum surface tension (γ_{min}) and lowest

maximum surface tension (γ_{max}) possible [7, 10]. Figure 4.5 displays the surface tension as a function of bubble surface area for lipid mixtures with and without the SP-C peptide (4.5A) and those containing Mimics 1-n (4.5B) and Mimics 2-n (4.5C). Key parameters of the dynamic compression cycles are also listed in Table 4.2.

The lipid mixture, when used alone, exhibits high γ_{min} and γ_{max} of ~ 12 mN/m and ~ 67 mN/m respectively. In addition, a surface tension below 20 mN/m for the lipid formulation is only reached with a significant degree of film compression, ~ 46% compression (Table 4.2). With these properties, this material would be inadequate as a lung surfactant replacement. The addition of SP-C_{Lff} to the lipid mixture dramatically improves the surface activity of the film relative to that of the lipids alone, as indicated by the significantly lower γ_{min} of < 1 mN/m and γ_{max} of ~ 51 mN/m (Figure 4.5A). The addition of SP-C_{Lff} to the lipid formulation also significantly decreases the compressibility of the surfactant, requiring much less compression, ~ 26%, to reach a γ below 20 mN/m.

The addition of Mimics 1-n to the lipid formulation results in surface behavior rather similar to that observed with the SP-C peptide formulation (Figure 4.5B). Mimics 1-8, 1-11 and 1-14 exhibit similar compression-expansion loops, all reaching a γ_{min} of < 1 mN/m upon compression. Not only is γ_{min} greatly reduced with the addition of the *N*spe-based mimics, but the amount of compression require to reach γ_{min} is also much less than for the lipids alone and is similar to the SP-C_{Lff} formulation (~ 31-34% compression). Upon expansion to the maximum surface area, these formulations obtained a γ_{max} that was also significantly lower than the lipid formulation and similar to the SP-C peptide (γ_{max} ~ 56 mN/m for Mimic 1-8 and ~ 53 mN/m for

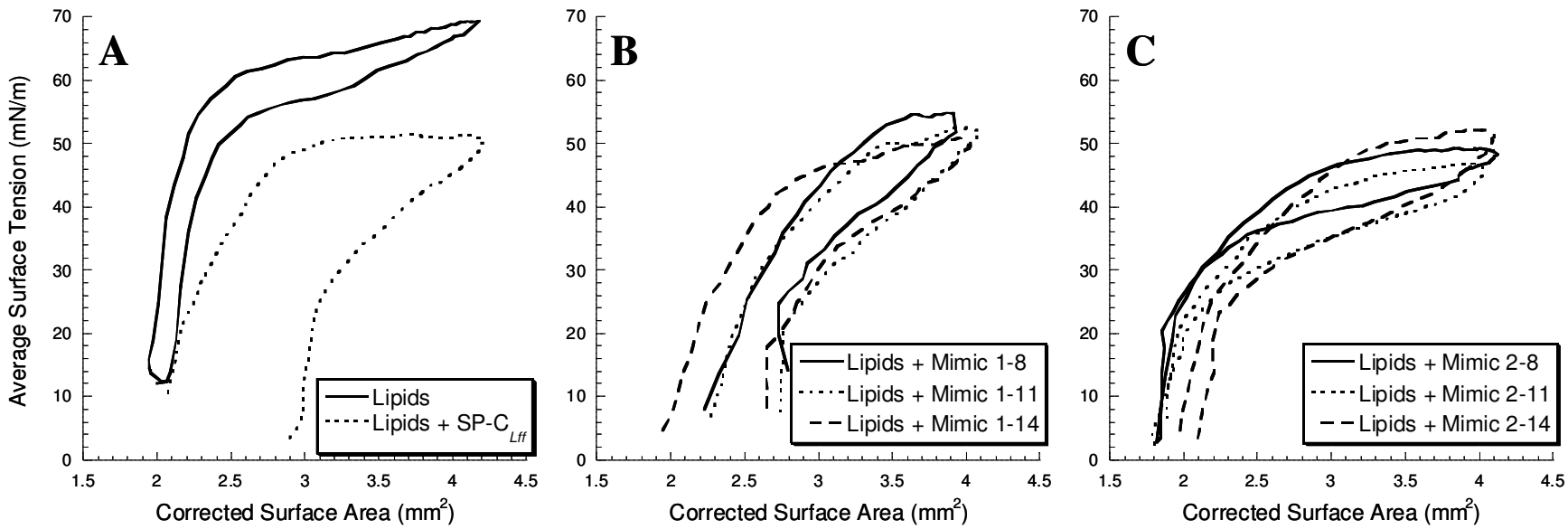

Figure 4.5: Dynamic PBS results displaying surface tension as a function of surface area at an oscillation frequency of 20 cycles/min, after 10 minutes of initial cycling. Measurements were taken at a bulk surfactant concentration of 1 mg/mL lipids and at 37°C. (A) Lipid mixture alone and with 1.6 mol% SP-C_{Lff}; (B) Lipid mixtures with 1.6 mol% *N*spe-based peptoids (Mimics 1-8, 1-11, and 1-14); (C) Lipid mixtures with 1.6 mol% *N*ssb-based peptoids (Mimics 2-8, 2-11, and 2-14).

Table 4.2: Dynamic pulsating bubble surfactometry (PBS) properties

Formulation	γ_{max} (mN/m)	γ_{min} (mN/m)*	Compression (%)†
Lipids	66.9 ± 2.12	11.6 ± 1.40	46.3 ± 3.17
Lipids + SP-C_{Lff}	51.3 ± 1.75	< 1	25.8 ± 2.67
Lipids + Mimic 1-8	55.5 ± 0.75	< 1	31.7 ± 1.71
Lipids + Mimic 1-11	53.3 ± 0.68	< 1	31.2 ± 1.54
Lipids + Mimic 1-14	52.9 ± 2.07	< 1	33.9 ± 4.14
Lipids + Mimic 2-8	49.7 ± 1.47	1.39 ± 2.05	55.3 ± 2.68
Lipids + Mimic 2-11	48.9 ± 1.56	< 1 ± 0.98	52.9 ± 3.15
Lipids + Mimic 2-14	51.2 ± 1.49	< 1	48.2 ± 1.78

Data are mean ± SD. * All experimental runs reached a γ_{min} less than 1 mN/m except for formulations comprised of lipids without any added SP-C analogue and those containing the shorter length *N*ssb-based analogues, Mimics 2-8 and 2-11. † Compression refers to the amount of compression necessary to reach a γ less than 20 mN/m.

Mimic 1-11 and Mimic 1-14). An increase in the amount of hysteresis in the compression expansion loop corresponding with increasing helical length was also observed in the aromatic mimics, which is indicative of the decreased compressibility and increased elasticity of the films containing the *N*spe-based analogues.

Compression-expansion loops obtained with lipid mixtures containing Mimics 2-n are shown in Figure 4.5C. These mimics also display enhanced surface activity in comparison to the "lipids-alone" mixture, with a significant reduction in both maximum and minimum surface tension values (γ_{max} ~ 49 to 51 mN/m and γ_{min} < 1 to just over 1 mN/m). Despite the improvement over lipids alone, none of the *N*ssb-based mimics were able to replicate the surface-activity of either the *N*spe-based mimics or the SP-C peptide. Specifically, all aliphatic-based formulations required significantly more compression to reach low surface tension values. Also observed was an elevated γ_{min} for the Mimic 2-8 containing formulation. Although the inclusion of the *N*ssb-based mimics provides an improvement over the surface activity observed for the lipids alone, it does so to a lesser extent than the corresponding *N*spe-based mimics. The reduced surface activity of the *N*ssb-based mimics is consistent with the static measurements of surface tension *vs.* time, which showed the aromatic-based mimics to have superior activity compared to the aliphatic-based mimics.

It is possible that the less rigid and slightly less hydrophobic *N*ssb-based helices are not able to associate as well with the lipid acyl chains as the *N*spe-based helices and, as a result, are not as efficient in the formation of lipid bilayers, yielding a more compressible surfactant film and a higher γ_{min}. This hypothesis is consistent with both the LWSB and the FM studies of the peptoid-based formulations. Each of the *N*spe-based formulations contained a more pronounced

plateau region than the *N*ssb-based formulations in the Π-A isotherms, suggesting a greater structural transition at higher surface pressures. The FM studies also showed that the formulation containing the aromatic mimic, Mimic 1-14, was better able to replicate the film morphology of the SP-C peptide than the aliphatic mimic, Mimic 2-14, with the occurrence of bright vesicle domains also consistent with multilayer formation. These multilayer protrusions induced by the presence of SP-C have been shown to coincide with a dramatic increase in film viscosity, providing low surface tension with minimal compression while respreading rapidly on expansion [40, 99, 160, 162].

4.4 Conclusions

Two classes of peptoid mimics of SP-C were synthesized, designed, and characterized to have either an aromatic-based or aliphatic-based hydrophobic helix in order to investigate the effect of side chain biomimicry on surface activity. The length of the helical region of these mimics was also varied in order to determine an optimal helix length. These peptoid-based SP-C mimics preserve the longitudinally amphipathic patterning and helical secondary structure of the native SP-C molecule. The secondary structure of each mimic was determined by CD spectroscopy and found to conform to a stable helical structure with an increase in spectra intensity corresponding with increasing helical length for both classes of mimics. The peptoid mimics of SP-C were then combined with a synthetic phospholipid formulation and characterized *in vitro* by LWSB, FM, and PBS studies. In general, the aromatic-based peptoid mimics showed superior surface activity relative to the aliphatic-based mimics. An increase in surface activity of the aromatic-based mimics was also observed coinciding with an increase in the number of helix-forming peptoid residues in the hydrophobic region of the molecule.

LWSB and FM studies confirm that the aromatic-based mimics are able to more closely mimic the surface behavior of the SP-C peptide. The formulation containing Mimic 1-14 showed an earlier lift-off, more pronounced plateau, and a much more biomimetic phase morphology than the other peptoid-based mimic formulations and most closely replicated the SP-C peptide formulation. Static PBS adsorption studies showed that the addition of either class of peptoid mimic to a lipid formulation results in improved surface film adsorption kinetics over lipids alone; however, the aromatic-based peptoid mimics displays superior adsorption (to a lower surface tension) compared to the aliphatic mimics with the longest helical mimic, Mimic 1-14, having the most SP-C-like surface adsorption. Dynamic compression and expansion cycles on the PBS revealed that while both classes of mimics are able to reduce the γ_{max} and γ_{min} of the lipid formulation in a similar manner as the SP-C peptide, only the aromatic-based mimics are able to significantly reduce the amount of compression required to reach γ_{min}. An increase in the amount of hysteresis was also observed in the PBS loops as the length of the helical region is increased, similar to what was observed for the adsorption experiments.

While all the aromatic-based peptoid mimics exhibit improved surface activity over lipids alone, only the longest length aromatic mimic with 14 *N*spe residues in the helical region was able to most closely replicate the surface activity of the full-length SP-C peptide. It is hypothesized that this longer length mimic with a helical region that is approximately 28 Å in length is better able to anchor in the lipid film than the truncated mimics. This is in agreement with previous studies of synthetic SP-C peptides, which showed that oligomers of varying lengths exhibited similar activity, as long as a certain core sequence (residues 5-32) was conserved [51].

The specific side chain chemistry of the hydrophobic helix also significantly alters the surface activity of the peptoid mimics. All the aromatic-based mimics exhibited superior surface activity compared to the aliphatic-based mimics as observed by LWSB, FM, and PBS. This was somewhat unexpected given that the side chains present in mammalian SP-C are closer in structure to the aliphatic mimics. This may be the case for two specific reasons: 1) peptoids composed of α-chiral, aromatic residues adopt a tighter, more rigid helix than aliphatic-based peptoids, and that this more rigid helix is necessary for modulating the surface film, and 2) the α-chiral, aromatic residues used in the aromatic mimics are slightly more hydrophobic than the α-chiral, aliphatic residues studied, which may facilitate better insertion into the alkyl region of the lipid film and surface activity. This suggests that the important structural feature of SP-C to mimic is its rigid, hydrophobic helical region rather than the exact side chain chemistry.

The peptoid-based analogues also have the added advantages that they are less prone to aggregation in solution, protease degradation, and structural transformations than natural or synthetic SP-C analogues. The added stability is likely to be an advantage in a biomimetic SRT as it would ease the synthesis and purification as well as increase the shelf-life and bioavailability after administration of the SRT. While it has been shown that excessive accumulation of misfolded SP-C in the airspaces is associated with pulmonary alveolar proteinosis, specific protease degradation sites can be engineered in the analogues, aiding their clearance from the airways should it be determined that these analogues are not biocompatible [44].

Taken together, this study has shown that peptoid-based mimics of SP-C are able to exhibit biophysical activities highly similar to that of the SP-C peptide when combined with a

biomimetic phospholipid formulation. It was also found that the same design considerations occurring in the peptide are also applicable in the development of peptoid-based mimics of SP-C. Specifically, the surface activity of the peptoid-based compounds was found to be dependent upon the conservation of the basic amphipathic sequence patterning and the maintenance of a hydrophobic, helical region of approximately 14 *N*spe residues in length and that the critical feature of the carboxy-terminal region of SP-C is its rigid helical structure and overall hydrophobic content, enabling the molecule to be anchored in the lipid film. Therefore, the results observed are promising for the development of a synthetic, biomimetic, peptoid-based lung surfactant formulation for the treatment of RDS or other medical applications.

Chapter 5: *N*-terminal alkylation of a peptoid analogue of surfactant protein C

Surfactant protein C (SP-C) is a hydrophobic lipopeptide that is critically important for the physiological functioning of lung surfactant. SP-C's addition to the phospholipids of lung surfactant dramatically improves their biophysical activity, resulting in improved surfactant adsorption and respreading. While many of SP-C's biophysical properties are derived from its extremely hydrophobic and structurally rigid helical region, recent evidence indicates that the amphipathic *N*-terminal region also contributes to these properties. In all species studied thus far, the *N*-terminal cysteine residues are palmitoylated. While the precise function of the thioester-linked palmitoyl chains is not precisely known, they are thought to be important in the maintenance of a surface-associated surfactant reservoir. Attempts to study this motif in the natural protein have been complicated by SP-C's extreme hydrophobicity and propensity to misfold and aggregate, make direct comparisons between the acylated and deacylated protein difficult.

Here, a synthetic, biomimetic platform has been used to study the effects of *N*-terminal alkylation of a peptoid-based mimic of SP-C. Peptoids have close structural similarity to peptides, form stable helices, do not irreversibly aggregate, and resist protease degradation. These properties make peptoids excellent candidates for the mimicry of natural molecules that rely on helical structure for proper functionality, such as SP-C. The peptoid mimics reported emulate the amphipathic patterning, highly helical nature, and extreme hydrophobicity of SP-C and have been designed to study the functional importance the palmitoyl modification by incorporating none, one, and two amide-linked alkyl chains in the *N*-terminal region. This

hydrophobic modification mimics the length and hydrophobicity of the native thioester-linked alkyl chains. The amide-linked alkyl chains are also efficiently incorporated into the growing peptoid backbone during solid phase synthesis, making them more selective and efficient than other synthetic protein alkylation methods. The SP-C peptoid species were observed by circular dichroism to be structured and helical in solution, mimicking SP-C secondary structure. *In vitro* surface activity measurements provide evidence that alkylation of the SP-C mimics greatly improves their surface activity, resulting in greater film stability and a significantly lower maximum dynamic surface tension. With improved stability, greater production potential, and elimination of possible pathogenic contamination, these biomimetic protein analogues offer the potential to improve the treatment of respiratory distress syndrome as well as the opportunity to treat other respiratory-related disorders.

5.1 Introduction

SP-C is one of four proteins that, along with saturated and unsaturated phospholipids, comprise the surfactant lining of the alveolar airways. Lung surfactant functions in the airways to reduce and control alveolar surface tension during respiration. This dramatically reduces the work of breathing and maintains alveolar patency, enabling proper respiration. Phospholipids make up nearly 80% of lung surfactant's mass, while neutral lipids and surfactant proteins each constitute approximately 10% [9, 64]. No single component is solely responsible for lung surfactant's unique activity; rather, each species contributes to its unique surface activity. The chief surface tension reducing component and most abundant phospholipid is dipalmitoyl phosphatidylcholine (DPPC). DPPC and other saturated phospholipids are largely responsible for lung surfactant's surface tension reduction properties; however, these species are poor lung

surfactants on their own as they slowly adsorb to the air-liquid interface and ineffectually respread upon inhalation. The addition of unsaturated phospholipids and neutral lipids improves these properties; however, not to an acceptable extent. The two hydrophobic proteins of lung surfactant, SP-B and SP-C, are required to retain the full surfactant activity repertoire. While only a minor component of lung surfactant, ~ 2% (w/w), the addition of SP-B and SP-C dramatically improves surfactant adsorption, stability, and recycling of the lipid film during the respiration cycle.

The study of the native SP-C protein and the subsequent development of SP-C analogues have been motivated by SP-C's functional importance in lung surfactant biophysical activity as well as the protein's inclusion in animal-derived exogenous surfactant preparations, which are currently used to treat neonatal respiratory distress syndrome (nRDS) in premature infants. Despite the dramatic efficacy of the animal-derived preparations for the treatment of nRDS, there are some drawbacks associated with their use including expensive and arduous purification, batch-to-batch variability, and the possible spread of infectious material [8, 12, 166]. In addition, exogenous surfactant may also be beneficial in the treatment of other respiratory disorders such as acute RDS in children and adults; however, this requires significantly more material than current surfactant isolation techniques can supply [12, 15]. To address these concerns, researchers have attempted to create synthetic analogues of the surfactant proteins for use in an entirely synthetic surfactant formulation [11]. However, SP-C's deceptively simple sequence and secondary structure have proven to be more difficult to emulate than first anticipated given the protein's extreme hydrophobicity and metastable secondary structure [45, 50].

SP-C is the smaller of the two hydrophobic lung surfactant proteins, at just 35 monomers in length [88]. SP-C is initially expressed as a larger precursor protein that is subsequently processed and secreted into the alveolar air-liquid interface by the alveolar type II pneumonocytes. The mature lipopeptide contains a high number of valine, leucine, and isoleucine residues as well as a di-palmitoylation motif in the *N*-terminal region, making SP-C one of the most hydrophobic proteins in the mammalian proteonome.

The three-dimensional structure and disposition of SP-C in a lipid environment are now known to a great extent [29, 39]. While SP-C lacks any tertiary structure, its secondary structure is dominated by a large C-terminal helical region that spans residues 9 to 34 [29]. The length of SP-C's helix, 37 Å, precisely matches that of a fluid DPPC bilayer and within this region resides a 23 Å valyl-rich region of hydrophobic amino acids that also closely matches the alkyl chain length of a DPPC bilayer. These dimensions closely support SP-C's disposition in a lipid environment where, in a lipid monolayer, SP-C orientates approximately 70° relative to the interfacial plane and nearly parallel with the lipid acyl chains in a lipid bilayer, thereby maximizing the interactions between the poly-valyl helix and the lipid acyl chains [32, 33]. SP-C's strong lipid association is also enhanced by the presence of two positively charged residues, lysine and arginine, at positions 11 and 12 that promote protein binding to anionic phospholipid headgroups through ionic interactions [34]. The *N*-terminal region of SP-C was found to assume a flexible disordered orientation in solution, but more recent investigations have suggested that this region possess an intrinsic capability to interact with and to perturb phospholipid monolayers and bilayers [167, 168].

While only a minor component of lung surfactant, ~ 1% (w/w), SP-C has a dramatic effect on the surface activity of the lung surfactant phospholipids [169]. The addition of SP-C (along with SP-B) to surfactant phospholipids dispersed in an aqueous subphase accelerates the adsorption and transfer of surfactant phospholipids from the subphase to the air-liquid interface, rapidly forming an interfacial surfactant layer [38]. SP-C also promotes further binding of dispersed lipid vesicles to the newly formed surfactant layer, assisting in the formation of a surface-associated surfactant reservoir [37, 90]. Upon compression at high surface pressures, SP-C also catalyzes the formation of stacked bilayers of excluded surfactant material [20, 39, 139, 164, 170]. These protrusions aid in the interfacial retainment of excluded material, providing a continuous supply of surface-active molecules to replenish the interfacial film during successive respiratory cycles. The three-dimensional structures are also likely to contribute to the SP-C-induced surfactant viscosity regulation, preventing surfactant outflow from alveoli to the upper airways at very low surface tensions [42].

SP-C's unique molecular features make the protein ideally suited for its interaction with phospholipids and its functionality; however, they also make working with and studying the native protein and synthetic SP-C analogues problematic. SP-C's seemingly simple sequence is extremely hydrophobic and the high content of valine residues causes the secondary structure to be discordant, i.e. composed of amino acids with a high propensity to form β-strands [4, 171]. Consequently, the helix is metastable in solution and spontaneously converts in β-strand aggregates and amyloid fibrils with have inferior surface activity compared to the correctly folded, helical protein [44, 45]. This makes the isolation of the native protein or the synthesis of synthetic analogues very difficult. The aggregation propensity may also limit the shelf-life of

exogenous surfactant preparations, hampering their therapeutic availability [5]. As a result, researchers have utilized a variety of unique strategies to mimic SP-C for mechanistic studies of the protein as well as for possible use in a synthetic lung surfactant formulation [10, 47, 54, 62, 93, 94]. These strategies include using recombinant proteins, synthetic peptide analogues with engineered sequences, and, more recently, non-natural oligomers [46-48, 50, 61, 62, 94, 172]. Because of SP-C's high degree of sequence conservation and uniqueness, all of these analogues preserve SP-C's key molecular and structural features, which include its extreme hydrophobicity, helical secondary structure, and amphipathic *N*-terminal region.

An interesting biomimetic approach, which overcomes many of the difficulties associated with the natural protein, is the use of poly-*N*-substituted glycines or "peptoids" for the mimicry of SP-C [61, 62, 162]. Peptoids share the same backbone structure as peptides, but have their side chains appended to the amide nitrogens rather than the α-carbons [86]. This feature renders peptoids essentially invulnerable to protease degradation, improving the bioavailability [55]. Despite having an achiral backbone structure and the absence of hydrogen bond donors, peptoids are able to adopt stable, chiral helices [115, 116]. When substituted with α-chiral, sterically bulky side chains, steric and, in some instances, electronic repulsion between adjacent residues cause peptoids to adopt a secondary structure similar to a polyproline type I helix with ~ 3 residues per turn and a pitch of ~ 6-6.7 Å [58, 115, 160]. Since peptoid secondary structure does not depend on hydrogen bonding, the resulting structures are extremely stable and do not appreciably aggregate over time [60]. Peptoids are also relatively easy and cost-effective to synthesize with coupling efficiencies comparable to those of solid phase peptide synthesis [173]. These features make peptoids a promising candidate for the mimicry of proteins that rely on

helical structure for proper function, such as the hydrophobic protein, SP-C. In fact, the same design considerations present in peptide analogues of SP-C have been shown to be applicable to peptoid-based analogues [45, 61, 63].

While many of the biophysical properties attributed to SP-C are heavily influenced by contributions from the hydrophobic, helical region, recent evidence suggests that the *N*-terminal segment of the protein is also responsible for many important surface-active properties [31, 167, 168]. This region was found to insert into and perturb phospholipid monolayers and bilayers, likely facilitating SP-C-catalyzed reinsertion of surfactant material to the alveolar air-liquid interface during the respiration cycle. These effects were observed in the absence of the *N*-terminal palmitoyl chains; however, palmitoylation appears to be an important SP-C modification. Palmitoylated variants of SP-C were shown to stabilize ordered domain structures and to promote the formation of extended multilayers of a surface-associated surfactant reservoir [31, 41]. Despite this, the exact function and relative importance of this hydrophobic modification in dynamically compressed films are not precisely known.

Unlike other palmitoylated proteins that become closely associated with a phospholipid membrane upon acylation [174, 175]. SP-C's hydrophobic helical region is sufficiently lipophilic on its own and readily associates with the phospholipid acyl chains even in the absence of the palmitoyl groups [7]. The palmitoyl chains are also not required for proper targeting of the lipophilic protein as the alteration of the acylated cysteine residues to either alanine or serine in the precursor protein has no influence on the protein targeting [176, 177]. More recent studies have indicated that the palmitoylated cysteines assist in lipid film stability under compression; however, the stabilizing effect at low surface tensions has recently come under scrutiny [40, 41,

178]. SP-C palmitoylation has also been shown to be important in the maintenance of the *N*-terminal region of the protein with highly compressed interfacial films, whereby this region is able to induce a structural transition in the compressed film that leads to the formation of surface-associated multilayered structures [31, 41]. In the absence of the palmitoyl chains, SP-C only forms bilayers rather than the multilayer structures and has a reduced association with the compressed surface film [40, 41]. The SP-C-catalyzed multilayered structures act as a surfactant reservoir, improving surfactant reincorporation and adsorption upon cycling of the film during respiration.

Here the previous studies of a peptoid-based analogue of SP-C have been expanded by focusing on the *N*-terminal region of the peptide analogue. Specifically, the biophysical role of the palmitoyl chains were investigated in these synthetic analogues by creating a series of alkylated and non-alkylated analogues and, subsequently, characterizing the *in vitro* surface properties of the peptoid mimics.

5.2 Materials and methods

5.2.1 Materials

Peptoid synthesis reagents, primary amines, and palmitic acid (PA) were purchased from Sigma-Aldrich (Milwaukee, WI). Fmoc-protected proline and Rink amide resin were purchased from NovaBiochem (San Diego, CA). All organic solvents used for sample synthesis, purification, and preparation were HPLC-grade or better and were purchased from Fisher Scientific (Pittsburgh, PA). The synthetic phospholipids DPPC and palmitoyloleoyl phosphatidylglycerol (POPG) were purchased from Avanti Polar Lipids (Alabaster, AL) and were used as received. Texas-Red® 1,2-dihexadecanoyl-*sn*-glycero-3-phosphoethanolamine,

triethylammonium salt (TR-DHPE) was purchased from Molecular Probes (Eugene, OR). The native SP-C used in these studies was a kind gift from Dr. Perez-Gil and Dr. Ines Plasencia and was extracted from porcine lung surfactant utilizing the methodology of Perez-Gil et al. [179].

5.2.2 Peptoid synthesis

The peptoid-based SP-C mimics shown in Table 5.1 were synthesized on an automated 433A ABI Peptide Synthesizer (Foster City, CA) on solid support (Rink amide resin), following a two-step submonomer method as described by Zuckermann et al. [86]. Briefly, synthesis was carried out on 0.25 mmol Rink amide resin. After the removal of the first Fmoc protecting group from the resin with 20% piperidine in *N,N*-dimethylformamide (DMF) and rinsing of the resin with DMF, the monomer addition cycle was performed by first acetylating the resin with the addition of 1.2 M bromoacetic acid in DMF, followed by the addition of *N,N*-diisopropyl carbodiimide (DIC). The acetylation step was carried out for 45 minutes and then the resin was washed with DMF. The resin-bound halogen was then displaced by 1.0 M primary amine submonomer in *N*-methylpyrrolidinone, which was added to the resin and allowed to react for 90 minutes. Due to poor solubility of the *N*-octadecylamine (*N*ocd) submonomer, *N*ocd was dissolved at 0.8 M in methanol:dichloromethane (1:1). The two-step cycle was repeated until the desired length and sequence of the peptoid was obtained. The displacement step for the Boc-protected *N*lys and *N*ocd residues was extended to 120 minutes while for the addition of the proline residue, a PyBrop activating system was employed. After the proline addition, the Fmoc

Table 5.1: Structu re of porcine SP-C and peptoid-based SP-C analogues.

Compound	Structure
Porcine SP-C	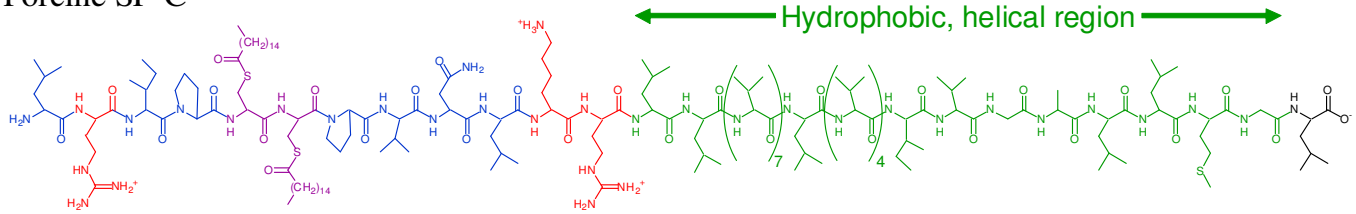
Mimic C	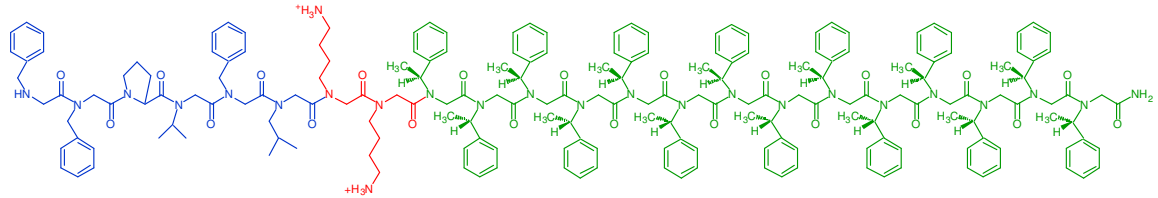
Mimic pC	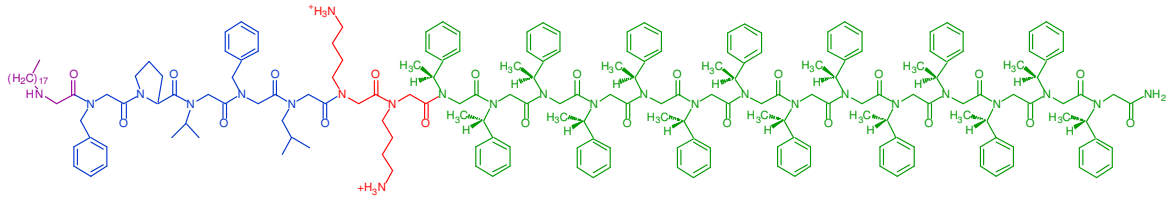
Mimic di-pC	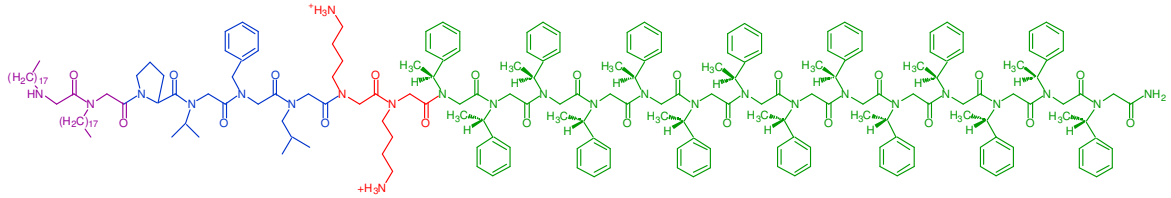

group was removed with piperidine and the peptoid cycle was continued. Peptoid oligomers were cleaved from the resin and deprotected with 90% TFA along with necessary scavengers for 5 minutes. The crude products were then purified by RP-HPLC on a Waters system with a Vydac C4 column and a linear gradient of 40-90% solvent B in solvent A over 80 minutes (solvent A= 0.1% TFA in water and solvent B = 0.1% TFA in isopropanol). The final purity of the peptoids was confirmed by analytical RP-HPLC to be > 97%. Electrospray ionization mass spectrometry was used to confirm correct molar masses.

5.2.3 Circular dichroism spectroscopy

Circular dichroism (CD) measurements were performed on a Jasco model 715 spectropolarimeter (Easton, MD). Stock solutions for dilution to appropriate concentrations for CD were made immediately before analysis in tared glass vials by precise weighing of added solvent to at least 2 mg of lyophilized peptoid powder, to produce a sample of accurately known concentration. The stock solutions were then diluted to a concentration of ~ 60 μM. CD spectra were then acquired in a quartz cylindrical cell (Hellma model 121-QS, Forest Hills, NY) with a path length of 0.02 cm, employing a scan rate of 100 nm/min. CD spectra reported here represent the average of 40 successive spectral accumulations. Data are expressed in terms of per-residue molar ellipticity (deg cm^2/dmol), as calculated per mole of amide groups present and normalized by the molar concentration of peptoid.

5.2.4 Pulsating bubble surfactometer

Static and dynamic characterization of surfactant film properties were performed on a modified PBS (General Transco, Largo, FL) as described by Seurynck et al., in which an imaging system is employed to accurately track bubble size and shape throughout the experiment

[27]. Briefly, the lipid mixture (DPPC:POPG:PA, 68:22:9 (by weight)) was dissolved in chloroform:methanol (3:1) alone or with 1.6 mol% SP-C additive, analogous to 10 wt% porcine SP-C to mimic the entire lung surfactant protein content [104]. The PBS samples were prepared in Eppendorf tubes, dried under vacuum, and re-suspended in an aqueous buffer solution (0.15 M NaCl, 5 mM $CaCl_2$, and 10 mM HEPES at pH 6.90) to a phospholipid concentration of 1.0 mg/mL. Samples were then loaded into the sample chamber using a modified leak-free methodology and placed on the PBS instrument at 37°C [26]. A bubble with a radius of 0.4 mm was then formed and an imaging acquisition system used to determine the bubble size. For static adsorption experiments, trans-film bubble pressure was recorded as a function of time while holding bubble radius static for 20 minutes. Dynamic measurements of surface tension as a function of bubble surface area were subsequently collected by cycling the bubble radius between approximately 0.4 mm and 0.55 mm at an oscillation frequency of 20 cycles/min for 10 minutes.

5.2.5 Langmuir-Wilhelmy surface balance and fluorescent microscopy

Surface pressure-area isotherms were obtained using a home-built Langmuir-Wilhelmy surface balance as previously described [112]. For each experiment, the subphase was filled with a buffered suphase (0.15 M NaCl, 5 mM $CaCl_2$, and 10 mM HEPES at pH 6.90) and heated to 37°C. A Wilhelmy surface balance (Reigler & Kirstein, Berlin, Germany) was then calibrated and used to monitor the surface pressure as the area of the trough was either expanded or compressed. The surfactant material in an organic solution was spread at the air-liquid interface using a syringe and the solvent was allowed to evaporate for 10 minutes. The barriers were then compressed at a rate of 30 mm/min.

In order to obtain fluorescence microscopic (FM) images, a Nikon MM40 compact microscope stand with a 100W mercury lamp (Tokyo, Japan) was used in conjunction with the Langmuir trough. Fluorescence was detected by a Dage-MTI three-chip color camera (Dage-MTI, Michigan City, IN) in conjunction with a generation II intensifier (Fryer, Huntley, IL). Samples were spiked with 0.5 mol% of a fluorescently labeled lipid, TR-DHPE, for detection. Previous studies have shown that inclusion of the labeled lipid at this concentration does not alter surfactant film morphology [119]. FM experiments were also performed on an aqueous buffered subphase at 37ºC with a barrier speed of 5 mm/min. The images were resized and enhanced in contrast and brightness within reasonable limits to make the features discernible for the purpose of display when warranted [147].

5.3 Results and discussion

5.3.1 Peptoid design and rationale

Previous efforts to develop a peptoid-based analogue of SP-C utilized similar design strategies as those used in the creation of peptide-based SP-C analogues [61, 62]. Namely, these peptoid analogues maintained the essential molecular and structural features of SP-C including: SP-C's extreme hydrophobicity, the positioning of the polar residues, and SP-C's rigid, helical secondary structure. Subsequent detailed structure-function studies with these analogues focused on the optimization of the length and side chain chemistry of the helical region. These studies revealed that it is more important to preserve the rigid nature of the helix rather than the exact side chain chemistry. Recent studies with peptide SP-C constructs have shown that the *N*-terminal region including the thioester-linked palmitoyl chains of this region also play an important biophysical role in SP-C-related surfactant homeostasis [31, 41, 167, 168].

A method for palmitoylation of peptides containing either non-protected cysteine, threonine, or serine residues has previously been developed to study the presence of the acyl chains in peptide-based mimics of SP-C [99]. This method involves reacting unprotected cysteine and/or serine containing peptides dissolved in TFA with palmitoyl chloride, which efficiently acetylates the peptide chains. Despite the effectiveness of this method, there are some drawbacks associated with the O- and S-palmitoylation technique. First, the peptide species must first be purified and then reacted and purified again as the added palmitoyl groups are unstable under peptide synthesis conditions and cannot be added on-resin during synthesis. Additionally, the method is non-selective in that any non-protected cysteine or serine side chain is subject to palmitoylation. Although, this is not a concern with SP-C mimetics as no other reactive side chains are present, it could present difficulties in other palmitoylated protein species. The reaction also requires exposure to very harsh conditions, which can be problematic in sequences with acid labile side chains such as the α-chiral, aromatic side chains used in peptoid analogues of SP-C.

An alternative approach that overcomes these difficulties is the use of a long, primary alkyl amine in a peptoid submonomer that mimics the length of a palmitoyl chain such as *N*-octadecylamine (*N*ocd). The *N*ocd side submonomer is readily incorporated into a growing peptoid backbone with coupling efficiencies on the order of ~ 95%. By using this strategy, the acyl chains can be introduced on-resin during the synthesis as the amide linkage is stable against hydrolysis under alkaline conditions. This eliminates the needed for additional purification and minimizes exposure to harsh reaction conditions. This also allows specific placement of the alkyl motif in sequences with other reactive side chains without the need for orthogonal

protecting groups. This method can also be extended to peptide analogues as the peptoid coupling chemistry is compatible with routine peptide synthesis.

Using this methodology, two alkylated analogues were designed having one or two *N*ocd residues in the *N*-terminal region, mimicking canine and human SP-C, respectively. The sequences of the peptoid analogues are shown in Table 5.1. These analogues mimic SP-C 5-32 and consist of 14 α-chiral, aromatic residues in the helical region along with an achiral amino-terminal stretch that mimics the side chains present in human SP-C except that the conserved arginine-lysine dibasic pair was replaced with a lysine-like pair. This replacement was necessary as the removal of the pmc-protecting group from the arginine peptoid side chain takes considerable time, causing degradation of the acid labile chiral, aromatic side chains. This substitution did not alter either the secondary structure or the surface activity of the peptoid analogue (data not shown).

5.3.2 Secondary structure

CD was used to characterize and compare the secondary structure of the peptoid-based SP-C mimics shown in Table 5.1. The highly helical nature of SP-C has been shown to be essential for its surfactant activity [45, 63]. CD spectra of the peptoid-based SP-C mimics are displayed in Figure 5.1. The non-alkylated and alkylated peptoid-based SP-C mimics containing α-chiral, aromatic residues exhibit CD spectral features that are similar to a peptide α-helix, with each showing an intense maximum at λ ~ 192 nm and double minima at λ ~ 205 nm and ~ 220 nm (Figure 5.1). These spectral features are characteristic signatures of a helical peptoid structure in oligomers of this class, which have highly ordered backbone amide bonds that adopt

right-handed conformations with a periodicity of about three residues per turn and a pitch of ~ 6 Å [59, 115].

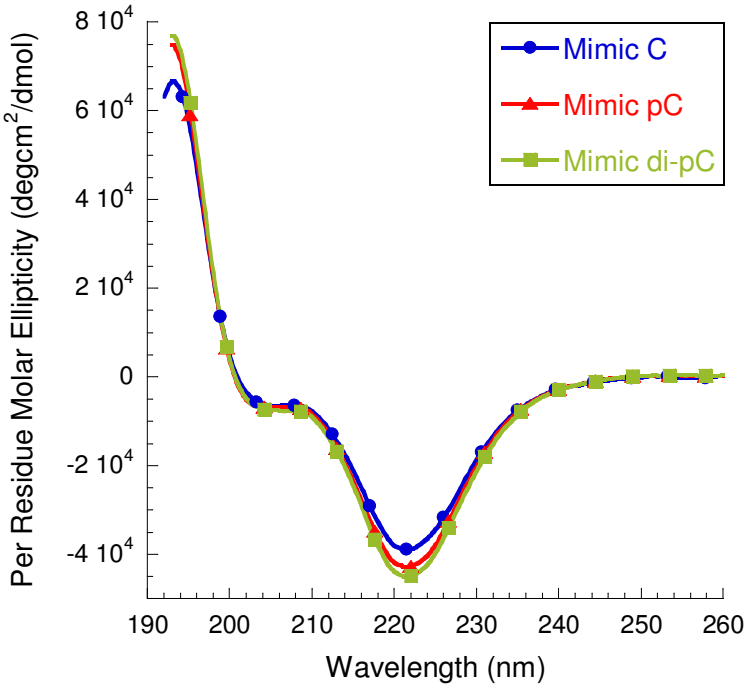

Figure 5.1: Circular dichroism (CD) spectra of peptoid-based SP-C mimics (Mimics C, pC, and di-pC), showing qualitatively similar characteristics of peptoid helices. Spectra were acquired in methanol at a concentration of ~ 60 µM at room temperature.

The intensities of the helical spectrum for the aromatic-based mimics are very similar, with the alkylated mimics, Mimics pC and di-pC, having slightly stronger intensities than the non-alkylated mimic, Mimic C. The increase in intensity of the helical signal of the alkylated mimics is likely due to confinement of the achiral amino-terminal stretch into a preferred confirmation. Similar increases in helicity of the native protein have been reported; however, either the method of deacylation or the metastable nature of the poly-valyl helix may have influenced the difference in helicity of the native protein, making a definitive conclusion difficult

[33, 43, 89]. Regardless of the slight variance in the CD intensities observed for the peptoid-based analogues, all of the SP-C mimics are shown to be helical and structured in solution, satisfying one of the structural criteria, helicity, believed to be of importance for the surface activity of SP-C [63].

5.3.3 Langmuir-Wilhelmy surface balance studies

To determine the effect of the peptoid-based SP-C mimics on the monolayer phase behavior of a synthetic lipid formulation, the mimics were combined at 1.6 mol% with a biomimetic lipid formulation comprised of DPPC:POPG:PA (68:22:9, by weight). This formulation has been shown to closely mimic the behaviors of the lipid portion of lung surfactant [104, 162]. While PA does not constitute a significant portion of natural lung surfactant, it has been successfully included in effective clinical preparations and is widely used for both *in vitro* and *in vivo* testing. The resulting formulations were studied on the LWSB as previously described. The surface pressure-area isotherms for the lipid formulation alone and with porcine SP-C and the peptoid analogues at 37°C are shown in Figure 5.2. Similar trends were observed at 25°C (data not shown).

The surface pressure-area isotherm observed for lipids alone has a lift-off point (defined as the molecular area where surface pressure first increases) of ~ 90 Å^2/molecule. The slope of the LWSB isotherm is relatively small up to a surface pressure of ~10 mN/m, indicating a highly compressible film typical of the liquid expanded (LE) phase. As the surface layer is further compressed from 10 mN/m to ~ 44 mN/m, the slope of the isotherm increases indicating a less compressible film, which is consistent with the formation of condensed domains of DPPC that are co-crystallizing with PA, forming liquid condensed (LC) domains in co-existence with the

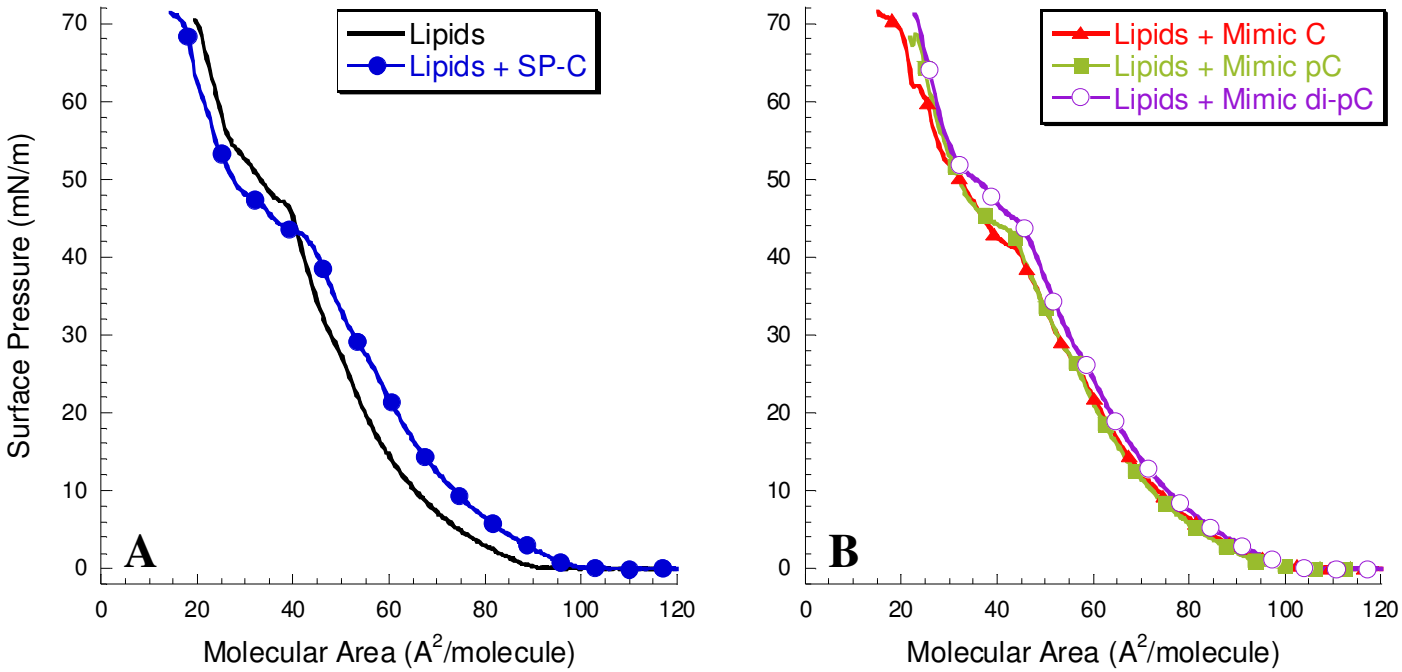

Figure 5.2: Langmuir-Wilhelmy surface balance (LWSB) studies at 37°C. (A) Surface pressure-area isotherms obtained for DPPC:POPG:PA (68:22:9, by weight) alone, and with 1.6 mol% SP-C; (B) Lipids with 1.6 mol% peptoid-based SP-C mimics (Mimics C, pC, and di-pC). Isotherms were collected on a buffered subphase (150 mM NaCl, 10 mM HEPES, 5 mM $CaCl_2$, pH=6.9 0) at 37°C.

LE phase [145, 163]. Further compression of the lipid film leads to a kink in the isotherm at ~ 47 mN/m. Eventually the compression leads to film collapse at a surface pressure of ~ 72 mN/m. The addition of SP-C to the lipid mixture shifts the lift-off to a greater molecular area (~ 98 $Å^2$/molecule vs. ~ 90 $Å^2$/molecule) indicating increased surface activity and an earlier transition to a LE state due to the presence of the natural SP-C protein at the air-liquid interface. At lower surface pressures, the isotherm is similar to lipids alone, only shifted towards higher molecular area. However, further compression results in the occurrence of a more dramatic, dual plateau region with the first break in the isotherm occurring at ~ 43 mN/m and the second plateau occurring at ~ 47 mN/m. An extended isotherm plateau is also observed for natural lung surfactant and is believed to indicate a phase transition in the lipid film or the reversible removal of lipids and proteins from the monolayer, forming a surface-associated surfactant reservoir that remains associated with the interface [149]. The presence of such a surfactant reservoir offers an explanation how the SP-C protein is able to interact with lipids to provide low surface tension upon compression and to respread rapidly on expansion [149, 164]. A dramatic increase in surface viscosity is also observed for SP-C containing films at or above the plateau and is thought to help minimize the loss of surfactant material from the alveoli at low surface tensions [42]. Further compression of the SP-C containing formulation leads to a high collapse pressure of ~ 72 mN/m.

The addition of the non-alkylated analogue, Mimic C, to the lipid formulation results in a similar increase as the native protein in the lift-off area to ~ 100 $Å^2$/molecule (Figure 5.2B). This increase is likely due to an orientation that is closely associated with the air-liquid interface that is similar to SP-C, maximizing the interactions between the hydrophobic helix and the lipid

acyl chains [32]. As the interfacial film is further compressed, the isotherm is nearly identical to the formulation containing the SP-C protein until at a surface pressure of ~ 42 mN/m a biomimetic plateau region is observed in the isotherm that is less pronounced than with the porcine SP-C formulation. Similar to the other surfactant formulations, the Mimic C formulation also exhibits a high collapse pressure of ~ 72 mN/m.

Adding one alkyl chain to the *N*-terminal end of the peptoid analogue results in a LWSB isotherm that is nearly identical to the non-alkylated mimic with a molecular area at lift-off of ~ 100 $Å^2$/molecule and a plateau region in the isotherm starting at ~ 43 mN/m. The addition of a second *N*ocd residue to the peptoid analogue similarly increases the lift-off to ~ 102 $Å^2$/molecule. Compression of the Mimic di-pC formulation reveals that the film is slightly less compressible than any of the other formulations. The plateau region is also slightly altered and most similar to the SP-C containing formulation with a dual plateau region in which the first plateau occurs at ~ 45 mN/m and with the second plateau or kink occurring at ~ 49 mN/m. These changes suggest either a slightly different orientation in the surfactant film or an alteration in the lipid film packing that is different than the other peptoid-based analogues. While all the peptoid-based analogues alter the surfactant film phase behavior in a manner that is similar to the SP-C protein, the formulation containing Mimic di-pC is closest in monolayer phase behavior to the SP-C system.

5.3.4 Fluorescence microscopy imaging of film morphology

To gain greater insight into the specific interactions between the surfactant lipids and the SP-C mimetics, the surface phase morphology as a function of surface pressure was investigated by FM. FM provides for the direct visualization of the surfactant monolayer at the air-liquid

interface, enabling analysis of the impact the added species have on the formation and transition of the surfactant domain structures. Figure 5.3 displays the FM images of the surfactant films at ~ 35 mN/m (panels A-E) and at ~ 50 mN/m (panels F-J). The pure lipid system displays nucleation of the dark LC domains beginning at ~ 20 mN/m, and a continuous growth of larger, circular-shaped LC domains with increased compression (Figure 5.3, panel A and F). The coexistence of both LE and LC domains is a common feature of most lung surfactant formulations. This phase coexistence is important in controlling surface viscosity and film mechanical properties, promoting high collapse pressure. At a surface pressure of ~ 35 mN/m, the lipid film exhibits dark, circular LC domains of ~ 71 μm^2 that occupy ~ 18% of the total film area. At ~ 50 mN/m, the LC domains of the lipid system have coalesced into much larger circular domains with an average size of ~ 190 μm^2 and occupy approximately the same area of the interface (Figure 5.3, panel F).

At ~ 35 mN/m, the film containing SP-C has a morphology similar to the lipids alone with the appearance of circular LC domains; however, the LC domains are significantly smaller, ~ 25 μm^2, and occupy 17% of the film area (Figure 5.3, panel B). The LC domains for the non-alkylated Mimic C are slightly smaller in size than the lipids alone, ~ 53 μm^2, and occupy only 14% of the film area (Figure 5.3, panel C). Adding Mimic pC to the lipid formulation results in LC domains that are much smaller than either the lipids alone or with Mimic C, ~ 29 μm^2, and occupy ~ 9% of the film area (Figure 5.3, panel D). When the di-alkylated mimic, Mimic di-pC, is added to the lipid formulation, the LC domains are similarly smaller, ~ 29 μm^2, and occupy ~ 10% of the film area (Figure 5.3, panel E). The alkylated mimics produce LC domains that are most similar in size and shape to those of the native SP-C-containing films.

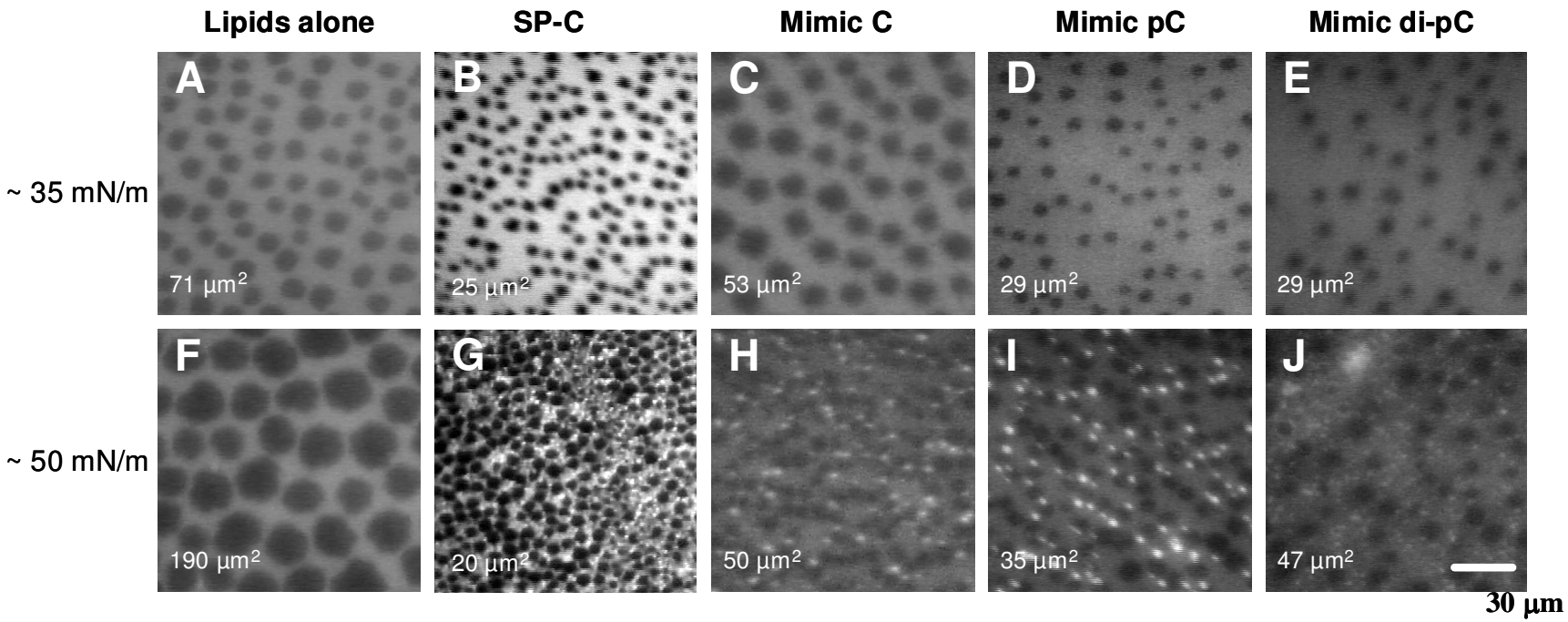

Figure 5.3: Fluorescence microscopy (FM) micrographs at 37°C corresponding to a surface pressure of ~ 35 mN/m and ~ 50 mN/m for DPPC:POPG:PA (68:22:9, by weight) alone (panels A and F), with 1.6 mol% SP-C (panels B and G), Mimic C (panels C and H), Mimic pC (panels D and I), and Mimic di-pC (panels E and J). Average size of the dark LC domains for each film is indicated in the lower left of each panel.

Increasing the surface pressure to 50 mN/m results in similar film morphologies for all the surfactants containing either the SP-C protein or the peptoid-based analogues, which are different than that observed for the lipid formulation without any added SP-C-related species. For the formulation containing SP-C, the LC domains remain approximately the same size, ~ 20 μm^2, covering the same amount of the film, ~ 17%, which is consistent with previous observations with native SP-C [126, 180]. SP-C preferentially partitions into the fluid or LE phase of the monolayer, causing perturbations in the lipid film that alters the packing of the neutral and anionic monolayer film [126, 180]. This perturbation causes a condensation and reduction in film area of the LC domains across all surface pressures, the degree of which is dependent on the concentration of SP-C.

The presence of the SP-C protein also induces the formation of small, bright vesicle-like domains in the surfactant film. These anomalies have been shown to be three-dimensional protrusions in the surfactant film [147]. These protrusions are anchored to the interfacial film and form a surfactant reservoir that assists in the respreading of the surfactant during expansion of the film. The presence and thickness of these structural transitions are directly linked with the presence of SP-C [20, 41, 164, 181].

At ~ 50 mN/m, the morphology of the Mimic C formulation is similar to the lower surface pressure morphology with LC domains that are nearly the same size, ~ 50 μm^2, and that occupy the same area of the film, ~ 14%. Similar to the SP-C film, Mimic C results in the occurrence of bright, vesicle-like domains. Adding either Mimic pC or Mimic di-pC also produces a similar film morphology with an average LC domain size ~ 35 μm^2 and ~ 47 μm^2, respectively, and a film coverage of ~ 12% for both formulations. Based upon these results, all

of the peptoid-based mimics interact with the surfactant lipids in a biomimetic manner, altering the lipid film morphology in a manner similar to the native SP-C protein. Addition of the mimics caused both a condensation of the LC domain sizes and a reduction of the LC film coverage as well as the occurrence of the bright, vesicle-like domains at higher surface pressures. Given these characteristics, all the added analogues interact favorably in a SP-C-like manner, consistent with previous observations of peptoid SP-C mimics [61, 62].

5.3.5 Static-bubble pulsating bubble surfactometry

One of the essential biophysical properties of native lung surfactant is its unique ability to rapidly adsorb from the alveolar subphase to the air-liquid interface, forming a surface-active layer that regulates surface tension during the respiration cycle [7, 10]. On their own, the phospholipids of lung surfactant exhibit poor adsorption kinetics and ineffectual spreading properties; however, the addition of the hydrophobic surfactant proteins to the phospholipids dramatically improves these characteristics, reaching an equilibrium surface tension of ~ 25 mN/m in less than a minute [38, 66, 81, 127, 182]. A modified PBS run in static mode was used to characterize the adsorption kinetics of the lipid mixture alone and with the addition of 1.6 mol% SP-C protein and SP-C mimics. Figure 5.4A displays the static surface tension as a function of time for the various surfactant formulations.

In the absence of SP-C protein or SP-C mimetics, the lipid mixture displays very slow surface adsorption and fails to reach an equilibrium surface tension lower than 51 mN/m even after 20 minutes of static adsorption (Figure 5.4A). The addition of the SP-C protein to the lipid formulation significantly accelerates the kinetics of surfactant adsorption to the interface. The presence of the SP-C protein allows the film to reach a surface tension of approximately 26

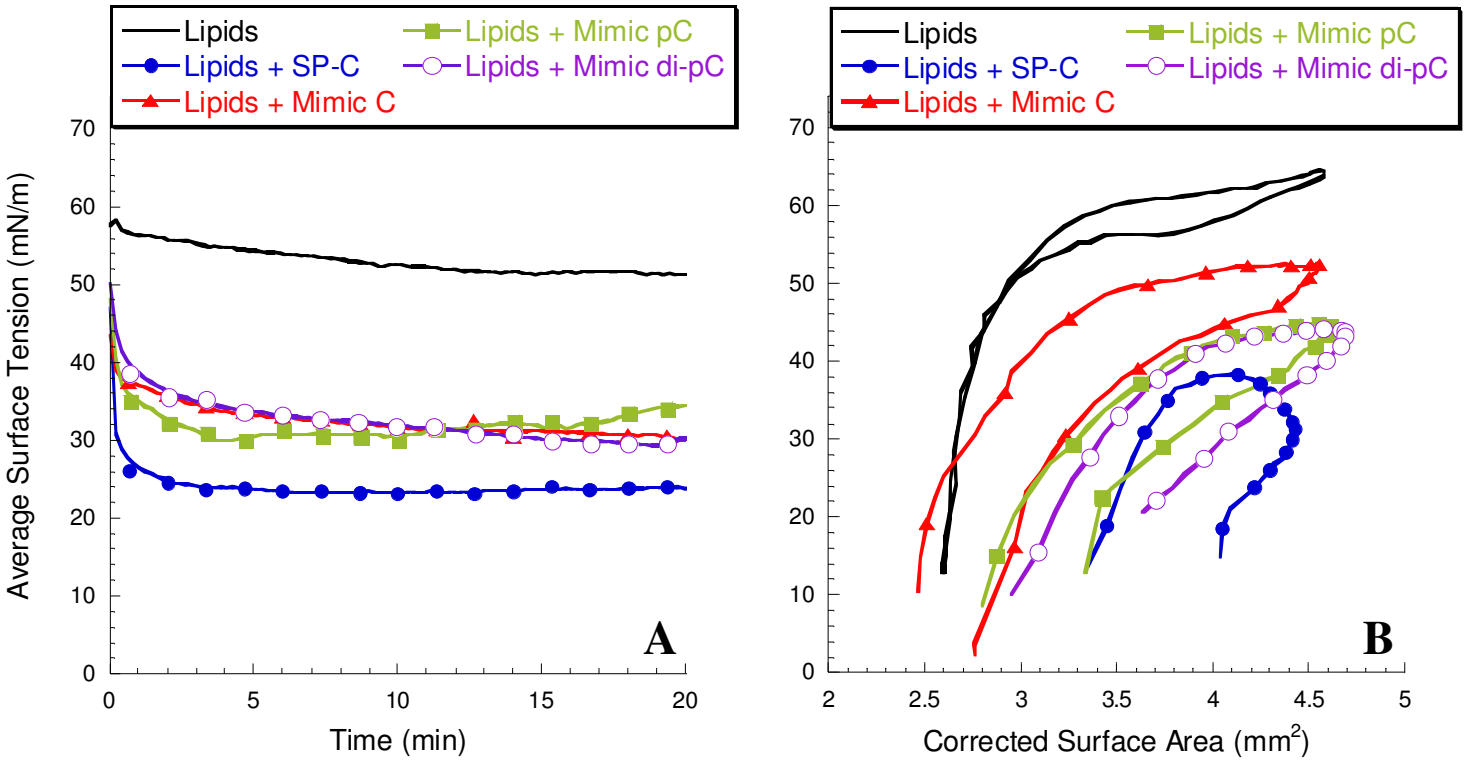

Figure 5.4: (A) Static pulsating bubble surfactometry (PBS) results displaying surface tension as a function of time and (B) dynamic PBS results displaying surface tension as a function of surface area at an oscillation frequency of 20 cycles/min after 5 minutes of cycling. Measurements were taken at a bulk surfactant concentration of 1 mg/mL lipids at 37°C.

mN/m in under one minute and a final equilibrium surface tension of ~ 24 mN/m. The addition of the non-alkylated peptoid mimic, Mimic C, to the lipid formulation also results in accelerated adsorption kinetics over the lipids alone, although, the rate is slower than the formulation containing SP-C, reaching a static adsorptive surface tension of ~ 37 mN/m after 1 minute and a final equilibrium surface tension of ~ 30 mN/m. Introducing one or two alkyl chains in the *N*-terminal region of the peptoid does not significantly alter the film adsorption kinetics. Both the formulations containing either Mimic pC or Mimic di-pC exhibit much improved adsorption kinetics over the lipid formulation alone, although, not quite to the extent that the native protein does so. The formulation containing Mimic pC has slightly improved adsorption kinetic over the other peptoid-based mimics initially, reaching a static surface tension of ~ 30 mN/m within 4 minutes; however, the equilibrium surface tension begins to rise slowly after ~ 10 minutes and is likely due to slight increases in the bubble size over time due to bubble drift [27].

The di-alkylated mimic formulation displays surface adsorption kinetics that are almost identical to the Mimic C formulation, reaching an equilibrium surface tension of ~ 30 mN/m. From these results, it is apparent that the kinetic adsorption behavior of the surfactant is significantly enhanced with the addition of the peptoid mimics to the lipid formulation, although to a lesser extent than SP-C. Also observed is that the introduction of either one or two alkyl chains into the peptoid mimic does not greatly affect the adsorption behavior of the surfactant formulation and, likely, does not facilitate surfactant adsorption to the air-liquid interface in this system.

5.3.6 Dynamic pulsating bubble surfactometry

The ability to modulate alveolar surface tension as a function of surface area is a unique feature of lung surfactant that is critical for proper respiration. As the alveoli become small during expiration, the surfactant at the air-liquid interface is compressed, resulting in a dramatic decrease in alveolar surface tension to very low values that approach ~ 0 mN/m [183]. Then during inspiration, the alveoli are enlarged and the surfactant film is expanded, causing an increase in alveolar surface tension. This dynamic behavior leads to a more uniform ratio of surface tension to alveolar radius during respiration, minimizing pressure inequalities amongst the alveoli and maintaining alveolar patency and stability.

To investigate the effectiveness of the peptoid-based SP-C mimic formulations to reduce and control surface tension as a function of surface area, dynamic PBS experiments were performed at 37°C with an oscillation frequency of 20 cycles/min and ~ 50% reduction in surface area. Features that are important in the compression-expansion loops for biomimetic surfactant film behavior include: (1) the attainment of a very low surface tension with a small amount of compression; (2) rapid respreading upon expansion, and (3) modulation of surface tension as a function of bubble surface area with a very low minimum surface tension and a low maximum surface tension [7, 10]. Figure 5.4B displays the PBS compression-expansion loops for the lipid mixture alone and with the added SP-C protein and SP-C mimetics. Key parameters of the dynamic compression-expansion cycles are also listed in Table 5.2.

During dynamic cycling, the lipid mixture without any added protein or mimic exhibits high a maximum and minimum surface tensions of ~ 64 mN/m and ~ 12 mN/m, respectively. In addition, a significant amount of compression (~ 45%) is required before the surface tension

reaches below 20 mN/m (Table 5.2). With these properties, the lipid formulation without any added species would be inadequate as a lung surfactant replacement. The addition of native SP-C to the lipid mixture dramatically improves the surface-activity of the film relative to that of the lipids alone, as indicated by the significantly lower maximum surface tension of ~ 36 mN/m and minimum surface tension below 1 mN/m (Figure 5.4B). The presence of porcine SP-C in the lipid formulation also significantly decreases the compressibility of the surfactant, requiring much less compression, ~ 8%, to reach a surface tension below 20 mN/m. These features are very similar to those of a natural surfactant formulation currently used to treat nRDS [27].

The addition of the peptoid mimics to the lipid formulation greatly improves the dynamic film behavior in a similar manner as the SP-C protein (Figure 5.4B). Adding the non-alkylated Mimic C to the lipid formulation reduces both the maximum and minimum surface tension to ~ 51 mN/m and < 1 mN/m, respectively. The inclusion of Mimic C also causes a reduction in the degree of compression required to reach a surface tension below 20 mN/m, ~ 30% compression (Table 5.2). The improvements in dynamic surface activity observed with the addition of Mimic C are similar to those previously observed with a non-acylated, synthetic SP-C peptide mimic; however, they are not as significant as those of the native SP-C protein [61].

Compression-expansion loops of the mono-alkylated Mimic pC and the di-alkylated Mimic di-pC, are shown in Figure 5.4B. With the addition of either one or two alkyl chains to the peptoid mimic, a minimum surface tension of < 1 mN/m is also observed for both formulations. Interestingly, the compression-expansion loops for the alkylated mimics show further improvement in the dynamic surface-active properties over the non-alkylated, Mimic C, formulation. The maximum surface tensions for the formulations containing Mimic pC and

Table 5.2: Dynamic pulsating bubble surfactometry (PBS) properties.

Formulation	γ_{max} (mN/m)	γ_{min} (mN/m)*	Compression (%)†
Lipids	64.2 ± 2.82	11.6 ± 1.40	45.1 ± 4.02
Lipids + SP-C	36.1 ± 2.04	< 1	8.1 ± 2.32
Lipids + Mimic C	51.1 ± 1.30	< 1	30.5 ± 2.24
Lipids + Mimic pC	45.1 ± 2.80	< 1	25.1 ± 3.22
Lipids + Mimic di-pC	45.5 ± 2.21	< 1	22.9 ± 2.53

Data are mean ± SD. * All experimental runs reached a minimum surface tension (γ_{min}) less than 1 mN/m except for formulations comprised of lipids without any added SP-C analogue.
† Compression refers to the amount of compression necessary to reach a surface tension less than 20 mN/m.

Mimic di-pC are reduced even further to ~ 45 mN/m (vs. 51 mN/m) and the amount of compression to reach 20 mN/m is also decreased to ~ 25 % and ~ 23% for Mimic pC and Mimic di-pC, respectively. These results indicate that the added alkyl chains are favorably interacting with the lipids, causing both a reduction in surface film compressibility during compression and improved retainment and respreadability of the surfactant at the air-liquid interface upon expansion. These improvements lead to PBS compression-expansion loops for the Mimic pC and Mimic di-pC formulations that are much more similar in shape to that observed for natural lung surfactant, although with higher maximum surface tensions (~ 45 mN/m versus ~ 35 mN/m for natural lung surfactant). These dynamic features for the alkylated analogues support a supposed disposition in which the palmitoyl chains act as a hydrophobic, lipid anchor, creating a surface-associated surfactant reservoir that is readily reincorporated into the expanding lipid film, reducing the maximum surface tension [31, 41, 118]. Despite the dominant role of the helical region in many of SP-C's observed surface-active properties, the *N*-terminal region and, specifically, the palmitoyl chains contribute to the surface activity of SP-C and SP-C-like molecules. The addition of a second alkyl chain to the peptoid mimic does not significantly alter the dynamic behavior of the surfactant formulation; however, this is not totally unexpected as both canine and mink SP-C contain only one palmitoylated cysteine in the *N*-terminal region.

5.4 Conclusions

A series of peptoid analogues of SP-C were designed, synthesized, and characterized to investigate the effect of alkylation on the surface activity of peptoid-based mimics of SP-C. These mimics were all designed to capture the essential features of SP-C including: SP-C's extreme hydrophobicity, longitudinal amphipathicity, and highly helical secondary structure.

The *N*ocd submonomer was incorporated into the achiral, *N*-terminal region, preserving both the hydrophobicity and chain length of the natural palmitoyl chains. The secondary structure of each mimic was determined by CD spectroscopy and found to conform to a stable helical structure in solution with a slight increase in spectra intensity upon the introduction of either one or two alkyl chains in the *N*-terminal region. The increase in spectra intensity is likely due to the alkyl chains restraining the flexible *N*-terminal region into a better-defined orientation. Ultimately, though, all of the mimics capture SP-C's highly helical nature, which is essential to its surface activity [45]. The helical structures were also stable over time, indicating that the peptoid-based analogues are not prone to misfolding and aggregation like the native protein. The peptoid SP-C mimics were then combined with a synthetic phospholipid formulation and the surface-active properties of the formulations with the native SP-C protein and the peptoid SP-C mimics were characterized *in vitro* by LWSB, FM, and PBS experiments.

With these systems, it is found that the peptoid-based SP-C analogues replicate many aspects of the *in vitro* surface activities of the native SP-C protein. Quasi-equilibrium surface pressure-area isotherms on a LWSB instrument reveal that the addition of the peptoid analogues to the lipid film causes an increase in the molecular area lift-off and a biomimetic kink or plateau region in the isotherm, which were both similar to the SP-C protein. FM images also reveal that the peptoid mimics induce biomimetic phase morphologies that are similar to those of SP-C containing films at all surface pressures. The added species cause condensation and a reduction in film coverage of the LC domains and induce the formation of bright, vesicle-like domains at higher surface pressures that are indicative of three-dimensional structure formation [20, 118]. This effect is highly similar to SP-C and is linked to the formation of a surface-associated

surfactant reservoir that causes an improvement in mechanical film stability at low surface tensions and that can be readily reincorporated upon expansion of the surfactant film, dramatically improving respreadability [16]. Interestingly, the inclusion of the alkyl chains in the peptoid analogues did not significantly affect either the quasi-equilibrium isotherms or the surfactant film phase morphology.

Static-bubble adsorption kinetics obtained with a modified PBS instrument similarly show a marked improvement in adsorption of surfactant material to the air-liquid interface with the addition of the peptoid SP-C mimetics. This improvement is similar to the SP-C protein, although to a lesser extent. The presence of the alkyl chains in the peptoid analogues did not further improve the adsorption kinetics, indicating that the alkyl chains do not alter the rate of diffusion of the surfactant aggregates towards the air-liquid interface nor the entrance of the dispersed surfactant material to the interface.

Dynamic compression-expansion cycles on the PBS reveal that the SP-C peptoid mimics also reduce both the maximum and minimum surface tensions of the lipid formulation, similar to the SP-C protein. Here, the presence of the alkyl chains invokes a significant improvement of the surface activity of the surfactant formulations. Adding one or two alkyl chains to the peptoid analogues causes a marked reduction in the maximum surface tension during dynamic cycling, ~ 45 mN/m for the alkylated mimics versus ~ 51 mN/m for the non-alkylated mimic. The reduced maximum surface tension, while not as low as native SP-C, is a significant improvement in the replenishment of the surface film during surface expansion, which is likely to significantly reduce the work of breathing *in vivo* [10]. The compressibility of the surfactants is also reduced with the presence of the alkyl chains, leading to a rapid reduction in surface tension with a

minimal amount of compression and a better ability to stabilize the alveolar network during respiration.

These experiments demonstrate that while all the peptoid analogues are able to reproduce many of SP-C's biophysical activities, the presence of the alkyl chains greatly increases the biomimicry of the synthetic analogues. The precise role of the thioester-linked palmitoyl chains in SP-C is not entirely known; however, their strict conservation amongst all species suggests an important role in SP-C and lung surfactant homeostasis. SP-C, even in the absence of palmitoylation, has been shown to promote the transfer of material from the air-liquid interface to surface-associated bilayer forming a surfactant reservoir that is readily reincorporated upon expansion or inhalation [20]. However, the palmitoyl chains are absolutely required for the formation of multilayered structures upon compression, forming a multilayered, surfactant reservoir that is readily reincorporated upon expansion or inhalation [41]. As the palmitoyl chains of SP-C are well suited for the insertion into and interaction with the membrane structures of lung surfactant films at high surface pressures, it is possible that the alkyl chains are able to link excluded surfactant material to the air-liquid surface as well as to link adjacent bilayers together, forming multilayered surfactant structures [31, 35, 40, 184]. The presence of the palmitoyl chains would, therefore, increase the retainment and respreading of the excluded material during respiration, reducing film compressibility and lowering the maximum surface tension during dynamic cycling. These results support this hypothesis and are comparable to experimental work with acylated and non-acylated SP-C peptides [40].

Taken together, this study has shown that peptoid-based mimics of SP-C are able to exhibit biophysical activities that are similar to SP-C when combined with a biomimetic

phospholipid formulation and that the extent of the biomimicry is significantly improved with the addition of an alkyl chain moiety to the *N*-terminal region of the peptoid analogues. These novel species replicate SP-C's key molecular and structural motifs, but because of their side chain chemistry and their unique backbone structure, reduce or eliminate many of the difficulties associated with the native protein. With improved stability, greater production potential, and elimination of possible pathogenic contamination, not only do peptoid-based biomimetic surfactant replacement therapies offer the potential to improve the treatment of nRDS, but they may also see wider application in the treatment of other, more prevalent, respiratory-related disorders where greater quantities of the surface-active material are required, such as in the treatment of acute RDS.

Chapter 6: Side chain chemistry of the C-terminal helix of a peptoid analogue of SP-C: balancing structural rigidity and biomimicry

Surfactant protein C (SP-C) is a unique lipoprotein that acts to modulate the biophysical surface activity of lung surfactant during respiration and is a necessary component of exogenous surfactant to treat neonatal respiratory distress syndrome (nRDS). However, the native SP-C protein is exceeding difficult to work with and in limited supply, prompting the development of functional SP-C analogues. Structure-function studies with various peptide and non-natural oligomer mimics of SP-C have shown that SP-C's biophysical activity is dependent upon the maintenance of a rigid, C-terminal helix and an amphipathic *N*-terminal region. These studies have also indicated that the secondary structure of the helical region, rather than the precise covalent side chain structure, is important for the biological function of the protein. However, SP-C is highly conserved amongst all mammalian species studied thus far, which suggests that the β-branched, aliphatic side chains of the C-terminal helix are also of importance. Here, several mimics of non-natural, helical mimics of SP-C were created that are based upon a poly-*N*-substituted glycine, or "peptoid," backbone in order to investigate specific covalent structural requirements of the C-terminal region in these analogues. These novel mimics incorporate varying amounts of α-chiral, aromatic and α-chiral, aliphatic side chains in the helical region, imparting structural rigidity and biomimicry into this region, respectively. Circular dichroism confirms that all the peptoid-based mimics emulate SP-C's secondary structure, forming stable, helical structures in solution. Langmuir-Wilhelmy surface balance, fluorescence microscopy, and pulsating bubble surfactometry experiments indicate the peptoid mimics in combination with

a synthetic phospholipid mixture, replicate many surface-active features of the native SP-C protein. Specifically, it was found that both structural rigidity and side chain chemistry are necessary requirements to emulate SP-C's unique surface activity. A structurally rigid helix results in a less compressible film, requiring less compression to reach a minimum surface tension while side chain biomimicry dramatically reduces the maximum surface tension of a dynamically cycled film in a stepwise fashion. By balancing these features in one SP-C mimic, a novel analogue of SP-C was created that, by *in vitro* characterization, emulates native SP-C's surface activity. With increased production potential and a stable secondary structure, peptoid-based analogues of SP-C hold great promise for use in a functional, biomimetic surfactant replacement therapy to treat nRDS.

6.1 Introduction

Premature infants born less than 32 weeks gestation have a high incidence of respiratory distress due to a lack of functional lung surfactant material [7, 185]. nRDS was a leading cause of infant mortality, but is now routinely treated with the instillation of exogenous surfactant material into the immature airways. The exogenous material functions in place of the native surfactant to open the airways and reduce the work of breathing until the infant is able to produce its own functional surfactant material. The adoption of surfactant replacement therapy (SRT) is one of the main contributors to the dramatic decline in infant mortality rates observed in the 1980s [15]. Despite the significant efficacy of natural, animal-derived surfactant preparations, there are still some concerns associated with their use. Because natural surfactants are extracted from animal lungs, there is a possibility of cross-species transfer infectious agents as well as high production costs and batch-to-batch variability [12]. Recent evidence has also suggested that the

use of SRT may also be beneficial in the treatment of other respiratory-related disorders; however, to increase the applicability of SRT, a much greater quantity is needed at a reasonable cost [49, 186]. These concerns and limited production potential have provided the motivation for the development of a synthetic surfactant formulation that functions as well as the native material, but overcomes these concerns and difficulties [11]. However, this endeavor has turned out much more complex than originally anticipated and is largely due to the difficulty in producing or mimicking the hydrophobic proteins of lung surfactant, SP-B and SP-C.

While the hydrophobic proteins of lung surfactant, SP-B and SP-C, represent only a small portion of lung surfactant (1-2 wt%), they are an essential component and necessary for the proper biophysical function of lung surfactant. Lung surfactant is a complex biomaterial composed of ~ 90% lipids and ~ 10% proteins that is essential for proper respiration. In the airways, this dynamic biomaterial functions to: 1) rapidly adsorb to the alveolar air-liquid interface, forming an interfacial surfactant layer, 2) greatly reduce the interfacial surface tension upon compression (expiration), preventing alveolar collapse and 3) efficiently respread the excluded surfactant material upon expansion (inhalation), reducing the maximum surface tension and diminishing the work of breathing [10]. Dipalmitoyl phosphatidylcholine (DPPC), the main lipid component of lung surfactant, along with the other saturated phospholipids are the main surface tension reducing entities; however, the molecular characteristics that allow DPPC and other saturated lipids to reach very low surface tensions, prevent them from rapidly reabsorbing and respreading upon expansion [9]. The inclusion of fluid, unsaturated phospholipids in lung surfactant provides better respreadability and slightly improved surfactant adsorption to the air-liquid interface, but results in an increase in minimum surface tension [9]. The addition of the

hydrophobic proteins, SP-B and SP-C, to the lipid portion greatly enhances surfactant adsorption, stability, and recycling of the phospholipid film [65, 66]. The presence of these surfactant-specific proteins is required for proper respiration as their absence in either genetically manipulated animal models or in individuals with inherited genetic deficiencies leads to lethal respiratory failure [68-71].

SP-C is an extraordinarily hydrophobic, helical protein that is comprised of 35 amino acids [7]. SP-C's sequence is highly conserved amongst all mammalian species and contains four functional regions [28]. The largest motif is a valyl-rich region that consists entirely of aliphatic residues with β-branched side chains that stretches from residue 13 to 28. This region is flanked on the C-terminal side by a conserved heptapeptide segment and on the *N*-terminal side by a lysine and arginine dibasic pair at positions 11 and 12, respectively. The final conserved segment consists of a flexible *N*-terminal region containing two palmitoylated cysteine residues at positions 5 and 6, which are bordered by two prolines at positions 4 and 7. SP-C lacks any tertiary structure, but its secondary structure is dominated by a α-helix that is approximately 37 Å long, extending from residue 9 to 34. Within this helical region is a 23 Å-long, valyl-rich stretch of hydrophobic amino acids. The lengths of the helix and valyl-rich region closely match the thickness of a DPPC bilayer and its acyl-chain portion, respectively, supporting its orientation in lipid monolayers and bilayers [32].

SP-C's important biophysical activities and inclusion in animal-derived surfactants suggests that the protein is a critical constituent of a synthetic surfactant preparation; however, the large scale production of the hydrophobic protein is exceedingly difficult [12]. While SP-C is relatively small and lacks any tertiary structure, the native protein and sequence identical

analogues are difficult to handle at all stages of experimentation. SP-C's poly-valyl helix is composed of amino acids with a high propensity to form -strands, which in the absence of phospholipids, spontaneously convert into -sheet aggregate structures with reduced surface activity [4, 43, 44]. The difficulties associated with native SP-C have lead researchers to employ a variety of unique strategies to overcome the metastable secondary structure and aggregation propensity by producing and mimicking SP-C in heterologous systems, synthetic peptide synthesis, and, more recently, non-natural peptidomimetic materials [12, 15].

Structure-function studies with synthetic SP-C analogues have revealed certain molecular features that are necessary to retain SP-C's functionality. These features include: SP-C's extreme hydrophobicity, the patterning of hydrophobic and polar residues, and, especially, the maintenance of SP-C's rigid, helical secondary structure [34, 45, 51, 54, 61, 105]. Many of SP-C's surface-active properties are dominated by the presence of the 37 Å-long helical region [167]. Several studies of synthetic mimics have focused on this region and concluded that the α-helical conformation rather than the exact side chain chemistry is of importance for capturing SP-C's surface-active properties [45, 50, 54, 61, 94]. Therefore, it is possible to preserve the requisite SP-C molecular parameters with alternative covalent structures, simplifying the production and handling of SP-C analogues.

One interesting approach to mimic SP-C is the utilization of poly-*N*-substituted glycines or "peptoids" [61, 62, 162]. Peptoids have close structural similarity to peptides, but have their side chains appended to the amide nitrogens rather than to the α-carbons. This feature renders peptoids essentially invulnerable to protease degradation, making them more biostable than peptides [55]. Despite the achirality of the *N*-substituted glycine backbone and its lack of

hydrogen bond donors, peptoids are able to adopt extraordinarily stable, chiral helices when substituted with α-chiral, sterically bulky side chains [59, 60, 116]. These helical structures are similar to a polyproline type I helix with ~ 3 residues per turn and a helical pitch of ~ 6-6.7 Å [58, 115]. This ability to form stable helices makes peptoids an excellent candidate for mimicry of bioactive molecules that rely on helical structure for proper function, such as the hydrophobic proteins of lung surfactant [62, 112]. In addition, many of the same design strategies used in the development of synthetic peptide analogues of SP-C are also applicable to peptoid analogues. Similar to the peptide analogues, peptoid analogues containing a more rigid, aromatic-based helix displayed superior SP-C-like behaviors in comparison to peptoid analogues containing a more biomimetic, aliphatic-based helix, which suggested that the overall secondary structure of SP-C is the important feature to mimic rather than the exact side chain chemistry [45, 61].

Despite the superior surface activities of the aromatic-based mimics, the aliphatic mimics did display a lower maximum surface tension during dynamic cycling. This suggests that perhaps there are specific favorable interactions between the branched aliphatic side chains of the helical region and the lipid acyl chains. The preservation of these specific interactions may be functionally important considering that the poly-valyl helix is also conserved amongst all species studied thus far; however, it is still unclear as to whether or not this is simply an adaption to the extremely hydrophobic lipid environment or out of functional necessity.

To investigate the helical side chain properties further in peptoid analogues of SP-C, a group of peptoid-based mimics were created and characterized that attempts to optimize the molecular features of both the α-chiral, aromatic and the α-chiral, aliphatic side chains: structural rigidity from the aromatic side chains and side chain biomimicry from the aliphatic side chains.

Specifically, the mimics incorporate varying amounts of aromatic and aliphatic residues in the helical region, balancing the two molecular characteristics in one mimic. It was found that increasing the aliphatic content in the helical region incrementally increases the surface activity of the peptoid mimics, reducing the maximum surface tension during dynamic cycling. With the incorporation of approximately one-third aromatic side chains for structural rigidity and two-thirds aliphatic side chains for side chain biomimicry in the helical region, the structural and biomimicry requirements in this region were balanced and optimized, resulting in a mimic that displays superior surface activity than mimics composed solely of either aromatic or aliphatic side chains in the helical region. To further improve the surface activity of the optimized mimic, two alkyl chains were introduced in the *N*-terminal region of the balanced mimic. The amide-linked alkyl chains mimic the structure and hydrophobicity of the palmitoyl chains of SP-C. Alkylation of the optimized mimic further improved the surface activity, resulting in a surfactant film with comparable *in vitro* surface activities as a natural SP-C-containing formulation.

6.2 Materials and methods

6.2.1 Materials

Peptoid synthesis reagents were purchased from Applied Biosystems (Foster City, CA) and Sigma-Aldrich (Milwaukee, WI). Fmoc-protected amino acids, resins, and di-tert-butyl dicarbonate were purchased from NovaBiochem (San Diego, CA). The primary amines and palmitic acid (PA) were purchased from Sigma-Aldrich in the highest purity available. All organic solvents used for sample synthesis, purification, and preparation were HPLC-grade or better and were purchased from Fisher Scientific (Pittsburgh, PA). The synthetic phospholipids DPPC and palmitoyloleoyl phosphatidylglycerol (POPG) were purchased from Avanti Polar

Lipids (Alabaster, AL) and were used as received. Texas-Red® 1,2-dihexadecanoyl-*sn*-glycero-3-phosphoethanolamine, triethylammonium salt (TR-DHPE) was purchased from Molecular Probes (Eugene, OR). The native SP-C used in these studies was a kind gift from Dr. Perez-Gil and Dr. Ines Plasencia and was extracted from porcine lung surfactant utilizing the methodology of Perez-Gil et al. [179].

6.2.2 Peptoid synthesis

The peptoid-based SP-C mimics shown in Table 6.1 were synthesized on an automated 433A ABI Peptide Synthesizer (Foster City, CA) on solid support (Rink amide resin), following a two-step submonomer method as described by Zuckermann et al. [86]. Briefly, synthesis was carried out on 0.25 mmol Rink amide resin (NovaBiochem, San Diego, CA). After the removal of the first Fmoc protecting group from the resin with 20% piperidine in *N,N*-dimethylformamide (DMF) and rinsing of the resin with DMF, the monomer addition cycle was performed by first acetylating the resin with the addition of 1.2 M bromoacetic acid in DMF, followed by *N,N*-diisopropyl carbodiimide (DIC). The acetylation step was carried out for 45 minutes and then the resin was washed with DMF. The resin-bound halogen was then displaced by the addition of 1.0 M primary amine submonomer in *N*-methylpyrrolidinone (NMP) for 90 minutes. The two-step cycle was repeated until the desired length and sequence of the peptoid was obtained, except for the addition of the lysine-like submonomer, the alkyl chains, and the proline residues. The displacement step for the Boc-protected lysine-like and alkyl chain submonomers was extended to 120 minutes while for the addition of the proline residue, a PyBrop activating system was employed. Additionally, due to poor solubility in NMP, the alkyl submonomer was dissolved at

Table 6.1: Structures of peptoid-based SP-C analogues.

Compound	Structure
Mimic C	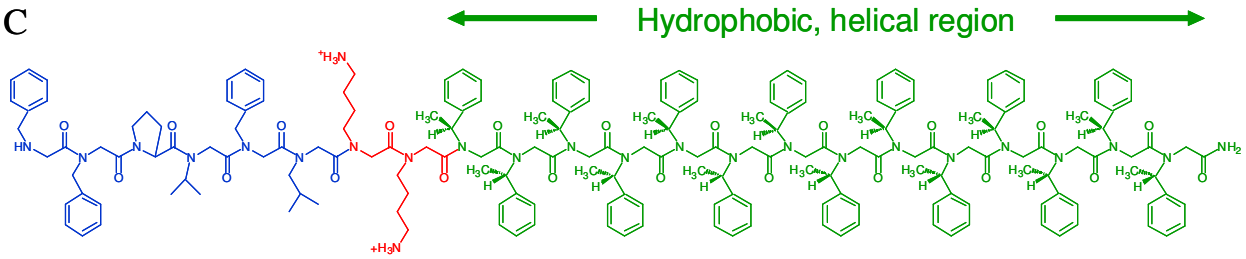
Mimic CIle1	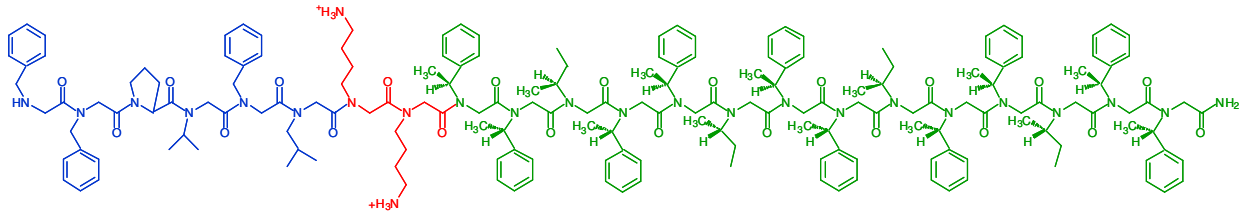
Mimic CIle2	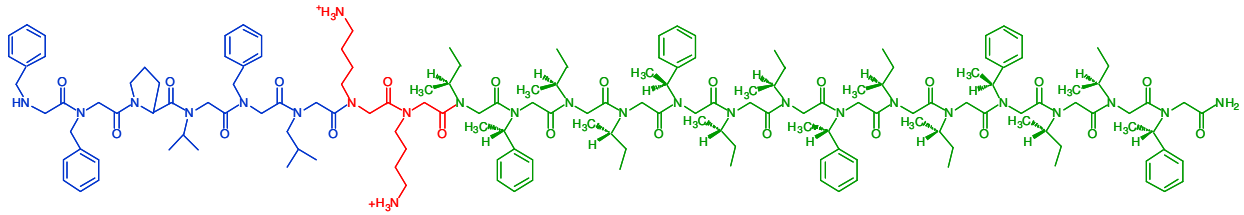
Mimic di-pCIle2	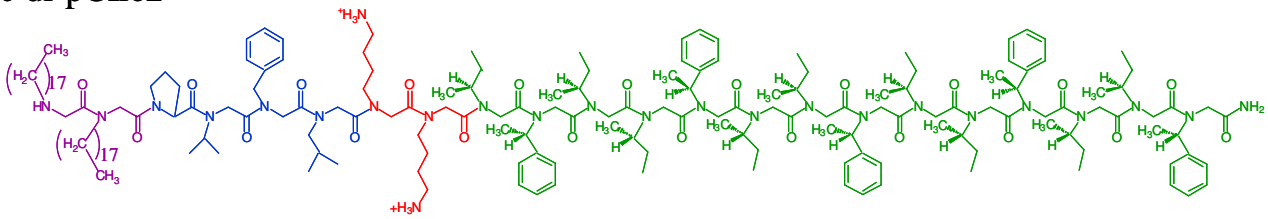

0.8 M in dichloromethane:methanol (1:1). After the proline addition, the Fmoc group was removed with piperidine as before and the peptoid cycle was continued. Peptoid oligomers were cleaved from the resin and deprotected with 90% TFA along with necessary scavengers for 5 minutes. The crude products were then purified by preparative HPLC on a Waters system with a Vydac C4 column and a linear gradient of 30-80% solvent C in solvent A over 70 minutes (solvent C = 0.1% TFA in isopropanol:acetonitrile, 1:1). The final purity of the peptoids was confirmed by reversed-phase HPLC to be > 97%. Electrospray mass spectrometry was used to confirm the correct molar masses.

6.2.3 Circular dichroism spectroscopy

Circular dichroism (CD) spectroscopy measurements were performed on a Jasco model 715 spectropolarimeter (Easton, MD). Stock solutions for dilution to appropriate concentrations for CD were made immediately before analysis in tared vials by precise weighing of added solvent and at least 2 mg of lyophilized peptoid powder, to produce a sample of accurately known concentration. The peptoid samples initially in methanol were diluted with additional methanol to a concentration of ~ 60 μM. CD spectra were acquired in a quartz cylindrical cell (Hellma model 121-QS, Forest Hills, NY) with a path length of 0.02 cm, employing a scan rate of 100 nm/min between 190-280 nm with 0.2 nm data pitch, 1 nm bandwidth, 2 second response, 100 mdeg sensitivity, and 40 successive spectral accumulations. Data are expressed in terms of per-residue molar ellipticity (deg cm^2/dmol), as calculated per mole of amide residues and normalized by the molar concentration of the peptoid.

6.2.4 Langmuir-Wilhelmy surface balance and fluorescent microscopy

Surface pressure-area isotherms were obtained using a home-built Langmuir-Wilhelmy surface balance (LWSB) as previously described [112]. For each experiment, the subphase was filled with a buffered suphase (0.15 M NaCl, 5 mM $CaCl_2$, and 10 mM HEPES at pH 6.90) and heated to either 25°C or 37°C. A Wilhelmy surface balance (Reigler & Kirstein, Berlin, Germany) was then calibrated and used to monitor the surface pressure as the area of the trough was either expanded or compressed. The surfactant material in an organic solution was spread at the air-water interface using a syringe and allowed to equilibrate for 10 minutes. The barriers were then compressed at a rate of 30 mm/min.

In order to obtain fluorescence microscopic (FM) images, a Nikon MM40 compact microscope stand with a 100W mercury lamp (Tokyo, Japan) was used in conjunction with the Langmuir trough. Fluorescence was detected by a Dage-MTI three-chip color camera (Dage-MTI, Michigan City, IN) in conjunction with a generation II intensifier (Fryer, Huntley, IL). Samples were spiked with 0.5 mol% of a fluorescently labeled lipid, TR-DHPE, for detection. Previous studies have shown that inclusion of the labeled lipid at this concentration does not alter surfactant film morphology [119]. Experiments were performed on an aqueous buffered subphase (0.15 M NaCl, 5 mM $CaCl_2$, and 10 mM HEPES at pH 6.90) at 37ºC with a barrier speed of 5 mm/min. The images were resized and enhanced in contrast and brightness within reasonable limits to make the features discernible for the purpose of display when warranted [147].

6.2.5 Pulsating bubble surfactometer

Static and dynamic characterization of surfactant film properties were performed on a modified pulsating bubble surfactometer (PBS) (General Transco, Largo, FL) as described by Seurynck et al., in which an imaging system is employed to accurately track bubble size and shape throughout the experiment [27]. Briefly, the lipid mixture (DPPC:POPG:PA, 68:22:9 (by weight)) was dissolved in chloroform:methanol (3:1) and spiked with 1.6 mol% SP-C protein or peptoid mimic, which is analogous to 10 wt% SP-C [104]. The samples were then prepared in Eppendorf tubes, dried under vacuum, and resuspended at room temperature in an aqueous buffer solution (0.15 M NaCl, 5 mM $CaCl_2$, and 10 mM HEPES at pH 6.90) to a phospholipid concentration of 1.0 mg/mL. Samples were then mixed with a pipette 20 times, sonicated with a probe sonicator for 15 seconds twice, and then mixed again 20 times with a pipette. Samples were then loaded into the sample chamber using a modified leak-free methodology [26]. The sample chamber was then placed on the PBS instrument at a temperature of 37°C. A bubble with a radius of 0.4 mm was then formed and an imaging acquisition system was used to determine the bubble size. Trans-film bubble pressure was recorded as a function of time while holding bubble radius static for 20 minutes during static adsorption experiments. Dynamic measurements of surface tension as a function of bubble surface area were subsequently collected by cycling the bubble radius between approximately 0.4 mm and 0.55 mm at an oscillation frequency of 20 cycles/min for 10 minutes.

6.3 Results and discussion

6.3.1 Peptoid design and rationale

SP-C is a functionally important constituent of lung surfactant. Its inclusion with the lung surfactant phospholipids greatly improves the adsorption of surfactant to the air-liquid interface and improves the respreading of the surfactant film during expansion of the film area, lowering the maximum surface tension. SP-C's biophysical activity is dominated by the presence of an extremely hydrophobic, rigid helix that contains only β-branch amino acids (predominately valine, leucine, and isoleucine). The exact side chain chemistry of this region seems to be of a lesser importance than the overall secondary structure of this regions as the replacement of SP-C's helix with the transmembrane segment of bacteriorhodopsin did not alter SP-C's surface activity [45, 63]. A similar finding was also observed in peptoid analogues of SP-C, in which a rigid, aromatic helix was superior in replicating a synthetic SP-C peptide's surface activity than a more biomimetic, aliphatic helix that was less structurally rigid [61]. Despite the superiority of the aromatic-based helix, the aliphatic-based mimic did display some favorable surface activities including a lower maximum surface tension during dynamic cycling. This suggests that a favorable interaction between the aliphatic peptoid side chains and the lipid acyl chains is present.

In order to combine features of both side chain chemistries in one mimic, varying amounts of α-chiral, aliphatic and α-chiral, aromatic residues were incorporated in the helical region of a peptoid mimic of SP-C. By doing this, it is desired to retain rigidity from the presence of the aromatic side chains, which provides bulky steric repulsion while also retaining the biomimicry from the presence of the isoleucine-like side chains of the α-chiral, aliphatic

residues. The designed peptoid SP-C mimics are shown in Table 6.1. Each of the analogues was designed to retain the patterning of polar and non-polar residues in SP-C as well as its helical secondary structure. The SP-C designed mimics consist of an achiral *N*-terminal region with side chain covalent structures analogous to those of human SP-C and a hydrophobic, α-chiral helical region, mimicking SP-C's helical secondary structure. The helical region in these analogues contains either entirely aromatic residues (Mimic C), one-third aliphatic, isoleucine-like residues (Mimic CIle1), or two-thirds aliphatic residues (Mimic CIle2), creating a range from the most rigid (Mimic C) to biomimetic (Mimic CIle2). Because of the 3-residue periodicity of peptoid helices, the α-chiral, aliphatic and aromatic residues were positioned in helical region to align facially so that Mimic CIle1 contains one aliphatic face and Mimic CIle2 contains two aliphatic faces. An entirely aliphatic mimic was not investigated as previous studies have shown that this mimic was inferior overall in comparison to the aromatic-based mimic [61]. Two *N*-terminal alkyl chains were also included in Mimic CIle2, resulting in Mimic di-pCIle2. These amide-linked alkyl chains mimic the length and hydrophobicity of the palmitoyl chains of SP-C and have been found to have a significant impact on the surface activity of a peptoid analogue of SP-C (Chapter 5).

6.3.2 Circular dichroism

SP-C's highly helical secondary structure in solution is critical to capture in a synthetic mimic as slight differences in helical content greatly impacts SP-C's biophysical surface activity [45]. The secondary structure must also be stable over time in solution, decreasing the difficulty associated with the metastable protein and increasing the lifetime of an SP-C-containing surfactant formulation. To characterize the secondary structure of the peptoid mimics, CD was

performed in methanol at room temperature (Figure 6.1). All the peptoid-based mimics exhibit spectral features consistent with helical structure. The spectrum for Mimic C is qualitatively similar to that of a peptide α-helix with an intense maximum at ~ 192 nm and a double minimum at ~ 205 nm and ~ 220 nm, which is indicative of a polyproline type-I-like peptoid helix and similar to other peptoids containing chiral, aromatic side chains [59, 115, 116, 160]. Increasing the aliphatic content in the helical region, results in a CD spectrum that is progressively similar to a typical polyproline type I peptide helix. The CD spectra for Mimics CIle1, CIle2, and di-pCIle2 contain a minimum at ~ 220 nm that is progressively weaker and the local minimum at ~ 205 nm is gradually shifted towards shorter wave-lengths. A local maximum is also observed at ~ 208 nm. The degree of spectral shift coincides with the amount of α-chiral, aliphatic side chains present with Mimic CIle2 and Mimic di-pCIle2 displaying spectra that are most similar to a polyproline type I helix. The presence of the alkyl chains in the peptoid analogue decreases the minimum at ~ 220 nm, but, otherwise, the CD spectrum is very similar to the unalkylated mimic (Mimic CIle2) and does not significantly alter the secondary structure of the peptoid mimic. Overall, the peptoid mimics are all structured and helical in solution and no change in helicity was observed over time, indicating that the secondary structures of the analogues are stable.

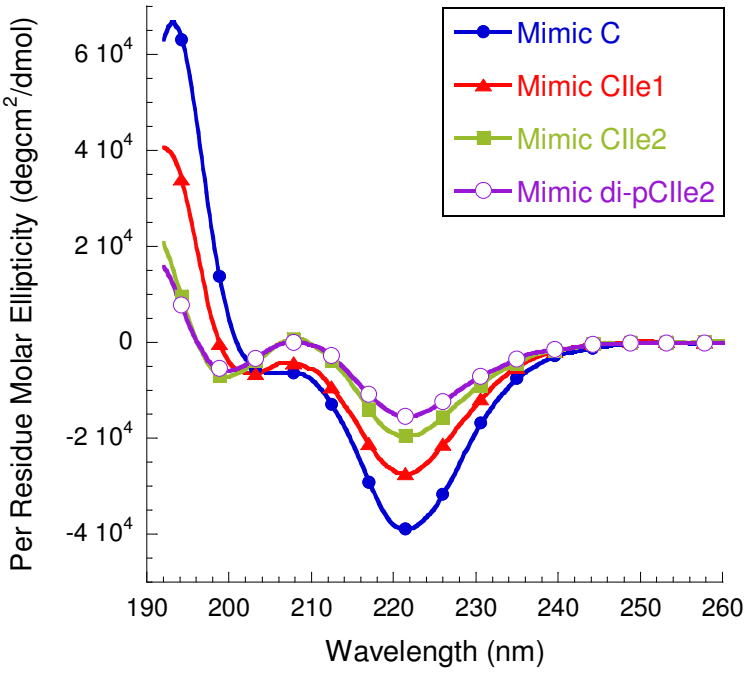

Figure 6.1: Circular dichroism (CD) spectra of the peptoid-based SP-C mimics (Mimics C, CIle1, CIle2, and di-pCIle2) showing qualitatively similar characteristics of peptoid helices. As the aliphatic content is increased, the CD spectra display features that are progressively similar to a polyproline type I peptide helix. Spectra were acquired in methanol at a concentration of ~ 60 µM at room temperature.

6.3.3 Langmuir-Wilhelmy surface balance

To determine the influence of the peptoid analogues on the monolayer phase behavior of a lipid film, the mimics were combined at 1.6 mol% with an optimized lipid formulation comprised of DPPC:POPG:PA (68:22:9, by weight). This formulation has been shown to closely mimic the behaviors of the lipid portion of lung surfactant [104, 162]. The resulting surfactant formulations were studied on the LWSB as previously described. The surface pressure-area LWSB isotherms at 37°C are shown in Figure 6.2. Similar trends were also observed at 25°C, but are omitted for clarity.

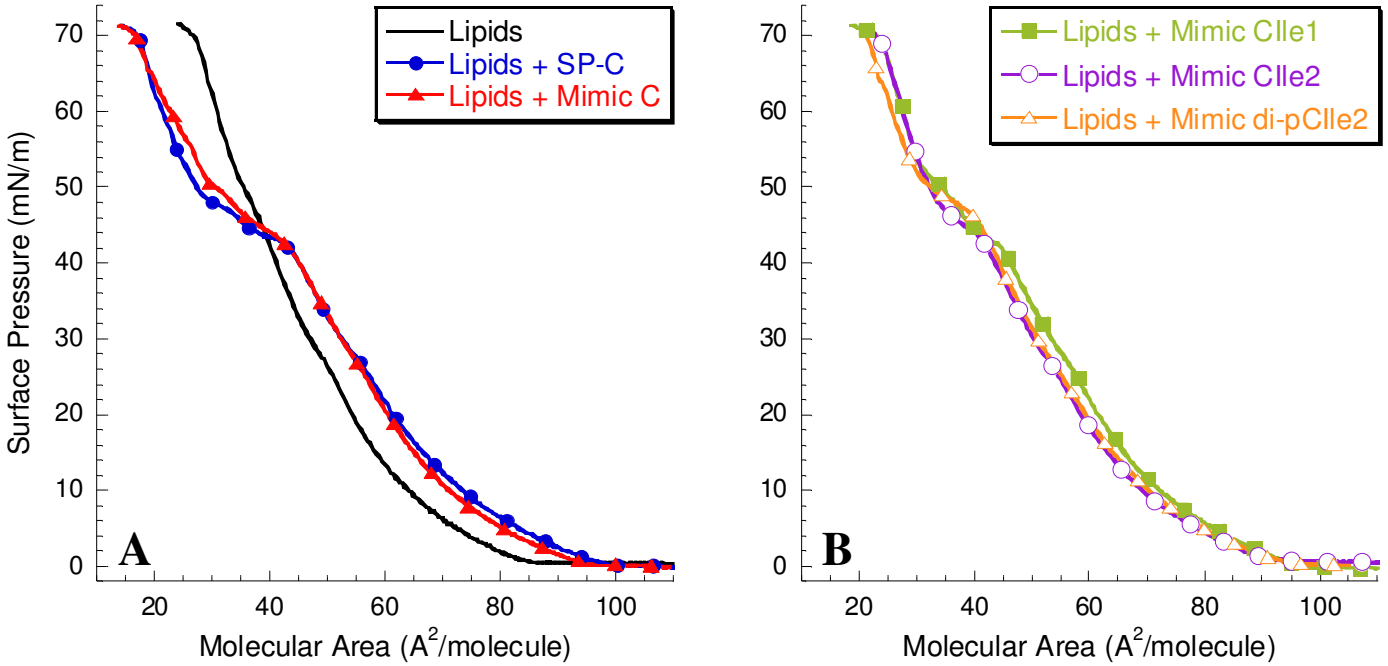

Figure 6.2: Langmuir-Wilhelmy surface balance (LWSB) studies at 37°C. (A) Surface pressure-area isotherms obtained for DPPC:POPG:PA (68:22:9, by weight) alone, with 1.6 mol% SP-C, and with 1.6 mol% Mimic C; (B) Lipids with 1.6 mol% Mimic CIIe1, Mimic CIIe2, and Mimic di-pCIIe2. Isotherms were collected on a buffered subphase (150 mM NaCl, 10 mM HEPES, 5 mM $CaCl_2$, pH=6.90).

For LWSB isotherms of lung surfactant, initially the material spread at the air-liquid interface is typically in the gaseous phase, where there is little interaction between the molecular species and no change in surface pressure. As the area available to the molecules is decreased with compression of the barriers, the molecules are in closer proximity and begin to interact with one another, forming a uniform liquid expanded (LE) phase. An initial increase in surface pressure (decrease in surface tension) is observed at this point and is termed "lift-off." An early lift-off (> 100 $Å^2$/molecule) is an important characteristic of lung surfactant [144]. Further compression of the interfacial surfactant layer causes increased interactions amongst the surfactant species and an increase in surface pressure leading to the coexistence of the LE and liquid condensed (LC) phases. As the surface layer is further compressed, a biomimetic plateau region in the isotherm is observed between 40-55 mN/m. This is likely due to the removal and rearrangement of the material from the interface and is more pronounced in the presence of SP-C [42, 149]. Eventually, the surface layer reaches a state of compression where interfacial layer can no longer accommodate a further reduction in surface area without being excluded from the interface, this point is termed collapse. Lung surfactant has a very high collapse pressure near 72 mN/m, corresponding to a low surface tension of ~ 0 mN/m.

Figure 6.2A shows that the LWSB isotherm for the lipid formulation without any added SP-C species has a lift-off point of ~ 85 $Å^2$/molecule. The slope of the isotherm is relatively small up to a surface pressure of ~12 mN/m, indicating high compressibility that is typical of the LE phase. As the surface layer is further compressed from 12 mN/m to ~ 48 mN/m, the slope of the isotherm increases, indicating a less compressible film consistent with the formation of LC domains of DPPC that are co-crystallizing with PA, which is in co-existence with the LE phase

[145, 163]. Further compression of the lipid film leads to a subtle shift in the isotherm at ~ 50 mN/m and a collapse pressure of ~ 72 mN/m. The addition of porcine SP-C to the lipid formulation dramatically alters the surface pressure-area isotherm characteristics. The lift-off is shifted to a greater molecular area (~ 97 $Å^2$/molecule vs. ~ 85 $Å^2$/molecule), indicating increased surface activity due to the presence of SP-C in the interfacial surfactant layer. At lower surface pressures, the isotherm is similar to the lipids alone, but shifted towards a greater molecular area. Further compression results in the occurrence of a dramatic, biomimetic plateau region beginning at ~ 42 mN/m. This is likely due to the formation of the surface-associated surfactant reservoir [149]. The presence of such a surfactant reservoir offers an explanation for how the SP-C protein is able to interact with lipids to provide low surface tension upon compression and to respread rapidly on expansion [149, 164]. A dramatic increase in surface viscosity is also observed for SP-C containing films at or above the plateau, which is thought to help minimize the loss of surfactant material from the alveoli at low surface tensions, and may be partially responsible for the high collapse pressure associated with lung surfactant [42]. Further compression of the SP-C containing formulation leads to a similar collapse pressure of ~ 72 mN/m.

The Mimic C containing formulation displays a LWSB isotherm that is nearly identical to SP-C, with a similar lift-off point of ~ 96 $Å^2$/molecule and a pronounce plateau at ~ 43 mN/m (Figure 6.2A). The entirely aromatic mimic replicates SP-C's monolayer phase behavior quite well. Adding one aliphatic face to the helical region, Mimic CIle1, similarly alters the surfactant film characteristics of the lipid formulation, but with some variation in the plateau region (Figure 6.2B). Lift-off is also shifted to higher molecular area, ~ 95 $Å^2$/molecule; however, the plateau

region is different than that observed for either SP-C or Mimic C. The Mimic CIle1 formulation displays a dual plateau at surface pressures ~ 43 mN/m and ~ 50 mN/m, but the extent of both of these regions together is equally pronounced as the single plateau region for SP-C and Mimic C. Adding Mimic CIle2 and Mimic di-pCIle2 also results in a similar isotherm with a lift-off of ~ 95 $Å^2$/molecule for both formulations. The plateau region is more similar to the SP-C and Mimic C containing films with only one kink in the isotherm occurring at ~ 43 mN/m for Mimic CIle2 and ~ 47 mN/m for Mimic di-pCIle2. The increase in the plateau pressure for the alkylated mimic is consistent with studies of an alkylated aromatic peptoid mimic of SP-C (Chapter 5). The formulations containing Mimic CIle2 and di-pCIle2 also have a high collapse pressure of ~ 72 mN/m.

6.3.4 Fluorescent microscopy

To further investigate the influence of SP-C and the peptoid SP-C mimics on the monolayer phase behavior, FM was used to characterize the surface film morphology as a function of surface pressure for the surfactant formulations. FM provides for the direct visualization of the surfactant monolayer at the air-liquid interface, enabling analysis of the impact the added species have on the formation and transition of the surfactant domain structures. Figure 6.3 displays the FM images obtained at 37°C at ~ 35 mN/m and ~ 50 mN/m for lipids alone (Figure 6.3, panels A and G), lipids with SP-C (Figure 6.3, panels B and H), lipids with Mimic C (Figure 6.3, panels C and I), lipids with Mimic CIle1 (Figure 6.3, panels D and J), with lipids and Mimic CIle2 (Figure 6.3, panels E and K), and lipids with Mimic di-pCIle2 (Figure 6.3, panels F and L).

Below the plateau region in the LWSB isotherm at a surface pressure of ~ 35 mN/m, all

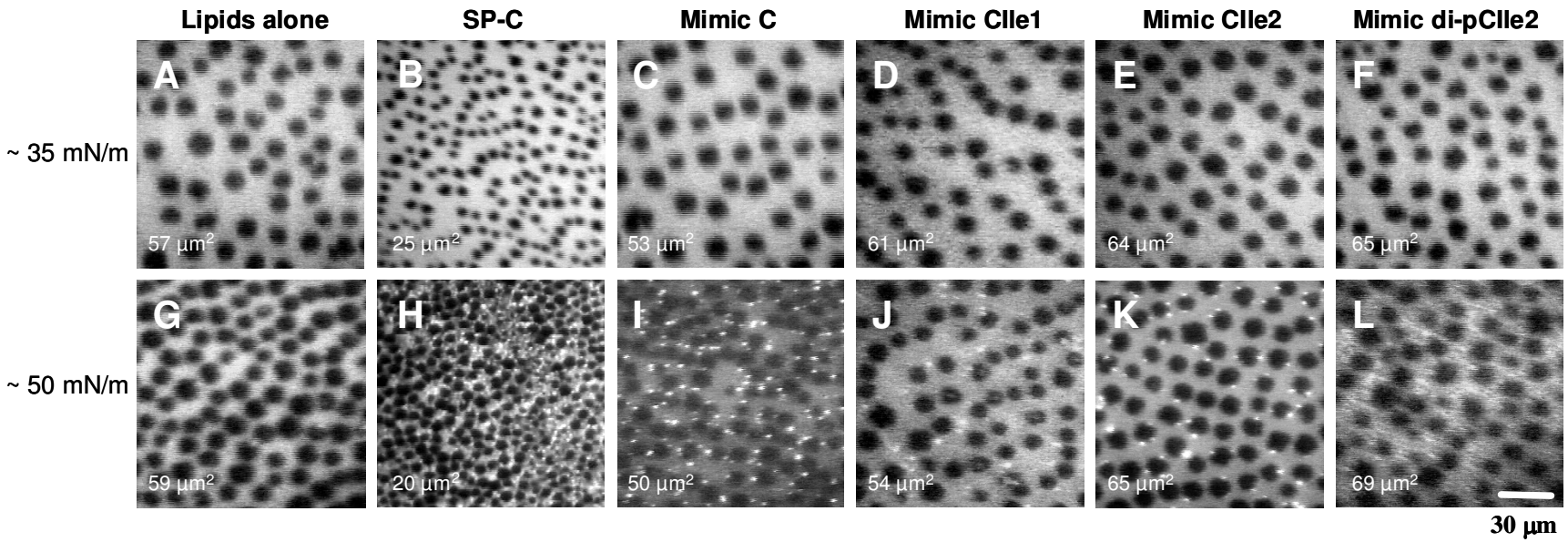

Figure 6.3: Fluorescence microscopy (FM) micrographs at 37°C corresponding to a surface pressure of ~ 35 mN/m and ~ 50 mN/m for DPPC:POPG:PA (68:22:9, by weight) alone (panels A and G), with 1.6 mol% SP-C (panels B and H), Mimic C (panels C and I), Mimic CIle (panels D and J), Mimic CIle2 (panels E and K), and Mimic di-pCIle2 (panels F and L). Average size of the dark LC domains for each film is indicated in the lower left of each panel.

the surfactant formulations exhibit a film morphology that is highly similar with the coexistence of a fluid LE phase with dark, circular LC phases. The film coverage and LC domain size (53-65 μm^2) are similar for all the formulations except the SP-C-containing formulation, which has much smaller LC domains, ~ 25 μm^2. Above the plateau region at ~ 50 mN/m, the film morphologies and trends in LC size are similar to those observed at the lower surface pressure except bright, vesicle-like domains are now present for all of the surfactant formulations excluding the lipids alone. These vesicles likely correspond to removal of surfactant material from the interface and the formation of a surface-associated surfactant reservoir. Their formation in the SP-C and SP-C mimic-containing films is also supported by the pronounce plateau region in the LWSB isotherms. All the peptoid-containing films display similar morphology to the SP-C film; however, the native protein is better able to condense the LC domains.

6.3.5 Static adsorption

Native lung surfactant initially dispersed in an aqueous subphase rapidly adsorbs to the air-liquid interface, reaching a surface tension below 25 mN/m in less than a minute. This rapid adsorption is one of the essential biophysical characteristics to mimic with a synthetic lung surfactant formulation and is enhanced by the presence of SP-C and SP-B [7, 10]. The static adsorption kinetics of the lipid mixture alone, and with the addition of 1.6 mol% SP-C and peptoid analogues, were characterized with a modified PBS run in static mode with a bubble radius of approximately 0.40 mm at 37°C. Figure 6.4 displays the adsorption surface tension as a function of time for the various surfactant formulations.

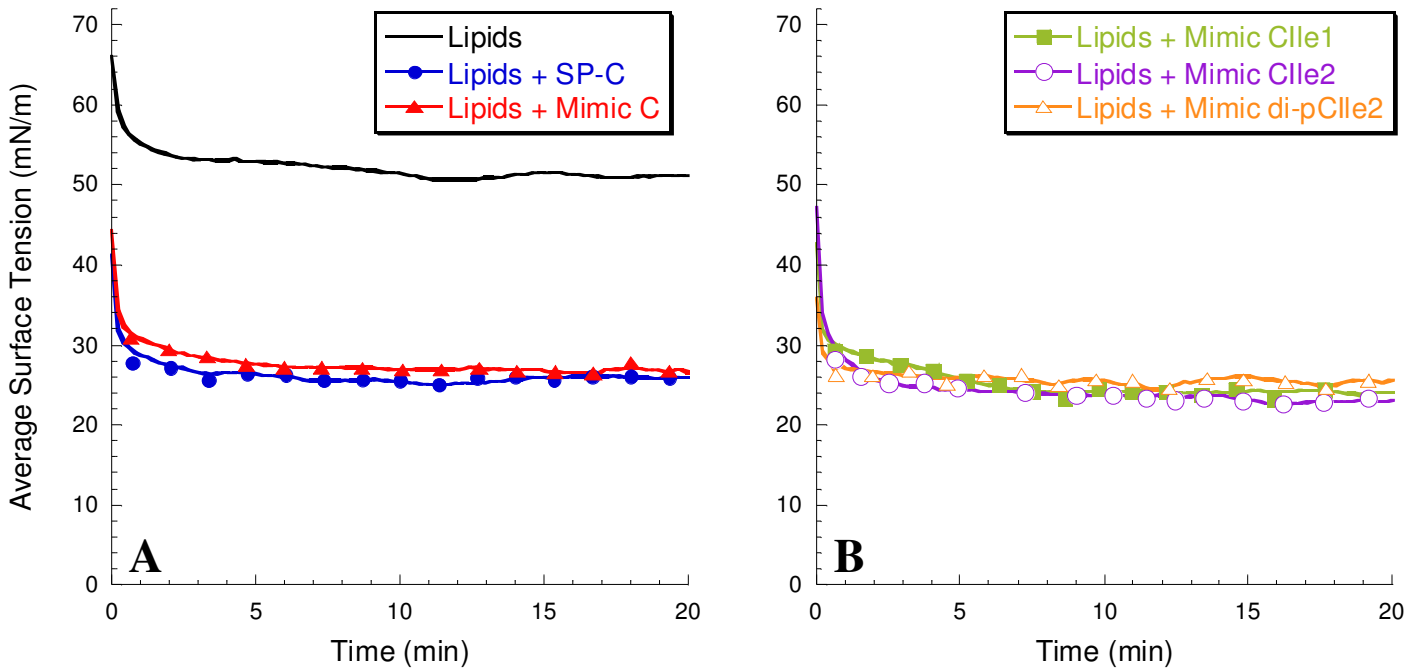

Figure 6.4: Static pulsating bubble surfactometry (PBS) results displaying surface tension as a function of time. (A) Lipid mixture alone and with 1.6 mol% SP-C and Mimic C; (B) Lipid mixture with 1.6 mol% Mimics CIIe1, CIIe2, and di-pCIIe2. Measurements were taken at a bulk surfactant concentration of 1 mg/mL lipids and at 37°C.

In the absence of any of the SP-C species, the lipid mixture displays very slow surface adsorption and fails to reach an equilibrium surface tension lower than ~ 50 mN/m even after 20 minutes of static adsorption. Adding SP-C to the lipid formulation dramatically improves the static adsorption kinetics, reaching an adsorption surface tension below 30 mN/m in less than a minute and a final surface tension of ~ 26 mN/m. All of the peptoid mimics similarly improve the surface adsorption of the lipid formulation. The formulations containing Mimics C, CIle1, CIle2, and di-pCIle2 all reach a static surface tension below 30 mN/m in less than one minute and a final surface tension of ~ 24-27 mN/m. The peptoid mimics appear to facilitate the adsorption and insertion of the dispersed surfactant material to the air-liquid interface in a manner very similar to SP-C. The presence of the aliphatic side chains in the helical region does not significantly alter the adsorption profile, which is somewhat surprising given that an entirely aliphatic peptoid mimic previously did not display favorable adsorption in a synthetic lipid formulation [61]. It is hypothesized that the maintenance of the aromatic side chains in the helical region increases the rigidity of the helical region due to increased steric repulsion, facilitating disruption and fusion of the dispersed surfactant structures to the air-liquid interface.

6.3.6 Dynamic cycling

Once at the air-liquid interface, lung surfactant exhibits several features that are important to mimic during dynamic compression and expansion cycles. These features include: (1) the ability to reach a very low surface tension with a small amount of compression; (2) an ability to respread rapidly upon expansion, and (3) an ability to control surface tension as a function of bubble surface area with the lowest minimum surface tension and a low maximum

surface tension [7, 10]. To investigate the effectiveness of the peptoid-based SP-C formulations to reduce and control surface tension as a function of surface area, PBS experiments were performed at 37°C in a dynamic mode with an oscillation frequency of 20 cycles/min and ~ 50% reduction in surface area. Figure 6.5 displays the surface tension as a function of bubble surface area for lipid mixtures with and without SP-C and Mimic C (6.5A) and those containing Mimics CIle1, CIle2, and di-pCIle2 (6.5B).

The lipid mixture without any added SP-C species is unable to reduce the surface tension below 13 mN/m during compression and, upon expansion, the maximum surface tension rises to ~ 61 mN/m. Also, a large amount of compression is required for the lipid formulation to reach its lowest surface tension. These dynamic compression-expansion characteristics are not acceptable for a biomimetic SRT. The addition of SP-C to the lipid formulation results in surface-active features that are significantly improved relative to the lipid formulation alone. Both the minimum and maximum surface tensions are significantly lower, < 1 mN/m and ~ 39 mN/m, respectively. The surfactant film with SP-C is also much less compressible, requiring less compression to reach a low surface tension.

The addition of the peptoid-based SP-C mimics to the lipid formulation also results in an improvement of the lipid formulation's surface-active features during dynamic cycling. The presence of Mimic C causes a reduction in the maximum and minimum surface tensions to ~ 53 mN/m and <1 mN/m, respectively. These improvements are significantly better than the lipid formulation, but are inferior relative to native SP-C. Adding one aliphatic face into the helical region (Mimic CIle1) results in a compression-expansion loop that is very similar to Mimic C, but with the maximum surface tension slightly reduced to ~ 50 mN/m. The introduction of a

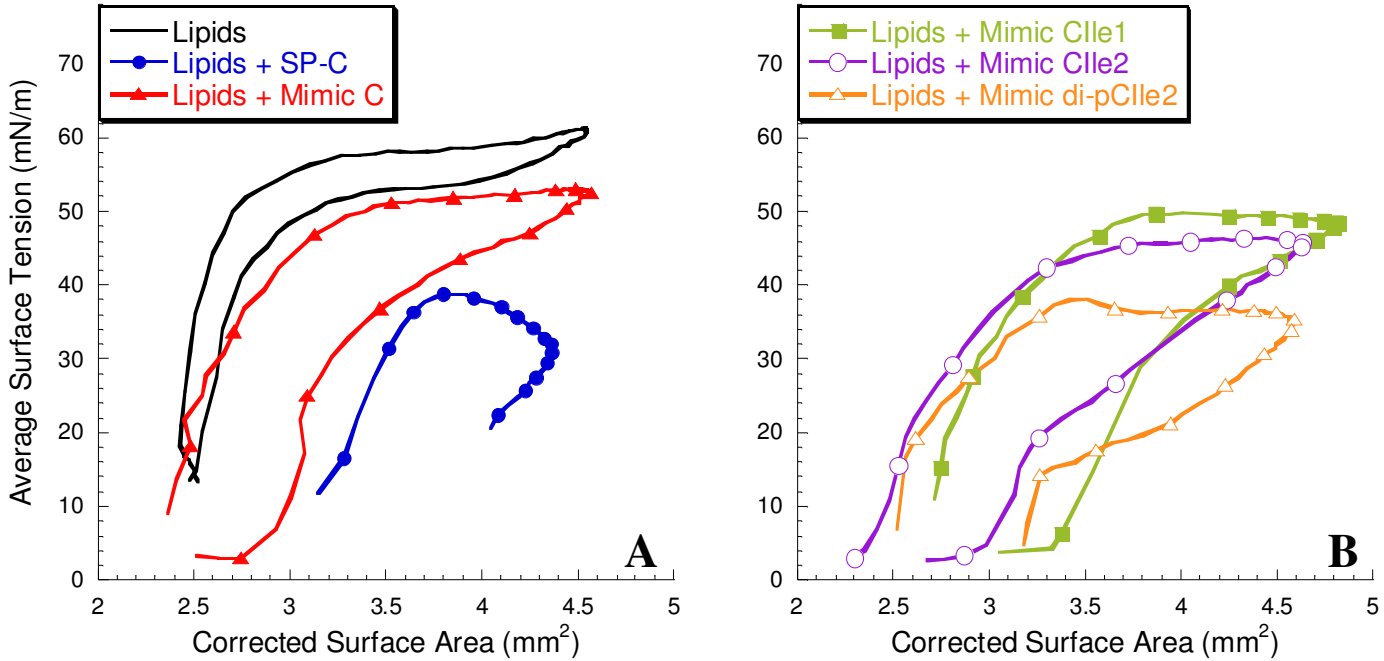

Figure 6.5: Dynamic pulsating bubble surfactometry (PBS) results displaying surface tension as a function of surface area at an oscillation frequency of 20 cycles/min, after 5 minutes of initial cycling. (A) Lipid mixture alone and with 1.6 mol% SP-C and Mimic C. (B) Lipid mixtures with 1.6 mol% Mimics CIIe1, CIIe2, and di-pCIIe2. Measurements were taken at a bulk surfactant concentration of 1 mg/mL lipids and at 37°C.

second α-chiral, aliphatic face into the helical region (Mimic CIle2) further improves the dynamic compression-expansion film behavior, resulting in a maximum surface tension of ~ 47 mN/m. The reduction in maximum surface tension indicates that the inclusion of aliphatic side chains in the helical region is promoting favorable interactions between the lipid acyl chains and the hydrophobic helices of the peptoid analogues. This interaction is thought to increase the aliphatic-containing peptoid mimics' association with excluded surfactant material, better enabling the reincorporation of this material upon expansion and reducing the maximum surface tension. The maintenance of the α-chiral, aromatic side chains is also necessary as their removal leads to a surfactant film that requires a significant amount of compression to reach a low surface tension [61]. By creating a mimic that utilizes features of both aromatic and aliphatic side chain chemistries, the structural and biomimetic requirements of the hydrophobic helical region were balanced and the surface activity of the SP-C mimic optimized.

Despite the much improved surface activity, Mimic CIle2 does not fully replicate the very low maximum surface tension exhibited by SP-C-containing surfactant film. This is likely due to the presence of the two palmitoyl chains in the *N*-terminal region of natural SP-C. These structural motifs are thought to play an important role in maintaining SP-C and associated phospholipids with the interfacial surfactant film at very high levels of compression, acting as a hydrophobic "anchor" for the excluded surfactant material and aiding in the reincorporation of this material during expansion. When two alkyl chains are added to the *N*-terminal region of Mimic CIle2 (Mimic di-pCIle2), it is found that the maximum surface tension during dynamic cycling is dramatically reduced to ~ 39 mN/m (Figure 6.5B). Both the maximum and minimum

surface tensions of the Mimic di-pCIle2 formulation are comparable to the SP-C formulation and have great promise for use in a biomimetic SRT formulation.

6.4 Conclusions

The C-terminal hydrophobic helix of SP-C has been shown to greatly influence SP-C's many reported interactions and surface activities in a phospholipid environment; however, because of the high content of β-branched amino acids, the helix is metastable in solution and prone to misfolding into inactive, non-helical conformations [44, 63]. This makes working with the natural protein and sequence identical analogues very difficult. To address this, researchers have pursued synthetic peptide mimics of SP-C in which the molecular parameters of the hydrophobic helix are preserved with alternative covalent structures [45, 50, 54, 93, 94]. This strategy attempts to retain SP-C's functionality while overcoming its aggregation propensity for possible use in a biomimetic SRT for the treatment of RDS. Corresponding structure-function studies of the helical region have confirmed that the secondary structure of this region is the dominant feature to mimic rather than the exact side chain chemistry.

Despite this, the poly-valyl helix of SP-C is highly conserved amongst all species studied thus far, suggesting an important functional role; however, it is still unclear whether this unique stretch of amino acids is an adaptation to the extreme hydrophobic environment or due to functional necessity [28, 105]. Similar work with peptoid-based analogues of SP-C has also shown that the overall secondary structure of the helical region was also the predominate feature to emulate rather than the exact side chain chemistry [61, 62]. Peptoid mimics utilizing structurally rigid, aromatic residues in the helical region were found to have superior SP-C-like behaviors than more biomimetic analogues containing a less structurally rigid, aliphatic helix;

however, the aliphatic-based peptoid mimics did display a lower maximum surface tension during dynamic cycling of the surfactant film. This suggests a specific interaction between the lipid acyl chains and the aliphatic side chains of the peptoid helix. To further investigate this, a set of peptoid SP-C analogues was created that incorporate both aromatic and aliphatic residues in the helical region in an attempt to combine structural features of the aromatic residues and biomimetic features of the aliphatic residues in one SP-C mimic. The analogues studied were an entirely aromatic mimic (Mimic C), a mimic with one aliphatic, isoleucine-like, face (Mimic CIle1), and a mimic containing two aliphatic faces, (Mimic CIle2).

CD spectroscopy studies of the synthetic analogues showed that all the peptoid-based mimics were structured, helical, in solution and the spectral characteristics did not change over time. The surface activities of these analogues in a surfactant lipid film were characterized *in vitro* using LWSB, FM, and PBS, and compared to native porcine SP-C. These studies revealed that both the side chain chemistry and the rigid secondary structure of the helical region are necessary components of an analogue of SP-C. All the peptoid analogues displayed favorable surface-active features when combined with a synthetic lipid formulation; however, increasing the aliphatic content of the helical region incrementally increased the surface activity of the peptoid mimics. The surfactant containing Mimic CIle2 displayed the lowest maximum surface tension during dynamic cycling while retaining a low compressibility due to the presence of the aromatic residues. Despite the favorable surface activity of Mimic CIle2, it was not as great as natural SP-C. To further improve the activity of Mimic CIle2, two alkyl chains were included in the *N*-terminal region. These amide-linked alkyl chains are similar to the palmitoyl chains of natural SP-C. This modification dramatically reduced the maximum surface tension of the

surfactant formulation and was comparable to natural SP-C. Therefore, the structural and biomimetic requirements of SP-C in a peptoid analogue were optimized by balancing the molecular and structural characteristics of both the helical C-terminal region and the amphipathic *N*-terminal region. These novel mimics capture the requisite features of SP-C, but because of their unique sequences, overcome many of the difficulties associated with the natural protein. Therefore, peptoid-based analogues hold great potential for use in a biomimetic SRT for the treatment of RDS.

Chapter 7: SP-C peptoid biomimicry: combining structural rigidity and side chain biomimicry in one peptoid residue

The use of non-natural oligomers to mimic the secondary structure and function of native protein species is an active area of research with great therapeutic potential. One interesting approach that is particularly promising is the use of a poly-*N*-substituted glycines, or peptoids. Peptoids have been recently used in a variety of applications to successfully mimic the secondary structure and hydrophobic patterning of simple, helical proteins; however, because of their unique structure, overcome some of the therapeutic difficulties associated with the native protein species. Here, a group of peptoid oligomers is reported with designed sequences and structures to mimic the hydrophobic and helical protein of the lung surfactant system, surfactant protein C (SP-C).

SP-C is a critical constituent of lung surfactant and is included in exogenous surfactant replacement therapies for the treatment of respiratory distress syndrome in premature infants. However, the native protein is exceedingly difficult to work with and in limited supply. Building upon previous structure-function studies of peptoid-based mimics of SP-C, a new helix-inducing side chain is utilized that combines the structural and biomimetic sequence requirements of the hydrophobic helix in a single side chain structure. Peptoid mimics incorporating varying amounts of this bulky, aliphatic residue in the helical region were investigated for their ability to mimic native SP-C's unique surface activity in a phospholipid film. *N*-terminal alkyl chains were also added to one of the mimics to investigate the influence of the palmitoyl-like modification on structure and surface activity. The secondary structures of the peptoid SP-C

mimics were assessed in organic solution using circular dichroism. Pulsating bubble surfactometry and fluorescence imaging of giant unilamellar vesicles were used to characterize the static and dynamic surface activity and film morphology of the mimics in a biomimetic phospholipid formulation. The results show that the rationally designed peptoid analogues are able to fully replicate not only the biophysical activity of native SP-C, but also display similar compression-expansion behavior as natural lung surfactant containing both SP-B and SP-C proteins. These studies provide strong evidence that peptoid analogues of SP-C hold forth significant promise for use in a synthetic surfactant replacement therapy for the treatment of respiratory distress syndrome.

7.1 Introduction

Lung surfactant is a unique biomaterial that is formed in alveolar epithelium. This material is essential for proper respiration as it functions at the alveolar air-liquid interface to dramatically reduce the surface tension at end expiration, preventing the lungs from collapsing. A lack or a deficiency of functional lung surfactant due to alveolar immaturity in premature infants leads to neonatal respiratory distress syndrome (nRDS). nRDS was a leading cause of infant mortality, but is now routinely treated by the airway instillation of exogenous surfactant extracted from animal lungs. The adoption of surfactant replacement therapy (SRT) has is largely responsible for the dramatic decline in infant mortality rates observed in the past 20 years [15, 72]. Despite the efficacy of SRT, there still exist several concerns associated with the use of natural surfactant including: cost, batch-to-batch variability, and possible infectious complications [5, 8, 12, 15]. Recent evidence has also shown that SRTs may be beneficial in the

treatment of other respiratory-related disorders in adult airways; however, this would require significantly more material than current isolation procedures can produce [49, 186, 187].

The concerns associated with natural SRTs as well as the limited production potential have prompted investigation towards the creation of an entirely synthetic SRT with the same efficacy as the natural material; however, this endeavor is much more complicated than first thought, largely due to the great complexity of the lung surfactant components [12]. Lung surfactant is made up of ~ 90% lipids and ~ 10% proteins. The lipid portion of lung surfactant consists of at least 50 different lipid species with dipalmitoyl phosphatidylcholine (DPPC) being the main surface tension reducing agent along with the other saturated phospholipids. Four surfactant proteins, SP-A, SP-B, SP-C, and SP-D, are also present in lung surfactant. The two hydrophilic proteins, SP-A and SP-D, belong to the C-type collagenous lectin protein family and are primarily responsible in the host-defense activities of the airways. These proteins are not included in animal-derived SRTs due to the organic extraction procedures used to obtain the exogenous surfactant [8]. While the hydrophobic proteins of lung surfactant, SP-B and SP-C, only constitute ~ 1-2% of lung surfactant's mass, they are critical constituents of lung surfactant and are necessary components in exogenous SRTs to treat nRDS [8, 14]. Their inclusion with the phospholipids dramatically increases surfactant adsorption and spreading at the alveolar air-liquid interface.

Synthetic surfactants have attempted to mimic the functional constituents of lung surfactant; however, mimicking the hydrophobic proteins, SP-B and SP-C, has proven to be rather difficult. SP-B is too large (79 amino acids) and structurally complex to mimic with synthetic peptides and no recombinant form of SP-B has yet been reported. SP-C, on the other

hand, is relatively small (35 amino acids) and lacks any tertiary structure; however, SP-C is extraordinarily hydrophobic and has a high propensity to misfold and aggregate into inactive conformations [44]. Recently, simplified peptide sequences and non-natural oligomers have been used to mimic the activities of SP-B and SP-C [46, 50, 54, 62, 94, 111, 112, 132, 188]. One interesting approach is the use of poly-*N*-substituted glycines or "peptoids" for the mimicry of small proteins [56, 61, 62, 112, 189]. Peptoids are similar to peptides except that the side chains are appended to the amide nitrogens rather than to the α-carbons [86]. This feature renders peptoids essentially invulnerable to protease degradation, making them more biostable than peptides [55]. Despite the achirality of the *N*-substituted glycine backbone and its lack of hydrogen bond donors, peptoids are able to adopt extraordinarily stable, chiral helices when substituted with α-chiral, sterically bulky side chains [59, 60, 116]. This ability to form stable helices makes peptoids an excellent candidate for mimicry of bioactive molecules that rely on helical structure for proper function, such as the hydrophobic proteins of lung surfactant [58, 61, 112].

Here, continued work is reported on structure-activity relationships in peptoid-based analogues of SP-C. It was previously shown that similar design strategies present in peptide analogues of SP-C are also present in peptoid analogues [62]. Peptoid analogues of SP-C that emulated SP-C's extreme hydrophobicity, highly helical structure, and longitudinal amphipathicity are able to reproduce many of SP-C's biophysical properties [62]. Subsequent work has also shown that the side chain chemistry and structural rigidity of the C-terminal helical region along with the alkyl chains of the *N*-terminal region are important for the biophysical activity of the peptoid-based mimics (Chapters 5 and 6). Building upon this

structural insight, a new helix-inducing side chain, *N*-S-dipropylamine (*N*sdp) was utilized, that is thought to better combine the structural and biomimetic sequence requirements of the hydrophobic helix in a single side chain structure. Peptoid mimics incorporating varying amounts of *N*sdp in the helical region were synthesized and subsequently characterized. An alkylated version of a mimic containing solely *N*sdp residues in the helical region was also studied as this modification greatly increases the surface activity of peptoid-based SP-C mimics. The secondary structures of the peptoid SP-C mimics were assessed in organic solution using circular dichroism (CD) spectroscopy. Pulsating bubble surfactometry (PBS) and fluorescence imaging of giant unilamellar vesicles (GUVs) were used to characterize the static and dynamic surface activity and film morphology of the mimics in a biomimetic phospholipid formulation.

7.2 Materials and methods

7.2.1 Materials

Peptoid synthesis reagents were purchased from Applied Biosystems (Foster City, CA) and Sigma-Aldrich (Milwaukee, WI). Fmoc-protected amino acids, resins, and di-tert-butyl dicarbonate were purchased from NovaBiochem (San Diego, CA). The primary amines and palmitic acid (PA) were purchased from Sigma-Aldrich in the highest purity available. All organic solvents used for sample synthesis, purification, and preparation were HPLC-grade or better and were purchased from Fisher Scientific (Pittsburgh, PA). The synthetic phospholipids DPPC and palmitoyloleoyl phosphatidylglycerol (POPG) were purchased from Avanti Polar Lipids (Alabaster, AL) and were used as received. Alexa Fluor® 488 carboxylic acid, succinimidyl ester was purchased from Invitrogen (Carlsbad, CA). The native SP-C used in

these studies was a kind gift from Dr. Perez-Gil and Dr. Ines Plasencia and was extracted from porcine lung surfactant utilizing the methodology of Perez-Gil et al. [179].

7.2.2 Peptoid synthesis

The peptoid-based SP-C mimics shown in Table 7.1 were synthesized on an automated 433A ABI Peptide Synthesizer (Foster City, CA) on solid support (Rink amide resin), following a two-step submonomer method as described by Zuckermann et al. [86]. Briefly, synthesis was carried out on 0.25 mmol Rink amide resin (NovaBiochem, San Diego, CA). After the removal of the first Fmoc protecting group from the resin with 20% piperidine in *N,N*-dimethylformamide (DMF) and rinsing of the resin with DMF, the monomer addition cycle was performed by first acetylating the resin with the addition of 1.2 M bromoacetic acid in DMF, followed by *N,N*-diisopropyl carbodiimide (DIC). The acetylation step was carried out for 45 minutes and then the resin was washed with DMF. The resin-bound halogen was then displaced by 1.0 M primary amine submonomer in *N*-methylpyrrolidinone (NMP), which was added to the resin and allowed to react for 90 minutes. The two-step cycle was repeated until the desired length and sequence of the peptoid was obtained, except for the addition of the lysine-like submonomer (*N*Lys), the alkyl submonomers (*N*ocd), and the proline residue. The displacement step for the Boc-protected *N*Lys submonomer and the *N*ocd submonomers was extended to 120 minutes while for the addition of the proline residue, a PyBrop activating system was employed. Additionally, due to poor solubility in NMP, the *N*ocd submonomer was dissolved at 0.8 M in dichloromethane:methanol (1:1). After the proline addition, the Fmoc group was removed with piperidine as before and the peptoid cycle was continued.

Table 7.1: Structures of peptoid-based SP-C analogues.

Compound	Structure
Mimic C	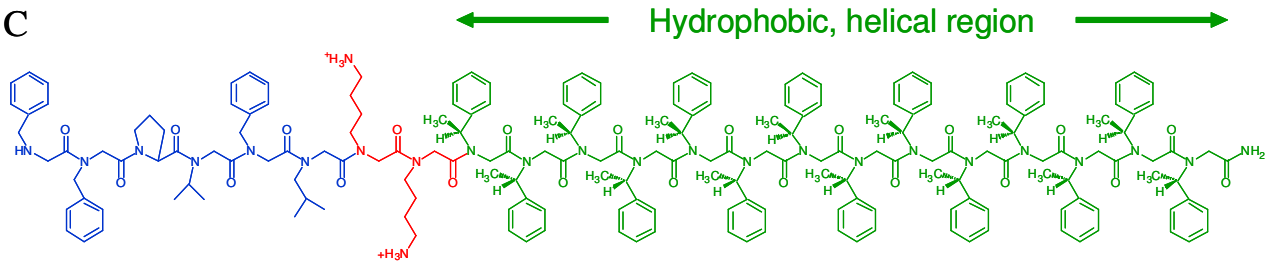
Mimic CLeu2	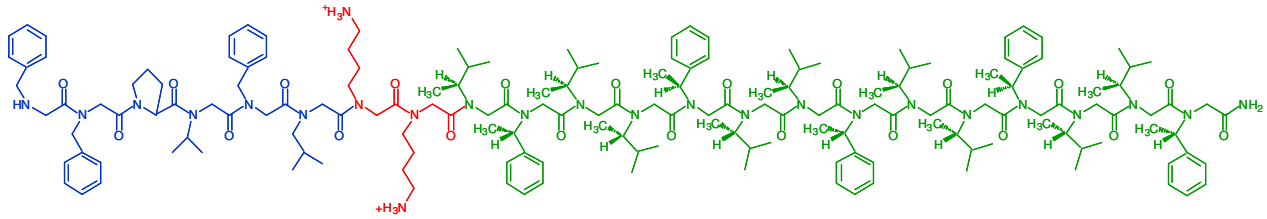
Mimic CLeu3	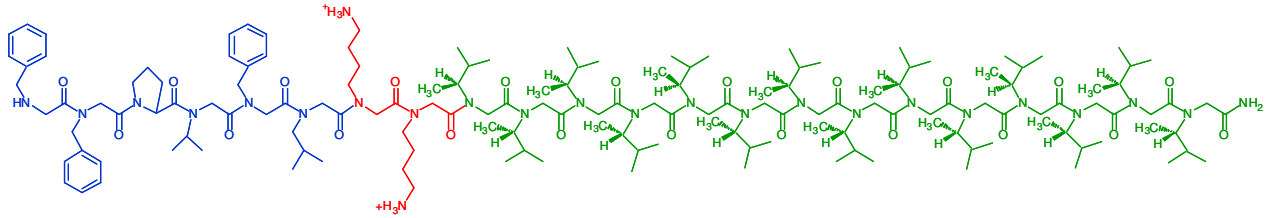
Mimic di-pCLeu3	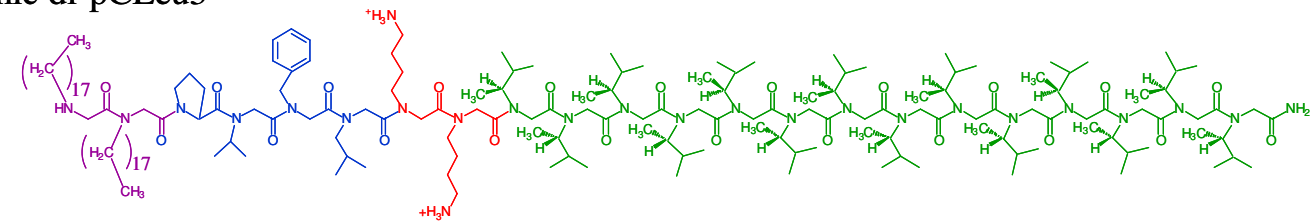

Peptoid oligomers were cleaved from the resin and deprotected with 90% TFA along with necessary scavengers for 5 minutes. The crude products were then purified by preparative HPLC on a Waters system with a Vydac C4 column and a linear gradient of 50-90% solvent B in solvent A over 70 minutes (solvent A = 0.1% TFA in water and solvent B = 0.1% TFA in isopropanol). The final purity of the peptoids was confirmed by reversed-phase HPLC to be > 97%. Electrospray mass spectrometry was used to confirm correct molar masses of the peptoids.

7.2.3 Natural lung surfactant isolation and extraction

Native lung surfactant was obtained from freshly slaughtered ovine lungs (Chiappetti Lamb and Veal, Chicago, IL) following procedures previously reported [80-82]. Briefly, excised lungs with trachea and bronchi intact were lavaged with ~ 2 liters of cold (4°C) 0.15 M NaCl under 25 cm H_2O of pressure within 1 hour of tissue procurement. After instillation of the saline solution, the filled lungs were elevated and the return collected by passive drainage. Collected lavage material showing any signs of contamination with blood was discarded. Blood-free lavage fluid was then pooled and centrifuged at 150 x g at 4°C for 10 minutes to remove any cellular debris. The supernatant containing the surfactant material was retained and pooled again. The crude surfactant was then harvested by medium-speed centrifugation at 20,000 x g at 4°C for 45 minutes. The pelleted surfactant was resuspended in 0.15 M NaCl and dispersed by injection through a syringe fitted with a 22-gauge needle. The resuspended material was then layered over 0.8 M sucrose in 0.15 M NaCl and centrifuged at 30,000 x g at 4°C for 45 minutes using a swinging bucket rotor. Pellicles at the interface were aspirated, pooled, and resuspended in 0.15 M NaCl as before. The collected material was then ultracentrifuged at 60,000 x g at 4°C

for 30 minutes to wash and concentrate the whole surfactant. The supernatant from this step was discarded and the pelleted material was resuspended in a small amount of 0.15 M NaCl.

The surfactant lipids and the hydrophobic proteins were then extracted from the isolated whole surfactant by the method of Bligh and Dyer [83]. The extracted surfactant dissolved in the organic solvent was dried under a stream of nitrogen and then placed under high vacuum overnight. The fully dried material was then reconstituted by adding a small amount of aqueous buffer (0.15 M NaCl, 5 mM $CaCl_2$, and 10 mM HEPES at pH 6.90) and aspirated through a 22-gauge needle. The lipid concentration of the purified surfactant was then quantified using the method of Stewart while the protein content was determined using a BCA protein assay kit (Thermo Fisher Scientific, Rockford, IL) [84].

7.2.4 Peptide synthesis

A di-alkylated peptide mimic of SP-C (di-pSP-C) was used for the giant unilamellar vesicle (GUV) studies as the labeling of native SP-C is quite problematic due to the unstable secondary structure. di-pSP-C was synthesized on a 0.25 mmol scale on an Applied Biosystems 433A automated peptide synthesizer, using standard Fmoc chemistry, and a prederivatized low-loading, Wang-Leu resin except for the acetylation and deprotection steps in which dimethyl sulfoxide was used as the solvent during acetylation and a 4% (v/v) 1,8-diazabicyclo-[5.4.0]undec-7-ene:piperidine (1:1) in DMF solution was used for deprotection. Cleavage and deprotection of the peptide-resin was carried out by mixing with aqueous 90% TFA and necessary scavengers for 2 hours. The reaction mixture was then immediately filtered, diluted with isopropanol and water, frozen, and lyophilized to yield the crude peptide. The crude material was then dissolved with hexafluoroisopropanol and isopropanol.

The crude SP-C peptide was purified by preparative HPLC on a Waters system with a Vydac C4 column and a linear gradient of 60-100% solvent B in solvent A over 60 minutes (solvent A = 0.1% TFA in water and solvent B = 0.1% TFA in isopropanol). The final purity of the protein was confirmed by reversed-phase HPLC to be > 97%. Electrospray mass spectrometry was used to confirm correct molar mass.

7.2.5 Peptide and peptoid fluorescent labeling

Fluorescently labeled di-pSP-C and SP-C peptoid mimics were prepared by labeling the peptide in organic solvent as described previously [190]. Briefly, ~ 2 mg each of the purified peptide and peptoids were dissolved in a small amount of methanol, ~ 3 mL. The apparent pH of the peptide and peptoid solutions was adjusted to ~ 7.0 by adding an appropriate volume of 50 mM triethylamine in methanol. The pH adjustment is necessary so as to preferentially deprotonate the *N*-terminal amine group, allowing for more specific labeling. The peptide and peptoid solutions were then separately incubated in total darkness at 4°C with constant stirring in the presence of Alexa Fluor® 488 carboxylic acid, succinimidyl ester. The reaction was stopped after 12 hours by the addition of 2 M HCl until the pH decreased below 3. The unreacted probe was then immediately separated from the labeled compounds by reverse-phase HPLC on a Jupiter C18 column (Phenomenex, Torrance, CA) using a gradient of 30-90% solvent B in solvent A over 40 minutes (solvent A = 0.1% TFA in water and solvent B = 0.1% TFA in isopropanol). The isolated labeled compounds were collected in tared vials and lyophilized to remove excess solvent.

7.2.6 Circular dichroism spectroscopy

CD measurements were performed on a Jasco model 715 spectropolarimeter (Easton, MD). Stock solutions for dilution to appropriate concentrations for CD were made immediately before analysis in tared vials by precise weighing of added solvent and at least 2 mg of lyophilized peptoid powder, to produce a sample of accurately known concentration. The peptoid samples initially in methanol were diluted with additional methanol to a CD sample concentration of ~ 60 μM. CD spectra were acquired in a quartz cylindrical cell (Hellma model 121-QS, Forest Hills, NY) with a path length of 0.02 cm, employing a scan rate of 100 nm/min between 185-280 nm with 0.2 nm data pitch, 1 nm bandwidth, 2 second response, 100 mdeg sensitivity, and 40 successive spectral accumulations. Data are expressed in terms of per-residue molar ellipticity (deg cm^2/dmol), as calculated per mole of amide residues and normalized by the molar concentration of the peptoid.

7.2.7 Pulsating bubble surfactometer

Static and dynamic characterization of surfactant film properties were performed on a modified PBS (General Transco, Largo, FL) as described by Seurynck et al. in which an imaging system is employed to accurately track bubble size and shape throughout the experiment [27]. Briefly, the lipid mixture (DPPC:POPG:PA, 68:22:9 (by weight)) was dissolved in chloroform:methanol (3:1) and spiked with 1.6 mol% SP-C protein or peptoid mimic, analogous to 10 wt% SP-C [104]. The samples were prepared in Eppendorf tubes, dried under vacuum, and resuspended at room temperature in an aqueous buffer solution (0.15 M NaCl, 5 mM $CaCl_2$, and 10 mM HEPES at pH 6.90) to a phospholipid concentration of 1.0 mg/mL. Samples were then mixed with a pipette 20 times, sonicated with a probe sonicator for 15 seconds twice, and then

mixed again 20 times with a pipette. Samples were then loaded into the sample chamber using a modified leak-free methodology [26]. The sample chamber was placed in the PBS at a temperature of 37°C. A bubble with a radius of 0.4 mm was then formed and an imaging acquisition system was used to determine the bubble size. Trans-film bubble pressure was recorded as a function of time while holding bubble radius static for 20 minutes during static adsorption experiments. Dynamic measurements of surface tension as a function of bubble surface area were subsequently collected by cycling the bubble radius between approximately 0.4 mm and 0.55 mm at an oscillation frequency of 20 cycles/min for 10 minutes.

7.2.8 Giant unilamellar vesicles

GUVs of the synthetic lung surfactant mixtures were prepared as previously described [191]. Briefly, 0.5 mol%, of a fluorescently labeled lipid, DiI_{C18} (Sigma Aldrich, Milwaukee, WI) along with 10 wt% of the appropriate peptide or peptoid labeled with Alexa Fluor® 488 and dissolved in methanol was added to a 0.5 mg/mL lipid mixture (DPPC:POPG:PA, 68:22:9 (by weight)) dissolved in chloroform:methanol (3:1).

The GUVs were then formed using a electroformation method as described by Angelova and Dimitrov [192]. Approximately 3 μL of the labeled lipid or lipid and peptide/peptoid solution was spread onto the surface of a platinum wire electrode in a sample well of a specially designed Teflon chamber [193]. The chamber was then placed under vacuum in darkness for at least 1.5 hours to evaporate the trace solvent. After evaporation of the solvent, 500 mL of a 200 mOsM sucrose solution was added to each sample well and a low frequency AC field of 10 Hz and 1.5 V amplitude was applied for 1.5 hours using a function generator (Van Draper Digimess Fg 100, Stenson, Derby, UK). A circulating water bath was also used during this process to

maintain the temperature of the sample chamber at 60°C, which is sufficiently above the fluid/gel transition temperature. The resulting GUVs were then harvested with a pipette and transferred to a plastic vial.

Just prior to GUV imaging, 50 μL aliquots of the harvested GUV suspension was transferred into a single well of an eight-well cell culture plate (Lab-Tek Brand Products, Naperville, IL) containing 200 μL equi-osmolar glucose in each well. Due to the density difference between the sucrose and glucose, the suspended GUVs settled on the bottom of the plate. The GUVs were then imaged at room temperature, 21°C, using an inverted confocal microscope (Zeiss LSM 510 META). The excitation wavelengths were 543 nm for the DiI_{C18} and 488 nm for the Alexa Fluor® 488 labeled compounds.

7.3 Results and discussion

7.3.1 Peptoid design and rationale

SP-C is a 35 amino acid lipopeptide that is highly conserved amongst all mammalian species and is unique to lung surfactant. The high rate of sequence conservation and specificity to lung surfactant suggest not only a critical role in surfactant homeostasis, but also that its unique sequence is paramount to its biophysical activity.

SP-C's secondary structure is dominated by a 37 Å-long α-helix that stretches from residue 9 to 34 [29]. This valyl-rich helical region governs SP-C's disposition in and association with the phospholipids of lung surfactant [7]. Despite the high rate of sequence conservation of this region, it is thought that the helical conformation itself, rather than the precise covalent structure, is of prime importance for the biological function of synthetic SP-C analogues [45, 63]. This strategy allows for the replacement of the problematic, aggregation prone sequence

with side chain structures that are more stable, allowing for the efficient production of a synthetic SP-C analogue.

A similar conclusion was found in peptoid analogues of SP-C in which a peptoid mimic with an α-chiral, aromatic helix displayed superior surface-active features in comparison to a more biomimetic peptoid mimic with an α-chiral, aliphatic helix [61]. The difference in surface activity between the two mimics was attributed to the increased structural rigidity imparted in the helical region by the bulkier aromatic groups. However, more recent structure-function studies with peptoid mimics of SP-C have shown that both the side chain chemistry and the rigidity of the helical region are important in SP-C-related functions (Chapter 6). These mimics combined both helix-inducing α-chiral, aromatic and α-chiral, aliphatic residues in the helical region to optimize the structural rigidity from the bulky aromatic groups and sequence biomimicry from the isoleucine-like, aliphatic residues.

Here, the structural requirements of this critical region of SP-C are investigated further by increasing the structural rigidity of the peptoid helix by incorporating varying amounts of an α-chiral, aliphatic side chain, *N*sdp, in the helical region (Table 7.1). This side chain contains an extra methyl branch than the previously studied α-chiral, aliphatic side chain, *N*-(S)-sec-butylamine (*N*ssb), and, therefore, is likely to strengthen the helical structure due to the added steric repulsion [61]. Four peptoid-based analogues were studied: Mimic C, Mimic CLeu2, Mimic CLeu3, and Mimic di-pCLeu3. Mimic C contains an entirely α-chiral, aromatic peptoid helix that was previously shown to mimic the surface properties of a SP-C peptide well and is used here as a comparator species. Mimic CLeu2 is similar to Mimic C except that the helical region contains approximately two-thirds of the α-chiral, leucine-like, *N*sdp side chain and one-

third α-chiral, aromatic residues. Because of the periodicity of the peptoid helix and the placement of the side chains, Mimic CLeu2 is predicted to have two aliphatic faces and one aromatic face in the helical region. Mimic CLeu3 contains a helical region that is entirely composed of the α-chiral, aliphatic *N*sdp side chains and is closest to the native SP-C helix composition. An alkylated version of Mimic CLeu3 was also studied (Mimic di-pCLeu3), as *N*-terminal alkylation of peptoid SP-C analogues has previously been shown to improve the dynamic surface activity of the mimics (Chapter 5).

In addition to being more sterically bulky, the *N*sdp side chain is also more similar to valine and leucine side chains normally present in the SP-C helix. Especially, considering that the structural differences between a peptoid polyproline type I-like helix and a standard peptide α-helix cause the side chains to project out at different angles. This difference in orientation and projection in the elongated peptoid structure (~ 6-6.7 Å per turn) has been shown to be overcome by the placement of an extra methylene group in the side chain, making *N*sdp very similar to a valine side chain [194].

7.3.2 Circular dichroism

CD was used to characterize and compare the secondary structures of the peptoid analogues in solution. SP-C and synthetic SP-C peptide mimics form predominantly α-helical structures in solution, which correlate strongly with their surface activity [45]. CD spectra of the modified of the peptoid-based SP-C mimics, are displayed in Figure 7.1.

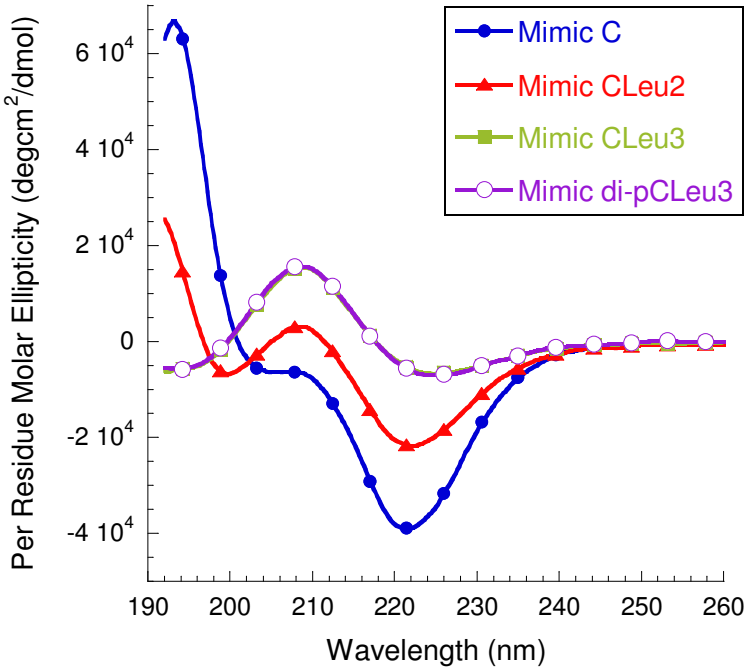

Figure 7.1: Circular dichroism (CD) spectra of the peptoid-based SP-C mimics showing qualitatively similar characteristics of peptoid helices. As the aliphatic content is increased, the CD spectra display features that are progressively similar to a polyproline type I peptide helix. Spectra were acquired in methanol at a concentration of ~ 60 μM at room temperature.

Mimic C, which contains solely α-chiral, aromatic residues in the helical region, exhibits CD features that are similar to a peptide α-helix with an intense maximum at λ ~ 192 nm and double minima at λ ~ 205 nm and ~ 220 nm (Figure 7.1). These spectral features are characteristic signatures of a helical peptoid structure in oligomers of this class with highly ordered backbone amide bonds [59]. Adding two *N*sdp faces in the helical region results in a slightly different type of CD spectrum for Mimic CLeu2. Mimic CLeu2 displays spectral features that are more similar to a polyproline type I peptide helix with a shallower minimum at λ ~ 220 nm and a shifted local minimum at λ ~ 200 nm. The spectrum for Mimic CLeu2 is very similar to that observed for a mixed aromatic and aliphatic mimic previously studied, although,

the intensity is increased, indicating a more confined, helical structure (Chapter 6). Mimic CLeu3 with only α-chiral, aliphatic residues in the helical region, displays a slightly different CD spectrum. These CD spectral features that are similar to those of a polyproline type I peptide helix, but blue-shifted, which is characteristic of peptoids of this class [58, 161]. Similar to Mimic CLeu2, t CD spectrum for the entirely *N*sdp mimic is also more intense than that of the corresponding *N*ssb-based mimic (Chapter 4). The addition of the amide-linked alkyl chains in the *N*-terminal region does not alter the CD spectrum of Mimic di-pCLeu3. This is consistent with other peptoid analogues of SP-C where only a minimal change in CD spectrum was observed (Chapters 5 and 6). Despite differences in the type of CD spectra observed for the various compounds, all of the SP-C mimics are shown to be helical and structured in solution, satisfying one of the structural criteria, helicity, believed to be of importance for the surface activity of SP-C [63]. In addition, the spectra for the peptoid-based mimics did not appreciably change over time, indicating the analogues are stable and not prone to aggregation in solution like the native protein [43, 44].

7.3.3 Static bubble adsorption

One of the key biophysical characteristics that is important to mimic with a synthetic, biomimetic lung surfactant formulation is natural lung surfactant's ability to rapidly adsorb to the alveolar air-liquid interface, immediately forming a surface-active layer [7, 10]. A modified PBS run in static mode with a bubble radius of approximately 0.40 mm at 37°C was used to characterize the adsorption kinetics of the surfactant formulations. Figure 7.2 shows the adsorption profile for natural lung surfactant (Natural LS) as well as a synthetic phospholipid mixture alone and with the addition of 1.6 mol% SP-C protein and SP-C analogues. Natural lung

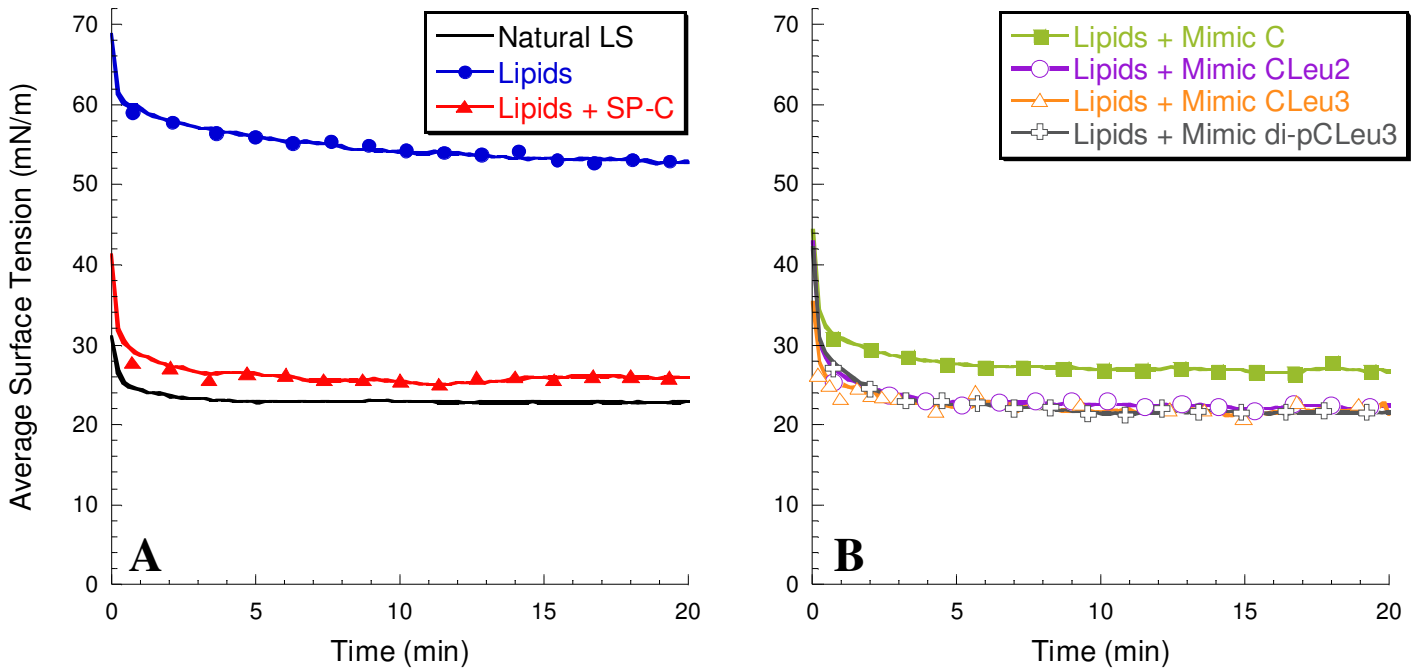

Figure 7.2: Static pulsating bubble surfactometry (PBS) results displaying surface tension as a function of time. (A) Natural lung surfactant and lipid mixture alone and with 1.6 mol% SP-C; (B) Lipid mixture with 1.6 mol% Mimics C, CLeu2, CLeu3, and di-pCLeu3. Measurements were taken at a bulk surfactant concentration of 1 mg/mL lipids and at 37°C.

surfactant displays very rapid adsorption kinetics, reaching a static surface tension < 25 mN/m in less than one minute and a final equilibrium surface tension of ~ 23 mN/m. In contrast, the lipid formulation without any protein or peptoid mimimetics displays very poor adsorption characteristics. The lipid formulation fails to reach a static adsorption surface tension lower than ~ 53 mN/m even after 20 minutes. The addition of natural SP-C to lipid formulation greatly accelerates the surfactant adsorption to the air-liquid interface, enabling the surfactant film to reach a surface tension of < 30 mN/m in less than one minute and a final static surface tension of ~ 26 mN/m. The addition of the peptoid analogues to the synthetic lipid formulation similarly improves the adsorption kinetics. All of the peptoid-containing formulations have similar adsorption profiles as the natural LS except for the Mimic C-containing formulation. While the Mimic C formulation only reaches a final surface tension of ~ 27 mN/m, this is comparable to the natural SP-C formulation.

Based upon these results, the kinetic adsorption behavior of the lipid formulation is significantly enhanced with the addition of the *N*sdp-containing peptoid SP-C mimics. The synthetic formulations not only show comparable adsorption to a natural SP-C-containing surfactant, but also to natural lung surfactant, which contains both SP-B and SP-C proteins. It is somewhat surprising that the Mimic CLeu3 formulation had such a rapid adsorption profile as previous studies with a *N*ssb-based mimic, containing solelyα-chiral, aliphatic residues in the helical region, did not display favorable adsorption (Chapter 4, Section 4.3.5). It is believed that the greater bulk and hydrophobicity of the *N*sdp residues results in greater structural rigidity and a better ability to perturb and fuse the dispersed surfactant structures to the air-liquid interface. The specific covalent structure of the *N*sdp side chain is also likely to be interacting in a specific

manner with the lipid acyl chains, as the aromatic-based mimic, Mimic C, was unable to produce as rapid surfactant adsorption despite its likely rigid helical structure.

7.3.4 Dynamic compression-expansion cycling

To investigate the effectiveness of the peptoid-based SP-C mimic formulations to reduce and control surface tension as a function of surface area, PBS experiments were performed in a dynamic mode at an oscillation frequency of 20 cycles/min and ~ 50% reduction in surface area. Features that are important in the compression-expansion loop for biomimetic surfactant film behavior include: (1) the ability to reach a very low surface tension with a small percentage of compression; (2) an ability to respread rapidly, and (3) an ability to control surface tension as a function of bubble surface area with the lowest minimum surface tension possible and a relatively low maximum surface tension [7, 10]. Figure 7.3 displays the surface tension as a function of bubble surface area for natural lung surfactant as well as the lipid mixture with and without SP-C (7.3A) and with the peptoid SP-C mimics (7.3B).

The natural lung surfactant is extraordinarily surface-active during the dynamic compression-expansion cycles. The maximum surface tension observed for the natural material is ~ 33 mN/m and the minimum surface tension reached upon compression is < 1 mN/m. These values are consistent with other studies of natural lung surfactant extracts [27, 82]. The lipid mixture, when used alone; however, exhibits a high maximum surface tension of ~ 60 mN/m and a high minimum surface tension of ~ 17 mN/m. The lipid formulation is also highly compressible, requiring a significant amount of compression to reach the minimum surface tension. With these properties, the lipid formulation would be a poor SRT. The addition of SP-C to the lipid formulation dramatically improves the surface activity of the film. The SP-C

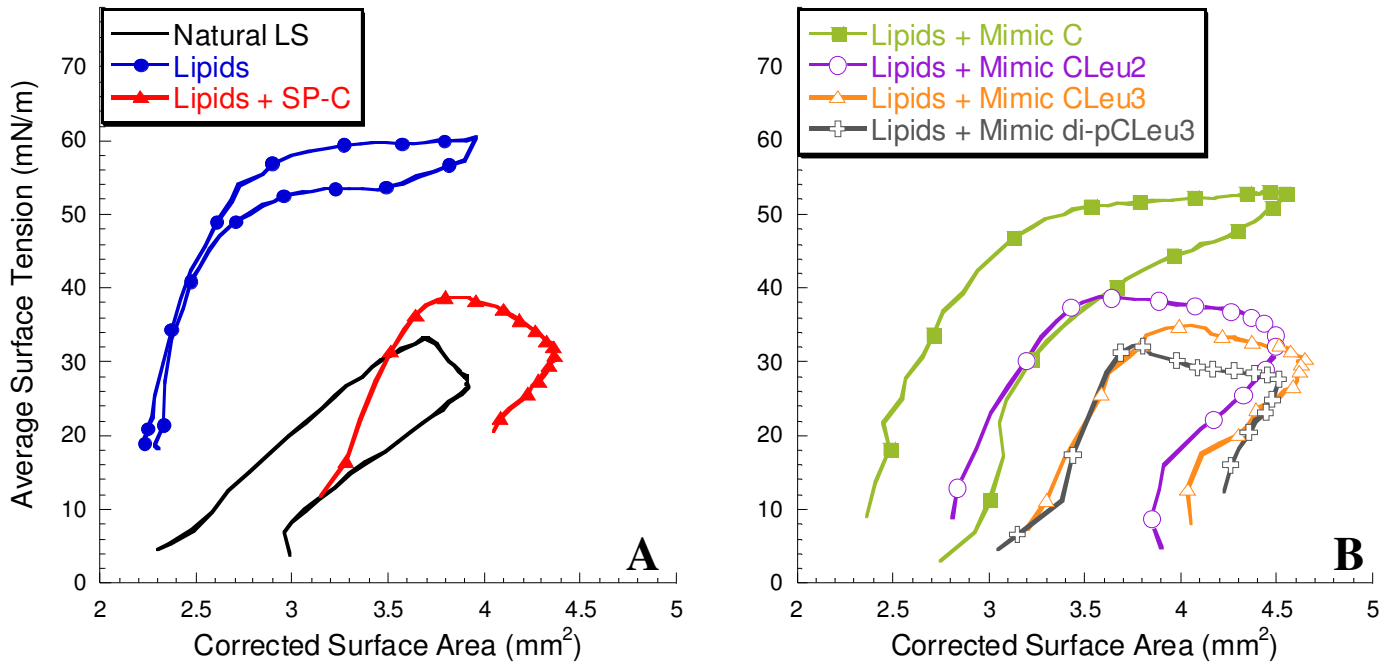

Figure 7.3: Dynamic pulsating bubble surfactometry (PBS) results displaying surface tension as a function of surface area at an oscillation frequency of 20 cycles/min. (A) Natural lung surfactant and lipid mixture alone and with 1.6 mol% SP-C. (B) Lipid mixtures with 1.6 mol% Mimics C, CLeu2, CLeu3, and di-pCLeu3. Measurements were taken at a bulk surfactant concentration of 1 mg/mL lipids and at 37°C.

containing film exhibits a maximum surface tension of ~ 39 mN/m and a minimum surface tension < 1 mN/m during dynamic PBS compression-expansion cycling. The compressibility of the film is also greatly reduced, requiring much less compression to reach a low minimum surface tension.

The addition of the aromatic-based peptoid mimic, Mimic C, to the lipid film also improves the compression-expansion behavior; however, not nearly to the extent of the natural protein (Figure 7.3B). The Mimic C film reduces the maximum surface tension of the lipid formulation to a modest 53 mN/m and the minimum surface tension to < 1 mN/m. The addition of Mimic CLeu2, containing two aliphatic faces in the helical region, to the lipid formulation results in a dramatic increase in surface activity. The Mimic CLeu2 formulation has a compression-expansion PBS loop that is very similar to the SP-C surfactant with a maximum surface tension of ~ 39 mN/m and a minimum surface tension < 1 mN/m. Mimic CLeu3 with an entirely aliphatic helical region results in a PBS loop that is further improved. The Mimic CLeu3 formulation exhibits a maximum surface tension of only ~ 35 mN/m and a minimum surface tension < 1 mN/m. This exceeds the performance of the SP-C-containing surfactant and approaches that of natural lung surfactant. This is extraordinarily surprising as previous studies with peptoid mimics composed of only aliphatic, *N*ssb residues in the helical region had inferior PBS cycling loops, which required a significant amount of compression to reach a minimum surface tension and the minimum surface tension was occasionally elevated (Chapter 4). Also surprising is that Mimic CLeu3 does this in the absence of an *N*-terminal alkylation motif. Addition of the alkyl chains to the *N*-terminal region of Mimic CLeu3 further improves the surface activity (Figure 7.3B). The alkylated Mimic di-pCLeu3 formulation displays

extraordinary surface activity during dynamic cycling with an extremely low maximum surface tension of ~ 33 mN/m and a minimum surface tension of < 1 mN/m. These values surpass the porcine SP-C formulation and are comparable to the natural lung surfactant formulation, representing the best performing synthetic surfactant formulation studied to date. Therefore, Mimic di-pCLeu3 has great potential for use in a biomimetic SRT for the treatment of nRDS given its relatively facile synthesis and purification as well as its stable secondary structure and extraordinary *in vitro* surface activity.

7.3.5 Fluorescently labeled SP-C mimics in lipid bilayers

To investigate the effect of the peptoid SP-C analogues on the lipid lateral organization and disposition in surfactant-like membranes, GUVs containing a fluorescently labeled SP-C peptide and labeled SP-C peptoid mimics were imaged by confocal fluorescence microscopy. The use of confocal fluorescence microscopy to visualize GUVs is an experimental technique that has recently been used to gain greater insight into the lateral organization and separation of lipid membranes [191, 195, 196]. Surfactant is a unique biomaterial, in that, the coexistence of the segregated lipid-protein domain structures provides a structural basis for its unique surface activity [191]. These small vesicles, ~ 20-35 μm diameter, allow the direct visualization of the lipid domain structures during experimentation. Figure 7.4 shows the fluorescent images of the lipids alone (panels A and E), with 10 wt% di-pSP-C (panels B and F), with 10 wt% Mimic CLeu3 (panels C and G), and with 10 wt% Mimic di-pCLeu3 (panels D and H). Natural SP-C was not used in this experiment due to the extreme difficulty associated with maintaining its proper secondary structure during the labeling procedure.

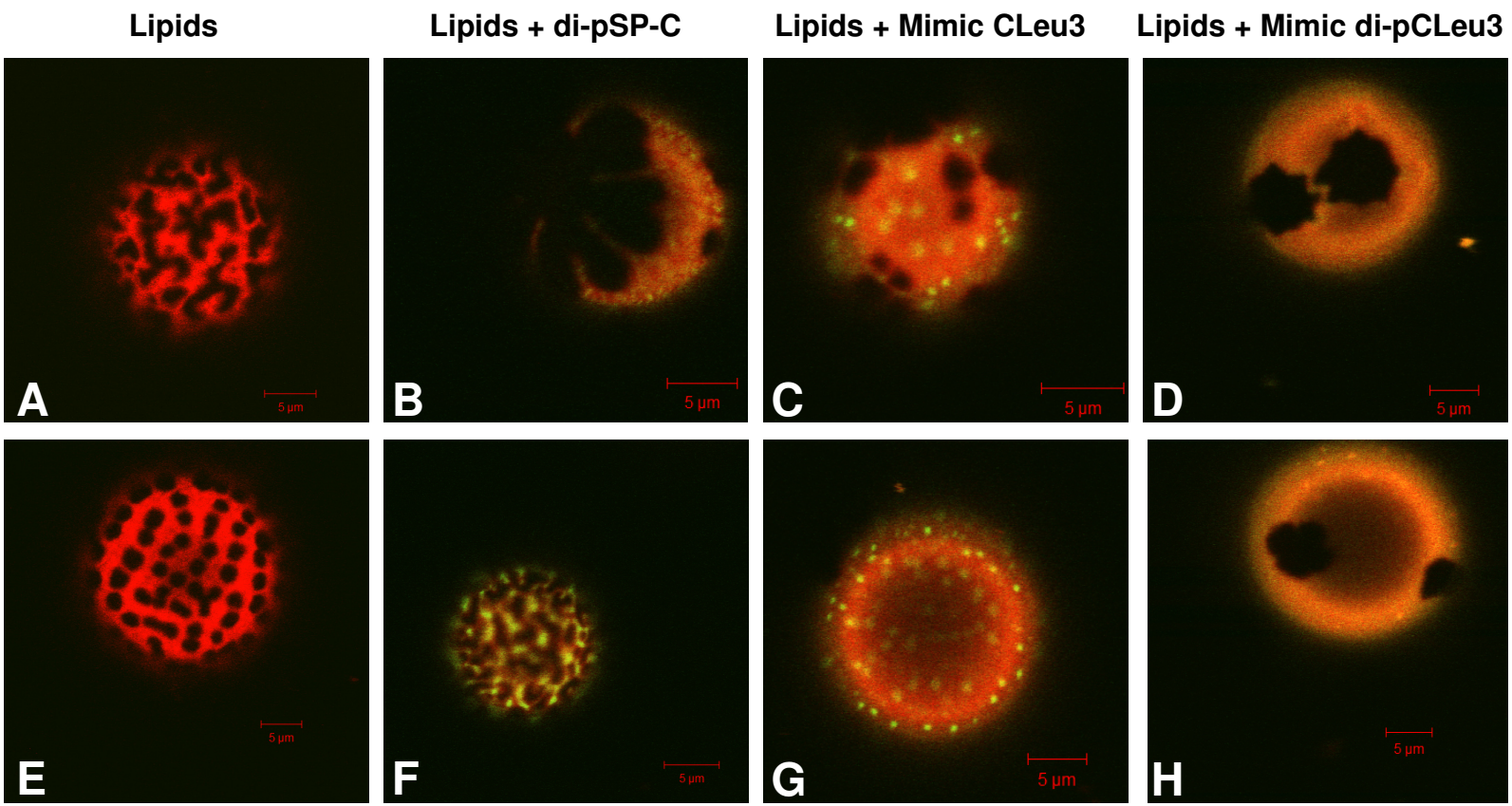

Figure 7.4: Confocal fluorescence microscopy imaging of giant unilamellar vesicles (GUVs) of lipids alone (A and E), lipids with 10 wt% di-pSP-C (B and F), lipids with 10 wt% Mimic CLeu3 (C and G), and lipids with 10 wt% Mimic di-pCLeu3. Scale bars correspond to 5 µm. Fluorescence images were taken at 21°C and are representative of the population observed. Red corresponds to the fluorescently labeled lipid species and yellow to the labeled peptide and peptoids.

The lipid formulation was doped with a lipid probe, DiI_{C18}, which preferentially segregates to the more fluid phase rather than the lipid ordered, gel phase. In the absence of any added peptide or peptoid species, coexistence of fluid and gel phases were observed at room temperature (Figure 7.4, panels A and E). The lipid formulation produced stable vesicles with large globular domains of segregated gel-like region (dark regions) that are devoid of the lipid probe (red) and are similar in morphology to lipid monolayer and bilayer films of this formulation at this temperature and estimated surface pressure [162, 195, 197]. Adding the labeled di-pSP-C peptide (yellow) to the lipid film causes a condensation of the solid domains, forming larger, flower-like domain structures in addition to condensed domains that are similar to those with lipid formulation (Figure 7.4, panels B and F). The labeled di-pSP-C peptide also preferentially segregates to the less ordered phase as seen by the orange color of the more fluid regions. This is consistent with other studies of SP-C in lipid bilayers where there is a hydrophobic mismatch between the length of the SP-C helix and the DPPC bilayer in the gel phase, causing phase segregation [198, 199]. The di-SP-C peptide also tends to self associated in these regions as evident by the regions of brighter intensity. This is also consistent with previous studies of SP-C at this temperature, where SP-C segregates and self associates at lower temperatures due to the hydrophobic mismatch [200].

The presence of the peptoid-based SP-C mimics in the lipid bilayers results in morphologies that are have some similarities and differences in comparison to the GUVs containing the SP-C peptide (Figure 7.4). Both Mimic CLeu3 and Mimic di-pCLeu3 are closely associated with the lipid bilayer as no fluorescence was observed in the interior of the GUVs. The mimics both preferentially associate with the less ordered lipid phase of the GUVs. Mimic

CLeu3 is most similar to the di-pSP-C peptide, in that, this species also segregates and self associates in the fluid regions (Figure 7.4, panels C and G). The peptoid helix is estimated to be slightly shorter than an SP-C helix; therefore, it is likely that a greater mismatch between the peptoid helix and the lipid acyl exists. Mimic CLeu3 also appears to have a fluidizing influence on the domain structures as the gel phase domains have coalesced, forming slightly larger domain structures. The addition of Mimic di-pCLeu3 results in a more uniform, fluid phase and does not appear to be strongly self associating (Figure 7.4, panels D and H). It is possible that the alkyl chains are assisting in Mimic di-pCLeu3's association with the lipid acyl region, decreasing the tendency for self association and causing the mimic to be more evenly dispersed. This greater dispersion likely contributes to the greater membrane fluidization observed with From these results, Mimic di-pCLeu3. Mimic di-pCLeu3 is very promising as the morphology induced by this mimic is very similar to GUVs containing both SP-B and SP-C peptide analogues.

7.4 Conclusions

The C-terminal, hydrophobic, helical region of SP-C is essential for the protein's proper biophysical activity. Research with synthetic peptide constructs of SP-C has shown that the overall secondary structure of this region rather than the exact side chain chemistry is more pertinent to its surface activity in phospholipid films [45, 63]. A similar finding with some of the peptoid SP-C analogues was also observed [61, 62]. However, more recent studies with peptoid analogues have shown that in addition to the rigid secondary structure, the specific side chain chemistry is also important in promoting favorable interactions between the SP-C mimics and the phospholipids (Chapter 6). In these peptoid constructs, it was beneficial to include both α-

chiral, aromatic and α-chiral, aliphatic residues to preserve SP-C's rigidity and side chain structure, respectively. Here, this was expanded by utilizing varying amounts of a bulkier, more rigid aliphatic side chain, *N*sdp.

CD was used to characterize the peptoid analogues' secondary structures in solution. All the peptoid analogues were found to replicate SP-C's helical secondary structure in solution. The spectral intensities of the *N*sdp-containing analogues were greater than those observed for previous α-chiral, aliphatic containing mimics, indicating increased helical propensity. The structures were also stable over time, which is a major advantage over the metastable natural SP-C protein. When combined with a biomimetic phospholipid formulation, the SP-C peptoid analogues significantly improved both the static and dynamic surfactant properties on a PBS instrument and were very similar to native, porcine SP-C. The peptoid mimic containing solely α-chiral, aliphatic residues in the helical region were observed to exhibit the greatest *in vitro* surface activity. The bulkier *N*sdp side chain is believed to result in a peptoid SP-C helix that is both structurally rigid and biomimetic. Adding two amide-linked alkyl chains, which mimic the palmitoyl chains of SP-C, further improved the PBS surface activity to comparable levels as natural lung surfactant containing both SP-B and SP-C proteins. The lateral organization of lipid bilayers and the disposition of the peptoid analogues in these films were also investigated by confocal fluorescence microscopy of GUVs. In the GUVs, it is found that the non-alkylated, aliphatic mimic has a similar influence on the lipid domain structures as a peptide SP-C mimic and that the non-alkylated peptoid mimic is also prone to self association in the more fluid and uniform regions. However, alkylating the mimic, results in a more fluid morphology and a lesser propensity to self associate.

Taken together, these studies show that both the specific side chain chemistry and the helical rigidity of the helix of peptoid-based SP-C mimics are important in the species' biophysical activity. The increased aliphatic content likely provides favorable interactions with the lipid acyl chains and better mimics the native protein. In fact, the *in vitro* surface activity of an alkylated peptoid mimic approaches that of natural lung surfactant. These studies are very promising for the development of a fully functional, biomimetic SRT for the treatment of respiratory-related disorders.

Chapter 8: Summary and future directions

8.1 Impact of the work presented

Animal-derived lung surfactant preparations have significantly reduced the morbidity and mortality associated with surfactant deficiency in the airways of premature infants; however, despite the great efficacy of these surfactant replacement therapies (SRTs), there still exist concerns and shortcomings associated with their use, including: possible spread of infectious material, batch-to-batch variability, and high production costs. Recent studies have also suggested that SRTs may be useful in the treatment of other respiratory-related disorders in adults; however, this requires significantly more surfactant material than current isolation techniques can supply. As a result, investigation has focused on the creation of a synthetic lung surfactant formulation that retains the functionality of the natural material, but overcomes the associated difficulties and concerns. This endeavor has proven to be much more difficult than first anticipated and is largely due to the great complexity of the lung surfactant phospholipids and, especially, the critically important hydrophobic surfactant proteins, SP-B and SP-C. SP-C is a particularly troublesome component as it is extremely hydrophobic and prone to misfolding and aggregation, significantly hampering efforts to synthetically produce the protein or analogue constructs.

Here, a novel methodology utilizing non-natural, sequence-specific oligomers to overcome the difficulties associated with the natural SP-C protein while retaining its unique and important biophysical activity is reported. Poly-*N*-substituted glycines, or peptoids, have close structural similarity to peptides; however, because of their unique structure, are protease resistant and form extremely stable helical structures. The ability to form stable helices makes peptoids

an excellent candidate for mimicry of SP-C, which relies on a helical secondary structure for its biophysical activity. Utilizing similar design strategies as peptide analogues of SP-C, a range of peptoid-based SP-C analogues were created and characterized, forming in-depth structure-activity relationships of these unique biopolymers. These studies have lead to the creation of a fully functional SP-C mimic that retains the protein's unique *in vitro* surface activity, but because of its unique structure, overcomes the difficulties associated with the native protein. Therefore, peptoids have significant potential for use in a biomimetic SRT, improving the treatment of respiratory-related disorders by increasing the production potential, eliminating possible pathogenic transmission, and minimizing surfactant variability. In order to further improve our understanding of the peptoid analogues' interaction and association with phospholipid films, further mechanistic investigation is warranted. This increased understanding will aid in the future development of a fully functional, biomimetic SRT that is both safe and efficacious.

8.2 Future directions

8.2.1 Biomimetic SP-C structures

SP-C is predominately monomeric in solution in its active, helical conformation; however, recent NMR structural studies with a recombinant SP-C protein have discovered a population of dimeric, α-helical structures [201, 202]. These dimeric species appear to be oligomerizing in a specific fashion at a site located at the C-terminus of the helical region. Within this region is a strictly conserved heptapeptide segment, containing an AxxxG motif that is very similar to the GxxxG pattern of the van der Waals dimer of glycophorin [28, 203, 204]. It

is, therefore, very likely that this motif is responsible for the SP-C helix-helix *in vitro* association.

The SP-C dimeric structure is also likely to be present in the surfactant lamellar bilayer systems *in vivo*; however, the biological importance of this specific association is not known [201, 205]. Due to the difficulties associated with the native SP-C sequence, studying the effect of this structural motif upon SP-C's biophysical activity is rather difficult; however, given the similarities between the peptoid and peptide analogues of SP-C, it would be of interest to study this interaction in peptoid analogues of SP-C. Constructs of peptoid SP-C dimeric species could be created that are either chemically cross-linked at the C-terminal end or contain a C-terminal heptapeptide segment of amino acids that replicates the AxxxG motif, forming a peptoid-peptide chimeric oligomer.

8.2.2 Biophysical characterization

In these studies, many structural modifications have been shown to greatly affect the surface activity of the peptoid-based SP-C analogues. While it is believed that many of the same SP-C-phospholipid interactions are also present within these peptidomimetics, the precise mechanistic rationale for their activity is not known to a great extent. Therefore, more mechanistic, biophysical characterization of the peptoid mimics is warranted to better correlate the molecular and structural attributes of the peptoids with their surface-active properties. An increased understanding of the specific mechanisms of action and interaction would aid in the future design and development of more therapeutically active SP-C analogues.

8.2.2.1 Giant unilamellar vesicles

Giant unilamellar vesicles (GUVs) have recently become an important characterization tool in understanding lipid phase formation and dynamics in model membrane systems [191, 195, 196]. Fluorescence microscopy (FM) imaging of these bilayer vesicles allows for the direct visualization of the lipid phase morphology, including the size, shape, and formation of lipid domains over the course of experimentation and is complementary to FM imaging of Langmuir monolayers; however, unlike the monolayer studies, bilayers of GUVs may better represent the bi- and multilayered films of lung surfactant that occur *in vivo* [191, 197, 206, 207]. Therefore, the characterization of lipid-protein/peptoid morphologies in the lipid bilayers of GUVs is of interest to better understand these interactions in a more lung surfactant-like system.

Initial testing of the peptoid analogues in GUV model membrane systems (Chapter 7) has begun; and it was found that the peptoid-based analogues of SP-C strongly associate with the lipid bilayers and preferentially partition in the less-ordered phase of the vesicles. Both of these characteristics are similar to the native SP-C protein and peptide analogues, which suggest a similar mechanism of action. However, further characterization is warranted to better understand and quantify how the presence of the peptoid species alters the lipid phase coexistence. Further GUV characterization of the membrane system with and without added peptoid analogues using LAURDAN generalization polarization will aid in the precise quantification of membrane perturbation brought about by the peptoid mimics [208, 209]. Also, it would be of value to characterize the membrane partitioning and morphological changes incurred by the peptoid analogues in other model membrane systems that more accurately reflect the complex composition of natural lung surfactant [191]. These results can then be compared to the results

from corresponding studies using the natural surfactant proteins or native lung surfactant, aiding in the assessment of peptoid mimic *in vitro* efficacy, complementing the monolayer studies previously undertaken.

8.2.2.2 Atomic force microscopy

Atomic force microscopy (AFM) has been previously used to increase the understanding of the collapse mechanism and respreading behavior of lung surfactant [20, 42, 148, 149, 181, 210]. From these studies, it appears that the formation of a surface-associated surfactant reservoir is greatly influenced by the presence of the hydrophobic surfactant proteins, SP-B and SP-C. More recently, the *N*-terminal palmitoyl chains of SP-C have been shown by AFM to be critical in the formation of multilayered structures [41]. In the absence of these structural motifs, SP-C is able to form bilayer structures of surfactant during compression; however, only in the presence of the thioester-linked palmitoyl chains, does SP-C catalyze the formation of extended multilayered structures that remain associated with the interface at high surface pressures. This multilayer formation is believed to be not only important in the retainment and respreading of surfactant for the next respiration cycle, but also in the regulation of surfactant viscosity, preventing surfactant outflow form the alveoli at very low surface tensions [42, 144].

To better understand the mechanism of action of the SP-C peptoid analogues, AFM of deposited films of peptoid-based surfactants at various surface pressures would be of great interest. These studies would provide quantitative information as to whether the peptoid-based mimics of SP-C are able to form surface-associated surfactant reservoirs as suggested by previously FM studies. Also, AFM would be able to determine if different C-terminal side chain chemistries or *N*-terminal modifications (*N*-alkylation) influence the formation of bilayer and/or

multilayered surfactant structures, providing relevant structure-activity relationships for the formation of a surfactant reservoir with peptoid analogues.

8.2.2.3 Captive bubble surfactometry

One of the major criticisms of the PBS is the possible occurrence of surfactant leakage through the capillary of the sample chamber during dynamic cycling, which leads to a significant underestimation of the compression [16]. The technique of captive bubble surfactometry (CBS) overcomes this concern. Similar to the PBS, the CBS attempts to mimic a small alveolus dispersed in an aqueous solution; however, unlike the PBS, it consists of an air bubble floating against an agar gel in an airtight chamber [26, 211]. The subphase of the CBS can also be stirred during experimentation, allowing adsorption and film studies to be conducted without the complicating influence of diffusion.

These experimental differences have lead to the CBS being used primarily for more in-depth, mechanistic studies; therefore, it would be advantageous to compare the peptoid-based surfactant formulations in the CBS in addition to the PBS. This is especially true since the PBS instrument is modified to more accurately determine the surface area of the bubble in a similar manner as that used to in the CBS. A side-by-side comparison may provide validation for the modified PBS instrument as well as further mechanistic information of the surfactant formulations.

8.2.3 Formulation of a peptoid-based surfactant replacement therapy

Lung surfactant is a unique biomaterial composed of ~ 90% lipids and ~ 10% surfactant-associated proteins [9, 16]. No single constituent is responsible for the material's dynamic surface activity. The saturated phospholipids comprise the major of lung surfactant's mass and

are primarily responsible for lung surfactant's surface tension reduction; however, on their own, they are poor surfactants as they exhibit poor adsorption and respreading properties. The inclusion of more fluid, unsaturated phospholipids improves these characteristics, but also causes an increase in minimum surface tension. The hydrophobic surfactant proteins, SP-B and SP-C, significantly improve the adsorption and respreading properties of lung surfactant while not interfering with the saturated phospholipids' ability to reach very low surface tensions [178]. Therefore, SP-B and SP-C are critical components of lung surfactant. In fact, both SP-B and SP-C are ubiquitously expressed amongst all animal species studied thus far that breathe air via alveolar-like, lung structures. This strict conservation suggests that both proteins fulfill an important and specific functional role in surfactant homeostasis.

So far, only biomimetic surfactants containing either a peptoid analogue of SP-B or SP-C have been studied. It is, therefore, of great interest to combine both SP-B and SP-C peptoid analogues in the same surfactant formulation in order to investigate any possible synergistic effects of the two mimetics. In addition, recent *in vivo* studies have indicated that despite good in vitro efficacy for a given surfactant formulation, the same surfactant formulation may have inferior in vivo efficacy [143]. Therefore, it is also necessary to examine different surfactant compositions *in vitro* and in *vivo*.

8.2.4 Peptoid biocompatibility

In addition to determining the relative toxicity of the peptoid-based analogues of SP-C, the overall biocompatibility the species with the alveolar system needs to be investigated. While the inherent resistance to protease degradation of peptoids makes them promising therapeutic candidates due to increased bioavailability, the increased *in vivo* lifetime could also pose

potential problems. The accumulation of SP-C in the airways has been linked to pulmonary alveolar proteinosis, a lung disease characterized by alveolar accumulation of proteinacesous material, in particular, SP-C [212, 213]. While the accumulated SP-C is predominately misfolded SP-C protein fibrils, the prolonged *in vivo* lifetime of an SP-C analogue could potentially increase the susceptibility to this condition. This is especially valid for the treatment of acute respiratory distress syndrome, where a significant amount of surfactant material would be instilled into the airways. Therefore, studies focusing on the rate of alveolar processing and clearance, not just toxicity, should be further investigated *in vitro* and *in vivo* to ensure proper clearance and compatibility with the alveolar network.

8.3 Conclusion

Current, animal-derived SRT formulations are highly efficacious in the treatment of nRDS; however, there are still drawbacks associated with their use. This has prompted researchers to devise synthetic sources of the surface-active material, specifically creating mimics of the hydrophobic surfactant proteins, SP-B and SP-C. The importance of SP-C as a functional constituent of a biomimetic SRT is evidenced not only by its inclusion in natural exogenous surfactant formulations, but also by its ubiquitous expression in mammalian airways as well as its uniqueness, lacking any known sequence homologues. However, isolation and storage of either the native SP-C protein or sequence-identical analogues is extraordinarily difficult due to its extreme hydrophobicity and metastable secondary structure. As a result, detailed structural information and biophysical insight about native SP-C was used to create a number of novel peptoid-based analogues that mimic SP-C's key molecular and structural motifs, but because of their unique backbone structure, reduce or eliminate many of the

difficulties associated with the native protein. This work has demonstrated great promise for the use of peptoids in a biomimetic surfactant formulation and will hopefully lead to more sophisticated and bioactive designs for future peptoid-based mimics of SP-C. Further structural and mechanistic studies as well as formulation optimization is still needed to better understand the requisite features of a biomimetic SRT. Ultimately, with improved stability, greater production potential, and elimination of possible pathogenic contamination, not only do peptoid-based biomimetic SRTs offer the potential to improve the treatment of nRDS, but they may also see wider application in the treatment of other, more prevalent, respiratory-related disorders where greater quantities of the surface-active material are required, such as in the treatment of acute RDS.

References

1. Sato, A.K., M. Viswanathan, R.B. Kent, and C.R. Wood, *Therapeutic peptides: technological advances driving peptides into development.* Current Opinion in Biotechnology, 2006. **17**(6): p. 638-642.

2. Kuhlman, B., G. Dantas, G.C. Ireton, G. Varani, B.L. Stoddard, and D. Baker, *Design of a novel globular protein fold with atomic-level accuracy.* Science, 2003. **302**(5649): p. 1364-1368.

3. Czyzewski, A.M. and A.E. Barron, *Protein and peptide biomimicry: Gold-mining inspiration from nature's ingenuity.* Aiche Journal, 2008. **54**: p. 2-8.

4. Kallberg, Y., M. Gustafsson, B. Persson, J. Thyberg, and J. Johansson, *Prediction of amyloid fibril-forming proteins.* Journal of Biological Chemistry, 2001. **276**(16): p. 12945-12950.

5. Walther, F.J., A.J. Waring, M.A. Sherman, J.A. Zasadzinski, and L.M. Gordon, *Hydrophobic surfactant proteins and their analogues.* Neonatology, 2007. **91**(4): p. 303-310.

6. Orgeig, S., W. Bernhard, S.C. Biswas, C.B. Daniels, S.B. Hall, S.K. Hetz, C.J. Lang, J.N. Maina, A.K. Panda, J. Perez-Gil, F. Possmayer, R.A. Veldhuizen, and W. Yan, *The anatomy, physics, and physiology of gas exchange surfaces: is there a universal function for pulmonary surfactant in animal respiratory structures?* Integrative and Comparative Biology, 2007. **47**(4): p. 610-627.

7. Notter, R.H., *Lung surfactants : basic science and clinical applications*. Lung biology in health and disease ; v. 149. 2000, New York: Marcel Dekker. xiii, 444.

8. Blanco, O. and J. Perez-Gil, *Biochemical and pharmacological differences between preparations of exogenous natural surfactant used to treat Respiratory Distress Syndrome: Role of the different components in an efficient pulmonary surfactant.* European Journal of Pharmacology, 2007. **568**(1-3): p. 1-15.

9. Veldhuizen, R., K. Nag, S. Orgeig, and F. Possmayer, *The role of lipids in pulmonary surfactant.* Biochimica Et Biophysica Acta-Molecular Basis of Disease, 1998. **1408**(2-3): p. 90-108.

10. Johansson, J., T. Curstedt, and B. Robertson, *Artificial surfactants based on analogues of SP-B and SP-C.* Pediatric Pathology & Molecular Medicine, 2001. **20**(6): p. 501-518.

11. Wu, C.W. and A.E. Barron, *Biomimetic lung surfactant replacements*, in *Biomimetic Materials and Design: Interactive Biointerfacial Strategies, Tissue Engineering, and*

Drug Delivery, A.K. Dillow and A.M. Lowman, Editors. 2002, Marcel-Dekker: New York. p. 565-633.

12. Curstedt, T. and J. Johansson, *New synthetic surfactant - How and when?* Biology of the Neonate, 2006. **89**(4): p. 336-339.

13. Almlen, A., G. Stichtenoth, B. Linderholm, M. Haegerstrand-Bjorkman, B. Robertson, J. Johansson, and T. Curstedt, *Surfactant proteins B and C are both necessary for alveolar stability at end expiration in premature rabbits with respiratory distress syndrome.* Journal of Applied Physiology, 2008. **104**(4): p. 1101-1108.

14. Halliday, H.L., *Controversies: synthetic or natural surfactant. The case for natural surfactant.* J Perinat Med, 1996. **24**(5): p. 417-26.

15. Mingarro, I., D. Lukovic, M. Vilar, and J. Perez-Gil, *Synthetic pulmonary surfactant preparations: New developments and future trends.* Current Medicinal Chemistry, 2008. **15**(4): p. 393-403.

16. Serrano, A.G. and J. Perez-Gil, *Protein-lipid interactions and surface activity in the pulmonary surfactant system.* Chemistry and Physics of Lipids, 2006. **141**(1-2): p. 105-118.

17. Clements, J.A., *Surface Tension of Lung Extracts.* Proceedings of the Society for Experimental Biology and Medicine, 1957. **95**(1): p. 170-172.

18. Lee, K.Y.C., M.M. Lipp, D.Y. Takamoto, E. Ter-Ovanesyan, J.A. Zasadzinski, and A.J. Waring, *Apparatus for the continuous monitoring of surface morphology via fluorescence microscopy during monolayer transfer to substrates.* Langmuir, 1998. **14**(9): p. 2567-2572.

19. Honig, D. and D. Mobius, *Direct Visualization of Monolayers at the Air-Water-Interface by Brewster-Angle Microscopy.* Journal of Physical Chemistry, 1991. **95**(12): p. 4590-4592.

20. Ding, J.Q., D.Y. Takamoto, A. von Nahmen, M.M. Lipp, K.Y.C. Lee, A.J. Waring, and J.A. Zasadzinski, *Effects of lung surfactant proteins, SP-B and SP-C, and palmitic acid on monolayer stability.* Biophysical Journal, 2001. **80**(5): p. 2262-2272.

21. Gaines, G.L., *Insoluble monolayers at liquid-gas interfaces*. Interscience monographs on physical chemistry. 1966, New York,: Interscience Publishers. xiv, 386.

22. Lipp, M.M., K.Y.C. Lee, J.A. Zasadzinski, and A.J. Waring, *Phase and morphology changes in lipid monolayers induced by SP-B protein and its amino-terminal peptide.* Science, 1996. **273**(5279): p. 1196-1199.

23. Enhorning, G., *Pulsating Bubble Technique for Evaluating Pulmonary Surfactant.* Journal of Applied Physiology, 1977. **43**(2): p. 198-203.

24. Schurch, S., H. Bachofen, J. Goerke, and F. Possmayer, *A captive bubble method reproduces the in situ behavior of lung surfactant monolayers.* J Appl Physiol, 1989. **67**(6): p. 2389-2396.

25. Possmayer, F., S.H. Yu, J.M. Weber, and P.G.R. Harding, *Pulmonary Surfactant.* Canadian Journal of Biochemistry and Cell Biology, 1984. **62**(11): p. 1121-1133.

26. Putz, G., J. Goerke, H.W. Taeusch, and J.A. Clements, *Comparison of Captive and Pulsating Bubble Surfactometers with Use of Lung Surfactants.* Journal of Applied Physiology, 1994. **76**(4): p. 1425-1431.

27. Seurynck, S.L., N.J. Brown, C.W. Wu, K.W. Germino, E.K. Kohlmeir, E.P. Ingenito, M.R. Glucksberg, A.E. Barron, and M. Johnson, *Optical monitoring of bubble size and shape in a pulsating bubble surfactometer.* Journal of Applied Physiology, 2005. **99**(2): p. 624-633.

28. Foot, N.J., S. Orgeig, S. Donnellan, T. Bertozzi, and C.B. Daniels, *Positive selection in the N-terminal extramembrane domain of lung surfactant protein C (SP-C) in marine mammals.* Journal of Molecular Evolution, 2007. **65**(1): p. 12-22.

29. Johansson, J., T. Szyperski, T. Curstedt, and K. Wuthrich, *The Nmr Structure of the Pulmonary Surfactant-Associated Polypeptide Sp-C in an Apolar Solvent Contains a Valyl-Rich Alpha-Helix.* Biochemistry, 1994. **33**(19): p. 6015-6023.

30. Gonzalez-Horta, A., D. Andreu, M.R. Morrow, and J. Perez-Gil, *Effects of palmitoylation on dynamics and phospholipid-bilayer-perturbing properties of the N-terminal segment of pulmonary surfactant protein SP-C as shown by H-2-NMR.* Biophysical Journal, 2008. **95**(5): p. 2308-2317.

31. Plasencia, I., F. Baumgart, D. Andreu, D. Marsh, and J. Perez-Gil, *Effect of acylation on the interaction of the N-Terminal segment of pulmonary surfactant protein SP-C with phospholipid membranes.* Biochimica Et Biophysica Acta-Biomembranes, 2008. **1778**(5): p. 1274-1282.

32. Gericke, A., C.R. Flach, and R. Mendelsohn, *Structure and orientation of lung surfactant SP-C and L-alpha-dipalmitoylphosphatidylcholine in aqueous monolayers.* Biophysical Journal, 1997. **73**(1): p. 492-499.

33. Vandenbussche, G., A. Clercx, T. Curstedt, J. Johansson, H. Jornvall, and J.M. Ruysschaert, *Structure and Orientation of the Surfactant-Associated Protein-C in a Lipid Bilayer.* European Journal of Biochemistry, 1992. **203**(1-2): p. 201-209.

34. Creuwels, L., E.H. Boer, R.A. Demel, L.M.G. Vangolde, and H.P. Haagsman, *Neutralization of the Positive Charges of Surfactant Protein-C - Effects on Structure and Function.* Journal of Biological Chemistry, 1995. **270**(27): p. 16225-16229.

35. Bi, X.H., C.R. Flach, J. Perez-Gil, I. Plasencia, D. Andreu, E. Oliveira, and R. Mendelsohn, *Secondary structure and lipid interactions of the N-terminal segment of pulmonary surfactant SP-C in Langmuir films: IR reflection-absorption spectroscopy and surface pressure studies.* Biochemistry, 2002. **41**(26): p. 8385-8395.

36. Gustafsson, M., W.J. Griffiths, E. Furusjo, and J. Johansson, *The palmitoyl groups of lung surfactant protein C reduce unfolding into a fibrillogenic intermediate.* Journal of Molecular Biology, 2001. **310**(4): p. 937-950.

37. Wang, Z.D., O. Gurel, J.E. Baatz, and R.H. Notter, *Acylation of pulmonary surfactant protein-C is required for its optimal surface active interactions with phospholipids.* Journal of Biological Chemistry, 1996. **271**(32): p. 19104-19109.

38. Oosterlaken-Dijksterhuis, M.A., H.P. Haagsman, L.M.G. Vangolde, and R.A. Demel, *Characterization of Lipid Insertion into Monomolecular Layers Mediated by Lung Surfactant Proteins Sp-B and Sp-C.* Biochemistry, 1991. **30**(45): p. 10965-10971.

39. Wang, L., P. Cai, H.J. Galla, H.X. He, C.R. Flach, and R. Mendelsohn, *Monolayer-multilayer transitions in a lung surfactant model: IR reflection-absorption spectroscopy and atomic force microscopy.* European Biophysics Journal with Biophysics Letters, 2005. **34**(3): p. 243-254.

40. Gustafsson, M., M. Palmblad, T. Curstedt, J. Johansson, and S. Schurch, *Palmitoylation of a pulmonary surfactant protein C analogue affects the surface associated lipid reservoir and film stability.* Biochimica Et Biophysica Acta-Biomembranes, 2000. **1466**(1-2): p. 169-178.

41. Nakorn, P.N., M.C. Meyer, C.R. Flach, R. Mendelsohn, and H.J. Galla, *Surfactant protein C and lung function: new insights into the role of alpha-helical length and palmitoylation.* European Biophysics Journal with Biophysics Letters, 2007. **36**(4-5): p. 477-489.

42. Alonso, C., A. Waring, and J.A. Zasadzinski, *Keeping Lung Surfactant Where It Belongs: Protein Regulation of Two-Dimensional Viscosity.* Biophys. J., 2005. **89**(1): p. 266-273.

43. Szyperski, T., G. Vandenbussche, T. Curstedt, J.M. Ruysschaert, K. Wuthrich, and J. Johansson, *Pulmonary surfactant-associated polypeptide C in a mixed organic solvent transforms from a monomeric alpha-helical state into insoluble beta-sheet aggregates.* Protein Science, 1998. **7**(12): p. 2533-2540.

44. Gustafsson, M., J. Thyberg, J. Naslund, E. Eliasson, and J. Johansson, *Amyloid fibril formation by pulmonary surfactant protein C.* Febs Letters, 1999. **464**(3): p. 138-142.

45. Johansson, J., G. Nilsson, R. Stromberg, B. Robertson, H. Jornvall, and T. Curstedt, *Secondary Structure and Biophysical Activity of Synthetic Analogs of the Pulmonary Surfactant Polypeptide Sp-C.* Biochemical Journal, 1995. **307**: p. 535-541.

46. Hawgood, S., A. Ogawa, K. Yukitake, M. Schlueter, C. Brown, T. White, D. Buckley, D. Lesikar, and B. Benson, *Lung function in premature rabbits treated with recombinant human surfactant protein-C.* American Journal of Respiratory and Critical Care Medicine, 1996. **154**(2): p. 484-490.

47. Lukovic, D., I. Plasencia, F.J. Taberner, J. Salgado, J.J. Calvete, J. Perez-Gil, and I. Mingarro, *Production and characterisation of recombinant forms of human pulmonary surfactant protein C (SP-C): Structure and surface activity.* Biochimica Et Biophysica Acta-Biomembranes, 2006. **1758**(4): p. 509-518.

48. Davis, A.J., A.H. Jobe, D. Hafner, and M. Ikegami, *Lung function in premature lambs and rabbits treated with a recombinant SP-C surfactant.* American Journal of Respiratory and Critical Care Medicine, 1998. **157**(2): p. 553-559.

49. Spragg, R.G., J.F. Lewis, H. Walmrath, J. Johannigman, G. Bellingan, P. Laterre, M.C. Witte, G.A. Richards, G. Rippin, F. Rathgeb, D. Hafner, F.J.H. Taut, and W. Seeger, *Effect of recombinant surfactant protein C-based surfactant on the acute respiratory distress syndrome.* New England Journal of Medicine, 2004. **351**(9): p. 884-892.

50. Nilsson, G., M. Gustafsson, G. Vandenbussche, E. Veldhuizen, W.J. Griffiths, J. Sjovall, H.P. Haagsman, J.M. Ruysschaert, B. Robertson, T. Curstedt, and J. Johansson, *Synthetic peptide-containing surfactants - Evaluation of transmembrane versus amphipathic helices and surfactant protein C poly-valyl to poly-leucyl substitution.* European Journal of Biochemistry, 1998. **255**(1): p. 116-124.

51. Takei, T., Y. Hashimoto, T. Aiba, K. Sakai, and T. Fujiwara, *The surface properties of chemically synthesized peptides analogous to human pulmonary surfactant protein SP-C.* Biological & Pharmaceutical Bulletin, 1996. **19**(10): p. 1247-1253.

52. Johansson, J., M. Some, B.M. Linderholm, A. Almlen, T. Curstedt, and B. Robertson, *A synthetic surfactant based on a poly-Leu SP-C analog and phospholipids: effects on tidal volumes and lung gas volumes in ventilated immature newborn rabbits.* Journal of Applied Physiology, 2003. **95**(5): p. 2055-2063.

53. Palmblad, M., J. Johansson, B. Robertson, and T. Curstedt, *Biophysical activity of an artificial surfactant containing an analogue of surfactant protein (SP)-C and native SP-B.* Biochemical Journal, 1999. **339**: p. 381-386.

54. Almlen, A., G. Stichtenoth, B. Robertson, J. Johansson, and T. Curstedt, *Concentration dependence of a poly-leucine surfactant protein C analogue on in vitro and in vivo surfactant activity.* Neonatology, 2007. **92**(3): p. 194-200.

55. Miller, S.M., R.J. Simon, S. Ng, R.N. Zuckermann, J.M. Kerr, and W.H. Moos, *Comparison of the Proteolytic Susceptibilities of Homologous L-Amino-Acid, D-Amino-Acid, and N-Substituted Glycine Peptide and Peptoid Oligomers.* Drug Development Research, 1995. **35**(1): p. 20-32.

56. Chongsiriwatana, N.P., J.A. Patch, A.M. Czyzewski, M.T. Dohm, A. Ivankin, D. Gidalevitz, R.N. Zuckermann, and A.E. Barron, *Peptoids that mimic the structure, function, and mechanism of helical antimicrobial peptides.* Proceedings of the National Academy of Sciences of the United States of America, 2008. **105**(8): p. 2794-2799.

57. Gibbons, J.A., A.A. Hancock, C.R. Vitt, S. Knepper, S.A. Buckner, M.E. Brune, I. Milicic, J.F. Kerwin, L.S. Richter, E.W. Taylor, K.L. Spear, R.N. Zuckermann, D.C. Spellmeyer, R.A. Braeckman, and W.H. Moos, *Pharmacologic characterization of CHIR 2279, an N-substituted glycine peptoid with high-affinity binding for alpha(1)-adrenoceptors.* Journal of Pharmacology and Experimental Therapeutics, 1996. **277**(2): p. 885-899.

58. Wu, C.W., K. Kirshenbaum, T.J. Sanborn, J.A. Patch, K. Huang, K.A. Dill, R.N. Zuckermann, and A.E. Barron, *Structural and spectroscopic studies of peptoid oligomers with alpha-chiral aliphatic side chains.* Journal of the American Chemical Society, 2003. **125**(44): p. 13525-13530.

59. Wu, C.W., T.J. Sanborn, K. Huang, R.N. Zuckermann, and A.E. Barron, *Peptoid oligomers with alpha-chiral, aromatic side chains: Sequence requirements for the formation of stable peptoid helices.* Journal of the American Chemical Society, 2001. **123**(28): p. 6778-6784.

60. Sanborn, T.J., C.W. Wu, R.N. Zuckerman, and A.E. Barron, *Extreme stability of helices formed by water-soluble poly-N-substituted glycines (polypeptoids) with alpha-chiral side chains.* Biopolymers, 2002. **63**(1): p. 12-20.

61. Brown, N.J., C.W. Wu, S.L. Seurynck-Servoss, and A.E. Barron, *Effects of Hydrophobic Helix Length and Side Chain Chemistry on Biomimicry in Peptoid Analogues of SP-C.* Biochemistry, 2008. **47**(6): p. 1808-1818.

62. Wu, C.W., S.L. Seurynck, K.Y. Lee, and A.E. Barron, *Helical peptoid mimics of lung surfactant protein C.* Chem Biol, 2003. **10**(11): p. 1057-63.

63. Clercx, A., G. Vandenbussche, T. Curstedt, J. Johansson, H. Jornvall, and J.F. Ruysschaert, *Structural and Functional Importance of the C-Terminal Part of the*

Pulmonary Surfactant Polypeptide Sp-C. European Journal of Biochemistry, 1995. **229**(2): p. 465-472.

64. Goerke, J., *Pulmonary surfactant: functions and molecular composition.* Biochimica Et Biophysica Acta-Molecular Basis of Disease, 1998. **1408**(2-3): p. 79-89.

65. Hall, S.B., A.R. Venkitaraman, J.A. Whitsett, B.A. Holm, and R.H. Notter, *Importance of Hydrophobic Apoproteins as Constituents of Clinical Exogenous Surfactants.* American Review of Respiratory Disease, 1992. **145**(1): p. 24-30.

66. Wang, Z.D., S.B. Hall, and R.H. Notter, *Roles of different hydrophobic constituents in the adsorption of pulmonary surfactant.* Journal of Lipid Research, 1996. **37**(4): p. 790-798.

67. Poelma, D.L.H., L.J. Zimmermann, W.A. van Cappellen, J.J. Haitsma, B. Lachmann, and J.F. van Iwaarden, *Distinct effects of SP-B and SP-C on the uptake of surfactant-like liposomes by alveolar cells in vivo and in vitro.* American Journal of Physiology-Lung Cellular and Molecular Physiology, 2004. **287**(5): p. L1056-L1065.

68. Clark, J.C., S.E. Wert, C.J. Bachurski, M.T. Stahlman, B.R. Stripp, T.E. Weaver, and J.A. Whitsett, *Targeted Disruption of the Surfactant Protein-B Gene Disrupts Surfactant Homeostasis, Causing Respiratory-Failure in Newborn Mice.* Proceedings of the National Academy of Sciences of the United States of America, 1995. **92**(17): p. 7794-7798.

69. Nogee, L.M., D.E. Demello, L.P. Dehner, and H.R. Colten, *Brief Report - Deficiency of Pulmonary Surfactant Protein-B in Congenital Alveolar Proteinosis.* New England Journal of Medicine, 1993. **328**(6): p. 406-410.

70. Nogee, L.M., S.E. Wert, S.A. Proffit, W.M. Hull, and J.A. Whitsett, *Allelic heterogeneity in hereditary surfactant protein B (SP-B) deficiency.* American Journal of Respiratory and Critical Care Medicine, 2000. **161**(3): p. 973-981.

71. Vorbroker, D.K., S.A. Profitt, L.M. Nogee, and J.A. Whitsett, *Aberrant Processing of Surfactant Protein-C in Hereditary Sp-B Deficiency.* American Journal of Physiology-Lung Cellular and Molecular Physiology, 1995. **12**(4): p. L647-L656.

72. Saugstad, O.D., T. Curstedt, H.L. Halliday, B. Robertson, and C.R. Speer, *Surfactant replacement therapy from 1986 to 2006: A 20-year success story.* Biology of the Neonate, 2006. **89**(4): p. 282-283.

73. Robertson, B., J. Johansson, and T. Curstedt, *Synthetic surfactants to treat neonatal lung disease.* Molecular Medicine Today, 2000. **6**(3): p. 119-124.

74. Whitelaw, A., *Controversies: Synthetic or natural surfactant treatment for respiratory distress syndrome? The case for synthetic surfactant.* Journal of Perinatal Medicine, 1996. **24**(5): p. 427-435.

75. Moya, F.R., D.R. Hoffman, B. Zhao, and J.M. Johnston, *Platelet-activating factor in surfactant preparations.* Lancet, 1993. **341**(8849): p. 858-60.

76. Long, W., *Synthetic Surfactant.* Seminars in Perinatology, 1993. **17**(4): p. 275-284.

77. Sinha, S.K., T. Lacaze-Masmonteil, A.V.I. Soler, T.E. Wiswell, J. Gadzinowski, J. Hajdu, G. Bernstein, and R. d'Agostino, *A multicenter, randomized, controlled trial of lucinactant versus poractant alfa among very premature infants at high risk for respiratory distress syndrome.* Pediatrics, 2005. **115**(4): p. 1030-1038.

78. Czaja, A.S., *A critical appraisal of a randomized controlled trial: Willson et al: Effect of exogenous surfactant (calfactant) in pediatric acute lung injury (JAMA 2005, 293 : 470-476).* Pediatric Critical Care Medicine, 2007. **8**(1): p. 50-53.

79. Willson, D.F., N.J. Thomas, B.P. Markovitz, L.A. Bauman, J.V. DiCarlo, S. Pon, B.R. Jacobs, L.S. Jefferson, M.R. Conaway, and E.A. Egan, *Effect of exogenous surfactant (Calfactant) in pediatric acute lung injury - A randomized controlled trial.* Jama-Journal of the American Medical Association, 2005. **293**(4): p. 470-476.

80. Notter, R.H., J.N. Finkelstein, and R.D. Taubold, *Comparative Adsorption of Natural Lung Surfactant, Extracted Phospholipids, and Artificial Phospholipid Mixtures to the Air-Water-Interface.* Chemistry and Physics of Lipids, 1983. **33**(1): p. 67-80.

81. Whitsett, J.A., B.L. Ohning, G. Ross, J. Meuth, T. Weaver, B.A. Holm, D.L. Shapiro, and R.H. Notter, *Hydrophobic Surfactant-Associated Protein in Whole Lung Surfactant and Its Importance for Biophysical Activity in Lung Surfactant Extracts Used for Replacement Therapy.* Pediatric Research, 1986. **20**(5): p. 460-467.

82. Ingenito, E.P., L. Mark, J. Morris, F.F. Espinosa, R.D. Kamm, and M. Johnson, *Biophysical characterization and modeling of lung surfactant components.* Journal of Applied Physiology, 1999. **86**(5): p. 1702-1714.

83. Bligh, E.G. and W.J. Dyer, *A Rapid Method of Total Lipid Extraction and Purification.* Canadian Journal of Biochemistry and Physiology, 1959. **37**(8): p. 911-917.

84. Stewart, J.C.M., *Colorimetric Determination of Phospholipids with Ammonium Ferrothiocyanate.* Analytical Biochemistry, 1980. **104**(1): p. 10-14.

85. Kates, S.A., N.A. Sole, M. Beyermann, G. Barany, and F. Albericio, *Optimized preparation of deca(L-alanyl)-L-valinamide by 9-fluorenylmethyloxycarbonyl (Fmoc) solid-phase synthesis on polyethylene glycol-polystyrene (PEG-PS) graft supports, with*

1,8-diazobicyclo[5.4.0]-undec-7-ene (DBU) deprotection. Peptide Research, 1996. **9**(3): p. 106-113.

86. Zuckermann, R.N., J.M. Kerr, S.B.H. Kent, and W.H. Moos, *Efficient Method for the Preparation of Peptoids Oligo(N-Substituted Glycines) by Submonomer Solid-Phase Synthesis.* Journal of the American Chemical Society, 1992. **114**(26): p. 10646-10647.

87. Scarpelli, E.M., E. David, M. Cordova, and A.J. Mautone, *Surface-Tension of Therapeutic Surfactants (Exosurf Neonatal, Infasurf, and Survanta) as Evaluated by Standard Methods and Criteria.* American Journal of Perinatology, 1992. **9**(5-6): p. 414-419.

88. Johansson, J., *Structure and properties of surfactant protein C.* Biochimica Et Biophysica Acta-Molecular Basis of Disease, 1998. **1408**(2-3): p. 161-172.

89. Qanbar, R., S. Cheng, F. Possmayer, and S. Schurch, *Role of the palmitoylation of surfactant-associated protein C in surfactant film formation and stability.* American Journal of Physiology-Lung Cellular and Molecular Physiology, 1996. **15**(4): p. L572-L580.

90. Taneva, S.G. and K.M.W. Keough, *Dynamic Surface-Properties of Pulmonary Surfactant Proteins Sp-B and Sp-C and Their Mixtures with Dipalmitoylphosphatidylcholine.* Biochemistry, 1994. **33**(49): p. 14660-14670.

91. Johansson, J., M. Gustafsson, M. Palmblad, S. Zaltash, B. Robertson, and T. Curstedt, *Synthetic surfactant protein analogues.* Biology of the Neonate, 1998. **74**: p. 9-14.

92. Ikegami, M. and A.H. Jobe, *Surfactant protein-C in ventilated premature lamb lung.* Pediatric Research, 1998. **44**(6): p. 860-864.

93. Otsubo, E. and T. Takei, *Effects of the human pulmonary surfactant protein-C (SP-C, SP-CL16(6-28) on surface activities of surfactants with various phospholipids.* Biological & Pharmaceutical Bulletin, 2002. **25**(10): p. 1303-1306.

94. Takei, T., Y. Hashimoto, E. Ohtsubo, K. Sakai, and H. Ohkawa, *Characterization of poly-leucine substituted analogues of the human surfactant protein SP-C.* Biological & Pharmaceutical Bulletin, 1996. **19**(12): p. 1550-1555.

95. Chan, W.C. and P.D. White, *Fmoc solid phase peptide synthesis : a practical approach*. The practical approach series ; 222. 2000, New York: Oxford University Press. xxiv, 346 p.

96. Mayer-Fligge, P., J. Volz, U. Kruger, E. Sturm, W. Gernandt, K.P. Schafer, and M. Przybylski, *Synthesis and structural characterization of human-identical lung surfactant SP-C protein.* Journal of Peptide Science, 1998. **4**(5): p. 355-363.

97. Tickler, A.K., A.B. Clippingdale, and J.D. Wade, *Amyloid-beta as a "difficult sequence" in solid phase peptide synthesis.* Protein and Peptide Letters, 2004. **11**(4): p. 377-384.

98. Hyde, C., T. Johnson, and R.C. Sheppard, *Internal Aggregation During Solid-Phase Peptide-Synthesis - Dimethyl-Sulfoxide as a Powerful Dissociating Solvent.* Journal of the Chemical Society-Chemical Communications, 1992(21): p. 1573-1575.

99. Yousefi-Salakdeh, E., J. Johansson, and R. Stromberg, *A method for S- and O-palmitoylation of peptides: synthesis of pulmonary surfactant protein-C models.* Biochemical Journal, 1999. **343**: p. 557-562.

100. Johansson, J., T. Curstedt, and B. Robertson, *Synthetic protein analogues in artificial surfactants.* Acta Paediatrica, 1996. **85**(6): p. 642-646.

101. Creuwels, L., R.A. Demel, L.M.G. Vangolde, B.J. Benson, and H.P. Haagsman, *Effect of Acylation on Structure and Function of Surfactant Protein-C at the Air-Liquid Interface.* Journal of Biological Chemistry, 1993. **268**(35): p. 26752-26758.

102. Shiffer, K., S. Hawgood, H.P. Haagsman, B. Benson, J.A. Clements, and J. Goerke, *Lung Surfactant Proteins, Sp-B and Sp-C, Alter the Thermodynamic Properties of Phospholipid-Membranes - a Differential Calorimetry Study.* Biochemistry, 1993. **32**(2): p. 590-597.

103. Flach, C.R., A. Gericke, K.M.W. Keough, and R. Mendelsohn, *Palmitoylation of lung surfactant protein SP-C alters surface thermodynamics, but not protein secondary structure or orientation in 1,2-dipalmitoylphosphatidylcholine Langmuir films.* Biochimica Et Biophysica Acta-Biomembranes, 1999. **1416**(1-2): p. 11-20.

104. Tanaka, Y., T. Takei, T. Aiba, K. Masuda, A. Kiuchi, and T. Fujiwara, *Development of Synthetic Lung Surfactants.* Journal of Lipid Research, 1986. **27**(5): p. 475-485.

105. Johansson, J., T. Szyperski, and K. Wuthrich, *Pulmonary Surfactant-Associated Polypeptide Sp-C in Lipid Micelles - Cd Studies of Intact Sp-C and Nmr Secondary Structure Determination of Depalmitoyl-Sp-C(1-17).* Febs Letters, 1995. **362**(3): p. 261-265.

106. Johansson, J. and T. Curstedt, *Molecular structures and interactions of pulmonary surfactant components.* European Journal of Biochemistry, 1997. **244**(3): p. 675-693.

107. Schram, V. and S.B. Hall, *Thermodynamic effects of the hydrophobic surfactant proteins on the early adsorption of pulmonary surfactant.* Biophysical Journal, 2001. **81**(3): p. 1536-1546.

108. Schram, V. and S.B. Hall, *SP-13 and SP-C alter diffusion in Bilayers of pulmonary surfactant.* Biophysical Journal, 2004. **86**(6): p. 3734-3743.

109. Poynter, S.E. and A.M. LeVine, *Surfactant biology and clinical application.* Critical Care Clinics, 2003. **19**(3): p. 459-+.

110. Cochrane, C.G., S.D. Revak, A. Merritt, G.P. Heldt, M. Hallman, M.D. Cunningham, D. Easa, A. Pramanik, D.K. Edwards, and M.S. Alberts, *The efficacy and safety of KL(4)-surfactant in infants with respiratory distress syndrome.* American Journal of Respiratory and Critical Care Medicine, 1996. **153**(1): p. 404-410.

111. McLean, L.R., J.E. Lewis, J.L. Krstenansky, K.A. Hagaman, A.S. Cope, K.F. Olsen, E.R. Matthews, D.C. Uhrhammer, T.J. Owen, and M.H. Payne, *An Amphipathic Alpha-Helical Decapeptide in Phosphatidylcholine Is an Effective Synthetic Lung Surfactant.* American Review of Respiratory Disease, 1993. **147**(2): p. 462-465.

112. Seurynck, S.L., J.A. Patch, and A.E. Barron, *Simple, helical peptoid analogs of lung surfactant protein B.* Chemistry & Biology, 2005. **12**(1): p. 77-88.

113. Simon, R.J., R.S. Kania, R.N. Zuckermann, V.D. Huebner, D.A. Jewell, S. Banville, S. Ng, L. Wang, S. Rosenberg, C.K. Marlowe, D.C. Spellmeyer, R.Y. Tan, A.D. Frankel, D.V. Santi, F.E. Cohen, and P.A. Bartlett, *Peptoids - a Modular Approach to Drug Discovery.* Proceedings of the National Academy of Sciences of the United States of America, 1992. **89**(20): p. 9367-9371.

114. Borman, S., *Peptoids eyed for gene therapy applications.* Chemical & Engineering News, 1998. **76**(18): p. 56-57.

115. Armand, P., K. Kirshenbaum, R.A. Goldsmith, S. Farr-Jones, A.E. Barron, K.T.V. Truong, K.A. Dill, D.F. Mierke, F.E. Cohen, R.N. Zuckermann, and E.K. Bradley, *NMR determination of the major solution conformation of a peptoid pentamer with chiral side chains.* Proceedings of the National Academy of Sciences of the United States of America, 1998. **95**(8): p. 4309-4314.

116. Kirshenbaum, K., A.E. Barron, R.A. Goldsmith, P. Armand, E.K. Bradley, K.T.V. Truong, K.A. Dill, F.E. Cohen, and R.N. Zuckermann, *Sequence-specific polypeptoids: A diverse family of heteropolymers with stable secondary structure.* Proceedings of the National Academy of Sciences of the United States of America, 1998. **95**(8): p. 4303-4308.

117. Waring, A.J., F.J. Walther, L.M. Gordon, J.M. Hernandez-Juviel, T. Hong, M.A. Sherman, C. Alonso, T. Alig, A. Braun, D. Bacon, and J.A. Zasadzinski, *The role of charged amphipathic helices in the structure and function of surfactant protein B.* Journal of Peptide Research, 2005. **66**(6): p. 364-374.

118. Kruger, P., J.E. Baatz, R.A. Dluhy, and M. Losche, *Effect of hydrophobic surfactant protein SP-C on binary phospholipid monolayers. Molecular machinery at the air/water interface.* Biophysical Chemistry, 2002. **99**(3): p. 209-228.

119. Bringezu, F., J.Q. Ding, G. Brezesinski, and J.A. Zasadzinski, *Changes in model lung surfactant monolayers induced by palmitic acid.* Langmuir, 2001. **17**(15): p. 4641-4648.

120. Cruz, A., C. Casals, K.M.W. Keough, and J. PerezGil, *Different modes of interaction of pulmonary surfactant protein SP-B in phosphatidylcholine bilayers.* Biochemical Journal, 1997. **327**: p. 133-138.

121. Lipp, M.M., K.Y.C. Lee, J.A. Zasadzinski, and A.J. Waring, *Design and performance of an integrated fluorescence, polarized fluorescence, and Brewster angle microscope Langmuir trough assembly for the study of lung surfactant monolayers.* Review of Scientific Instruments, 1997. **68**(6): p. 2574-2582.

122. Oosterlaken-Dijksterhuis, M.A., M. Vaneijk, L.M.G. Vangolde, and H.P. Haagsman, *Lipid Mixing Is Mediated by the Hydrophobic Surfactant Protein Sp-B but Not by Sp-C.* Biochimica Et Biophysica Acta, 1992. **1110**(1): p. 45-50.

123. Taneva, S. and K.M.W. Keough, *Pulmonary Surfactant Proteins Sp-B and Sp-C in Spread Monolayers at the Air-Water-Interface .2. Monolayers of Pulmonary Surfactant Protein Sp-6 and Phospholipids.* Biophysical Journal, 1994. **66**(4): p. 1149-1157.

124. Cruz, A., L. Vazquez, M. Velez, and J. Perez-Gil, *Effect of pulmonary surfactant protein SP-B on the micro- and nanostructure of phospholipid films.* Biophysical Journal, 2004. **86**(1): p. 308-320.

125. Dico, A.S., J. Hancock, M.R. Morrow, J. Stewart, S. Harris, and K.M.W. Keough, *Pulmonary surfactant protein SP-B interacts similarly with dipalmitoylphosphatidylglycerol and dipalmitoylphosphatidylcholine in phosphatidylcholine/phosphatidylglycerol mixtures.* Biochemistry, 1997. **36**(14): p. 4172-4177.

126. Nag, K., J. PerezGil, A. Cruz, and K.M.W. Keough, *Fluorescently labeled pulmonary surfactant protein C in spread phospholipid monolayers.* Biophysical Journal, 1996. **71**(1): p. 246-256.

127. Yu, S.H. and F. Possmayer, *Role of Bovine Pulmonary Surfactant-Associated Proteins in the Surface-Active Property of Phospholipid Mixtures.* Biochimica Et Biophysica Acta, 1990. **1046**(3): p. 233-241.

128. Yu, S.H. and F. Possmayer, *Adsorption, Compression and Stability of Surface-Films from Natural, Lipid Extract and Reconstituted Pulmonary Surfactants.* Biochimica Et Biophysica Acta, 1993. **1167**(3): p. 264-271.

129. Amirkhanian, J.D., R. Bruni, A.J. Waring, C. Navar, and H.W. Taeusch, *Full-Length Synthetic Surfactant Proteins, Sp-B and Sp-C, Reduce Surfactant Inactivation by Serum.* Biochimica Et Biophysica Acta, 1993. **1168**(3): p. 315-320.

130. Amirkhanian, J.D., R. Bruni, A.J. Waring, and H.W. Taeusch, *Inhibition of Mixtures of Surfactant Lipids and Synthetic Sequences of Surfactant Proteins Sp-B and Sp-C.* Biochimica Et Biophysica Acta, 1991. **1096**(4): p. 355-360.

131. Bringezu, F., J.Q. Ding, G. Brezesinski, A.J. Waring, and J.A. Zasadzinski, *Influence of pulmonary surfactant protein B on model lung surfactant monolayers.* Langmuir, 2002. **18**(6): p. 2319-2325.

132. Gupta, M., J.M. Hernandez-Juviel, A.J. Waring, and F.J. Walther, *Function and inhibition sensitivity of the N-terminal segment of surfactant protein B (SP-B1-25) in preterm rabbits.* Thorax, 2001. **56**(11): p. 871-876.

133. Gustafsson, M., G. Vandenbussche, T. Curstedt, J.M. Ruysschaert, and J. Johansson, *The 21-residue surfactant peptide (LysLeu(4))(4)Lys(KL(4)) is a transmembrane alpha-helix with a mixed nonpolar/polar surface.* Febs Letters, 1996. **384**(2): p. 185-188.

134. Walther, F.J., J.M. Hernandez-Juviel, P.E. Mercado, L.M. Gordon, and A.J. Waring, *Surfactant with SP-B and SP-C analogues improves lung function in surfactant-deficient rats.* Biology of the Neonate, 2002. **82**(3): p. 181-187.

135. Diemel, R.V., M.M.E. Snel, L.M.G. van Golde, G. Putz, H.P. Haagsman, and J.J. Batenburg, *Effects of cholesterol on surface activity and surface topography of spread surfactant films.* Biochemistry, 2002. **41**(50): p. 15007-15016.

136. Discher, B.M., K.M. Maloney, D.W. Grainger, and S.B. Hall, *Effect of neutral lipids on coexisting phases in monolayers of pulmonary surfactant.* Biophysical Chemistry, 2002. **101**: p. 333-345.

137. Fleming, B.D. and K.M.W. Keough, *Surface Respreading after Collapse of Monolayers Containing Major Lipids of Pulmonary Surfactant.* Chemistry and Physics of Lipids, 1988. **49**(1-2): p. 81-86.

138. Larsson, M., K. Larsson, T. Nylander, and P. Wollmer, *The bilayer melting transition in lung surfactant bilayers: the role of cholesterol.* European Biophysics Journal with Biophysics Letters, 2003. **31**(8): p. 633-636.

139. Malcharek, S., A. Hinz, L. Hilterhaus, and H.-J. Galla, *Multilayer Structures in Lipid Monolayer Films Containing Surfactant Protein C: Effects of Cholesterol and POPE.* Biophys. J., 2005. **88**(4): p. 2638-2649.

140. Notter, R.H., S. Holcomb, and R.D. Mavis, *Dynamic Surface-Properties of Phosphatidylglycerol-Dipalmitoyl Phosphatidylcholine Mixed Films.* Chemistry and Physics of Lipids, 1980. **27**(4): p. 305-319.

141. Taneva, S. and K.M.W. Keough, *Cholesterol modifies the properties of surface films of dipalmitoylphosphatidylcholine plus pulmonary surfactant-associated protein B or C spread or adsorbed at the air-water interface.* Biochemistry, 1997. **36**(4): p. 912-922.

142. Tolle, A., W. Meier, M. Rudiger, K.P. Hofmann, and B. Rustow, *Effect of cholesterol and surfactant protein B on the viscosity of phospholipid mixtures.* Chemistry and Physics of Lipids, 2002. **114**(2): p. 159-168.

143. Walther, F.J., J.M. Hernandez-Juviel, L.M. Gordon, A.J. Waring, P. Stenger, and J.A. Zasadzinski, *Comparison of three lipid formulations for synthetic surfactant with a surfactant protein B analog.* Experimental Lung Research, 2005. **31**(6): p. 563-579.

144. Alonso, C., T. Alig, J. Yoon, F. Bringezu, H. Warriner, and J.A. Zasadzinski, *More than a monolayer: Relating lung surfactant structure and mechanics to composition.* Biophysical Journal, 2004. **87**(6): p. 4188-4202.

145. Lee, K.Y.C., A. Gopal, A. von Nahmen, J.A. Zasadzinski, J. Majewski, G.S. Smith, P.B. Howes, and K. Kjaer, *Influence of palmitic acid and hexadecanol on the phase transition temperature and molecular packing of dipalmitoylphosphatidyl-choline monolayers at the air-water interface.* Journal of Chemical Physics, 2002. **116**(2): p. 774-783.

146. Ege, C., M.K. Ratajczak, J. Majewski, K. Kjaer, and K.Y.C. Lee, *Evidence for lipid/cholesterol ordering in model lipid membranes.* Biophysical Journal, 2006. **91**(1): p. L1-L3.

147. Gopal, A. and K.Y.C. Lee, *Morphology and collapse transitions in binary phospholipid monolayers.* Journal of Physical Chemistry B, 2001. **105**(42): p. 10348-10354.

148. Krol, S., A. Janshoff, M. Ross, and H.J. Galla, *Structure and function of surfactant protein B and C in lipid monolayers: a scanning force microscopy study.* Physical Chemistry Chemical Physics, 2000. **2**(20): p. 4586-4593.

149. Takamoto, D.Y., M.M. Lipp, A. von Nahmen, K.Y.C. Lee, A.J. Waring, and J.A. Zasadzinski, *Interaction of lung surfactant proteins with anionic phospholipids.* Biophysical Journal, 2001. **81**(1): p. 153-169.

150. Veldhuizen, E.J.A. and H.P. Haagsman, *Role of pulmonary surfactant components in surface film formation and dynamics.* Biochimica Et Biophysica Acta-Biomembranes, 2000. **1467**(2): p. 255-270.

151. Gopal, A. and K.Y.C. Lee, *Headgroup percolation and collapse of condensed Langmuir monolayers.* Journal of Physical Chemistry B, 2006. **110**(44): p. 22079-22087.

152. Albrecht, O., H. Gruler, and E. Sackmann, *Pressure-Composition Phase-Diagrams of Cholesterol-Lecithin, Cholesterol-Phosphatidic Acid, and Lecithin-Phosphatidic Acid Mixed Monolayers - a Langmuir Film Balance Study.* Journal of Colloid and Interface Science, 1981. **79**(2): p. 319-338.

153. Weaver, T.E., *Synthesis, processing and secretion of surfactant proteins B and C.* Biochimica Et Biophysica Acta-Molecular Basis of Disease, 1998. **1408**(2-3): p. 173-179.

154. Curstedt, T., J. Johansson, P. Persson, A. Eklund, B. Robertson, B. Lowenadler, and H. Jornvall, *Hydrophobic Surfactant-Associated Polypeptides - Sp-C Is a Lipopeptide with 2 Palmitoylated Cysteine Residues, Whereas Sp-B Lacks Covalently Linked Fatty Acyl-Groups.* Proceedings of the National Academy of Sciences of the United States of America, 1990. **87**(8): p. 2985-2989.

155. Hosia, W., J. Johansson, and W.J. Griffiths, *Hydrogen/deuterium exchange and aggregation of a polyvaline and a polyleucine alpha-helix investigated by matrix-assisted laser desorption ionization mass spectrometry.* Molecular & Cellular Proteomics, 2002. **1**(8): p. 592-597.

156. Whitmore, L. and B.A. Wallace, *DICHROWEB, an online server for protein secondary structure analyses from circular dichroism spectroscopic data.* Nucleic Acids Research, 2004. **32**: p. W668-W673.

157. Lobley, A., L. Whitmore, and B.A. Wallace, *DICHROWEB: an interactive website for the analysis of protein secondary structure from circular dichroism spectra.* Bioinformatics, 2002. **18**(1): p. 211-212.

158. Sreerama, N., S.Y. Venyaminov, and R.W. Woody, *Estimation of the number of alpha-helical and beta-strand segments in proteins using circular dichroism spectroscopy.* Protein Science, 1999. **8**(2): p. 370-380.

159. Alig, T.F., H.E. Warriner, L. Lee, and J.A. Zasadzinski, *Electrostatic barrier to recovery of dipalmitoylphosphatidylglycerol monolayers after collapse.* Biophysical Journal, 2004. **86**(2): p. 897-904.

160. Wu, C.W., T.J. Sanborn, R.N. Zuckermann, and A.E. Barron, *Peptoid oligomers with alpha-chiral, aromatic side chains: Effects of chain length on secondary structure.* Journal of the American Chemical Society, 2001. **123**(13): p. 2958-2963.

161. Rabanal, F., M.D. Ludevid, M. Pons, and E. Giralt, *CD of proline-rich polypeptides: application to the study of the repetitive domain of maize glutelin-2.* Biopolymers, 1993. **33**(7): p. 1019-28.

162. Seurynck-Servoss, N.J. Brown, M.T. Dohm, C.W. Wu, and A.E. Barron, *Lipid composition greatly affects the in vitro surface activity of lung surfactant protein mimics.* Colloids and Surfaces B-Biointerfaces, 2007. **57**(1): p. 37-55.

163. Ding, J.Q., H.E. Warriner, and J.A. Zasadzinski, *Viscosity of two-dimensional suspensions.* Physical Review Letters, 2002. **88**(16): p. art. no. 168102.

164. vonNahmen, A., M. Schenk, M. Sieber, and M. Amrein, *The structure of a model pulmonary surfactant as revealed by scanning force microscopy.* Biophysical Journal, 1997. **72**(1): p. 463-469.

165. Otis, D.R., E.P. Ingenito, R.D. Kamm, and M. Johnson, *Dynamic Surface-Tension of Surfactant Ta - Experiments and Theory.* Journal of Applied Physiology, 1994. **77**(6): p. 2681-2688.

166. Kattwinkel, J., *Synthetic surfactants: The search goes on.* Pediatrics, 2005. **115**(4): p. 1075-1076.

167. Plasencia, I., K.M.W. Keough, and J. Perez-Gil, *Interaction of the N-terminal segment of pulmonary surfactant protein SP-C with interfacial phospholipid films.* Biochimica Et Biophysica Acta-Biomembranes, 2005. **1713**(2): p. 118-128.

168. Plasencia, I., L. Rivas, K.M.W. Keough, D. Marsh, and J. Perez-Gil, *The N-terminal segment of pulmonary surfactant lipopeptide SP-C has intrinsic propensity to interact with and perturb phospholipid bilayers.* Biochemical Journal, 2004. **377**: p. 183-193.

169. Weaver, T.E. and J.J. Conkright, *Functions of surfactant proteins B and C.* Annual Review of Physiology, 2001. **63**: p. 555-578.

170. Kramer, A., A. Wintergalen, M. Sieber, H.J. Galla, M. Amrein, and R. Guckenberger, *Distribution of the surfactant-associated protein C within a lung surfactant model film investigated by near-field optical microscopy.* Biophysical Journal, 2000. **78**(1): p. 458-465.

171. Li, S.C. and C.M. Deber, *A Measure of Helical Propensity for Amino-Acids in Membrane Environments (Vol 1, Pg 368, 1994).* Nature Structural Biology, 1994. **1**(8): p. 558-558.

172. Otsubo, E., T. Takei, and M. Nomura, *Synthesis, purification and surface activities of the human pulmonary surfactant protein-C (SP-C) analogue, SP-CL16 (6-28).* Biological & Pharmaceutical Bulletin, 2001. **24**(12): p. 1362-1365.

173. Murphy, J.E., T. Uno, J.D. Hamer, F.E. Cohen, V. Dwarki, and R.N. Zuckermann, *A combinatorial approach to the discovery of efficient cationic peptoid reagents for gene delivery.* Proceedings of the National Academy of Sciences of the United States of America, 1998. **95**(4): p. 1517-1522.

174. Nadolski, M.J. and M.E. Linder, *Protein lipidation.* Febs Journal, 2007. **274**(20): p. 5202-5210.

175. Resh, M.D., *Use of analogs and inhibitors to study the functional significance of protein palmitoylation.* Methods, 2006. **40**(2): p. 191-197.

176. Conkright, J.J., J.P. Bridges, C.L. Na, W.F. Voorhout, B. Trapnell, S.W. Glasser, and T.E. Weaver, *Secretion of surfactant protein C, an integral membrane protein, requires the N-terminal propeptide.* Journal of Biological Chemistry, 2001. **276**(18): p. 14658-14664.

177. ten Brinke, A., J.J. Batenburg, B.M. Gadella, H.P. Haagsman, A.B. Vaandrager, and L.M.G. van Golde, *The juxtamembrane lysine and arginine residues of surfactant protein C precursor influence palmitoylation via effects on trafficking.* American Journal of Respiratory Cell and Molecular Biology, 2001. **25**(2): p. 156-163.

178. Lhert, F., W. Yan, S.C. Biswas, and S.B. Hall, *Effects of hydrophobic surfactant proteins on collapse of pulmonary surfactant monolayers.* Biophysical Journal, 2007. **93**(12): p. 4237-4243.

179. Perezgil, J., A. Cruz, and C. Casals, *Solubility of Hydrophobic Surfactant Proteins in Organic-Solvent Water Mixtures - Structural Studies on Sp-B and Sp-C in Aqueous-Organic Solvents and Lipids.* Biochimica Et Biophysica Acta, 1993. **1168**(3): p. 261-270.

180. Perezgil, J., K. Nag, S. Taneva, and K.M.W. Keough, *Pulmonary Surfactant Protein Sp-C Causes Packing Rearrangements of Dipalmitoylphosphatidylcholine in Spread Monolayers.* Biophysical Journal, 1992. **63**(1): p. 197-204.

181. Amrein, M., A. vonNahmen, and M. Sieber, *A scanning force and fluorescence light microscopy study of the structure and function of a model pulmonary surfactant.* European Biophysics Journal with Biophysics Letters, 1997. **26**(5): p. 349-357.

182. Perezgil, J., J. Tucker, G. Simatos, and K.M.W. Keough, *Interfacial Adsorption of Simple Lipid Mixtures Combined with Hydrophobic Surfactant Protein from Pig Lung.* Biochemistry and Cell Biology-Biochimie Et Biologie Cellulaire, 1992. **70**(5): p. 332-338.

183. Schurch, S., J. Goerke, and J.A. Clements, *Direct Determination of Volume-Dependence and Time-Dependence of Alveolar Surface-Tension in Excised Lungs.* Proceedings of the

National Academy of Sciences of the United States of America, 1978. **75**(7): p. 3417-3421.

184. ten Brinke, A., L.M.G. van Golde, and J.J. Batenburg, *Palmitoylation and processing of the lipopeptide surfactant protein C.* Biochimica Et Biophysica Acta-Molecular and Cell Biology of Lipids, 2002. **1583**(3): p. 253-265.

185. Avery, M.E. and J. Mead, *Surface properties in relation to atelectasis and hyaline membrane disease.* AMA J Dis Child, 1959. **97**(5, Part 1): p. 517-23.

186. Spragg, R., *Surfactant for acute lung injury.* American Journal of Respiratory Cell and Molecular Biology, 2007. **37**(4): p. 377-378.

187. Spragg, R.G., J.F. Lewis, W. Wurst, D. Hafner, R.P. Baughman, M.D. Wewers, and J.J. Marsh, *Treatment of acute respiratory distress syndrome with recombinant surfactant protein C surfactant.* American Journal of Respiratory and Critical Care Medicine, 2003. **167**(11): p. 1562-1566.

188. Veldhuizen, E.J.A., A.J. Waring, F.J. Walther, J.J. Batenburg, L.M.G. van Golde, and H.P. Haagsman, *Dimeric N-terminal segment of human surfactant protein B (dSP-B1-25) has enhanced surface properties compared to monomeric SP-B1-25.* Biophysical Journal, 2000. **79**(1): p. 377-384.

189. Patch, J.A. and A.E. Barron, *Helical peptoid mimics of magainin-2 amide.* Journal of the American Chemical Society, 2003. **125**(40): p. 12092-12093.

190. Plasencia, I., A. Cruz, J.L. Lopez-Lacomba, C. Casals, and J. Perez-Gil, *Selective labeling of pulmonary surfactant protein SP-C in organic solution.* Analytical Biochemistry, 2001. **296**(1): p. 49-56.

191. de la Serna, J.B., J. Perez-Gil, A.C. Simonsen, and L.A. Bagatolli, *Cholesterol rules - Direct observation of the coexistence of two fluid phases in native pulmonary surfactant membranes at physiological temperatures.* Journal of Biological Chemistry, 2004. **279**(39): p. 40715-40722.

192. Angelova, M.I. and D.S. Dimitrov, *Liposome Electroformation.* Faraday Discussions, 1986: p. 303-+.

193. Fidorra, M., L. Duelund, C. Leidy, A.C. Simonsen, and L.A. Bagatolli, *Absence of fluid-ordered/fluid-disordered phase coexistence in ceramide/POPC mixtures containing cholesterol.* Biophysical Journal, 2006. **90**(12): p. 4437-4451.

194. Hara, T., S.R. Durell, M.C. Myers, and D.H. Appella, *Probing the structural requirements of peptoids that inhibit HDM2-p53 interactions.* Journal of the American Chemical Society, 2006. **128**(6): p. 1995-2004.

195. Saenz, A., O. Canadas, L.A. Bagatolli, F. Sanchez-Barbero, M.E. Johnson, and C. Casals, *Effect of surfactant protein A on the physical properties and surface activity of KL4-surfactant.* Biophysical Journal, 2007. **92**(2): p. 482-492.

196. Plasencia, I., L. Norlen, and L.A. Bagatolli, *Direct visualization of lipid domains in human skin stratum corneum's lipid membranes: Effect of pH and temperature.* Biophysical Journal, 2007. **93**: p. 3142-3155.

197. Saenz, A., O. Canadas, L.A. Bagatolli, M.E. Johnson, and C. Casals, *Physical properties and surface activity of surfactant-like membranes containing the cationic and hydrophobic peptide KL4.* Febs Journal, 2006. **273**(11): p. 2515-2527.

198. Janiak, M.J., D.M. Small, and G.G. Shipley, *Nature of Thermal Pre-Transition of Synthetic Phospholipids - Dimyristoyllecithin and Dipalmitoyllecithin.* Biochemistry, 1976. **15**(21): p. 4575-4580.

199. Horowitz, A.D., *Exclusion of Sp-C, but Not Sp-B, by Gel Phase Palmitoyl Lipids.* Chemistry and Physics of Lipids, 1995. **76**(1): p. 27-39.

200. Horowitz, A.D., J.E. Baatz, and J.A. Whitsett, *Lipid Effects on Aggregation of Pulmonary Surfactant Protein Sp-C Studied by Fluorescence Energy-Transfer.* Biochemistry, 1993. **32**(37): p. 9513-9523.

201. Luy, B., A. Diener, R.P. Hummel, E. Sturm, W.R. Ulrich, and C. Griesinger, *Structure and potential C-terminal dimerization of a recombinant mutant of surfactant-associated protein C in chloroform/methanol.* European Journal of Biochemistry, 2004. **271**(11): p. 2076-2085.

202. Kairys, V., M.K. Gilson, and B. Luy, *Structural model for an AxxxG-mediated dimer of surfactant-associated protein C.* European Journal of Biochemistry, 2004. **271**(11): p. 2086-2092.

203. Smith, S.O., D. Song, S. Shekar, M. Groesbeek, M. Ziliox, and S. Aimoto, *Structure of the transmembrane dimer interface of glycophorin A in membrane bilayers.* Biochemistry, 2001. **40**(22): p. 6553-6558.

204. MacKenzie, K.R., J.H. Prestegard, and D.M. Engelman, *A transmembrane helix dimer: Structure and implications.* Science, 1997. **276**(5309): p. 131-133.

205. Wang, W.J., S.J. Russo, S. Mulugeta, and M.F. Beers, *Biosynthesis of surfactant protein C (SP-C) - Sorting of SP-C proprotein involves homomeric association via a signal anchor domain.* Journal of Biological Chemistry, 2002. **277**(22): p. 19929-19937.

206. Bagatolli, L.A., *To see or not to see: Lateral organization of biological membranes and fluorescence microscopy.* Biochimica Et Biophysica Acta-Biomembranes, 2006. **1758**(10): p. 1541-1556.

207. Kahya, N., D. Scherfeld, K. Bacia, and P. Schwille, *Lipid domain formation and dynamics in giant unilamellar vesicles explored by fluorescence correlation spectroscopy.* Journal of Structural Biology, 2004. **147**(1): p. 77-89.

208. Harris, F.M., K.B. Best, and J.D. Bell, *Use of laurdan fluorescence intensity and polarization to distinguish between changes in membrane fluidity and phospholipid order.* Biochimica Et Biophysica Acta-Biomembranes, 2002. **1565**(1): p. 123-128.

209. Bagatolli, L.A. and E. Gratton, *Direct observation of lipid domains in free-standing bilayers using two-photon excitation fluorescence microscopy.* Journal of Fluorescence, 2001. **11**(3): p. 141-160.

210. Bourdos, N., F. Kollmer, A. Benninghoven, M. Ross, M. Sieber, and H.J. Galla, *Analysis of lung surfactant model systems with time-of-flight secondary ion mass spectrometry.* Biophysical Journal, 2000. **79**(1): p. 357-369.

211. Schurch, S., H. Bachofen, J. Goerke, and F. Possmayer, *A Captive Bubble Method Reproduces the Insitu Behavior of Lung Surfactant Monolayers.* Journal of Applied Physiology, 1989. **67**(6): p. 2389-2396.

212. Johansson, H., K. Nordling, T.E. Weaver, and J. Johansson, *The Brichos domain-containing C-terminal part of pro-surfactant protein C binds to an unfolded poly-Val transmembrane segment.* Journal of Biological Chemistry, 2006. **281**(30): p. 21032-21039.

213. Ramirez, E., A. Santana, A. Cruz, I. Plasencia, and G.E. Lopez, *Molecular dynamics of surfactant protein C: From single molecule to heptameric aggregates.* Biophysical Journal, 2006. **90**(8): p. 2698-2705.

Appendices

Appendix A: SP-C Peptoid *N*- and C-terminal sequence biomimicry

A thorough understanding of the relationship between peptoid oligomer structure and function will aid in the rational design of SP-C mimics having the necessary molecular features to closely mimic the biophysical activities of the natural molecule. So far, the following structural features have been investigated: (i) side chain chemistry and helical rigidity of the C-terminal helical region, (ii) minimum helix length, and (iii) palmitoylation (alkylation) of the *N*-terminal region. The compounds listed in Table A.1 were similarly synthesized and purified as previously detailed in order to investigate the effect of the following structural features in peptoid analogues of SP-C: (i) extending the helical length to 17 *N*spe residues, ~ 34 Å, (Mimic C1-17), (ii) extending the length of the achiral region to mimic the entire *N*-terminal sequence of human SP-C (Mimic C7-6), and (iii) extending the helical region internally to include residues 5 and 6 (Mimic C6-120).

Table A.1: Peptoid sequences designed to better mimic the *N*- and C-terminal regions of SP-C.

Mimic C1-17	H-*N*pm-*N*pm-Pro-*N*Val-*N*pm-*N*Leu-*N*Lys-*N*Lys-(***N*spe**)$_{17}$-*N*H$_2$	Lengthen C-terminal helical region
Mimic C7-6	H-***N*pm-Gly-*N*Ile-Pro**-*N*pm-*N*pm-Pro-*N*Val-*N*pm-*N*Leu-*N*Lys-*N*Lys-(*N*spe)$_{14}$-*N*H$_2$	Full-length *N*-terminal region
Mimic C6-120	H-*N*pm-*N*pm-Pro-*N*Val-***N*spe-*N*ssb**-*N*Lys-*N*Lys-(*N*spe)$_{14}$-*N*H$_2$	Extended helical region

The purified sequences were then characterized by circular dichroism (CD) spectroscopy to ensure the designed mimetics conform to stable, helical structures in solution. Figure A.1 shows the CD spectra for the biomimetic sequences. In addition to the mimics listed in Table A.1, the *N*spe-based, aromatic mimic, Mimic C, is also shown for comparison.

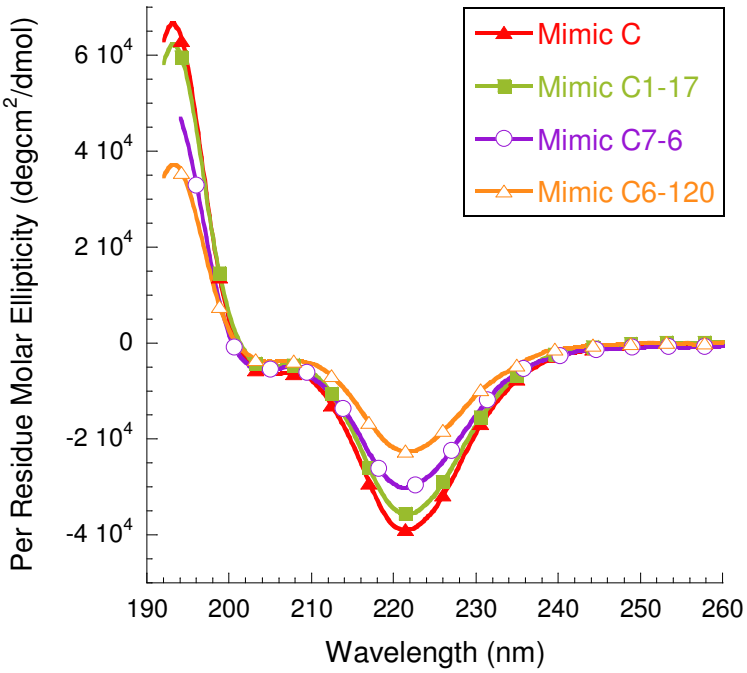

Figure A.1: Circular dichroism (CD) spectra of the peptoid-based SP-C mimics, showing qualitatively similar characteristics of peptoid helices. Spectra were acquired in methanol at a concentration of ~ 60 μM at room temperature.

All of the peptoid-based mimics of SP-C exhibit CD spectra that are qualitatively similar to a peptide α-helix with a double minima at λ ~ 220 nm and ~ 205 nm and an intense maximum at λ ~ 192 nm. Therefore, all the mimics are structured and helical in solution. Mimic C1-17 has a CD spectrum that is very similar to Mimic C, indicating that the helical region in Mimic C is already fully developed and that the inclusion of three additional α-chiral, aromatic residues does not further increase the helicity of the compound. Mimic C7-6 exhibits a slightly reduced CD

signal as a result of the inclusion of four additional residues in the *N*-terminal region. This is expected as the addition of these achiral residues lowers the percentage of chiral residues in the compound, lowering the per-residue molar ellipticity of the compound. Somewhat surprising is the decreased CD intensity observed for Mimic C6-120 as this compound contains two additional chiral residues; however, one of these is an α-chiral, aliphatic residue, *N*ssb, which likely shifts the CD spectrum slightly in a manner observed in Chapters 6 and 7 with the inclusion of both α-chiral, aromatic and α-chiral, aliphatic residues.

The *in vitro* surface activities of the mimics in a biomimetic phospholipid formulation were characterized by Langmuir-Wilhelmy surface balance (LWSB) studies as well as static and dynamic pulsating bubble surfactometry (PBS) as described in previous chapters. All mimics were compared to lipids alone, lipids with 1.6 mol% native porcine SP-C, and 1.6 mol% Mimic C. Figure A.2 shows the LWSB surface pressure-area isotherms for the mimics at 37°C.

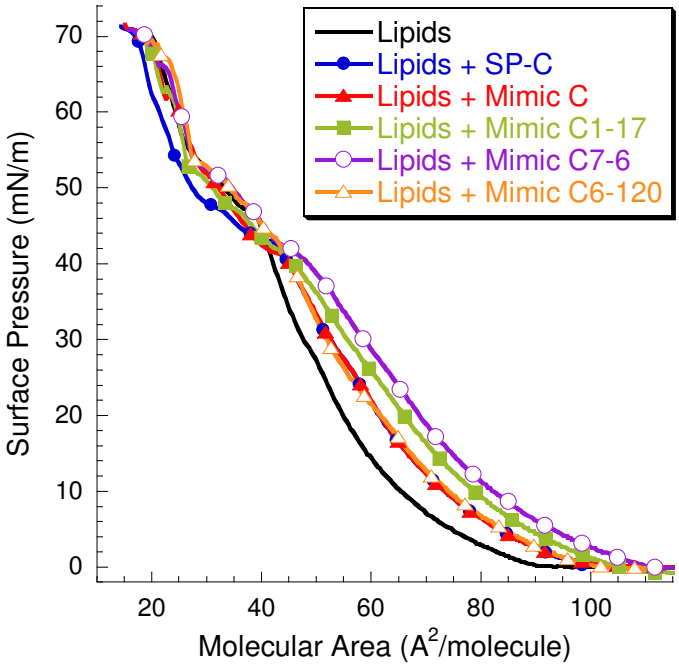

Figure A.2: Langmuir-Wilhelmy surface balance (LWSB) studies at 37°C. Surface pressure-area isotherms obtained for DPPC:POPG:PA (68:22:9, by weight) alone and with 1.6 mol% SP-C and SP-C mimics. Isotherms were collected on a buffered subphase (150 mM NaCl, 10 mM HEPES, 5 mM CaCl2, pH=6.90).

The LWSB isotherms in Figure A.2 show that increasing either the C-terminal helix length (Mimic C1-17) or the *N*-terminal length leads to an increase in the molecular area lift-off to ~ 110 $Å^2$/molecule and ~ 112 $Å^2$/molecule, respectively. The increase in molecular area lift-off is likely a result the increased length of the peptoid analogues rather than a specific interaction between these species and the phospholipids. Also, extending the helical region results in a lift-off for the Mimic C6-120 formulation of ~ 102 $Å^2$/molecule, which is similar to the Mimic C and porcine SP-C formulations. The plateau regions of the LWSB isotherms are all similar to Mimic C with that of Mimic C7-6 being slightly extended, which may indicate a slight increase in biomimicry.

Figure A.3A displays the static adsorption over time in a PBS instrument. All the peptoid analogues increase the adsorption kinetics of the phospholipid formulation, but not to the extent that SP-C does so. Specifically, increasing the length of the of the C-terminal helical region or the achiral, *N*-terminal region does not significantly alter the static adsorption kinetics significantly from Mimic C. Both formulations rapid reach an adsorptive surface tension of ~ 30-34 mN/m within one minute, which is slightly faster than Mimic C; however, the final equilibrium surface tensions are all similar, ~ 32 mN/m. Interestingly, while the addition of Mimic C6-120 with an internally extended helical region improves the adsorption kinetics over the lipids alone, it does so to a less extent than any of the other peptoid analogues, only reaching ~ 36 mN/m after 20 minutes.

Figure A.3B displays the dynamic PBS compression expansion cycles for the peptoid analogues. All the peptoid analogues display very similar dynamic PBS characteristics including PBS loop shape and maximum and minimum surface tensions. Also, the reduction in maximum surface tension was not as significant as native SP-C. Both the formulations containing Mimics C and C1-17 had a maximum surface tension of ~ 52 mN/m while those of Mimics C7-6 and C6-120 had a maximum surface tension of ~ 50 mN/m. This indicates a slight improvement in biomimicry by increasing the unstructured, amphipathic *N*-terminal region or by extending the helical region internally.

Here, a series of peptoid-based analogues of SP-C were created to better mimic both the C-terminal helical region and the unstructured, amphipathic *N*-terminal region. CD spectroscopy showed that all these peptoid analogues exhibit CD spectra that are similar to a peptide α-helix, which is typical of peptoids of this class, indicating that the compounds are structured and helical

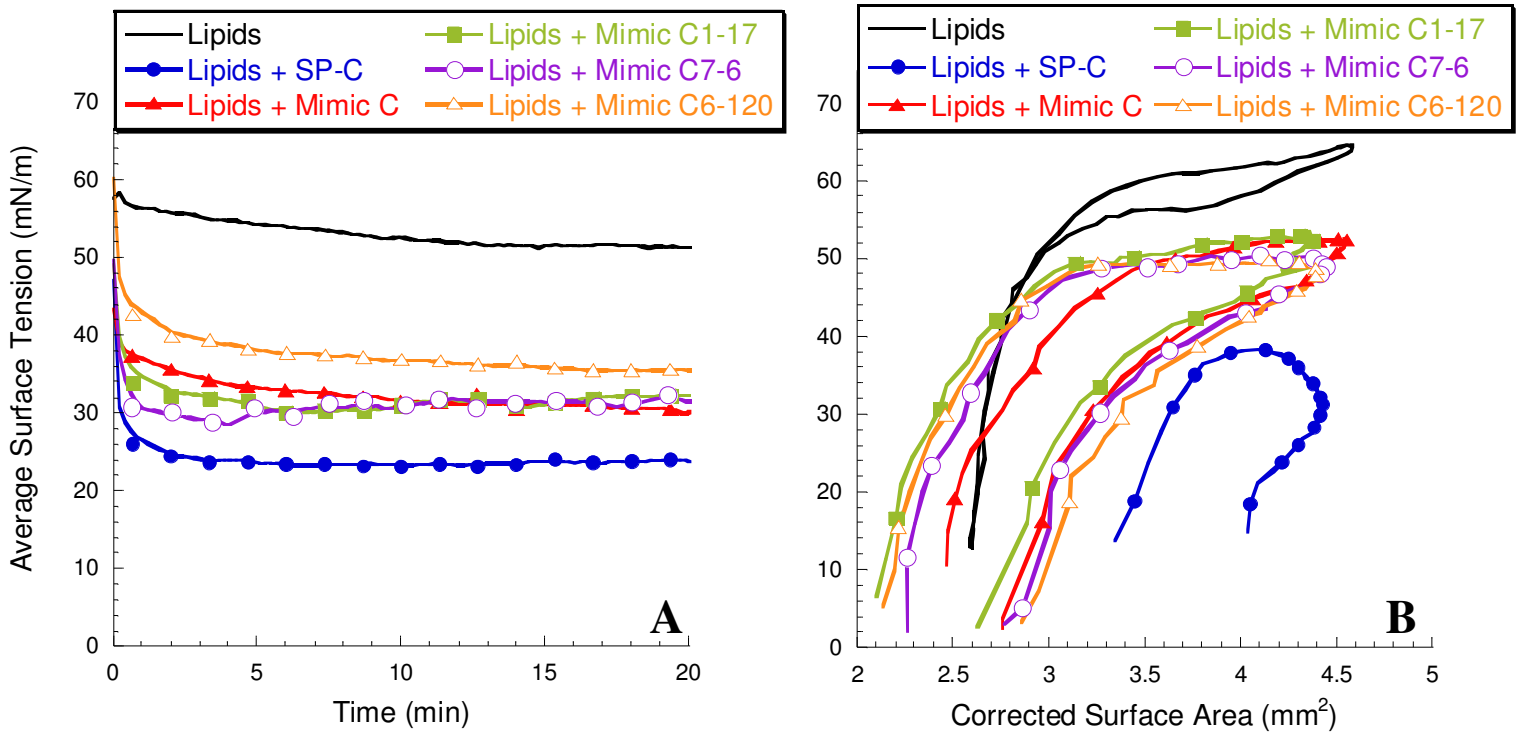

Figure A.3: (A) Static pulsating bubble surfactometry (PBS) results displaying surface tension as a function of time and (B) dynamic PBS results displaying surface tension as a function of surface area at an oscillation frequency of 20 cycles/min after 5 minutes of cycling. Measurements were taken at a bulk surfactant concentration of 1 mg/mL lipids [DPPC:POPG:PA (68:22:9, by weight)] at 37°C and dispersed in a buffered solution (150 mM NaCl, 10 mM HEPES, 5 mM CaCl2, pH=6.90).

in solution. LWSB and PBS studies showed that when combined with a synthetic phospholipid formulation, that the mimics improved the surface activity of the surfactants in a manner similar to SP-C, but not as significant as the native protein. Also, by dynamic PBS cycling, a slight increase in surface activity (reduced maximum surface tension) was observed by either extending the *N*-terminal sequence (Mimic C7-6) or increasing the extending the C-terminal helical region to included residues 5 and 6 of the peptoid mimic (Mimic C6-120); however, this increase in surface activity comes with a caveat. Lengthening of the *N*-terminal region by 4 peptoid residues in Mimic C7-6 increases the cost of production and decreases the overall yield of the peptoid analogue in comparison to Mimic C. Similarly, for Mimic C6-120, increasing the total number of α-chiral residues increases the cost as the chiral submonomers are significantly more expensive than the achiral peptoid submonomers. Furthermore, Mimic C6-120 was significantly more difficult to purify than the other peptoid oligomers. Therefore, the modest increases in surface activity observed with Mimics C7-6 and C6-120 do not warrant their sequence alterations. This is especially true in light of the dramatic effect that *N*-terminal alkylation (Chapter 5) and side chain chemistry of the helical region (Chapters 6 and 7) have upon surface activity.